See Docket 1 for encl.

CorSTAR

EECO INDUSTRIES AFFILIATE

WM DOCKET CONTROL CENTER

March 27, 1986

'86 MAR 31 P2:57

WM-RES
WM Record File
B6985
CorStar

WM Project 10,11,16
Docket No.
PDR ✓
LPDR B,M,S

Distribution:
X P. Brooks
Joan Tuckett
(Return to WM, 623-SS)

Pauline Brooks
Division of Waste Management
MS 623 SS
U.S. Nuclear Regulatory Commission
Washington, D.C. 20555

Subject: Contract No. NRC-02-81-026
Benchmarking of Computer Codes
and Licensing Assistance

Dear Pauline:

Enclosed are 5 copies of the draft report for Tasks 4 and 5 of the Radiological Assessment Codes. We will submit this report for External QA Review concurrent with the NRC's review of the report.

Contact me if you have questions on this matter.

Sincerely,

Douglas K. Vogt

Douglas K. Vogt
Project Manager

DKV:kg

2940

CORPORATE SYSTEMS, TECHNOLOGIES, AND RESOURCES
2121 ALLSTON WAY • BERKELEY, CALIFORNIA 94704 • (415) 548-4100

BERKELEY WASHINGTON, D.C. INCLINE VILLAGE

Sec B6985 3/27/86
TO: Pauline Brooks
Draft Report for Task 4&5

NUREG/CR-XXXX

BENCHMARK PROBLEM RESULTS FOR RADIOLOGICAL ASSESSMENT CODES

DRAFT FINAL REPORT

Submitted to:

Division of Waste Management
Office of Nuclear Materials Safety and Safeguards
U.S. Nuclear Regulatory Commission
Washington, D.C. 20555
NRC FIN B6985

Submitted from:

D. Vogt and M. Mills
CorSTAR Research, Inc.
2121 Allston Way
Berkeley, California 94704
(415)548-4100

RK-81-3009

CorSTAR

CONTENTS

CONTENTS
(Continued)

CONTENTS
(Continued)

CONTENTS
(Continued)

TABLES

TABLES
(Continued)

TABLES
(Continued)

FIGURES

FIGURES
(Continued)

FIGURES
(Continued)

FIGURES
(Continued)

FIGURES
(Continued)

FIGURES
(Continued)

FIGURES
(Continued)

I. INTRODUCTION

1.1 Background

The licensing of a repository for high-level radioactive waste will require the application of computer codes to analyze the numerous interrelated factors affecting the repository's performance. The Nuclear Regulatory Commission (NRC), which has the responsibility for reviewing repository license applications, is sponsoring an evaluation of computer codes in the following five areas of repository performance assessment: (1) repository siting; (2) radiological assessment; (3) repository design; (4) waste package design; and (5) overall systems analysis.

Repository siting codes deal with the analysis of saturated flow, unsaturated flow, surface-water flow, solute transport, and heat transport. Radiological assessment codes include computer programs for analyzing radionuclide source terms, the transport of radionuclides between various compartments of the surface environment, and the resulting dose to man due to ingestion, inhalation, and external exposure. The repository design codes will be used to analyze geomechanical processes, structural design, and heat transport. Waste package codes simulate the interactions taking place within the waste package and with the surrounding repository host rock. Overall systems codes will be used to address multiple areas of repository performance assessment. The radiological assessment codes PATH1 and BIODOSE, which are evaluated in this report, are actually components of larger systems codes.

This report is the fourth in a series dealing with the radiological assessment codes. The three preceding reports are listed in the reference section of this chapter (see Section 1.4).

The first report in this series (Reference 1) presents the results of a comprehensive survey of available radiological assessment codes. Those codes most applicable to high-level waste repository analysis are summarized on the basis of available code documentation. Each code summary deals both with the operating characteristics of the code (computing time, storage, input, and output) and with

the underlying theory upon which the code is based (equations, numerical approximations, and simplifications). In addition, the summary reports the extent to which the code has been subjected to verification, validation, and sensitivity analysis.

For each code summarized in the initial report, the second report (Reference 2) defines the code's independent and dependent variables and presents data indicating the ranges of values that can be assigned to these variables for repository assessment applications. The primary purpose of the second report is to provide users of the codes with a quick reference for aid in interpreting code input data requirements. The report is also designed to serve as a guide in the preparation of benchmark problems for the actual evaluation of computer codes.

The third report (Reference 3) describes these benchmark problems in detail. The set of benchmark problems for each code area was developed with several objectives in mind. In some cases the problems are based upon field or laboratory measurements, so that running the problem can serve as a validation of the code. In other cases the problems have analytic solutions, which can be used to verify the accuracy of numerical methods employed in the code. In still other cases, the problems are designed to test whether the code can even be used to analyze the hypothetical repository situation. By running these hypothetical problems, the following types of code errors and limitations can be uncovered:

- Code options advertised in the user's manual but not actually available in the program
- Parameter values set within the code, not to be overridden by the user
- Division by zero, logarithm of a negative number, etc.
- Array size constraints and excessive program run times
- Cumbersome input data requirements
- Options added to a code without having been checked out or even used by the developers of the code
- Vestigial sections of the code that cannot be accessed any longer or that cannot affect the outcome of the calculation

In addition to making it possible to evaluate a code, these test problems can serve as benchmarks by which the impact of future modifications to the codes can be judged. Also, since a coding error made during code modification can introduce problems within portions of the code that have been previously checked out, having a complete set of benchmark problems to rerun after each code modification permits timely discovery of the error.

The purpose and organization of the fourth report are discussed below.

1.2 Purpose of This Report

The benchmark problems documented in the third report were run using a subset of the codes presented in the first report as well as two new codes, ANSIDECH/BURNUP and CELLTRANS. ANSIDECH/BURNUP, presented as a solution to benchmark problems 2.1 and 2.2 in the third report, was included in the benchmark problem runs because it is based on an accepted method for estimating spent-fuel afterheat generation rates, the joint American National Standards Institute/American Nuclear Society standard for competing fission product after heat power. CELLTRANS was introduced because it provides an analytical solution to benchmark problems 3.1, 3.2, 3.3, 3.4, and 3.5. The purpose of this fourth report is to present the results of the benchmarking study.

The report is designed to be used in conjunction with accompanying listings of source code, benchmark problem input, and code input given on magnetic tape and micofiche. While much of this report is devoted to a comparison of codes in terms of their outputs, an effort has also been made to evaluate each code's ease of use. Ease of use is an important consideration for the environmental-pathway and dose-to-man codes, which require long times for the preparation of input data files. The steps and compromises involved in this input data preparation are documented in this report.

Although they have been grouped under the general heading of "radiological assessment," the codes covered in this report fall into two distinct categories. The codes in the first category, ORIGEN and ANSIDECH/BURNUP, calculate the

time-dependent radionuclide inventory (ORIGEN) or heat production rate (ORIGEN, ANSIDECH/BURNUP) within reacter fuel elements based upon the operating history of the reactor during the residence time of the fuel element. The codes in the second group (PATH1/DOSHEM, CELLTRANS, BIODOSE, PABLM, and LADTAP) simulate the transport of radionuclides through the surface environment, their movement through the food chain, and the eventual dose to man due to ingestion, inhalation, and external exposure. The connection between the two code groups is that the time-dependent radionuclide inventory is a required input to the solute transport model that provides the surface-water radionuclide input for environmental transport modeling. The benchmark problems for the two code groups are quite different. The problems for ORIGEN and ANSIDECH/BURNUP are based upon engineering data, while the problems for the environmental-pathway and dose-to-man codes are hypothetical. The primary reason for combining these code groups is that they deal with two closely related fields, nuclear engineering and health physics.

1.3 Organization of the Report

The organization of this report reflects the fact that two different types of codes are being benchmarked. In the discussion of benchmarking results and code-to-code comparisons, these two code types are treated separately.

In Chapter 2 of the report, the major findings of the study are summarized.

Chapter 3 deals with the benchmarking of the radionuclide inventory and heat generation codes: Section 3.1 addresses the code ORIGEN; and Section 3.2, the code ANSIDECH/BURNUP. For each code, the discussion is divided into three parts. The first part provides a description of the code. In the case of ORIGEN, this description just highlights the code's most important features and capabilities; for a more detailed discussion, the reader should consult the code user's manual or the code summary report (Reference 1) described earlier. In the case of ANSIDECH/BURNUP, the description is detailed, since this code was not discussed in the code summary report. The second part of the discussion for each code provides a detailed description of the benchmark problems to be

solved by the code. A benchmark problem described once is not described again when listed for use with subsequent codes; instead, only those aspects of the problem that cause difficulties for the code or that require a problem restatement are examined. In the third part of the discussion, the benchmarking results for each code are presented. Section 3.3 is devoted an evaluation of the ORIGEN and ANSIDECH/BURNUP codes and to a presentation of selected comparisons of code outputs.

Chapter 4 contains the benchmarking discussion for the environmental-pathway and dose-to-man codes, PATH1/DOSHEM, CELLTRANS, BIODOSE, PABLM, and LADTAP. The format is identical to that of Section 3. Except for CELLTRANS, the code descriptions highlight important features and capabilities; again, for further detail the reader should consult the code user's manual or the summary report. The code description for CELLTRANS is more detailed, since this code was not covered in that report.

1.4 References for Chapter 1

1. Mills, M.T., and Vogt, D.K. A Summary of Computer Codes for Radiological Assessment. NUREG/CR-3209. March 1983.

2. Mills, M.T.; Vogt, D.K.; and Mann, B. Parameters and Variables Appearing in Radiological Assessment Codes. NUREG/CR-3160. June 1983.

3. Mills, M.T.; Vogt, D.K.; and Mann, B. Benchmark Problems for Radiological Assessment Codes. NUREG/CR-3451. September 1983.

2. SUMMARY OF MAJOR FINDINGS

In a report of this type, there is the chance that the most important conclusions reached during the study will be obscured by the details of the individual code comparisons. Furthermore, there are a number of general observations that apply to more than one code. The purpose of this chapter is to present these important but more general findings at the outset of the report. Individual code evaluations are presented at the ends of Sections 3 and 4. As is the case throughout this report, each of the two code types is dealt with separately.

2.1 Radionuclide Inventory and Heat Generation Codes

Methods for estimating the decay heat from nuclear fuel and the isotopic buildup and decay in nuclear fuel have been used for over forty years, since the start-up of the first reactors during the Manhattan project. In spite of the relatively long period these methods have been used, there are relatively few publicly available data for measured decay heat or isotopic content of spent fuel assemblies representative of today's pressurized water reactor designs and almost no publicly available data for decay heat or spent fuel isotopic content are available for today's boiling water reactor fuel designs.

The estimation of decay heat and isotopic content of spent fuel requires an analytical method and an extensive data base of nuclear parameters. Performing engineering estimates of spent fuel isotopic content or decay heat requires both the choice of an appropriate analytical method and the use of properly generated nuclear data. One of the principal findings of this effort is that additional measured data for both spent fuel isotopic content and decay heat are required to better benchmark these computer codes.

Major conclusions from the benchmarking of the decay heat and isotopic buildup and decay codes are presented below:

- Our benchmarking results confirm the conservatism of the ANS Standard for estimating decay heat generation from spent fuel for time periods of up to thirty years following discharge from the reactor.

- Although the ANS Standard is meant to estimate the decay heat generation from fission products only, the results from the Standard provided a conservative estimate for the total decay heat, including that from fission products, transuranic elements, and activation products present in spent fuel.

- The ANS Standard is conservative in estimating decay heat generation for time periods of at least 100 years following discharge from reactor.

- The ANS Standard provides a conservative estimate of the decay heat generation rates when compared to available measurements.

- Decay heat generation rates estimated by both ORIGEN and the ANS Standard are an estimated 7% to 15% or more higher than measured decay heat generation rates. This may be due to conservatism in the ORIGEN and ANS standard methods or to measurement errors.

- ORIGEN estimates of the uranium isotopic content of spent fuel agree favorably with the available measured data. ORIGEN predictions of U-234, U-235, U-236, and U-238 isotopic content agree to within a nominal 2% of measured concentrations in spent fuel. Obtaining good estimates for the Uranium 234 content and spent fuel requires a reliable estimate of the U-234 content in initially loaded uranium fuel. A method to develop this estimate is presented in Appendix A to this report.

- ORIGEN estimates of the plutonium concentration in spent nuclear fuel range from fair to poor for individual plutonium isotopes. The ORIGEN estimate of the total quantity of plutonium present in spent fuel was generally in good agreement with measurements.

- ORIGEN estimates of other transuranic elements range from poor to unacceptable. Often the error in estimating the quantities of these transuranic elements was a factor of two or more. If the quantities of these transuranic elements present in high-level waste are of importance to high-level waste management, a better method of estimating them is required.

- ORIGEN estimates of the concentration of individual fission products present in spent fuel range from marginal to acceptable. Some of the disagreement may be due to errors in the measurement of fission products in spent fuel. Additional disagreement may be due to migration of fission products from the fuel pellets to the fuel cladding or the volatilization of fission products within the fuel pellets.

We found the code ORIGEN relatively easy to use for an experienced nuclear engineer. An individual without a nuclear engineering background may have difficulty in understanding the theory required to prepare certain inputs for the code. The code did provide adequate error messages when input mistakes were made. The empirical ANS Standard is relatively easy to use. It is recommended if a reliable estimate of decay heat is needed.

2.2 Environmental-Pathway and Dose-to-Man Codes

In view of the mathematical simplicity of the environmental-pathway and dose-to-man codes, there was some concern at the beginning of the project as to the justification of their being benchmarked. The assumption generally made is that, once the health physics expert has chosen his parameter values, the relatively mundane calculations will be performed correctly. Although it is true that these codes are inherently less complex mathematically than are the codes used in most engineering analyses, they can still pose problems. This point will be demonstrated in Section 4 of the report.

Although some of the environmental-pathway and dose-to-man codes covered in this report are advertised as general-purpose codes, the principal motivation for their development was the wish to solve specific problems. The generalization of these codes has been achieved by hanging on additional options that give the user more flexibility in the application of the code but rarely affect its basic structure. Furthermore, this complex array of options can make the preparation of code input data a cumbersome task. Sometimes options are added to a code without being thoroughly checked by the code developer. For example, the code BIODOSE, does not calculate time-dependent radionuclide concentrations correctly. Conversations with the consulting firm that developed the code revealed that the code was only run in the steady-state mode in support of high-level-waste assessment projects. A similar but less serious problem was discovered with the PATH1 code. Although no errors were found in the PATH1 calculations of time-dependent radionuclide concentrations, the numerical solution to the transport equations for groundwater radionuclide input would not converge using the integration method recommended in the code user's manual. Through

discussions with the code developers, it was discovered that this particular code option had not been exercised. The noncovergence problem was eliminated through the choice of a different integration method.

In contrast to the problem of numerous and sometimes unverified code options, some codes have "wired in" parameter values that may be applicable only to the specific problem for which the code was originally designed. The code LADTAP is necessarily written in this way, since it was designed to implement the recommendations of NRC Regulatory Guide 1.109. In the case of codes designed for more general purpose applications, one would not expect to find these internally assigned parameter values. The code PABLM, however, contains several assigned variables that can strongly affect the outcome of the calculation. These include the soil "surface density," rates of feed consumption and water consumption by farm animals, and the transfer rate of radionuclides between river and sediment. Although these assumed values are mentioned in the PABLM documentation, the user can be unaware of their role in the calculation. Furthermore, if the user wishes to change one or more of these values, he must find the variable within the source code, make the change, and then recompile the code.

The biggest challenge in this benchmarking study was to prepare the benchmark problem inputs in accordance with the input requirements of each code. In some cases a problem could not be run with a particular code. The lack of a groundwater compartment meant that the codes BIODOSE, PABLM, and LADTAP could not be used to solve problems 3.0, 3.0A, 3.1, 3.1A, and 3.2.* Furthermore, even if a code could be applied to a problem, it was often necessary to make approximations and simplifications in the preparation of input data sets. For example, the comparison between the codes BIODOSE and PATH1/DOSHEM required that a number of the environmental transport parameters needed by BIODOSE be selected so that the resultant transfer matrix would be the same as that used by PATH1/DOSHEM (see Section 4.2.3). The extraordinary measures required for this comparison constituted one reason for

---

* These benchmark problem numbers correspond to those used in the preceding report (see Reference 3 in the Chapter 1 reference list above).

our concluding that it might be easier to develop a code for a specific type of problem than spend the time trying to use a code not intended for the application. This conclusion becomes more reasonable when one considers that most of the statements in each of these programs are devoted to the retrieval of data and the tabulation of results. These applications are well suited to a number of programs currently available to run on microcomputers. Data retrieval and manipulation and the reporting of results could be handled through a sequence of higher-level-language commands, which could be easily modified, rather than with a FORTRAN program that would require considerable time to develop and debug. In this regard, there is the need for a data base of food chain and dose parameters able to run on a microcomputer. Such a data base would make it possible to set up problems rapidly and to avoid using inflexible codes not suited to the problem at hand.

During the course of the study a number of observations were made. These had less to do with the accuracy of the codes than with the practical difficulties encountered in their use. A number of the more important observations are given below. The remainder are discussed in conjunction with the individual code benchmarking writeups.

- The codes PATH1/DOSHEM and BIODOSE are parts of larger systems. In these systems, data are generally passed from one component to another in the form of disk files. When run in a stand-alone mode, these codes require that the data be manually entered in a rather cumbersome or confusing format. For example, DOSHEM input had to be prepared manually from PATH1 output, since only the steady-state version of PATH1 will generate a file for direct input to DOSHEM. The code developers never bothered to link the time-dependent version of PATH1 with DOSHEM, since the overall system was used to model steady-state conditions only. As for BIODOSE, when run in a stand-alone mode, this code does not allow the user to specify radionuclide inputs in conventional units such as Ci/yr. Instead, BIODOSE requires an inventory value for each radionuclide in units of Ci/MWe-yr. By consulting the documentation for the NUTRAN system, of which BIODOSE is a part, one finds that the BIODOSE-calculated dose reported in rem must be multiplied by the spent fuel stored (MWe-yr) and the transport rate from the repository to the surface environment (yr^{-1}).

- The separation of the radionuclide transport and food chain calculations from the dose-to-man calculation can facilitate the use of alternative dosimetry systems. The codes BIODOSE and PABLM will have to be substantially modified to accept a new system of dose factors, since the dose factor calculation is performed within these codes.

- The environmental compartment approach with solid and liquid components, as used in PATH1 and CELLTRANS, appears to offer the best general framework for handling environmental transport problems. From the user's point of view, it also seems to be the least confusing. Furthermore, with the eigenvector method used in CELLTRANS, these problems can be run on microcomputers.

- The preparation of input data for these codes could be facilitated by the use of input preprocessor programs. The approach would require no change to the code itself, which would still be run in a batch mode.

- The PABLM and LADTAP codes have poor internal documentation. This not only makes future improvements to the codes more difficult but also increases the probability that these modifications will introduce errors into the codes.

3. BENCHMARKING OF RADIONUCLIDE INVENTORY AND HEAT GENERATION CODES

3.1 ORIGEN/S

3.1.1 Code Description

The computer code ORIGEN simulates the buildup and decay of radionuclides at a point in a nuclear fuel assembly. ORIGEN can be used to calculate radionuclide inventories, heat production, decay product energies, and photon releases. Several versions of ORIGEN exist (see References 1 through 4 in the list at the end of this chapter). Here we present benchmark results for the version known as ORIGEN/S, a code that runs within the SCALE system (Reference 4).

ORIGEN is a zero-dimensional depletion code that solves the Bateman Equation (Reference 5) for radioactive growth and decay of large numbers of isotopes with arbitrary coupling. The code solves a matrix of coupled first-order ordinary differential equations with constant coefficients using the matrix exponential method. An extensive library of nuclear data has been compiled for use with the code, including half-lives and decay schemes, neutron absorption cross-sections, fission yields, disintegration energies, and multigroup photon release.

ORIGEN solves the following general expression for the formulation and disappearance of a nuclide by irradiation, nuclear transmutation, and decay at a point in a constant neutron flux of one effective energy group:

$$\frac{dN_i}{dt} = \sum_j \gamma_{ji}\sigma_{f,j}N_j\phi + \sigma_{c,i-1}N_{i-1}\phi + \lambda_i' N_i' - \sigma_{f,i}N_i\phi - \sigma_{c,i}N_i\phi - \lambda_i N_i \,, \qquad (3.1.1)$$

where ($i = 1, \ldots I$), and

$\sum_j \gamma_{ij} \sigma_{f,j} N_j \phi$	is the yield rate of N_i, due to the fission of all nuclides N_j
$\sigma_{c,i-1} N_{i-1} \phi$	is the rate of transmutation into N_i, due to radioactive neutron capture by nuclide N_{i-1}
$\lambda'_i N'_i$	is the rate of formation of N_i, due to the radioactive decay of nuclide N_i
$\sigma_{f,i} N_i \phi$	is the destruction rate of N_i, due to fission
$\sigma_{c,i} N_i \phi$	is the destruction rate of N_i, due to all forms of neutron capture ((n, ;n, ;n,p;n,2n;n,3n)
$\lambda_i N_i$	is the radioactive decay rate of N_i
I	the total number of nuclides under consideration

The analytical solution to this type of coupled differential equation is provided by the Bateman Equation (Reference 5). Bateman's solution for the i^{th} member in a decay chain is:

$$N_i = N_i(0)e^{-d_i t} + \sum_{k=1}^{i-1} N_k(0) \left[\sum_{j=k}^{i-1} \frac{e^{-d_j t} - e^{-d_i t}}{(d_i - d_j)} a_{j+1,j} \prod_{\substack{n=k \\ n \neq j}}^{i-1} \frac{a_{n+1,n}}{d_n - d_j} \right], \quad (3.1.2)$$

where d_i is the rate constant ($d_i = \quad _i + (\sigma_{f,i} + \sigma_{c,i})$)

where $N_i(O)$ is the amount of isotope i initially present and the members of the chain are numbered consecutively for simplicity.

ORIGEN/S was used to analyze each problem described in the following section with two cross-section sets:

- The cross-section set supplied with the code ORIGEN/S
- A cross-section set generated for each problem, taking into account reactor operating characteristics and specific fuel-design data

Cross-sections were generated using reactor design information and the codes NITAWL/S, XSDRNPM/S, and COUPLE. NITAWL/S uses the Nordheim integral method to account for resonance shelf shielding when generating group average cross-sections. XSDRNPM/S is used to collapse multigroup cross-sections in one dimension to few-group, cell-weighted cross-sections. The code COUPLE can be used to translate XSDRNPM/S output to a form suitable for use as input to the code ORIGEN.

It is generally believed that the use of cross-sections generated for specific reactor fuel designs and operating conditions yields a more accurate estimate of fuel actinide inventory at discharge and reactor decay heat. In this section of the report we compare the results of ORIGEN/S calculations in the benchmark problems for the existing ORIGEN cross-sections and for cross-sections generated for representative fuel designs and operating conditions.

3.1.2 Description of Benchmark Problems

3.1.2.1 Pressurized Water Reactor Afterheat Generation—ANS Standard (Benchmark Problem 2.1)*

Problem Statement. This problem presents two methods from the American National Standards Institute/American Nuclear Society standard** for computing fission-product afterheat power (Reference 6). These methods are available in the computer programs ANSIDECH and BURNUP (see Section 3.2). The purpose of the problem is to provide a semiempirical check of a code's ability to estimate decay heat generation rates.

The problem is designed to simulate the irradiation of a light water reactor fuel assembly and the decay heat generation during an extended cooling period. It is similar to a problem described in Reference 7.

---

* Note again that the number of each benchmark problem corresponds to the number used in the preceding report (Reference 3 in Chapter 1).

** Commonly called the ANS Standard and referred to as such in this report.

Physical Specifications. Pressurized water reactor fuel is irradiated at power levels ranging from about 20 MW/kg to about 45 MW/kg for periods of one to five years before being discharged. During irradiation, fission product concentrations increase; and, as a result, fission-product decay heat production after fission has ceased can be significant.

Selected design parameters for a Westinghouse 17x17 fuel assembly are given in Table 3-1. Analyses in Reference 7 indicate that, for similar fuel-assembly operating conditions and initial enrichment, this fuel assembly design will have the highest decay heat generation rate of any PWR zircalloy clad fuel design.

For benchmarking purposes, five subproblems are specified. The subproblems represent different combinations of fuel initial enrichment and operating conditions. Table 3-2 contains the problem-dependent input information for each of the five subproblems.

Assumptions. The initial nonactinide composition of the uranium oxide fuel pellets is given in Table 3-3. The weight of the fuel-assembly structural material is given in Table 3-4. The elemental composition of the structural materials is given in Table 3-5.

Output Specifications. The outputs for this problem are the decay heat generation rates in units of watts per initial metric ton of heavy metal at times of 1, 3, 10, 30, 100, 300, 1,000, 3,000, and 10,000 years following reactor shutdown. According to Reference 6, the ANS Standard is not applicable for cooling times greater than 10^9 seconds (31.7 years). However, Reference 7 reports excellent agreement between ANS Standard predictions and ORIGEN/S calculations for cooling times of up to 110 years.

3.1.2.2 Boiling Water Reactor Afterheat Generation—ANS Standard (Benchmark Problem 2.2)

Problem Statement. This problem presents two methods from the American National Standards Institute/American Nuclear Society standard for computing

Table 3-1

Data for PWR Fuel Decay Heat Generation Calculations

Percent theoretical density for UO_2*		93.844
Initial uranium composition (wt. %)	^{234}U	0.042
	^{235}U	3.200
	^{238}U	96.671
Initial uranium loading (kg/assembly)		461.4
Fuel rods per assembly		264 with zircaloy-4 clad
Rod pitch (cm)		1.25984
Pellet O.D. (cm)		0.81915
Gap O.D. (cm)		0.89281
Clad O.D. (cm)		0.94996
Active fuel length (cm)		365.76
Fuel temperature (^{o}K)		1000
Clad temperature (^{o}K)		605
Moderator temperature (^{o}K)		583
Moderator density (g cm^{-3})		0.706575
Average boron concentration (wt. ppm)		550

Source: Reference 7.

* Theoretical UO_2 density is 10.96 g cm^{-3}.

Table 3-2

Fuel Irradiation Data

Operating Conditions	Subproblems 1	2	3	4	5
^{235}U enrichment	1.5%	2.5%	3.5%	3.2%	3.2%
Irradiation History					
Time Period #1					
Duration (days)	370	370	370	1,080	150
Power level (MW/MTU)	41	43	28.5	31.25	34
Shutdown period (days)	–	60	60	–	0
Time Period #2					
Duration (days)	–	260	260	–	150
Power level (MW/MTU)	–	38	45	–	34
Shutdown period (days)	–	–	60	–	60
Time Period #3					
Duration (days)	–	–	300	–	150
Power level (MW/MTU)	–	–	42	–	41
Shutdown period (days)	–	–	–	–	15
Time Period #4					
Duration (days)	–	–	–	–	150
Power level (MW/MTU)	–	–	–	–	41
Shutdown period (days)	–	–	–	–	45
Time Period #5					
Duration (days)	–	–	–	–	150
Power level (MW/MTU)	–	–	–	–	37.5
Shutdown period (days)	–	–	–	–	15
Time Period #6					
Duration (days)	–	–	–	–	150
Power level (MW/MTU)	–	–	–	–	37.5
Shutdown period (days)	–	–	–	–	–

Table 3-3

Nonactinide Composition of LWR Oxide Fuels

Element	Atomic Number	Concentration (ppm)*
Li	3	1.0
B	5	1.0
C	6	89.4
N	7	25.0
O	8	134,454
F	9	10.7
Na	11	15.0
Mg	12	2.0
Al	13	16.7
Si	14	12.1
P	15	35.0
Cl	17	5.3
Ca	20	2.0
Ti	22	1.0
V	23	3.0
Cr	24	4.0
Mn	25	1.7
Fe	26	18.0
Co	27	1.0
Ni	28	24.0
Cu	29	1.0
Zn	30	40.3
Mo	42	10.0
Ag	47	0.1
Cd	48	25.0
In	49	2.0
Sn	50	4.0
Gd	64	2.5
W	74	2.0
Pb	82	1.0

Source: Reference 8.

* Parts of element per million parts of heavy metal by weight.

Table 3-4

Assumed Mass Distribution of PWR Fuel-Assembly Structural Materials

	Material	Mass (kg/MTHM)
Fuel Zone		
Cladding	Zircaloy-4	223.0
Fuel channel	–	–
Grid spacers	Inconel 718	12.8
Grid-spacer springs	Inconel 718	
Grid-brazing material	Nicrobraze 50	2.6
Miscellaneous	SS 304*	9.9
Fuel-gas Plenum Zone		
Cladding	Zircaloy-4	12.0
Fuel channel	–	–
Plenum spring	SS 302	4.2
End Fitting Zone		
Top end fitting	SS 304	14.8
Bottom end fitting	SS 304	12.4
Expansion springs	–	–
Total		291.7

Source: Reference 8.

* Distributed throughout the PWR core in sleeves.

Table 3-5

Assumed Elemental Compositions of LWR Fuel-Assembly Structural Materials

Element	Atomic Number	Structural Material Composition, Grams per Tonne of Metal				
		Zircaloy-4	Inconel-718	Stainless Steel 302	Stainless Steel 304	Nicrobraze 50
H	1	13	0	0	0	0
B	5	0.33	0	0	0	50
C	6	120	400	1,500	800	100
N	7	80	1,300	1,300	1,300	66
O	8	950	0	0	0	43
Al	13	24	5,992	0	0	100
Si	14	0	1,997	10,000	10,000	511
P	15	0	0	450	450	103,244
S	16	35	70	300	300	100
Ti	22	20	7,990	0	0	100
V	23	20	0	0	0	0
Cr	24	1,250	189,753	180,000	190,000	149,709
Mn*	25	20	1,997	20,000	20,000	100
Fe	26	2,250	179,766	697,740	688,440	471
Co*	27	10	4,694	800	800	381
Ni	28	20	519,625	89,200	89,200	744,438
Cu	29	20	999	0	0	0
Zr*	40	979,110	0	0	0	100
Nb	41	0	55,458	0	0	0
Mo	42	0	29,961	0	0	0
Cd	48	0.25	0.25	0	0	0
Sn	50	16,000	0	0	0	0
Hf	72	78	0	0	0	0
W	74	20	0	0	0	100
U	92	0.2	0	0	0	0
Density, grams/cm^3		6.56	8.19	8.02	8.02	—

Source: Reference 8.

* Value used in ORIGEN should be less than this (actual) value if the materials are not in the active fuel zone.

fission-product afterheat power (Reference 6). These methods are available in the computer program ANSIDECH (Reference 7). The purpose of this problem is to provide a semiempirical check of a code's ability to estimate decay heat generation rates. This problem is similar to benchmark problem 2.1, except that boiling water reactor fuel is simulated; the problem simulates the irradiation of a light water reactor fuel assembly and the decay heat generation during an extended cooling period.

Physical Specifications. Boiling water reactor fuel is irradiated at power levels ranging from about 15 MW/kg to about 30 MW/kg for periods of one to six years before being discharged. During irradiation, fission product concentrations increase; consequently, the fission-product decay heat production after fission has ceased can be significant.

Selected design parameters for a General Electric 8x8 fuel assembly are given in Tables 3-6 and 3-7. Analyses performed by CorSTAR indicate that, for similar operating conditions, this fuel assembly will be neutronically similar to other 8x8 and 7x7 fuel assemblies.

For benchmarking purposes, six subproblems are specified. The subproblems represent different combinations of fuel initial enrichment and operating conditions. Table 3-8 contains the problem-dependent input information for each of the six subproblems.

Assumptions. The initial nonactinide composition of the uranium oxide fuel pellets has already been given; see Table 3-3. For the elemental composition of the structural materials, see Table 3.5.

Problem Solution. This problem is to be solved using the method described for problem 2.1.

Output Specifications. The outputs for this problem are the decay heat generation rates in units of watts per initial metric ton of heavy metal at times

Table 3-6

Data for Calculations of BWR Fuel Decay Heat Generation

	Initial Uranium Composition (wt. %)		
	Subproblem 1	Subproblems 2,3	Subproblems 4,5,6
^{234}U	0.010	0.033	0.030
^{235}U	1.100	2.500	2.700
^{238}U	98.891	97.480	97.278

Percent theoretical density for UO_2*		95
Initial uranium loading (kg/assembly)		190
Fuel rods per assembly		63 with zircaloy-2 clad
Rod pitch (cm)		1.62560
Pellet O.D. (cm)		1.05664
Gap O.D. (cm)		1.07950
Clad O.D. (cm)		1.25222
Active fuel length (cm)		375.920
Fuel temperature (^oK)		900
Clad temperature (^oK)		605
Moderator temperature (^oK)		575
Moderator density (g cm^{-3} -	no voids)	0.743108
	20% voids	0.594486
	35% voids	0.483020
	50% voids	0.371554

Source: Reference 9.

* Theoretical UO_2 density is 10.96 g cm^{-3}.

Table 3-7

Assumed Mass Distribution of BWR Fuel-Assembly Structural Materials

	Material	Mass (kg/MTHM)
Fuel Zone		
Cladding	Zircaloy-2	279.5
Fuel channel*	Zircaloy-4	227.5
Grid spacers	Zircaloy-4	10.6
Grid-spacer springs	Inconel X-750	1.8
Fuel-gas Plenum Zone		
Cladding	Zircaloy-2	25.4
Fuel channel*	Zircaloy-4	20.7
Plenum spring	SS 302	6.0
End Fitting Zone		
Top end fitting	SS 304	10.9
Bottom end fitting	SS 304	26.1
Expansion springs	Inconel X-750	2.1
Total		610.6

Source: Reference 8.

* Assumed to be discharged with spent fuel.

Table 3-8

Fuel Irradiation Data

Operating Conditions	Subproblems 1	2	3	4	5	6
^{235}U enrichment	1.1%	2.5%	2.5%	2.7%	2.7%	2.7%
Irradiation History						
Time Period #1						
Duration (days)	370	370	370	1,080	150	150
Power level (MW/MTU)	30	30	20	25	27	31
Void percent	40	40	35	35	20	50
Shutdown period (days)	–	60	60	–	0	0
Time Period #2						
Duration (days)	–	260	260	–	150	150
Power level (MW/MTU)	–	27	30	–	31	27
Void percent	–	30	35	–	50	20
Shutdown period (days)	–	–	60	–	60	60
Time Period #3						
Duration (days)	–	–	300	–	150	150
Power level (MW/MTU)	–	–	30	–	29	33
Void percent	–	–	35	–	20	50
Shutdown period (days)	–	–	–	–	15	15
Time Period #4						
Duration (days)	–	–	–	–	150	150
Power level (MW/MTU)	–	–	–	–	33	29
Void percent	–	–	–	–	50	20
Shutdown period (days)	–	–	–	–	45	45
Time Period #5						
Duration (days)	–	–	–	–	150	150
Power level (MW/MTU)	–	–	–	–	28	32
Void percent	–	–	–	–	20	50
Shutdown period (days)	–	–	–	–	15	15
Time Period #6						
Duration (days)	–	–	–	–	150	150
Power level (MW/MTU)	–	–	–	–	32	28
Void percent	–	–	–	–	50	20
Shutdown period (days)	–	–	–	–	–	–

of 1, 3, 10, 30, 100, 1,000, 3,000, and 10,000 years following reactor shutdown. According to Reference 6, the ANS Standard is not applicable for cooling times greater than 10^9 seconds (31.7 years). However, Reference 7 reports excellent agreement between the ANS Standard predictions and ORIGEN/S calculations for cooling times of up to 110 years for PWR fuel.

3.1.2.3 Turkey Point Unit 3 Afterheat Power Study (Benchmark Problem 2.3)

Problem Statement. The afterheat power from a number of Turkey Point Unit 3 fuel assemblies has been measured by the Hanford Engineering Development Laboratory (Reference 10) during pretest characterization of assemblies for the Climax Spent Fuel Test. This benchmark problem is designed to predict the measured afterheat power values for three fuel assemblies. Results of a similar benchmark problem are described in Reference 7.

Physical Specifications. Turkey Point Unit 3 uses Westinghouse 15x15 fuel assemblies. Fuel-assembly design characteristics are given in Table 3-9. For the initial nonactinide composition of uranium fuel oxide pellets, the weights of fuel-assembly structural materials, and the elemental compositions of structural materials, see Tables 3-3, 3-4, and 3-5, respectively. Fuel-assembly operating conditions are summarized in Table 3-10. The concentrations of fuel-assembly structural material located in the end fitting zone should be multiplied by 0.011 to account for the lower activation levels near the ends of the fuel assembly due to flux levels lower than those present in the active fuel zone. In addition, the concentrations of manganese, cobalt, and zirconium in the end fitting zone should be multiplied by factors of 0.80, 0.67, and 0.40, respectively. These corrections account for the difference in the neutron energy spectrum from that in the active fuel zone. Both kinds of corrections are based on axial spectrum calculations for a Westinghouse PWR fuel assembly as reported in Reference 8. With these corrections, the ORIGEN/S calculations should predict more accurately the afterheat power and nuclide activities from structural materials.

Table 3-9

Data for Turkey Point Unit 3 Fuel Afterheat Calculations

Percent theoretical density for UO_2*		93.38
Initial uranium composition (wt. %)	^{234}U	0.031
	^{235}U	2.556
	^{236}U	0.01126
	^{238}U	97.41021
Initial uranium loading (kg/assembly)		456.9
Fuel rods per assembly		204 with zircaloy clad
Rod pitch (cm)		1.43002
Pellet O.D. (cm)		0.92964
Gap O.D. (cm)		0.948436
Clad O.D. (cm)		1.07188
Active fuel length (cm)		365.76
Fuel temperature (^{o}K)		922
Clad temperature (^{o}K)		595
Moderator temperature (^{o}K)		570
Moderator density (g cm^{-3})		0.731141
Average boron concentration (wt. ppm)		450

Source: Reference 7.

* Theoretical UO_2 density in SAS2 is 10.96 g cm^{-3}.

Table 3-10

Operating Histories for Turkey Point Unit 3
Afterheat Power Study

Time Period	Δ t (Days)*	Power (MW/MTU)**		
		D34	D15	D22
Cycle 1	310	28.462	29.041	27.054
Downtime	64	0.0	0.0	0.0
Cycle 2	321	31.827	32.475	30.253
Downtime	69	0.0	0.0	0.0
Cycle 3	305	28.929	29.518	27.498
Assembly				
Burnup (MWD/MTU)		27,863	28,430	26,485
Cooling time (days)		864	962	963

* Source: Reference 11.

** Best estimate based on operating experience at similar nuclear power plants.

Output Specifications. The outputs for this benchmark problem are the calculations of afterheat power in units of watts per assembly for each of the three fuel assemblies (D34, D15, and D22) at the cooling times at which the decay heat was measured in the Climax test. The afterheat power calculation should identify the contribution to afterheat power from activation products, actinides, and fission products. Calculated afterheat power values can be compared with the measured values given in Table 3-11.

3.1.2.4 Turkey Point Unit 3 Fuel Inventory Calculation (Benchmark Problem 2.4)

Problem Statement. Battelle Columbus Laboratories has performed five experimental measurements of spent-fuel inventory for three 3-cycle fuel rods from Turkey Point Unit 3 as a part of the pretest characterization of fuel assemblies for the Climax Spent Fuel Test (Reference 12). This problem presents information on the fuel operating conditions for these fuel rods and the measured isotopic data for plutonium and uranium. The purpose of the problem is to validate a fuel depletion code and cross-section libraries using measured parameters from an irradiated PWR fuel assembly. A similar problem for one fuel rod is discussed in Reference 7.

Physical Specifications. This problem includes the measured parameters for five fuel pin samples from the peak burnup region of the Turkey Point Unit 3 fuel assemblies DO1 and DO4. These fuel pins were irradiated from December 1974 to November 1977, to burnups of 30,510 to 31,560 MWD/MTU, and were cooled for 927 days before measurements were taken.

DO1 and DO4 are Westinghouse 15x15 fuel assemblies. Fuel initial composition, irradiation conditions, and mechanical design data are given in Table 3-12. For the initial nonactinide composition or uranium oxide fuel pellets, see Table 3-3; for the weight and composition of the fuel rod cladding, see Tables 3-4 and 3-5.

Output Specifications. The outputs of this problem are the quantities of each of the actinides produced, in grams per metric ton of initial uranium. These

Table 3-11

Measured Afterheat Power for Turkey Point Unit 3 Fuel Assemblies

Assembly	Cooling Time (Days)	Measured Total Power (Watts/Assembly)	Total Power (Watts/MTU)
D34	864	1,550	3,392
D15	962	1,423	3,114
D15	1,143	1,125	2,462
D22	963	1,284	2,810

Source: Reference 7.

Table 3-12

Data for Turkey Point Unit 3 Fuel
Inventory Calculations

Percent theoretical density for UO_2*		93.38
Initial uranium composition (wt. %)	^{234}U	0.031
	^{235}U	2.556
	^{236}U	0.01126
	^{238}U	97.4017
Initial uranium loading (kg/assembly)		456.9
Fuel rods per assembly		204 with zircaloy clad
Rod pitch (cm)		1.43002
Pellet O.D. (cm)		0.92964
Gap O.D. (cm)		0.948436
Clad O.D. (cm)		1.07188
Active fuel length (cm)		365.76
Fuel temperature (^{o}K)		922
Clad temperature (^{o}K)		595
Moderator temperature (^{o}K)		570
Moderator density (g cm^{-3})		0.731141
Average boron concentration (wt. ppm)		450
Nominal exposure (MWD/MTU)		30,720
Irradiation history: Δ t(days)**		
	Cycle 1	310
	Downtime	64
	Cycle 2	321
	Cooling time	69
	Cycle 3	305
	Cooling time	927

Source: Reference 7.

* Theoretical UO_2 density in SAS2 is 10.96 g cm^{-3}.

** From Reference 11.

concentrations should be corrected for a decay time of 927 days. Table 3-13 gives the measured concentrations of uranium and plutonium isotopes from the Turkey Point Unit 3 fuel.

The design and operating conditions of these Turkey Point fuel assemblies are similar to those of the H.B. Robinson 2 fuel assembly described in benchmark problem 2.5. Concentrations of fission products and transplutonics also should be calculated for a decay time of 669 days, for comparison with the measured data given in that problem.

3.1.2.5 H.B. Robinson Unit 2 Fuel Inventory (Benchmark Problem 2.5)

Problem Statement. As part of an experimental program centered around hot-cell tests of fuel processing operations (References 13 through 18), a portion of a fuel assembly from H.B. Robinson Unit 2 was analyzed. The analyses of this fuel included measurements of actinide and fission product inventories. This benchmark problem is designed to provide code and cross-section validation for fuel designs and operating conditions similar to those of H.B. Robinson Unit 2.

Physical Specifications. Fuel assembly B05 was irradiated in the H.B. Robinson Unit 2 reactor to an average burnup of 28,026 MWD/MTU. A portion of the fuel from the maximum burnup region (31,364 MWD/MTU) of this fuel assembly was analyzed at the Oak Ridge National Laboratory after 669 days of cooling time. Measured values of actinide and fission product activities are presented in Table 3-14. Actinide activities were determined by alpha counting, and fission product activities were derived from gamma- and beta-ray counting.

B05 is a Westinghouse 15x15 PWR fuel assembly. Fuel assembly design and operating characteristics are given in Table 3-14. For the initial nonactinide composition of uranium oxide fuel pellets and for the weight and elemental composition of the structural materials, see Table 3-4 and Table 3-5, respectively.

Table 3-13

Measured Isotopic Data for Turkey Point Unit 3
after 927 Days of Cooling Time

	D01-G9-15 65.75-66.25		D01-G10-4 65.5-66.0		D01-H9-7 66.5-66.0		D04-G9-9 65.75-66.25		D04-G10-7 65.5-66.0	
	g/kgU_i	Ci/kgU_i	g/kgU_i	Ci/kgU_i	g/kgU_i	Ci/kgU_i	g/kgU_i	Ci/kgU_i	g/kgU_i	Ci/kgU_i
^{234}U	.1321	8.26 E-1	.1321	8.26 E-1	.1225	7.66 E-1	.1132	7.07 E-1	.1321	8.26 E-1
^{235}U	5.8655	1.27 E-5	5.6773	1.23 E-2	5.5852	1.21 E-2	5.5114	1.19 E-2	5.6626	1.22 E-2
^{236}U	3.2545	2.11 E-1	3.2553	2.11 E-1	3.1753	2.05 E-1	3.1573	2.04 E-1	3.2523	2.10 E-2
^{238}U	950.3207	3.20 E-1	950.7448	3.20 E-1	949.7477	3.19 E-1	950.1843	3.20 E-1	949.8633	3.19 E-1
^{238}Pu	.1365	2.34 E+3	.1360	2.33 E+3	.1426	2.44 E+3	.1383	2.37 E+3	.1372	2.35 E+3
^{239}Pu	4.8382	3.01 E+2	4.8410	3.01 E+2	4.9291	3.06 E+2	4.9438	3.07 E+2	4.7891	2.98 E+2
^{240}Pu	2.2659	5.16 E+2	2.2946	5.23 E+2	2.2950	5.23 E+2	2.3211	5.29 E+2	2.2780	5.19 E+2
^{241}Pu	1.0610	1.09 E+5	1.0687	1.10 E+5	1.1043	1.14 E+5	1.1245	1.16 E+5	1.0719	1.10 E+5
^{242}Pu	.5020	1.92 E+0	.5249	2.00 E+0	.5477	2.09 E+0	.5430	2.07 E+0	.5235	2.00 E+0
Burnup (MWD/MTU)*	30,270		30,510		31,560		31,260		31,310	
Uf/U_i**	.959573		.959810		.958631		.958966		.958910	

Nominal Irradiation History — Power Levels in MW/MTU

Cycle 1	32.000
Cycle 2	35.000
Cycle 3	32.279

Source: Reference 12.

* Burnup measurements are accurate to ~ ± 1,000 MWD/MTU. The physics-calculated burnup value was 30,280 for approximately the same location.

** Discharge uranium metal weight divided by initial uranium metal weight; based on a proprietary CorSTAR correlation, accurate to ± .0001.

Table 3-14

Data for H.B. Robinson Unit 2 Fuel Inventory Calculations

Percent theoretical density for UO_2*		90.73
Initial uranium composition (wt. %)	^{234}U	0.031
	^{235}U	2.561
	^{236}U	0.013
	^{238}U	97.403
Initial uranium loading (kg/assembly)		443.7
Fuel rods per assembly		204 with zircaloy clad
Rod pitch (cm)		1.43002
Pellet O.D. (cm)		0.929386
Gap O.D. (cm)		0.948436
Clad O.D. (cm)		1.07188
Active fuel length (cm)		365.76
Fuel temperature (^oK)		922
Clad temperature (^oK)		595
Moderator temperature (^oK)		573
Moderator density (g cm^{-3})		0.72701
Average boron concentration (wt. ppm)		450
Burnup (MWD/MTU)		31,364

Irradiation history:**

	Δt(days)	Power (MW/MT)
Cycle 1	540	38.574
Downtime	62	0.0
Cycle 2	357	29.507
Cooling time	669	

Source: Reference 7.

* Theoretical UO_2 density in SAS2 is 10.96 g cm^{-3}.

** Corrected to agree with Reference 11.

Output Specifications. The outputs from this problem are the radionuclide activities in curies per metric ton of uranium and the radionuclide mass in kilograms per metric ton of initial uranium after 669 days of cooling time. These outputs should be compared with the values shown in Table 3-15.

3.1.3 Benchmarking Results and Conclusions

3.1.3.1 Problem 2.1

Each of the subproblems for benchmark problem 2.1 was run using the code ORIGEN/S with a previously generated nuclear cross-section library and using the codes NITAWL/S, XSDRNPM/S, and COUPLE to generate cross-sections for ORIGEN/S. No significant numerical problems were encountered using either cross-section library. The code functioned as intended and provided adequate error messages when input mistakes were made.

Table 3-16 summarizes the results for each of the benchmark subproblems. Decay heat predictions as a function of time are presented graphically in Figures 3-1 through 3-5.

For the time period of interest in this problem set, there was very good agreement between the decay heat predictions made using the existing cross-section library and those made using the generated cross-section library. For time periods of interest to waste management – that is, for periods of about 10 to 1,000 years following discharge from a reactor – the use of different cross-section sets resulted in less than a 2 percent difference in predicted decay heat. The differences between predictions were greater for shorter time periods following discharge and for the less enriched (less than 3 percent enriched) fuel that is more typical of first core loadings. One would expect to encounter these differences, since the existing cross-section library was developed for fuel of 3.2 percent enrichment.

For each of the five subproblems, Figure 3-6 permits a comparison of the two types of ORIGEN/S decay heat predictions, showing the percentage differences

Table 3-15

Isotopic Parameters for H. B. Robinson 2
Fuel after 669 Days of Cooling Time

Nuclide	Concentration (kg/MTU, Initial)*	Activity (Ci/MTU, Initial)**
^{234}U	1.323E-1	8.273E-1
^{235}U	6.201E+0	1.340E-2
^{236}U	3.309E+0	2.141E-1
^{238}U	9.519E+2	3.202E-1
^{238}Pu	1.407E-1	2.410E+3
^{239}Pu	5.054E+0	3.143E+2
^{240}Pu	2.226E+0	5.165E+2
^{241}Pu	1.123E+0	1.157E+5
^{242}Pu	5.000E-1	1.909E+0
^{241}Am	9.993E-2	3.410E+2
^{242m}Am	4.987E-3	4.848E+0
^{243}Am	5.985E-2	1.194E+1
^{242}Cm	8.404E-4	2.779E+3
^{243}Cm	3.113E-4	1.607E+1
^{244}Cm	2.342E-2	1.895E+3
^{245}Cm	1.149E-3	1.974E-1
^{246}Cm	1.180E-4	3.630E-2
^{247}Cm	1.046E-6	9.708E-7
^{248}Cm	2.626E-7	1.117E-8
^{106}Ru**	3.957E-2	1.269E+5
^{134}Cs**	5.232E-2	6.843E+4
^{137}Cs**	1.016E+0	8.861E+4
^{144}Ce**	5.655E-2	1.820E+5
^{129}I**	1.290E-1	2.257E-2
^{3}H***	2.814E-5	2.746E+2

* Derived from data in Reference 7 assuming that final uranium weight/initial uranium weight = .961570 (based on a correlation developed by Teknekron).

** Measured value believed to be too low by 15 percent to 25 percent (depending on gamma energy) due to problems with GeLi detector.

*** Approximately 41 percent to 46 percent of ^{3}H is probably trapped in the fuel clad and is not included in this measurement.

Table 3-16

Decay Thermal Power Prediction, in Watts

Problem Number	Time (Years)	ORIGEN Predictions: Existing Cross-Sections	ORIGEN Predictions: Generated Cross-Sections	Percent Difference
2.1.1	1	6810	6550	3.969
	3	1760	1690	4.142
	10	407	405	0.494
	30	228	228	0.000
	100	43.6	43.7	-0.229
	300	0.427	0.426	0.235
	1000	0.00831	0.00812	2.340
	3000	0.00809	0.008	1.125
	10000	0.0078	0.00771	1.167
2.1.2	1	8830	8600	2.674
	3	2610	2560	1.953
	10	717	711	0.844
	30	396	396	0.000
	100	75.4	75.4	0.000
	300	0.733	0.733	0.000
	1000	0.0134	0.0134	0.000
	3000	0.0132	0.0132	0.000
	10000	0.0127	0.0127	0.000
2.1.3	1	10600	10500	0.952
	3	3330	3350	-0.597
	10	990	983	0.712
	30	544	533	2.064
	100	103	101	1.980
	300	0.999	0.978	2.147
	1000	0.0174	0.0178	-2.247
	3000	0.0172	0.0175	-1.714
	10000	0.0166	0.0169	-1.775
2.1.4	1	9400	9260	1.512
	3	3070	3070	0.000
	10	944	937	0.747
	30	519	509	1.965
	100	98.7	96.7	2.068
	300	0.955	0.936	2.030
	1000	0.0172	0.0174	-1.149
	3000	0.0169	0.0166	1.807
	10000	0.0163	0.0163	0.000
2.1.5	1	9650	9550	1.047
	3	3100	3110	-0.322
	10	936	931	0.537
	30	514	506	1.581
	100	97.8	96.1	1.769
	300	0.946	0.93	1.720
	1000	0.0169	0.0172	-1.744
	3000	0.0167	0.017	-1.765
	10000	0.0161	0.0164	-1.829

Figure 3-1

ORIGEN-Predicted Decay Heat Generation Rate vs. Time
for Benchmark Problem 2.1.1

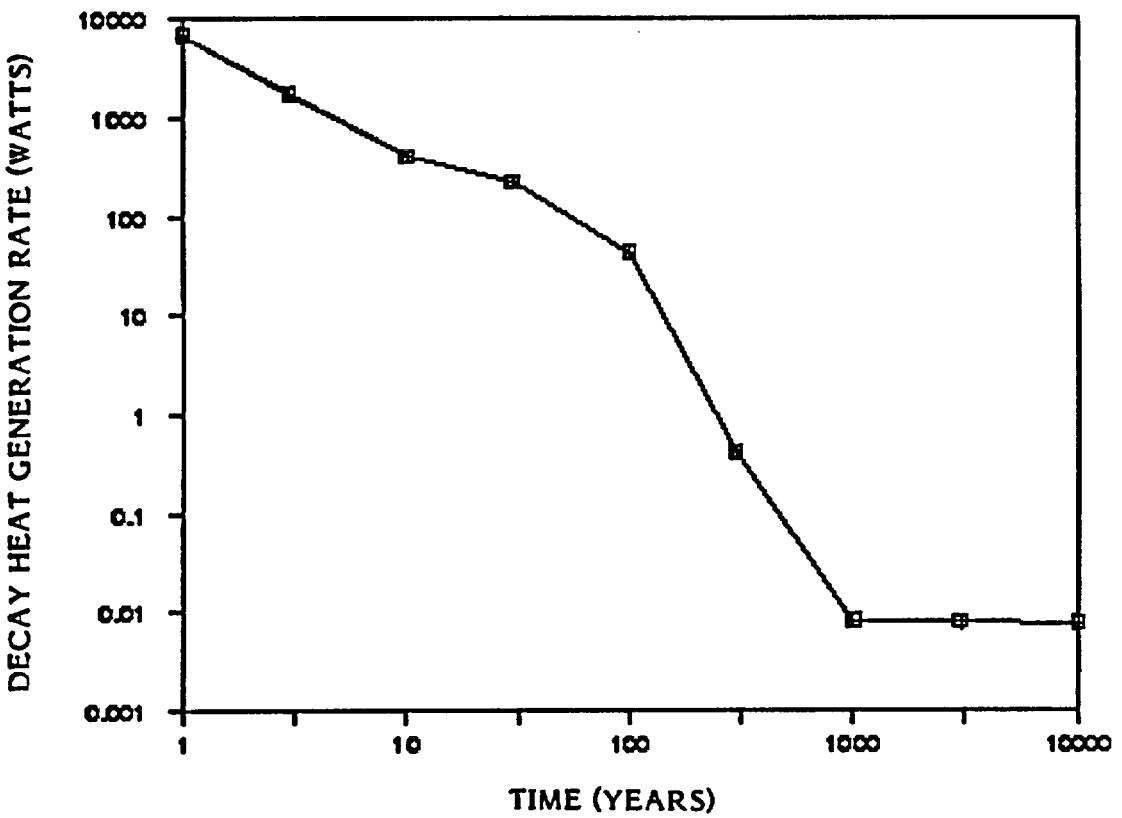

□ ORIGEN-predicted value using existing cross-sections

\+ ORIGEN-predicted value using generated cross-sections

Figure 3-2

ORIGEN-Predicted Decay Heat Generation Rate vs. Time
for Benchmark Problem 2.1.2

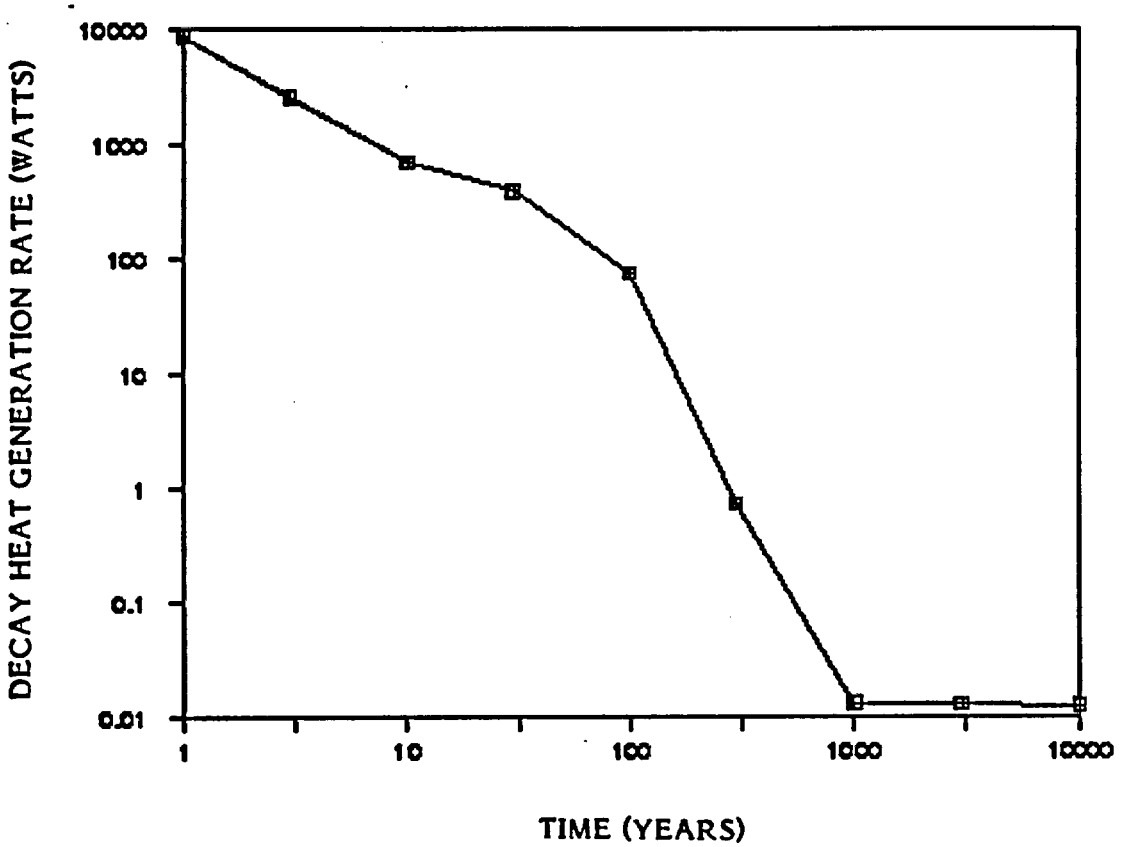

□ ORIGEN-predicted value using existing cross-sections

\+ ORIGEN-predicted value using generated cross-sections

Figure 3-3

ORIGEN-Predicted Decay Heat Generation Rate vs. Time
for Benchmark Problem 2.1.3

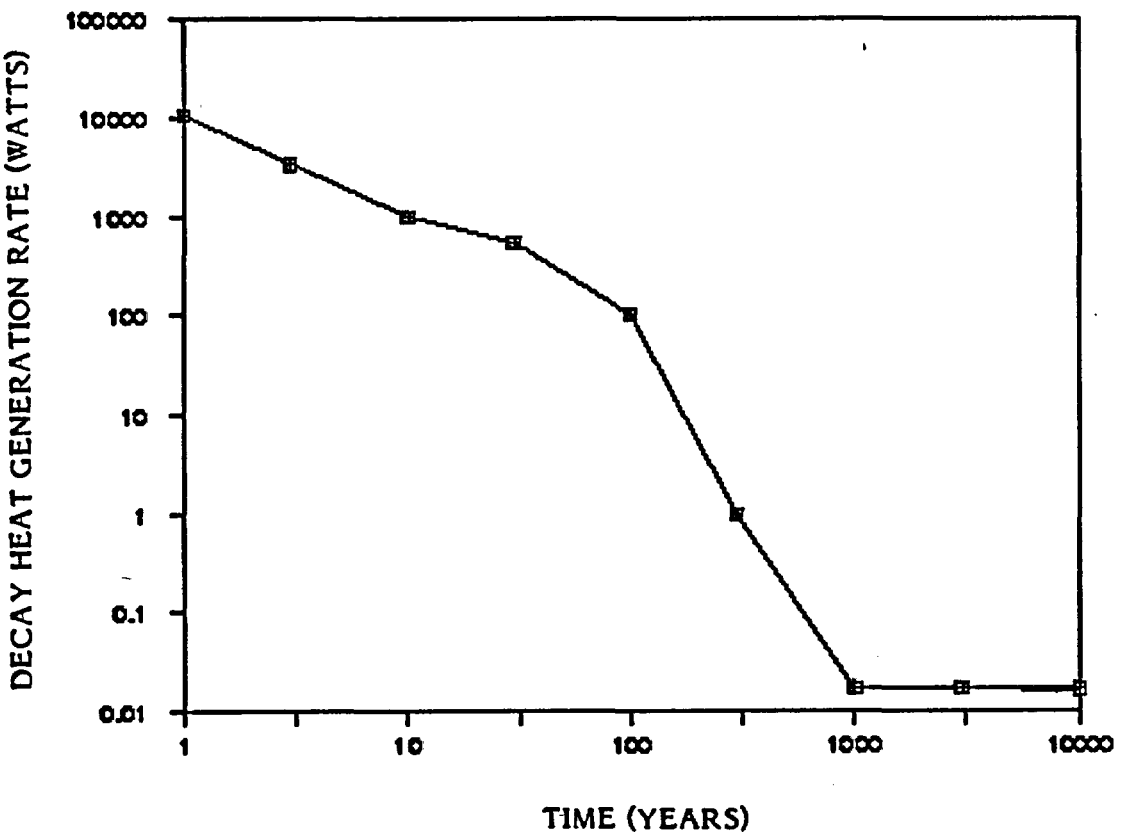

□ ORIGEN-predicted value using existing cross-sections

\+ ORIGEN-predicted value using generated cross-sections

Figure 3-4

ORIGEN-Predicted Decay Heat Generation Rate vs. Time
for Benchmark Problem 2.1.4

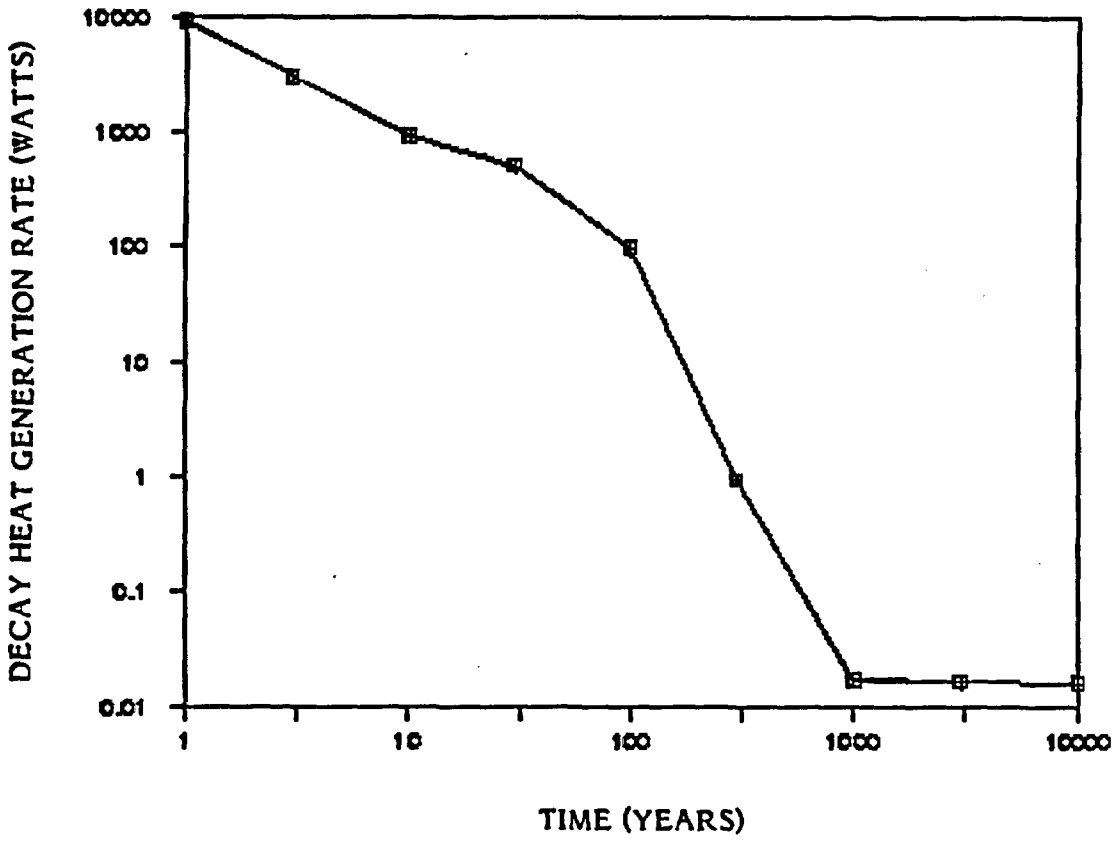

□ ORIGEN-predicted value using existing cross-sections

\+ ORIGEN-predicted value using generated cross-sections

Figure 3-5

ORIGEN-Predicted Decay Heat Generation Rate vs. Time
for Benchmark Problem 2.1.5

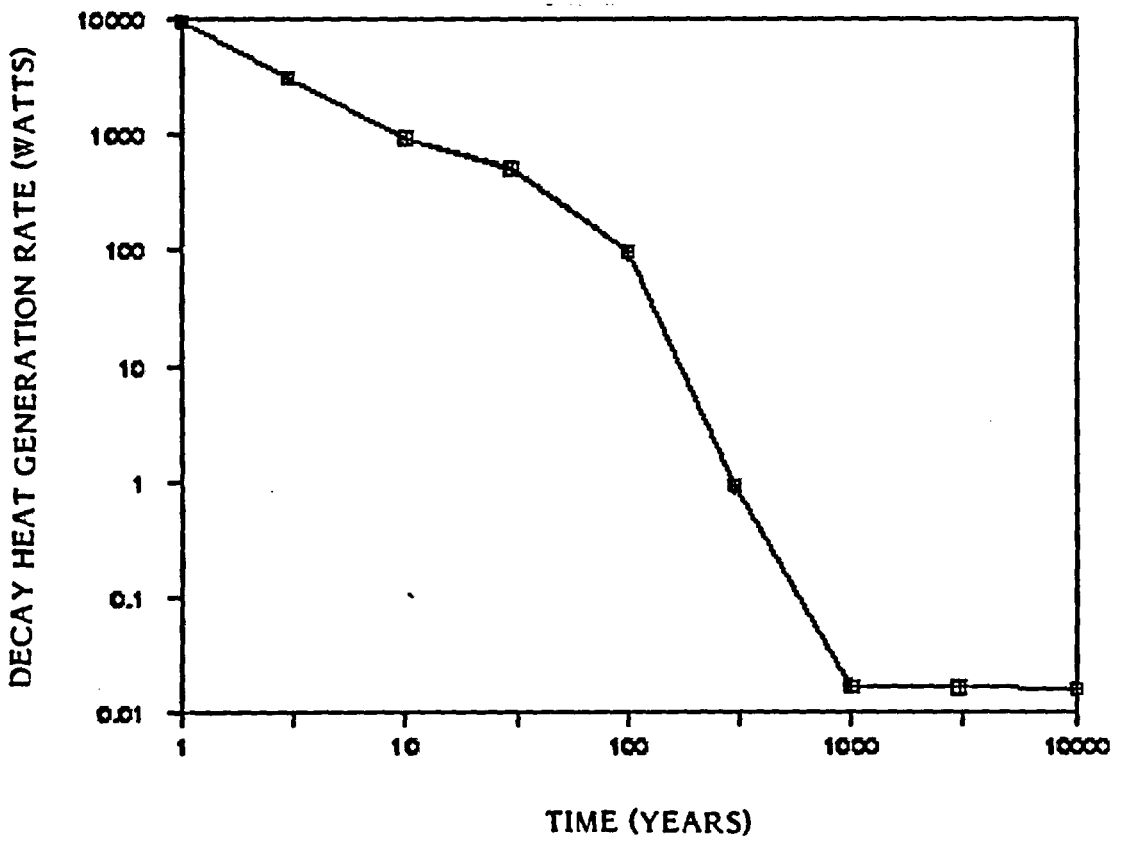

□ ORIGEN-predicted value using existing cross-sections

\+ ORIGEN-predicted value using generated cross-sections

Figure 3-6

Comparison of ORIGEN-Predicted Decay Heat Generation Rates Based on Existing vs. Newly Generated Cross-Sections for Benchmark Problems 2.1.1 through 2.1.5

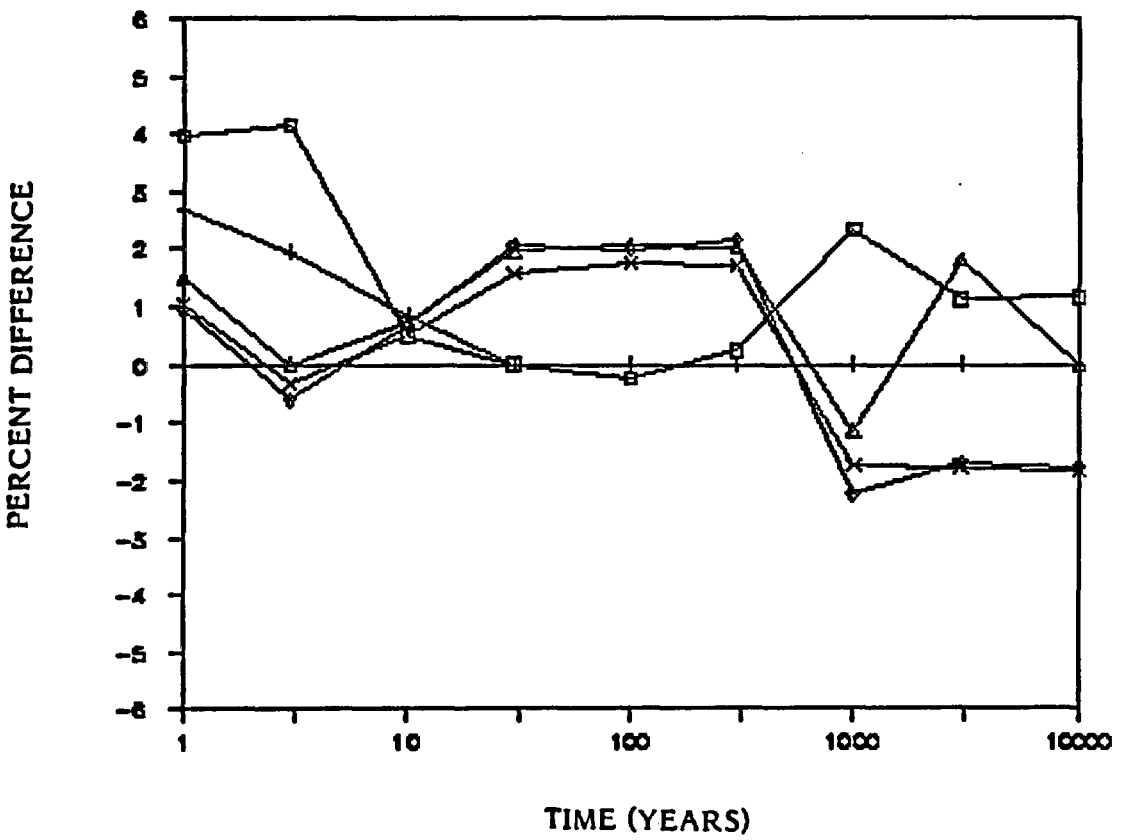

□ Problem 2.1.1
+ Problem 2.1.2
◇ Problem 2.1.3
△ Problem 2.1.4
× Problem 2.1.5

between the predictions using the existing cross-section library and those using the updated library.

3.1.3.2 Problem 2.2

Examination of the results from benchmark problem 2.2, the BWR problem, indicates that the existing ORIGEN cross-section library is adequate for analysis of decay heat generation for the time periods of interest to waste management. For these periods – about 10 to 1,000 years following discharge from the reactor – the differences between the decay heat predictions associated with generated cross-sections and those associated with the existing cross-section library were insignificant, amounting to less than 2 percent. For shorter time periods and fuel of lower enrichment, however, the differences for the different libraries were as great as 5 percent.

Table 3-17 summarizes the ORIGEN/S results for problem 2.2 Figures 3-7 through 3-12 provide a graphical display of decay heat generation as a function of time for each subproblem. Figure 3-13 provides a summary of the calculated differences in decay heat using the existing cross-section library versus an updated cross-section library.

3.1.3.3 Problem 2.3

Results from this problem are summarized in Table 3-18. The ORIGEN/S decay heat predictions using the existing versus updated cross-section libraries generally agreed within 2 percent of each other, with the latter – the cross-section set generated to be more representative of actual fuel operating conditions – providing more accurate predictions. All predictions of decay heat by ORIGEN/S were conservative. Predictions made using the updated cross-sections generated for analysis of this problem ranged from 7 to 11 percent over measured decay heat generation rates, whereas those made using the existing ORIGEN cross-section library ranged from 8 to 15 percent over the measured values. It is possible that this difference is due to measurement bias existing when the

Figure 3-7

ORIGEN-Predicted Decay Heat Generation Rate vs. Time
for Benchmark Problem 2.2.1

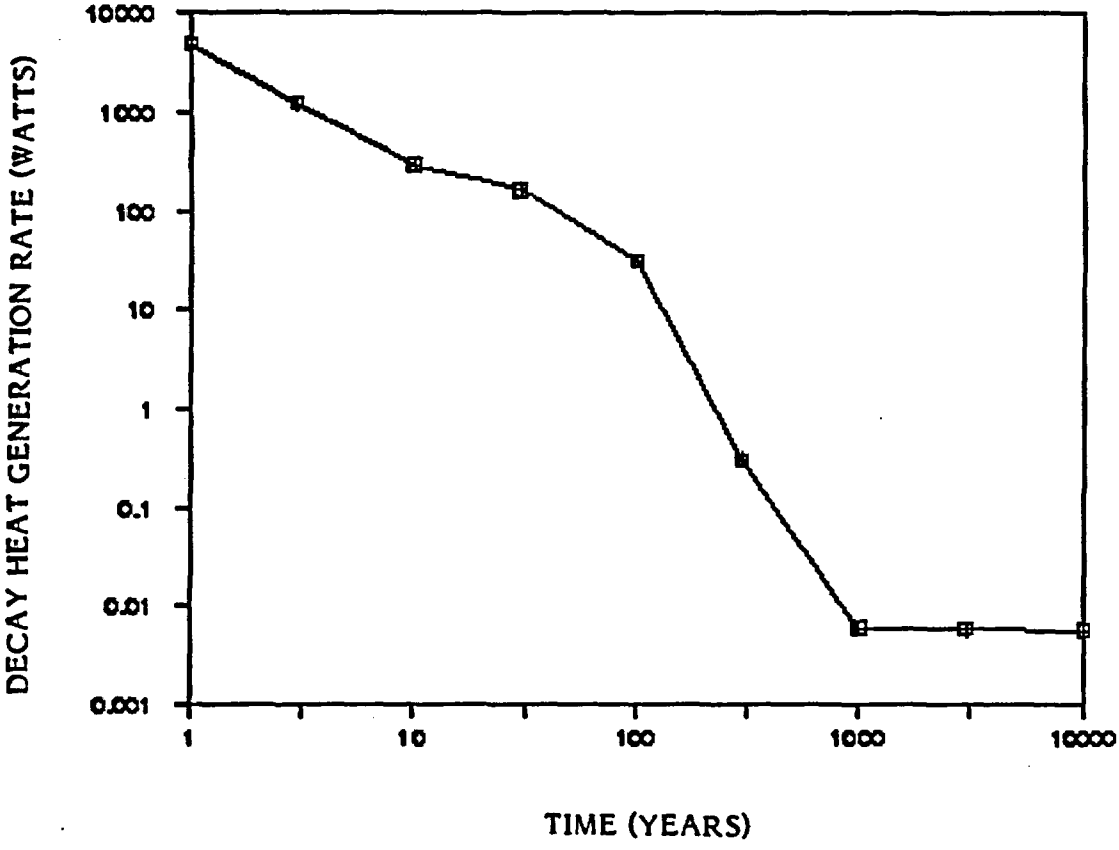

□ ORIGEN-predicted value using existing cross-sections

\+ ORIGEN-predicted value using generated cross-sections

Figure 3-8

ORIGEN-Predicted Decay Heat Generation Rate vs. Time
for Benchmark Problem 2.2.2

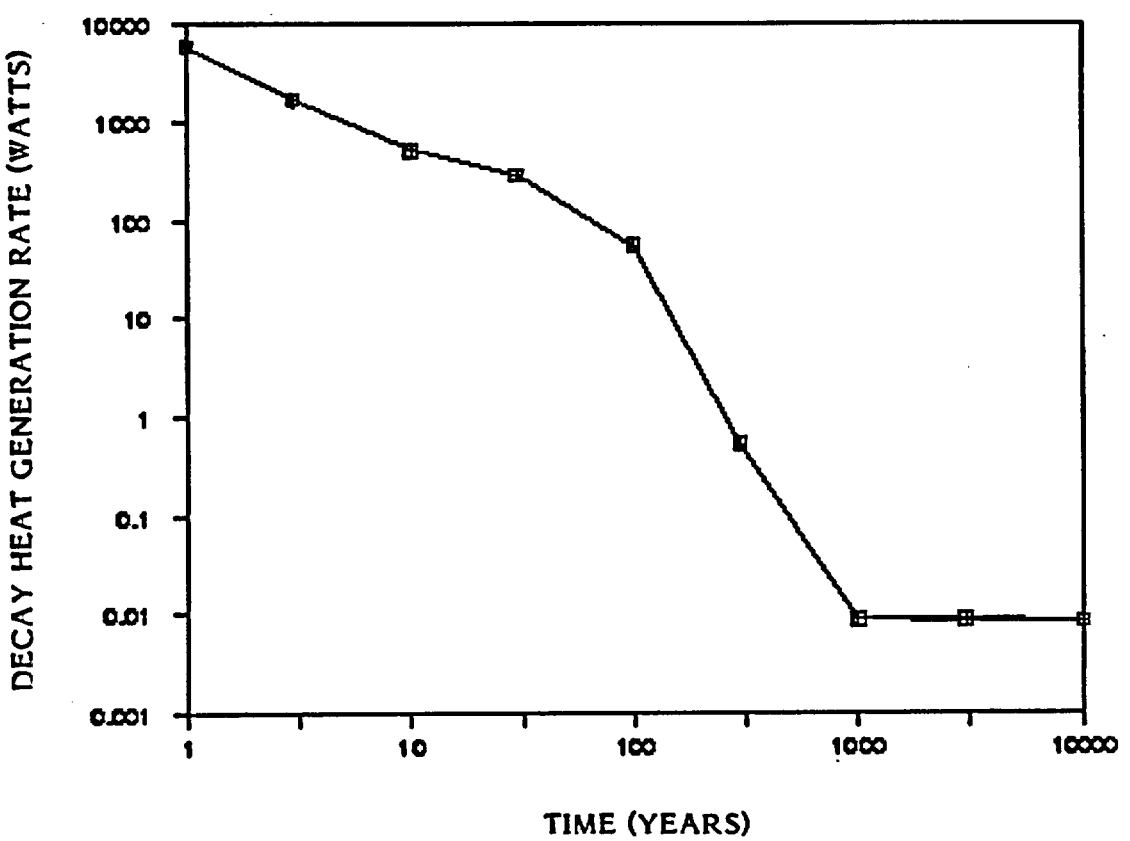

□ ORIGEN-predicted value using existing cross-sections

\+ ORIGEN-predicted value using generated cross-sections

Figure 3-9

ORIGEN-Predicted Decay Heat Generation Rate vs. Time
for Benchmark Problem 2.2.3

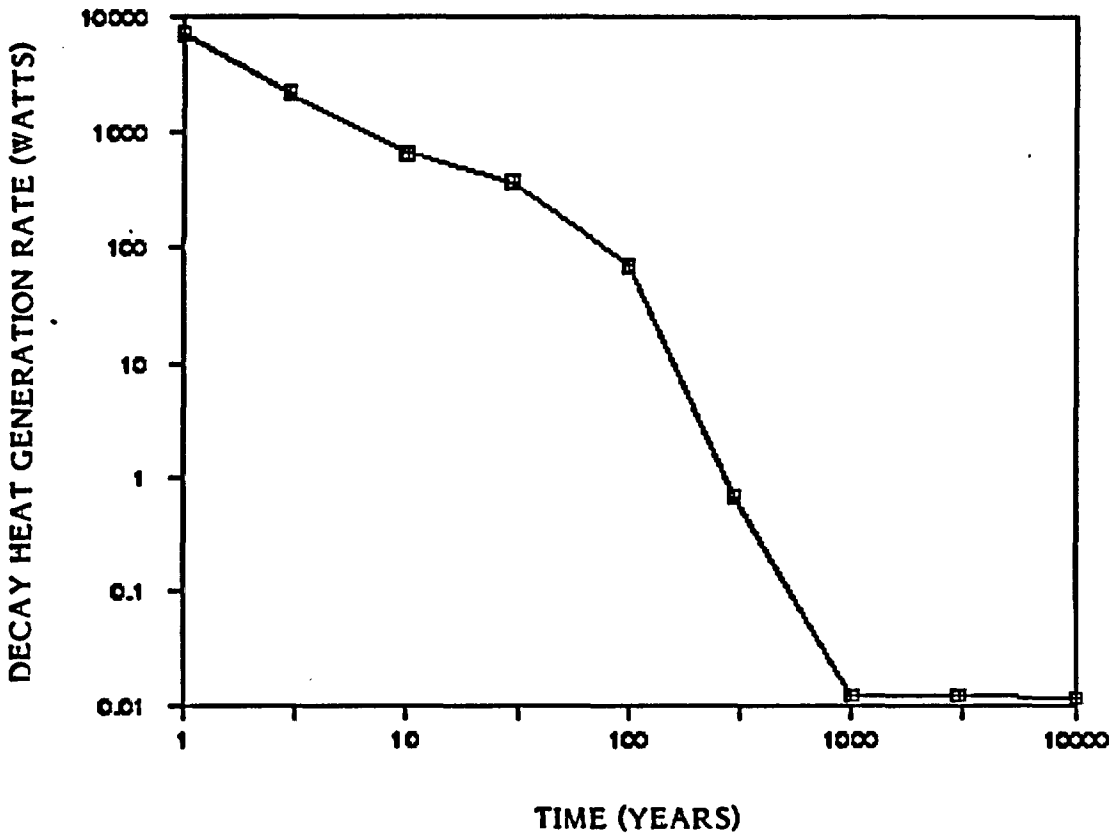

□ ORIGEN-predicted value using existing cross-sections

+ ORIGEN-predicted value using generated cross-sections

Figure 3-10

ORIGEN-Predicted Decay Heat Generation Rate vs. Time
for Benchmark Problem 2.2.4

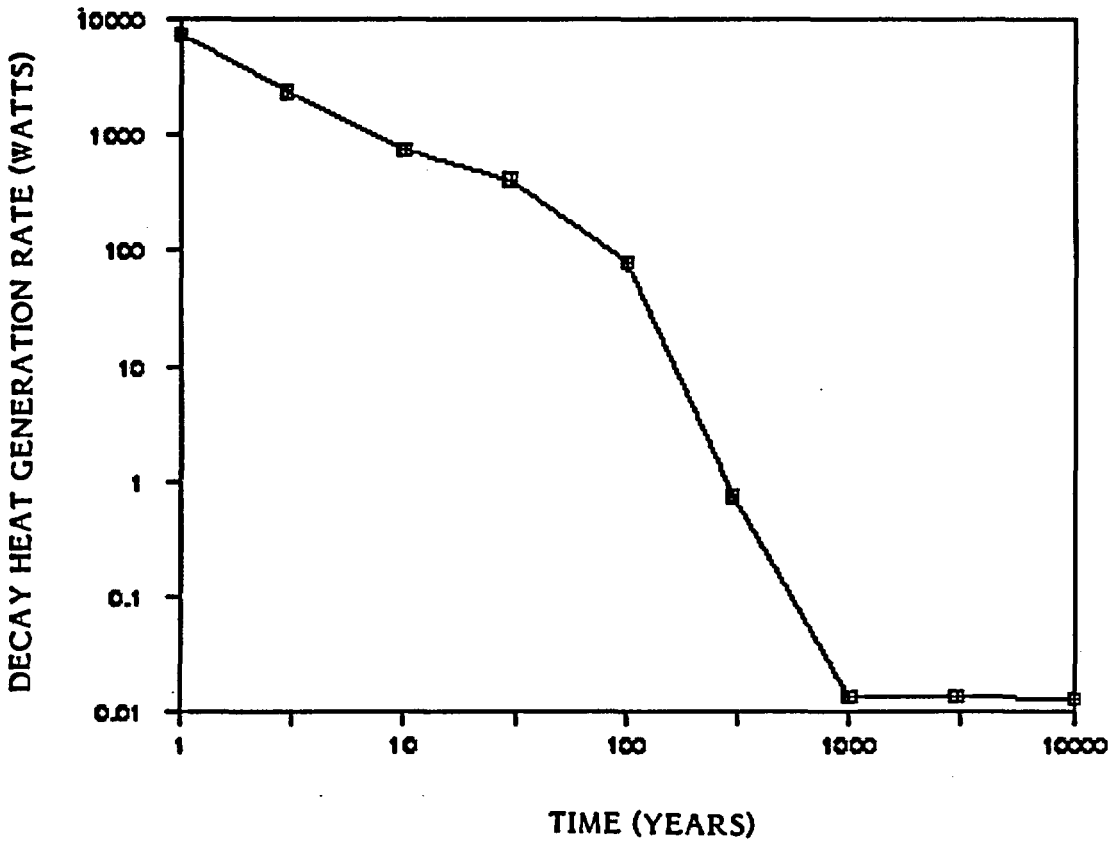

□ ORIGEN-predicted value using existing cross-sections

\+ ORIGEN-predicted value using generated cross-sections

Figure 3-11

ORIGEN-Predicted Decay Heat Generation Rate vs. Time
for Benchmark Problem 2.2.5

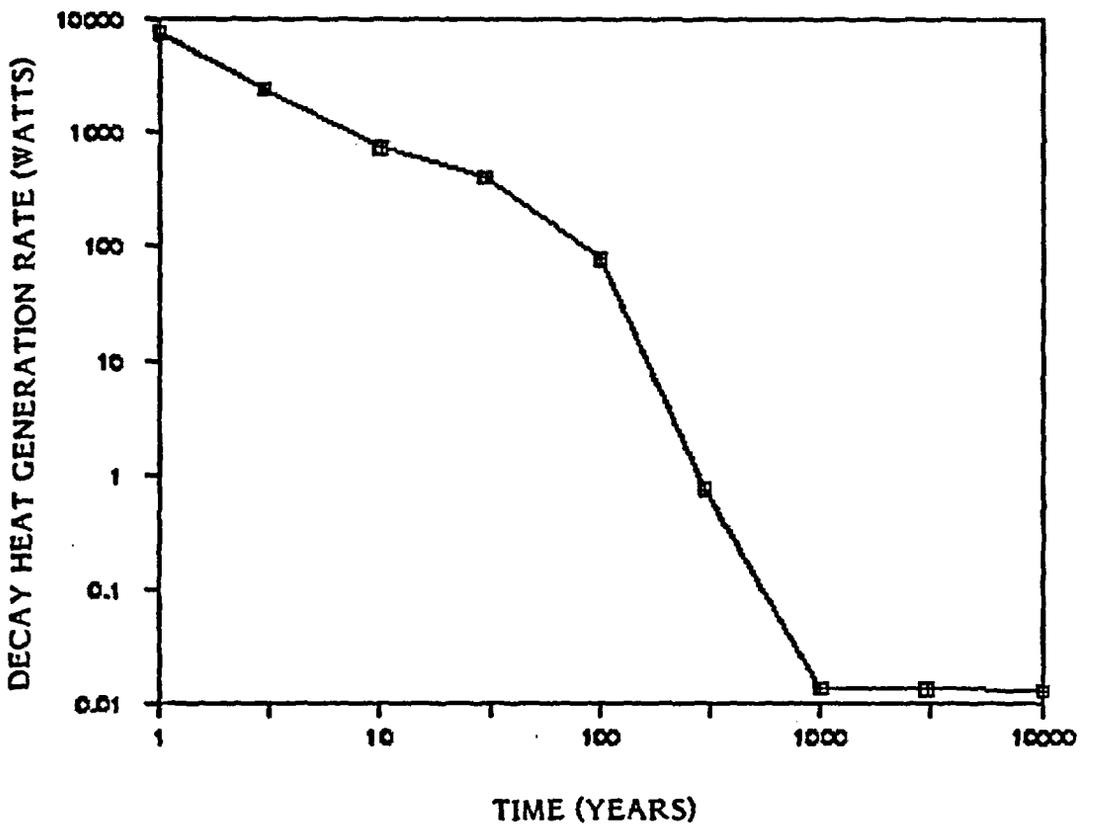

□ ORIGEN-predicted value using existing cross-sections

+ ORIGEN-predicted value using generated cross-sections

Figure 3-12

ORIGEN-Predicted Decay Heat Generation Rate vs. Time
for Benchmark Problem 2.2.6

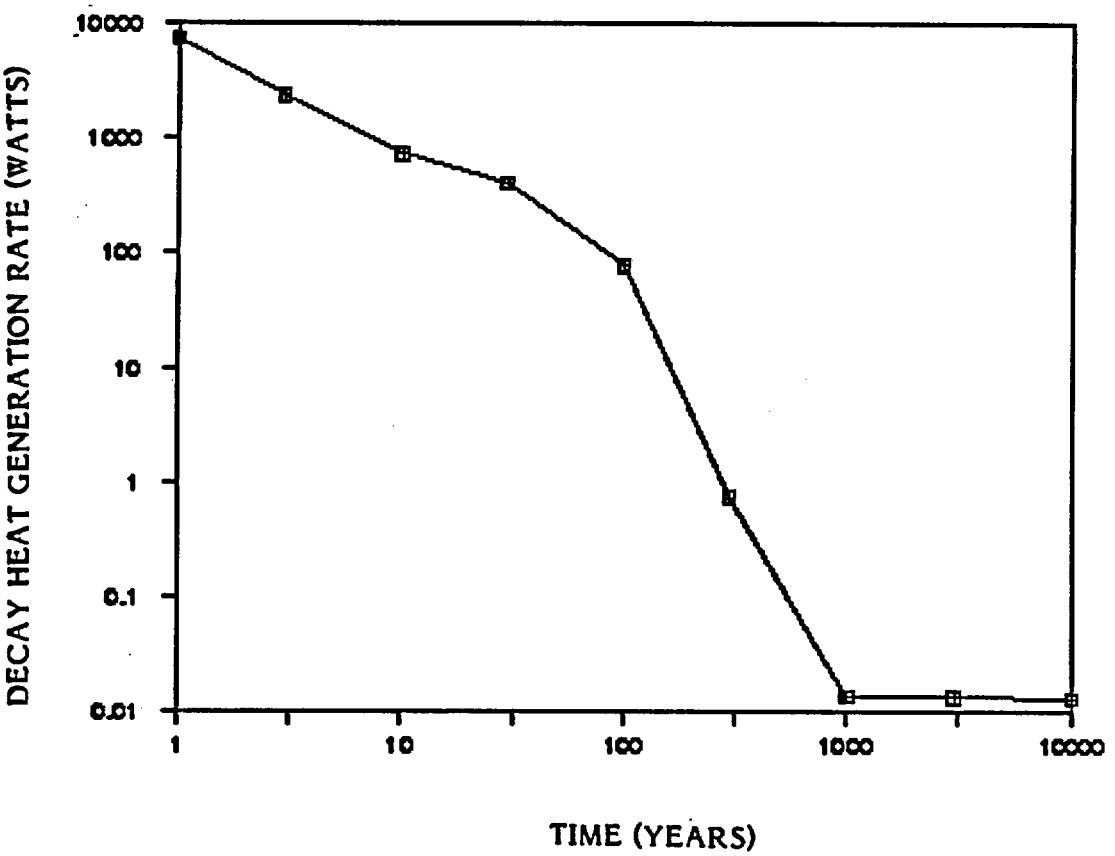

□ ORIGEN-predicted value using existing cross-sections

\+ ORIGEN-predicted value using generated cross-sections

Figure 3-13

Comparison of ORIGEN-Predicted Decay Heat Generation Rates Based on Existing vs. Newly Generated Cross-Sections for Problems 2.2.1 through 2.2.6

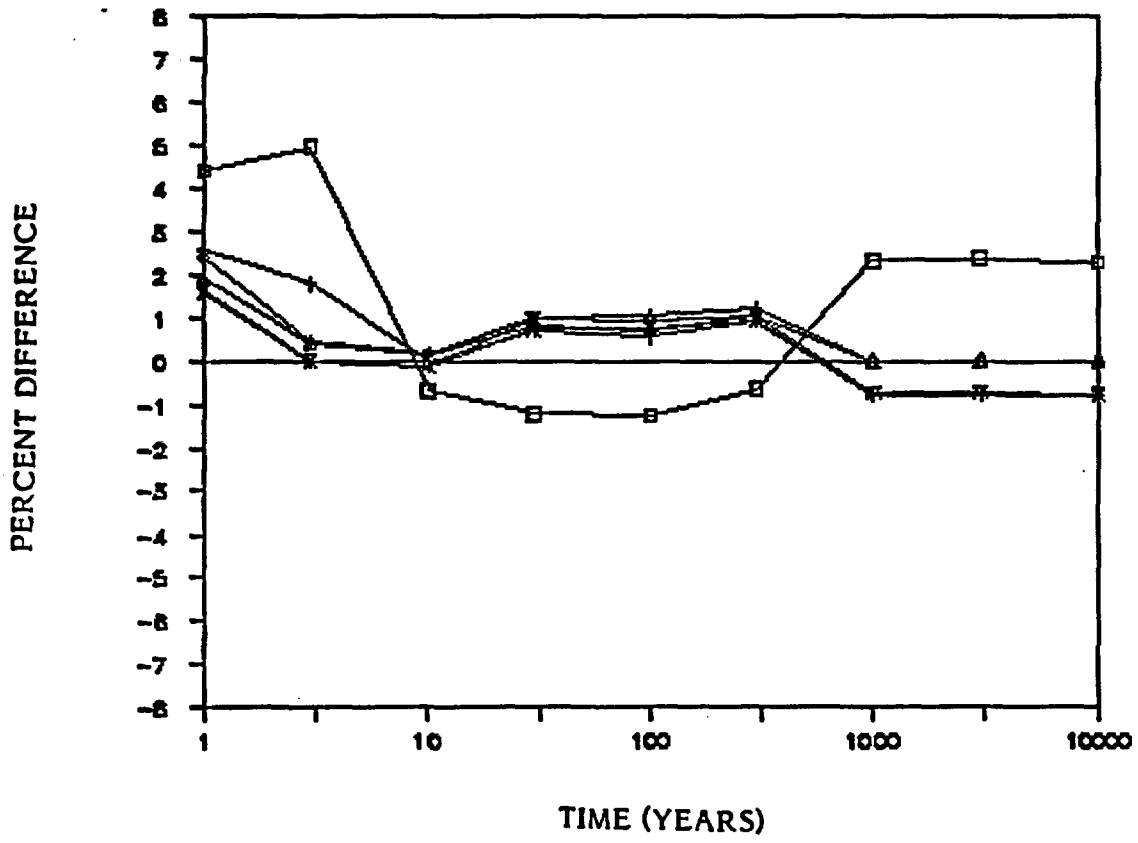

- □ Problem 2.2.1
- \+ Problem 2.2.2
- ◇ Problem 2.2.3
- △ Problem 2.2.4
- × Problem 2.2.5
- ▽ Problem 2.2.6

Table 3-17

Decay Thermal Power Prediction, in Watts

Problem Number	Time (Years)	ORIGEN Predictions: Existing Cross-Sections	ORIGEN Predictions: Generated Cross-Sections	Percent Difference
2.2.1	1	4970	4760	4.412
	3	1270	1210	4.959
	10	289	291	-0.687
	30	163	165	-1.212
	100	31.3	31.7	-1.262
	300	0.308	0.31	-0.645
	1000	0.00615	0.00601	2.329
	3000	0.00606	0.00592	2.365
	10000	0.00584	0.00571	2.277
2.2.2	1	5910	5760	2.604
	3	1700	1670	1.796
	10	502	502	0.000
	30	286	284	0.704
	100	54.8	54.5	0.550
	300	0.531	0.526	0.951
	1000	0.00899	0.00906	-0.773
	3000	0.00886	0.00893	-0.784
	10000	0.00855	0.00862	-0.812
2.2.3	1	7290	7120	2.388
	3	2230	2220	0.450
	10	665	664	0.151
	30	371	368	0.815
	100	70.7	70.2	0.712
	300	0.686	0.679	1.031
	1000	0.0125	0.0125	0.000
	3000	0.0123	0.0123	0.000
	10000	0.0119	0.0119	0.000
2.2.4	1	7390	7250	1.931
	3	2380	2370	0.422
	10	743	742	0.135
	30	413	409	0.978
	100	78.7	77.9	1.027
	300	0.763	0.754	1.194
	1000	0.0139	0.0139	0.000
	3000	0.0137	0.0137	0.000
	10000	0.0132	0.0132	0.000
2.2.5	1	7650	7530	1.594
	3	2410	2410	0.000
	10	737	738	-0.136
	30	410	407	0.737
	100	78.1	77.5	0.774
	300	0.757	0.75	0.933
	1000	0.0137	0.0138	-0.725
	3000	0.0135	0.0136	-0.735
	10000	0.013	0.0131	-0.763
2.2.6	1	7470	7350	1.633
	3	2380	2380	0.000
	10	736	737	-0.136
	30	410	406	0.985
	100	78.1	77.4	0.904
	300	0.757	0.749	1.068
	1000	0.0137	0.0138	-0.725
	3000	0.0135	0.0136	-0.735
	10000	0.013	0.0131	-0.763

Table 3-18

Decay Thermal Power Prediction, in Watts

Problem Number	Time (Days)		ORIGEN Predictions: Existing Cross-Sections	ORIGEN Predictions: Generated Cross-Sections
2.3.1	864	Fission Products	3380	3320
		Structural Material	118	127
		Actinides	205	226
		Total	3703	3673
2.3.2	962	Fission Products	3040	3000
		Structural Material	116	125
		Actinides	206	222
		Total	3362	3347
	1143	Fission Products	2450	2410
		Structural Material	107	116
		Actinides	191	207
		Total	2748	2733
2.3.3	963	Fission Products	2780	2740
		Structural Material	108	115
		Actinides	171	187
		Total	3059	3042

original decay heat measurements were taken or to a consistent overestimation of decay heat when the libraries associated with the code ORIGEN are used.

Measured values of decay heat are compared with ORIGEN/S predictions in Figure 3-14.

3.1.3.4 Problems 2.4 and 2.5

The results from benchmark problems 2.4 and 2.5 are summarized in Table 3-19 and in Figures 3-15 through 3-39. In general, the ORIGEN/S results associated with both the existing and newly generated cross-section libraries compared very favorably with measured values of the uranium isotopes in spent fuel assemblies. The uranium-236 predictions made by ORIGEN/S with existing cross-sections varied by about 10 percent from measured values. However, ^{236}U concentrations in spent fuel are probably not significant from a waste management perspective.

Accurate predictions of the U-234 content of spent fuel required a good estimate of the U-234 content in fresh fuel. The method to estimate the U-234 content of fresh fuel presented in Appendix A was used for this benchmark problem. By using this method, relatively good agreement was obtained between ORIGEN estimates and laboratory measurements.

In general, the agreement between ORIGEN/S plutonium predictions and measured values was poor. Concentrations of ^{239}PU, ^{241}Pu, and ^{242}Pu were consistently overpredicted. Concentrations of ^{240}Pu were consistently underpredicted. Overall, ORIGEN/S predictions of the total quantity of plutonium present in spent fuel agreed with measured values to within plus or minus 2 percent. For individual plutonium isotopes, however, the ORIGEN/S predictions were off by as much as 30 percent. It is likely that this phenomenon is caused by overly low capture and fission cross-sections for ^{239}Pu. While better agreement between calculated and measured values would be desirable for the plutonium isotopes, the predictions from ORIGEN/S are conservative from a waste management viewpoint.

Figure 3-14

Comparison of ORIGEN-Predicted vs. Measured Decay Heat Generation Rates for Turkey Point 3 Fuel

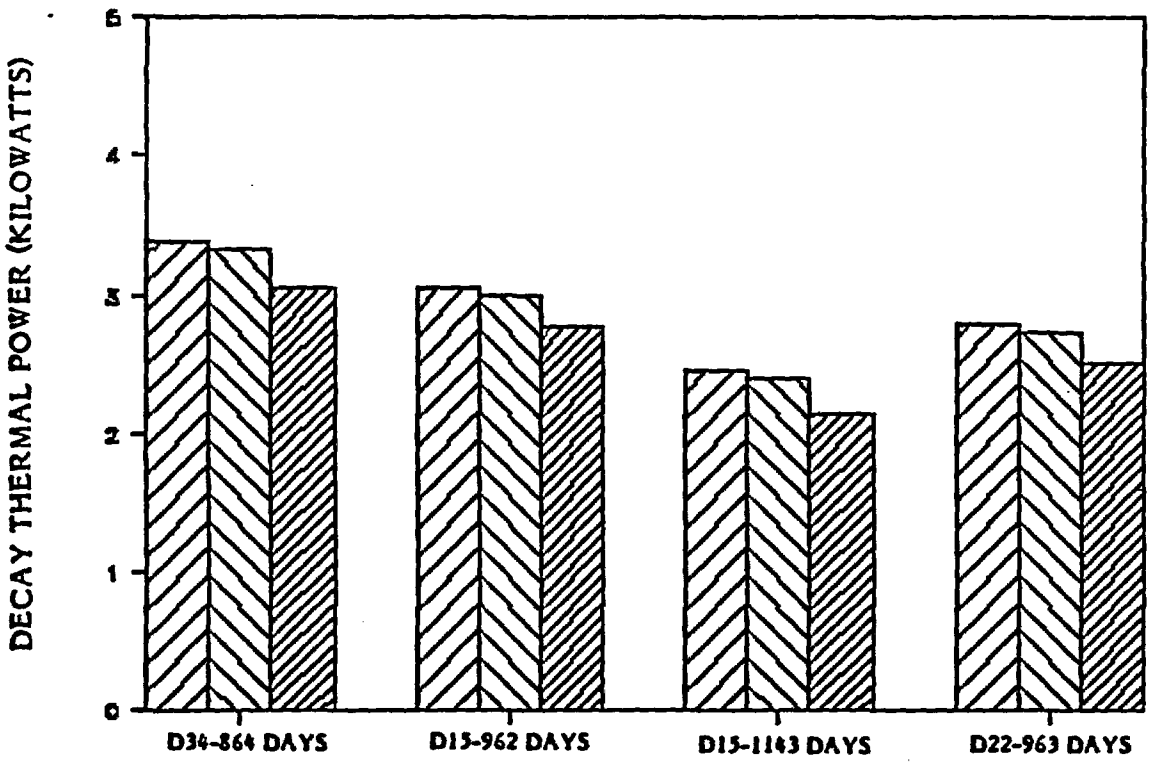

Table 3-19

Results of Benchmark Problems 2.0 and 2.3

Nuclide	Revised Estimate of U-234 Concentration: H. B. Robinson 2 ORIGEN Calculation, Existing Cross-Sections	H. B. Robinson 2 ORIGEN Calculation, Generated Cross-Sections	Turkey Point 3 ORIGEN Calculation, Existing Cross-Sections	Turkey Point 3 ORIGEN Calculation, Generated Cross-Sections	CorSTAR Cell Calculations, Westinghouse 15 X 15 Fuel	Measured Nuclide Concentrations: Turkey Pt. 3 Fuel Assembly and Rod ID: D01-G9-15	D01-G10-14	D01-H9-7	D04-G9-9	D04-G10-7	HB Robinson 2 Fuel	H.B. Robinson and Turkey Point 3 Average	Percent Standard Deviation	H.B. Robinson 2 ORIGEN A Relative Pct. Error	H.B. Robinson 2 ORIGEN B Relative Pct. Error	Turkey Point 3 ORIGEN A Relative Pct. Error	Turkey Point 3 ORIGEN B Relative Pct. Error
U-234	0.102	0.13	0.102	0.131	-	0.1321	0.1321	0.1225	0.1132	0.1321	0.1323	0.1274	5.70	-19.927	2.054	-19.927	2.839
U-235	5.61	5.56	5.69	5.67	5.5655	5.8655	5.8773	5.5853	5.114	5.6626	6.201	5.6843	5.72	-1.307	-2.186	0.101	-0.251
U-236	3.6	3.25	3.58	3.24	3.1923	3.2545	3.2553	3.1753	3.1573	3.2523	3.309	3.2340	1.60	11.319	0.496	10.701	0.187
U-238	948	949	949	949	950.929	950.321	950.7448	949.7477	950.1843	949.8633	951.9	950.4602	0.08	-0.259	-0.154	-0.154	-0.154
PU-238	0.161	0.166	0.157	0.163	-	0.1365	0.136	0.1426	0.1383	0.1372	0.1407	0.1386	1.71	16.204	19.812	13.316	17.647
PU-239	5.32	5.12	5.32	5.12	4.7705	4.8382	4.841	4.9291	4.9438	4.7891	5.054	4.8992	1.79	8.589	4.507	8.589	4.507
PU-240	2.26	1.86	2.25	1.86	2.0225	2.2659	2.2946	2.295	2.3211	2.278	2.226	2.2801	1.30	-0.882	-18.425	-1.320	-18.425
PU-241 CORR	1.02	1.4	1.01	1.39	1.1059	1.061	1.0687	1.1043	1.1245	1.0719	1.0844	1.0858	2.04	-6.060	28.937	-6.981	28.016
PU-242	0.408	0.58	0.4	0.566	0.5516	0.502	0.5249	0.5447	0.543	0.5235	0.5	0.5230	3.35	-21.991	10.895	-23.521	8.218
TOTAL PU	9.169	9.126	9.137	9.099	-	8.8036	8.8652	9.0157	9.0707	8.7997	9.0051	8.9267	1.21	2.715	2.233	2.356	1.931
PU W/O 238	9.008	8.96	8.98	8.936	8.4505	8.6671	8.7292	8.8731	8.9324	8.6625	8.8644	8.7881	1.21	2.502	1.956	2.183	1.683
AM-241	1.190E-01	1.630E-01	1.160E-01	1.590E-01							9.930E-02	9.930E-02		19.839	64.149	16.818	60.121
AM-242M	1.040E-03	1.390E-03	9.830E-04	1.320E-03							4.987E-03	4.987E-03		-79.146	-72.128	-80.289	-73.531
AM-243	1.170E-01	1.040E-01	1.130E-01	1.020E-01							5.985E-02	5.985E-02		95.489	77.109	88.805	70.426
CM-242	6.890E-04	1.020E-03	6.990E-04	1.040E-03							8.404E-04	8.404E-04		-18.015	21.371	-16.825	23.751
CM-243	9.020E-05	1.450E-04	9.370E-05	1.510E-04							3.113E-04	3.113E-04		-71.025	-53.421	-69.900	-51.494
CM-244	3.760E-02	3.610E-02	3.610E-02	3.430E-02							2.342E-02	2.342E-02		60.547	54.142	54.142	46.456
CM-245	2.700E-03	2.620E-03	2.570E-03	2.470E-03							1.149E-03	1.149E-03		134.987	128.024	123.673	114.970
CM-246	3.370E-04	3.570E-04	3.170E-04	3.320E-04							1.180E-04	1.180E-04		185.593	202.542	168.644	181.356
CM-247	4.650E-06	5.140E-06	4.330E-06	4.720E-06							1.046E-06	1.046E-06		344.551	391.396	313.958	351.243
CM-248	3.600E-07	3.990E-07	3.130E-07	3.610E-07							2.626E-07	2.626E-07		29.474	51.942	19.193	37.471
RU-106	4.920E-02	4.440E-02	4.900E-02	4.450E-02							3.957E-02	3.957E-02		24.337	12.206	23.831	12.459
CS-134	7.010E-02	7.540E-02	6.930E-02	7.550E-02							5.232E-02	5.232E-02		33.983	44.113	32.454	44.304
CS-137	1.110E+00	1.080E+00	1.100E+00	1.080E+00							1.016E+00	1.016E+00		9.252	6.299	8.268	6.299
CE-144	6.290E-02	6.180E-02	6.260E-02	6.170E-02							5.655E-02	5.655E-02		11.229	9.284	10.698	9.107
I-129	2.320E-01	1.820E-01	2.300E-01	1.820E-01							1.290E-01	1.290E-01		79.845	41.085	78.295	41.085
H-3	4.800E-05	4.920E-05	4.740E-05	4.930E-05							2.814E-05	2.814E-05		70.576	74.840	68.443	75.195
BURNUP	31364	31000	31364	31000	31000	30720	30510	31560	31260	31310	31364	31121	1.20	0.782	-0.388	0.782	-0.388

Figure 3-15

^{234}U – ORIGEN Results vs. Measured Data for Problems 2.4 and 2.5

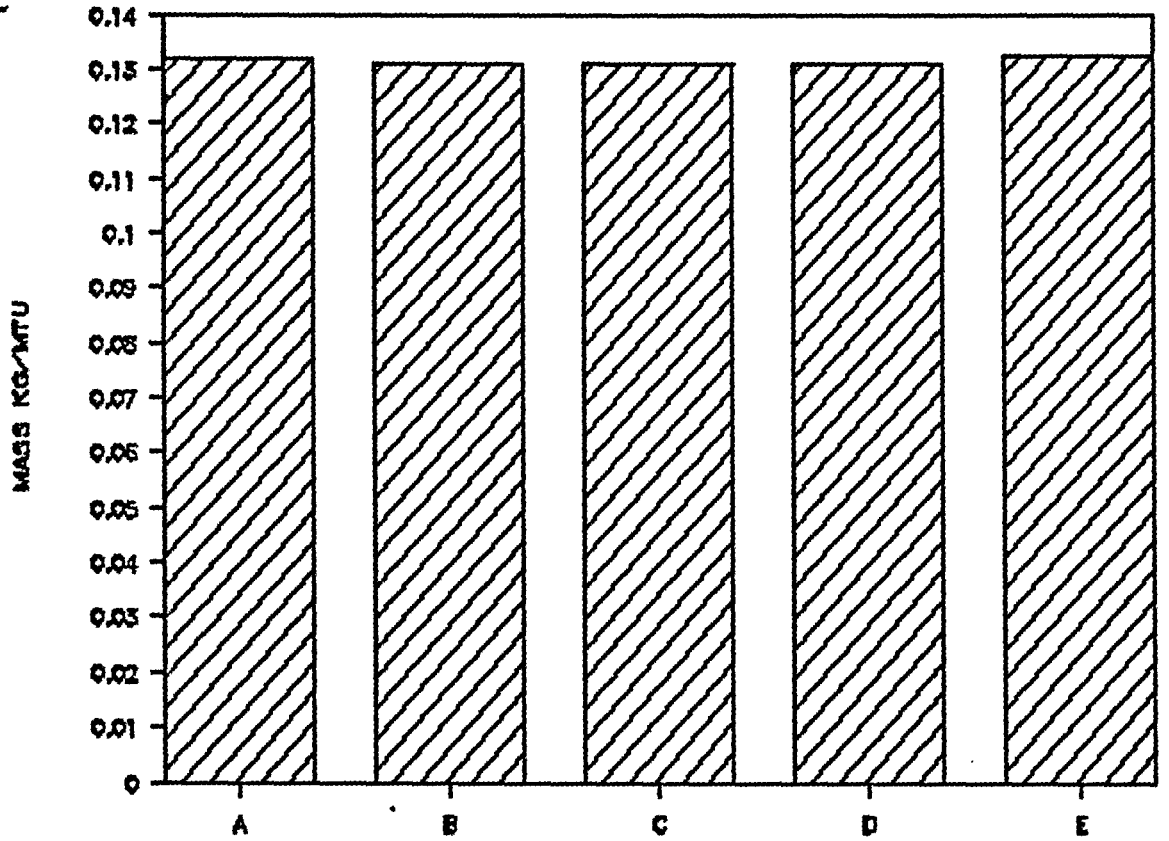

Note: A = ORIGEN-calculated results for H.B. Robinson 2, using existing cross-sections

B = ORIGEN-calculated results for H.B. Robinson 2, using newly generated cross-sections

C = ORIGEN-calculated results for Turkey Point 3, using existing cross-sections

D = ORIGEN-calculated results for Turkey Point 3, using newly generated cross-sections

E = Average of H.B. Robinson 2 and Turkey Point 3 measured data

Figure 3-16

^{235}U – ORIGEN Results vs. Measured Data for Problems 2.4 and 2.5

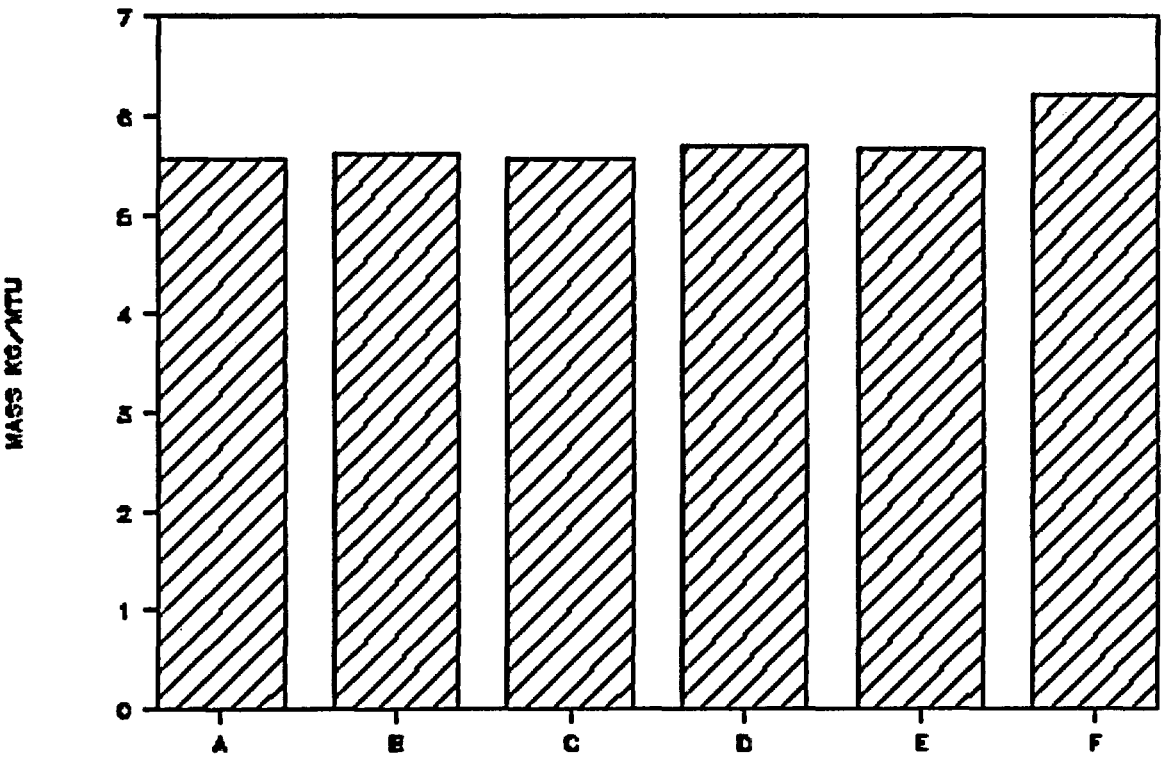

Note: A = Corstar Cell calculation for Westinghouse 15x15 fuel assembly

B = ORIGEN-calculated results for H.B. Robinson 2, using existing cross-sections

C = ORIGEN-calculated results for H. B. Robinson 2, using newly generated cross-sections

D = ORIGEN-calculated results for Turkey Point 3, using existing cross-sections

E = ORIGEN-calculated results for Turkey Point 3, using newly generated cross-sections

F = Average of H.B. Robinson 2 and Turkey Point 3 measured data

Figure 3-17

^{236}U – ORIGEN Results vs. Measured Data for Problems 2.4 and 2.5

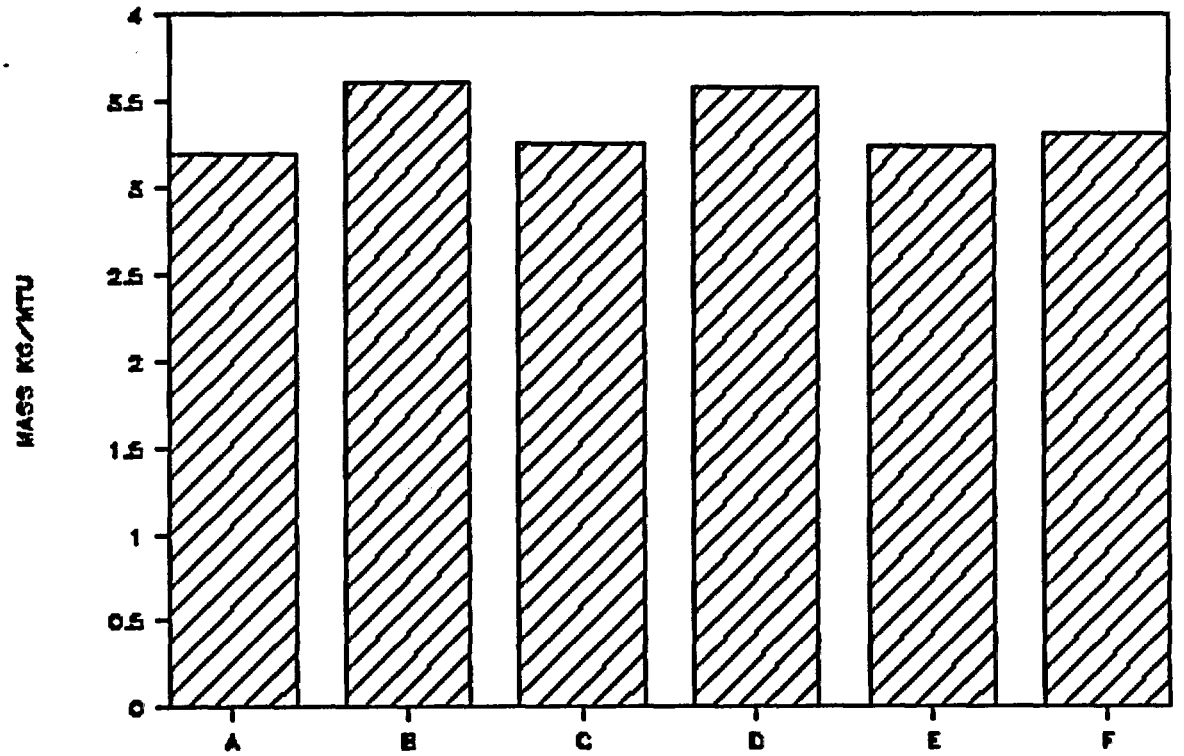

Note: A = Corstar Cell calculation for Westinghouse 15x15 fuel assembly

B = ORIGEN-calculated results for H.B. Robinson 2, using existing cross-sections

C = ORIGEN-calculated results for H. B. Robinson 2, using newly generated cross-sections

D = ORIGEN-calculated results for Turkey Point 3, using existing cross-sections

E = ORIGEN-calculated results for Turkey Point 3, using newly generated cross-sections

F = Average of H.B. Robinson 2 and Turkey Point 3 measured data

Figure 3-18

^{238}U – ORIGEN Results vs. Measured Data for Problems 2.4 and 2.5

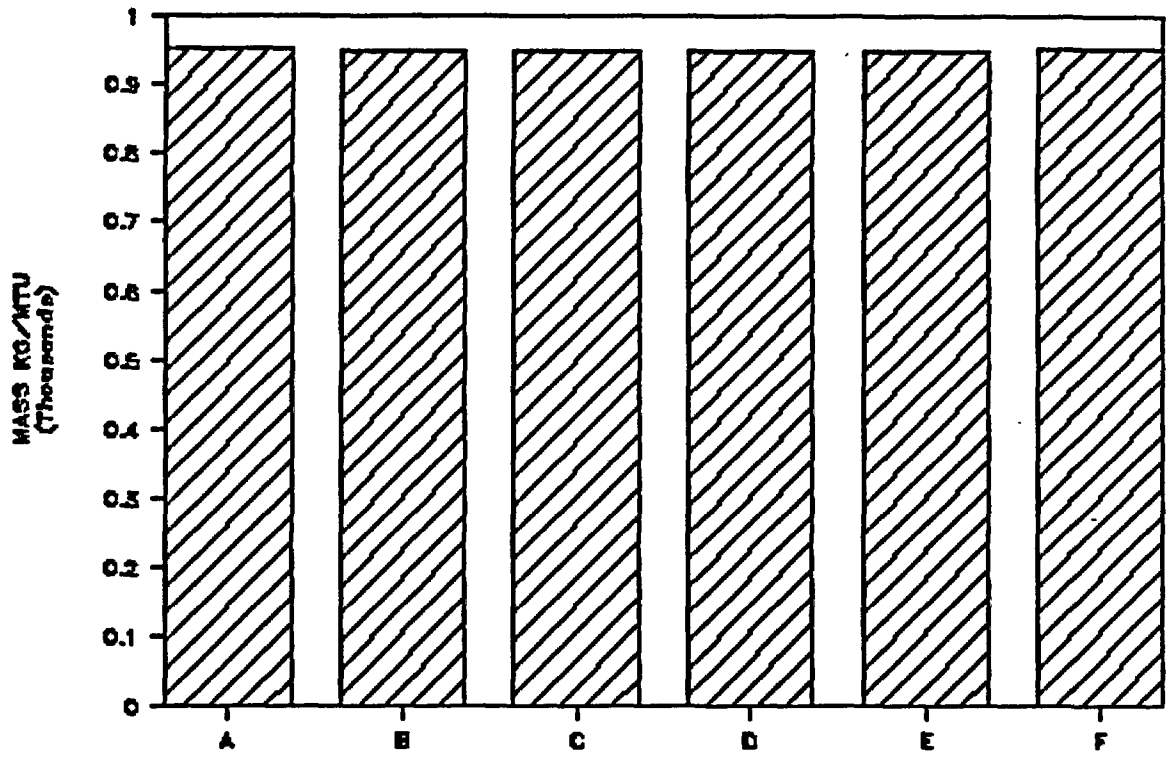

Note: A = Corstar Cell calculation for Westinghouse 15x15 fuel assembly

B = ORIGEN-calculated results for H.B. Robinson 2, using existing cross-sections

C = ORIGEN-calculated results for H. B. Robinson 2, using newly generated cross-sections

D = ORIGEN-calculated results for Turkey Point 3, using existing cross-sections

E = ORIGEN-calculated results for Turkey Point 3, using newly generated cross-sections

F = Average of H.B. Robinson 2 and Turkey Point 3 measured data

Figure 3-19

^{238}Pu – ORIGEN Results vs. Measured Data for Problems 2.4 and 2.5

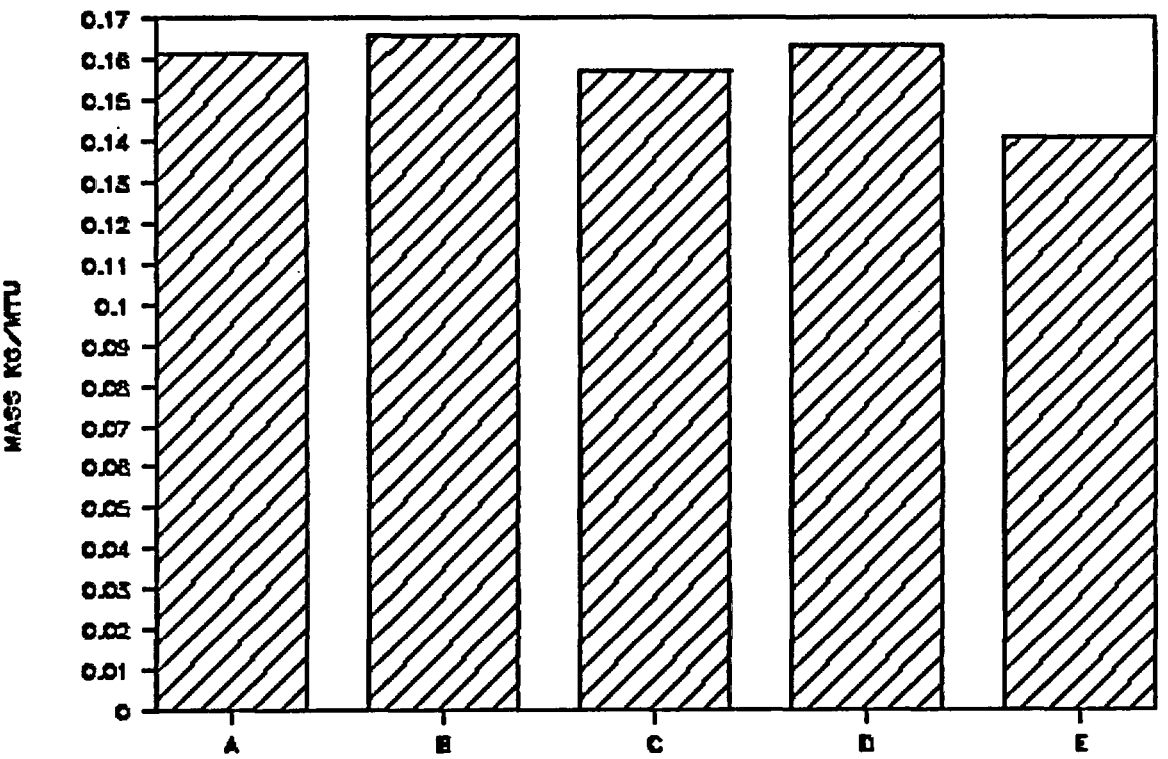

Note: A = ORIGEN-calculated results for H.B. Robinson 2, using existing cross-sections

B = ORIGEN-calculated results for H.B. Robinson 2, using newly generated cross-sections

C = ORIGEN-calculated results for Turkey Point 3, using existing cross-sections

D = ORIGEN-calculated results for Turkey Point 3, using newly generated cross-sections

E = Average of H.B. Robinson 2 and Turkey Point 3 measured data

Figure 3-20

^{239}Pu – ORIGEN Results vs. Measured Data for Problems 2.4 and 2.5

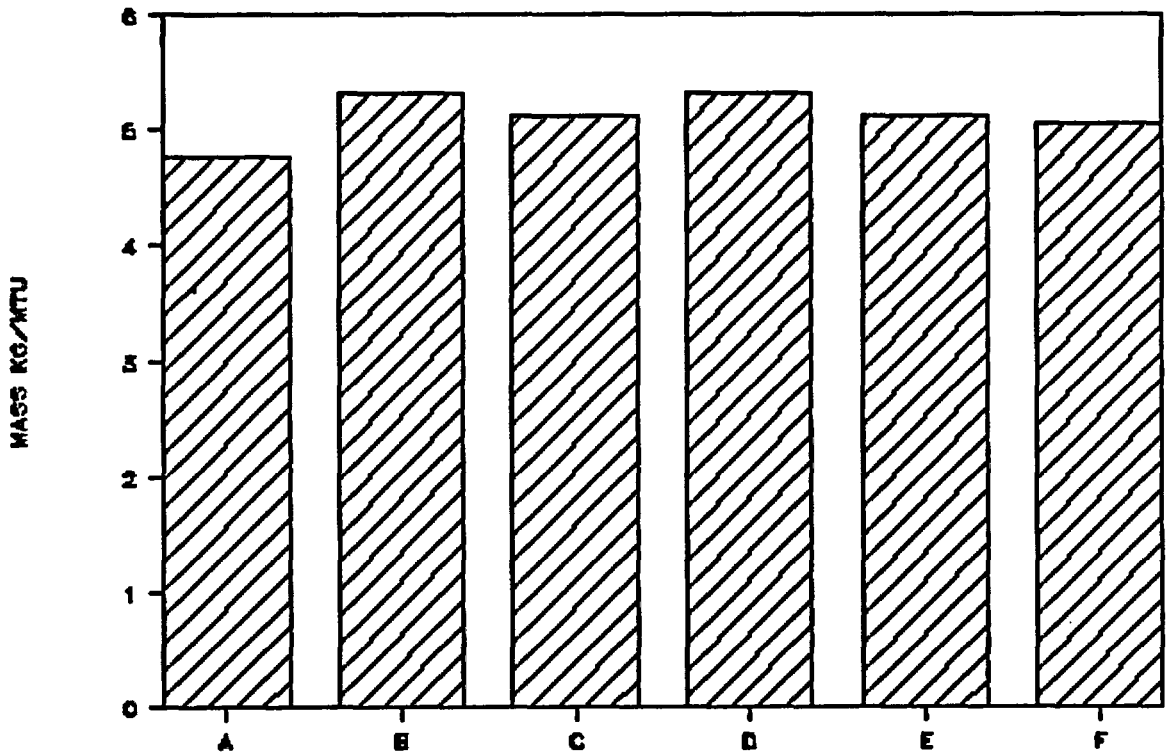

Note: A = Corstar Cell calculation for Westinghouse 15x15 fuel assembly

B = ORIGEN-calculated results for H.B. Robinson 2, using existing cross-sections

C = ORIGEN-calculated results for H. B. Robinson 2, using newly generated cross-sections

D = ORIGEN-calculated results for Turkey Point 3, using existing cross-sections

E = ORIGEN-calculated results for Turkey Point 3, using newly generated cross-sections

F = Average of H.B. Robinson 2 and Turkey Point 3 measured data

Figure 3-21

^{240}Pu – ORIGEN Results vs. Measured Data for Problems 2.4 and 2.5

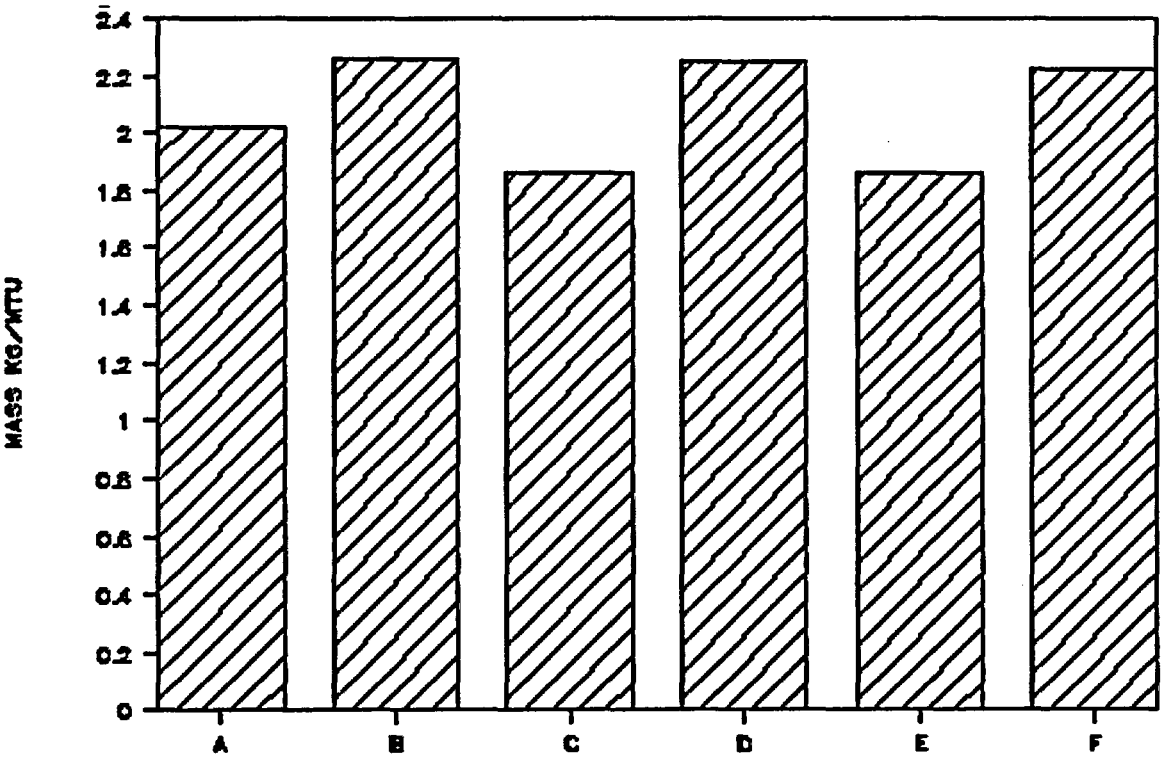

Note: A = Corstar Cell calculation for Westinghouse 15x15 fuel assembly

B = ORIGEN-calculated results for H.B. Robinson 2, using existing cross-sections

C = ORIGEN-calculated results for H. B. Robinson 2, using newly generated cross-sections

D = ORIGEN-calculated results for Turkey Point 3, using existing cross-sections

E = ORIGEN-calculated results for Turkey Point 3, using newly generated cross-sections

F = Average of H.B. Robinson 2 and Turkey Point 3 measured data

Figure 3-22

^{241}Pu – ORIGEN Results vs. Measured Data for Problems 2.4 and 2.5

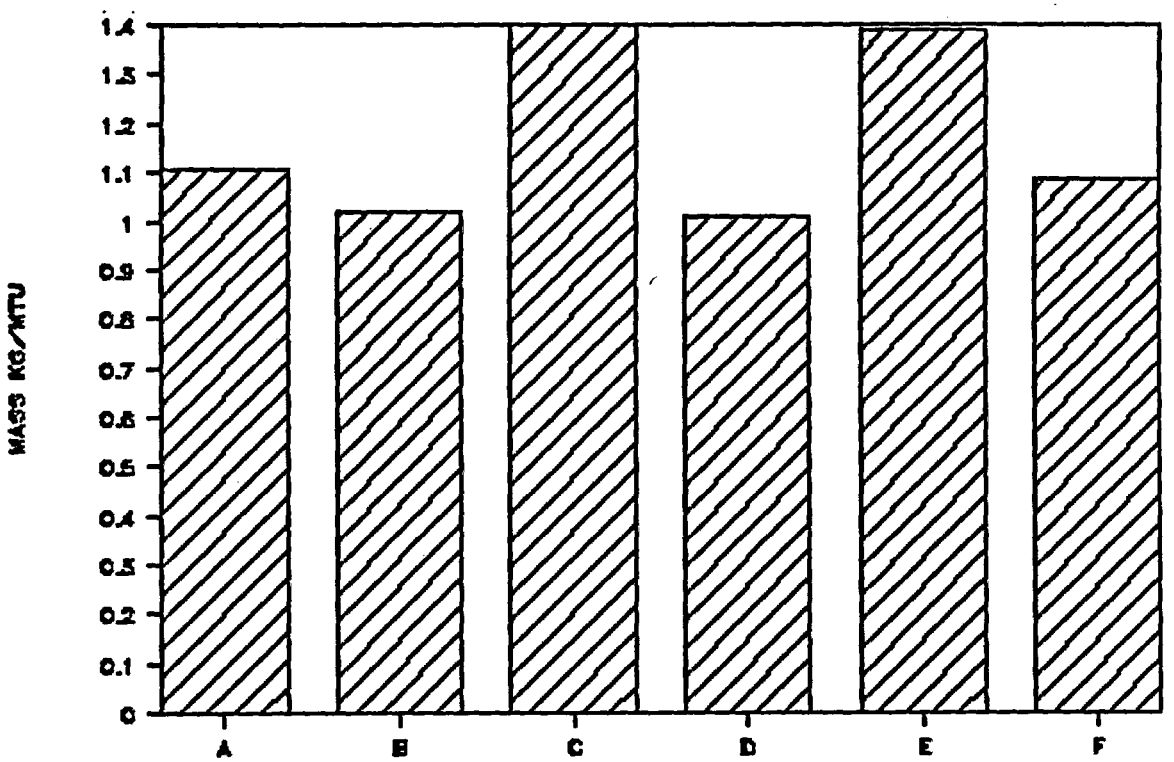

Note: A = Corstar Cell calculation for Westinghouse 15x15 fuel assembly

B = ORIGEN-calculated results for H.B. Robinson 2, using existing cross-sections

C = ORIGEN-calculated results for H. B. Robinson 2, using newly generated cross-sections

D = ORIGEN-calculated results for Turkey Point 3, using existing cross-sections

E = ORIGEN-calculated results for Turkey Point 3, using newly generated cross-sections

F = Average of H.B. Robinson 2 and Turkey Point 3 measured data

Figure 3-23

^{242}Pu – ORIGEN Results vs. Measured Data for Problems 2.4 and 2.5

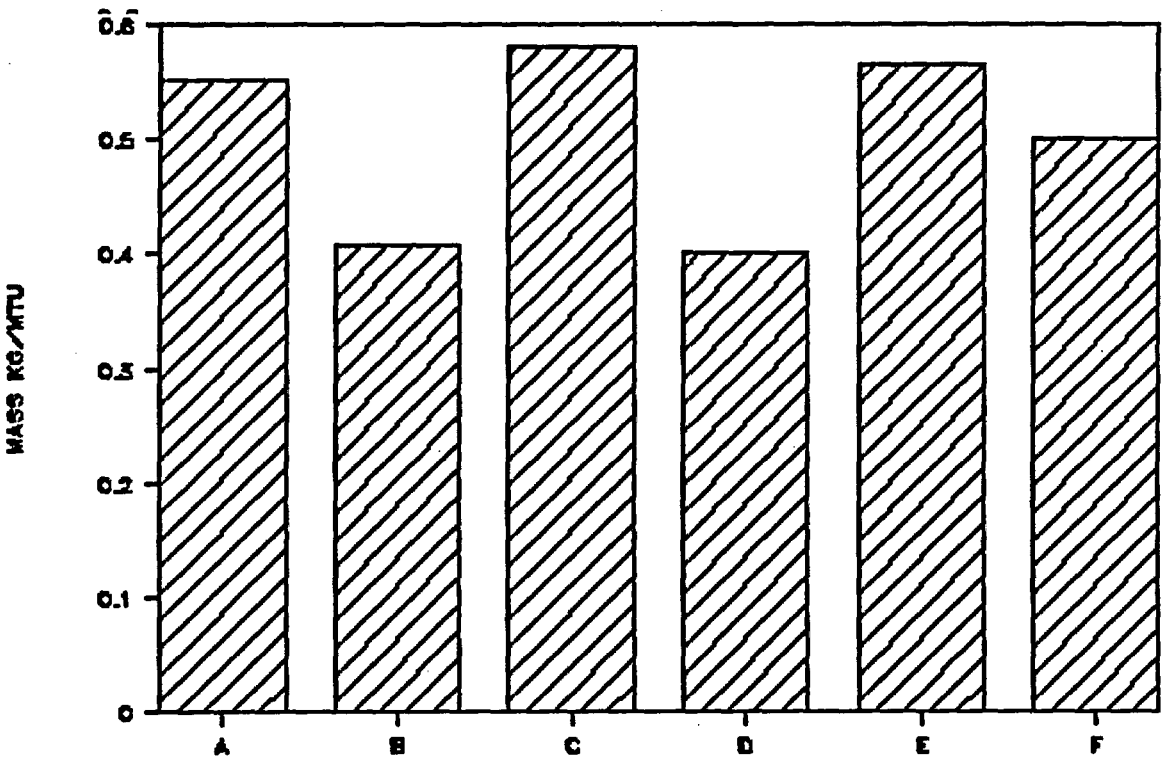

Note: A = Corstar Cell calculation for Westinghouse 15x15 fuel assembly

B = ORIGEN-calculated results for H.B. Robinson 2, using existing cross-sections

C = ORIGEN-calculated results for H. B. Robinson 2, using newly generated cross-sections

D = ORIGEN-calculated results for Turkey Point 3, using existing cross-sections

E = ORIGEN-calculated results for Turkey Point 3, using newly generated cross-sections

F = Average of H.B. Robinson 2 and Turkey Point 3 measured data

Figure 3-24

^{241}Am – ORIGEN Results vs. Measured Data for Problems 2.4 and 2.5

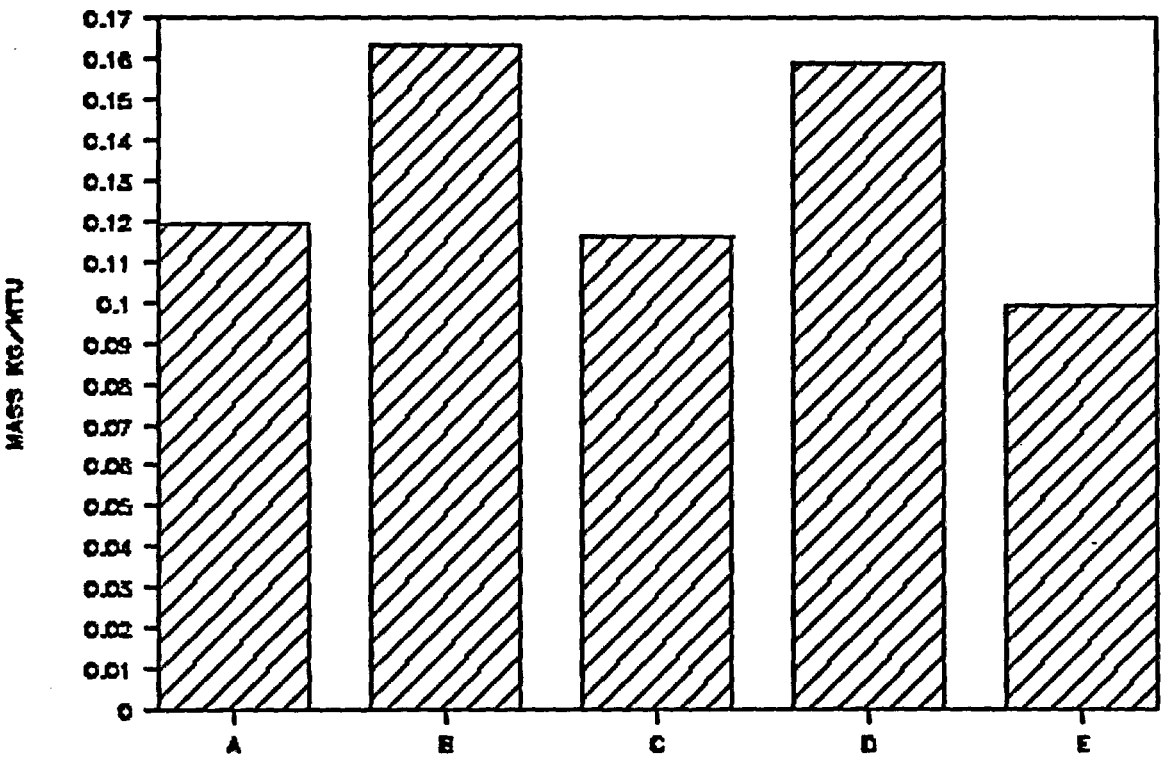

Note: A = ORIGEN-calculated results for H.B. Robinson 2, using existing cross-sections

B = ORIGEN-calculated results for H.B. Robinson 2, using newly generated cross-sections

C = ORIGEN-calculated results for Turkey Point 3, using existing cross-sections

D = ORIGEN-calculated results for Turkey Point 3, using newly generated cross-sections

E = Average of H.B. Robinson 2 and Turkey Point 3 measured data

Figure 3-25

^{242m}Am – ORIGEN Results vs. Measured Data for Problems 2.4 and 2.5

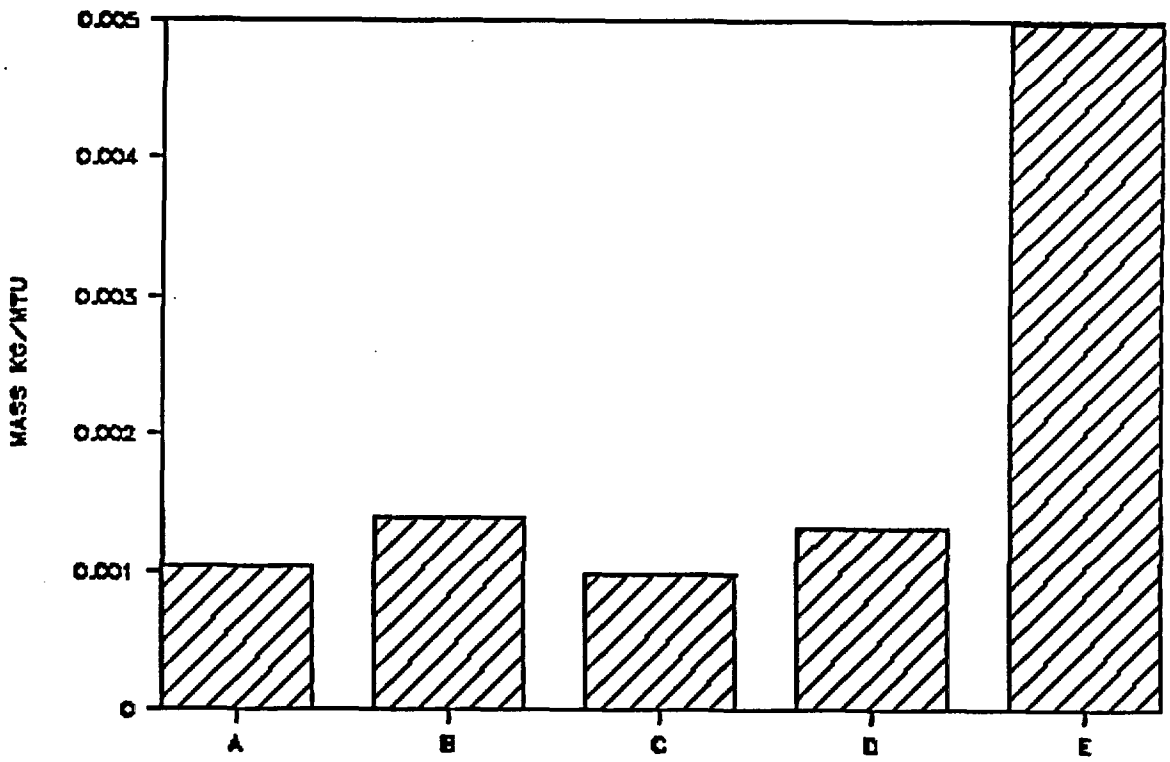

Note: A = ORIGEN-calculated results for H.B. Robinson 2, using existing cross-sections

B = ORIGEN-calculated results for H.B. Robinson 2, using newly generated cross-sections

C = ORIGEN-calculated results for Turkey Point 3, using existing cross-sections

D = ORIGEN-calculated results for Turkey Point 3, using newly generated cross-sections

E = Average of H.B. Robinson 2 and Turkey Point 3 measured data

Figure 3-26

^{243}Am – ORIGEN Results vs. Measured Data for Problems 2.4 and 2.5

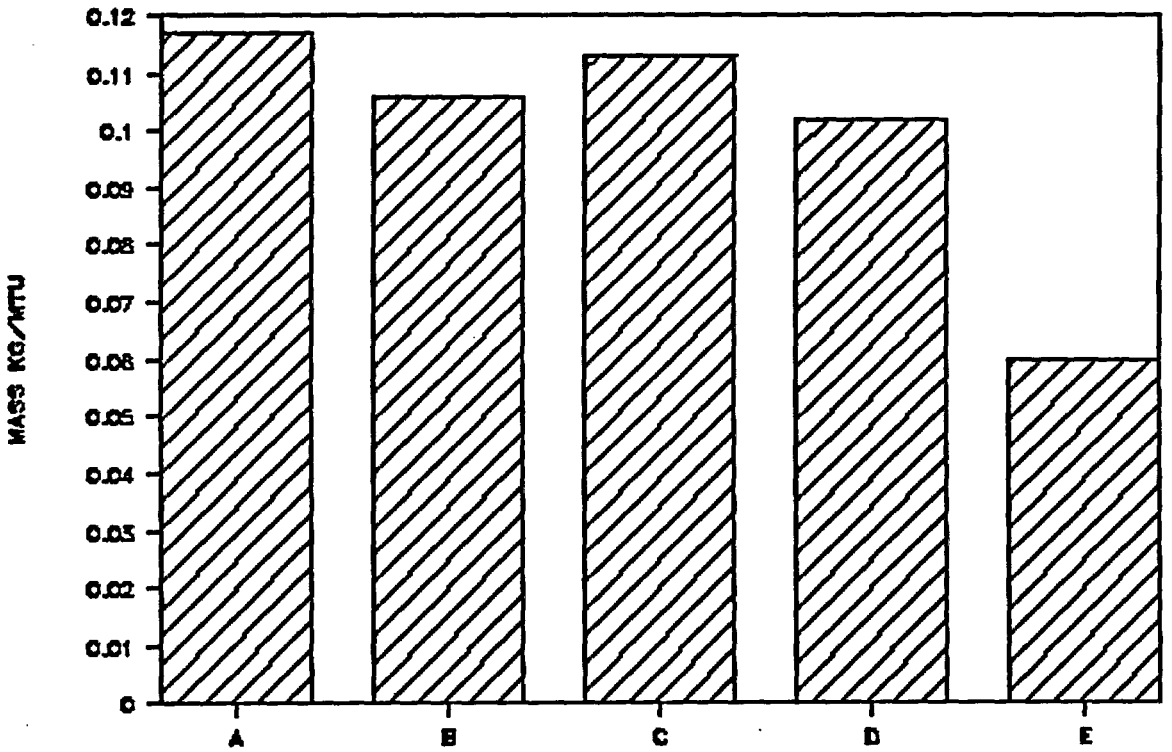

Note: A = ORIGEN-calculated results for H.B. Robinson 2, using existing cross-sections

B = ORIGEN-calculated results for H.B. Robinson 2, using newly generated cross-sections

C = ORIGEN-calculated results for Turkey Point 3, using existing cross-sections

D = ORIGEN-calculated results for Turkey Point 3, using newly generated cross-sections

E = Average of H.B. Robinson 2 and Turkey Point 3 measured data

Figure 3-27

^{242}Cm – ORIGEN Results vs. Measured Data for Problems 2.4 and 2.5

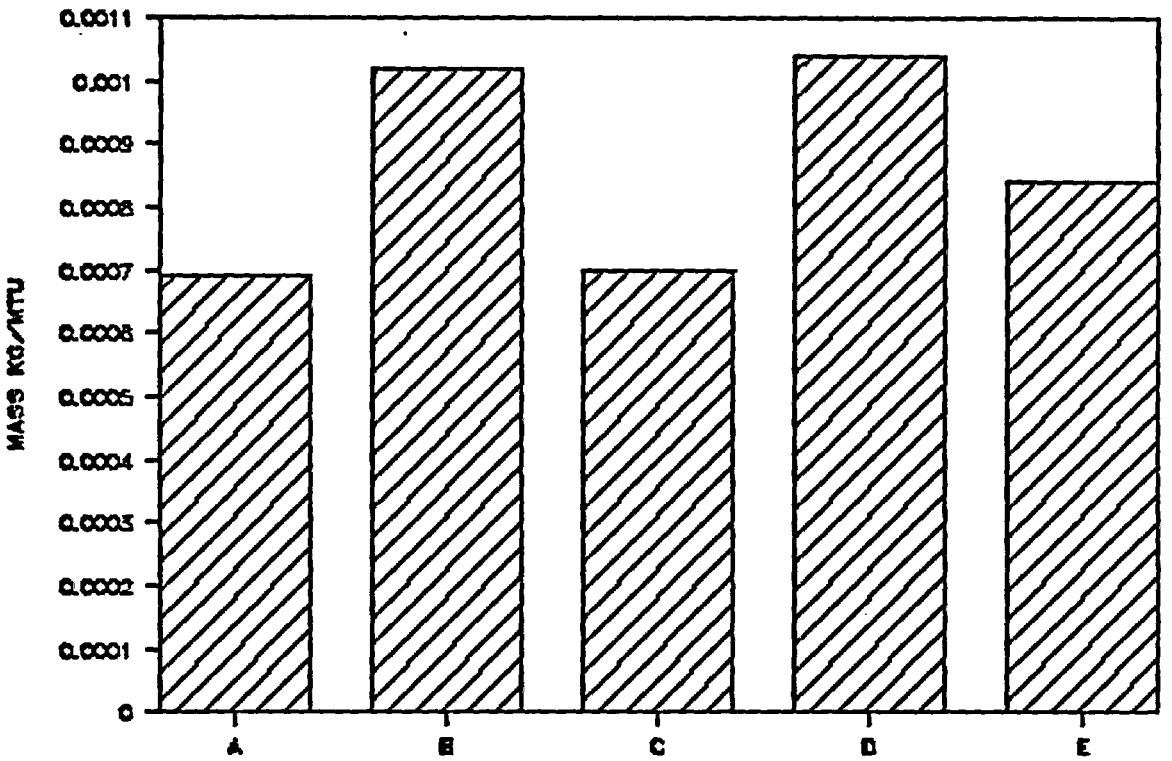

Note: A = ORIGEN-calculated results for H.B. Robinson 2, using existing cross-sections

B = ORIGEN-calculated results for H.B. Robinson 2, using newly generated cross-sections

C = ORIGEN-calculated results for Turkey Point 3, using existing cross-sections

D = ORIGEN-calculated results for Turkey Point 3, using newly generated cross-sections

E = Average of H.B. Robinson 2 and Turkey Point 3 measured data

Figure 3-28

^{243}Cm – ORIGEN Results vs. Measured Data for Problems 2.4 and 2.5

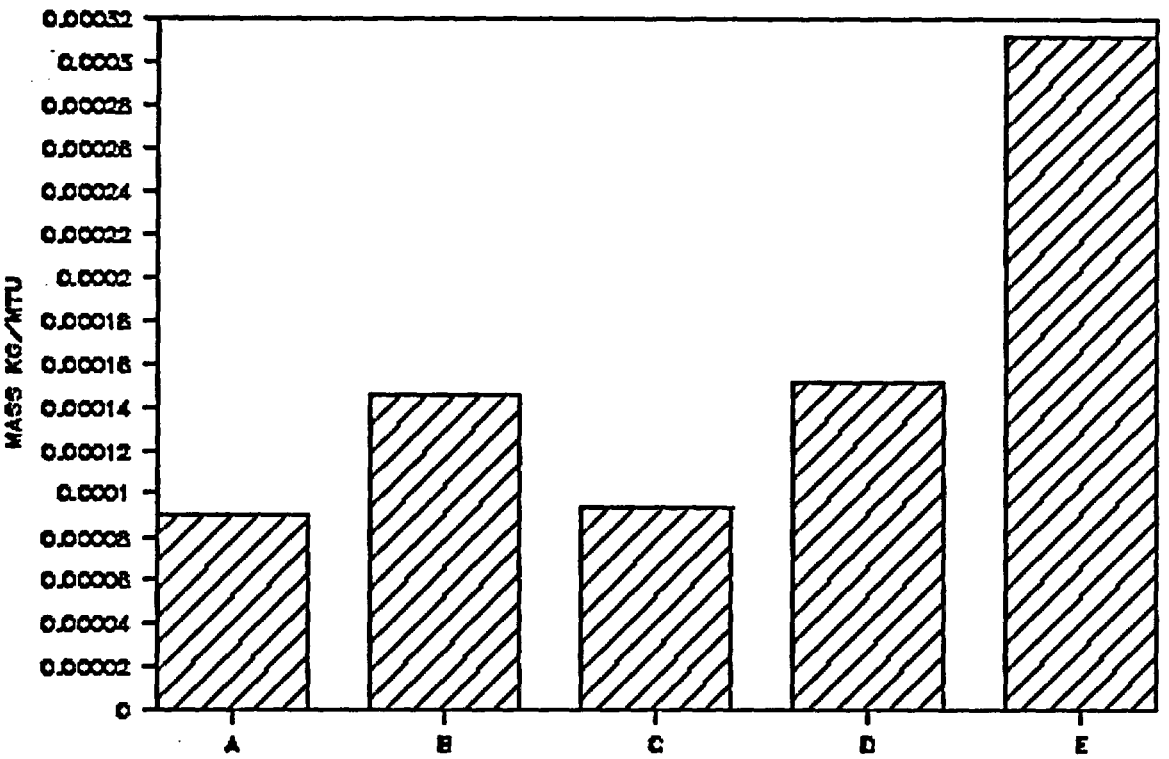

Note: A = ORIGEN-calculated results for H.B. Robinson 2, using existing cross-sections

B = ORIGEN-calculated results for H.B. Robinson 2, using newly generated cross-sections

C = ORIGEN-calculated results for Turkey Point 3, using existing cross-sections

D = ORIGEN-calculated results for Turkey Point 3, using newly generated cross-sections

E = Average of H.B. Robinson 2 and Turkey Point 3 measured data

Figure 3-29

^{244}Cm – ORIGEN Results vs. Measured Data for Problems 2.4 and 2.5

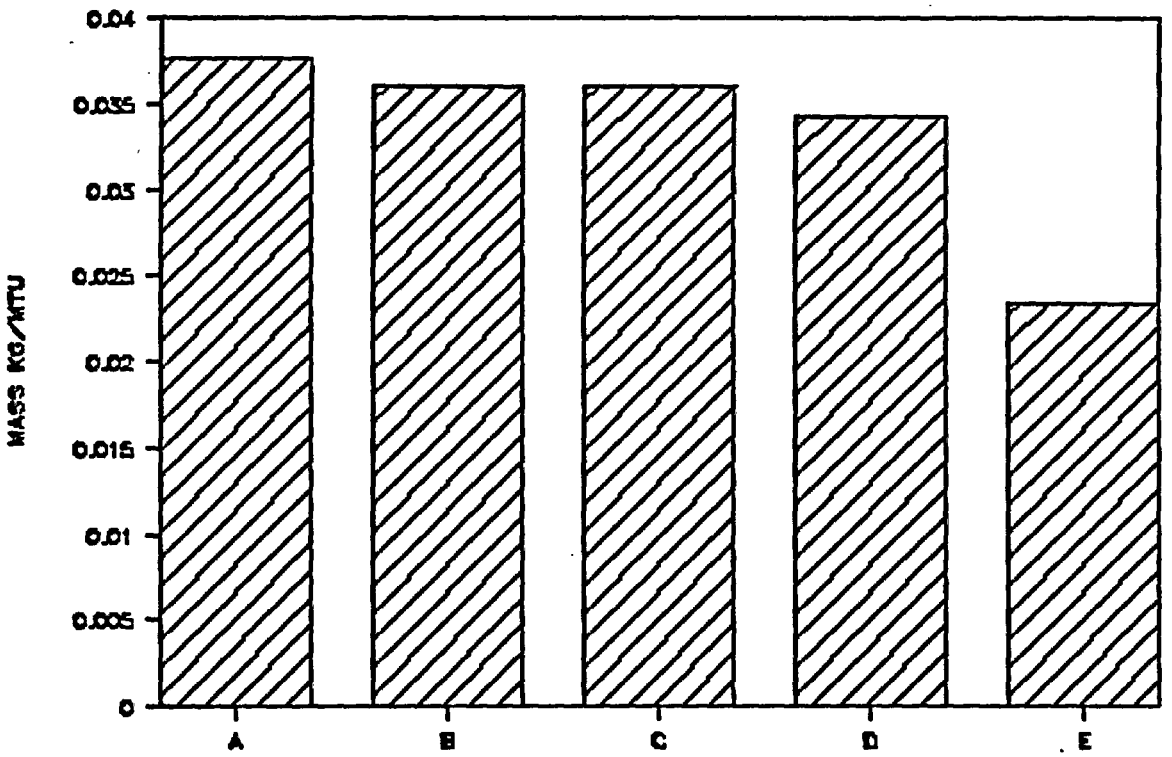

Note: A = ORIGEN-calculated results for H.B. Robinson 2, using existing cross-sections

B = ORIGEN-calculated results for H.B. Robinson 2, using newly generated cross-sections

C = ORIGEN-calculated results for Turkey Point 3, using existing cross-sections

D = ORIGEN-calculated results for Turkey Point 3, using newly generated cross-sections

E = Average of H.B. Robinson 2 and Turkey Point 3 measured data

Figure 3-30

^{245}Cm – ORIGEN Results vs. Measured Data for Problems 2.4 and 2.5

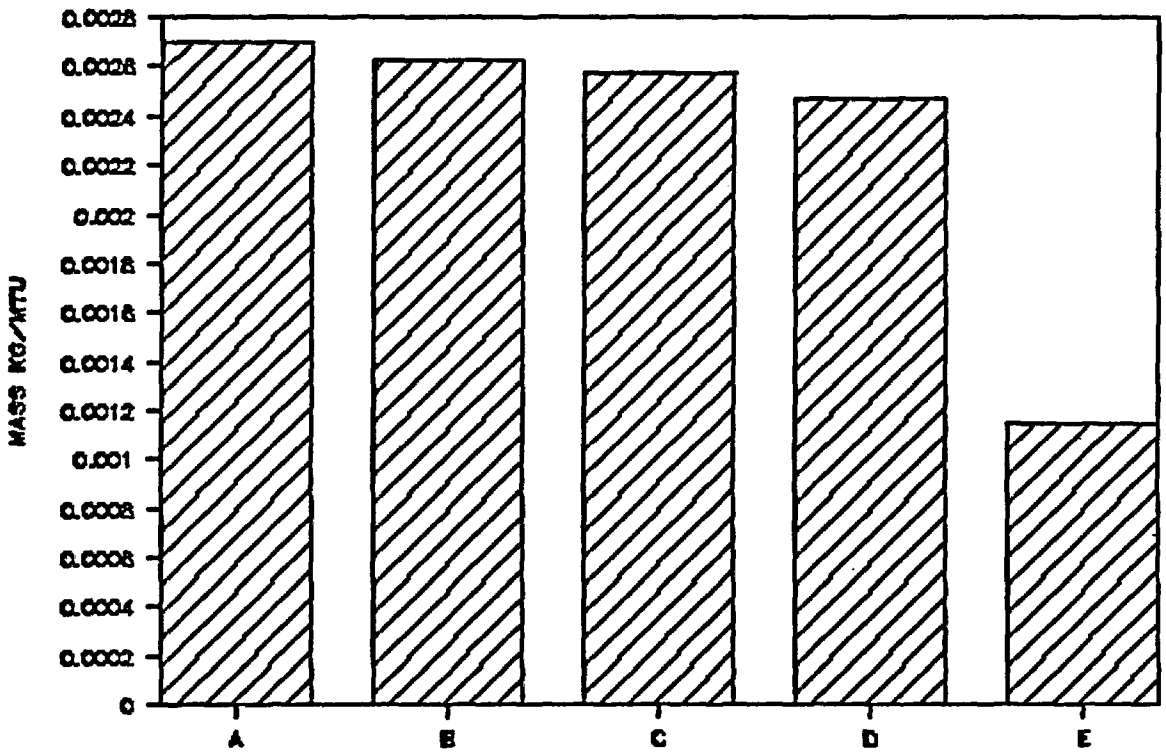

Note: A = ORIGEN-calculated results for H.B. Robinson 2, using existing cross-sections

B = ORIGEN-calculated results for H.B. Robinson 2, using newly generated cross-sections

C = ORIGEN-calculated results for Turkey Point 3, using existing cross-sections

D = ORIGEN-calculated results for Turkey Point 3, using newly generated cross-sections

E = Average of H.B. Robinson 2 and Turkey Point 3 measured data

Figure 3-31

^{246}Cm – ORIGEN Results vs. Measured Data for Problems 2.4 and 2.5

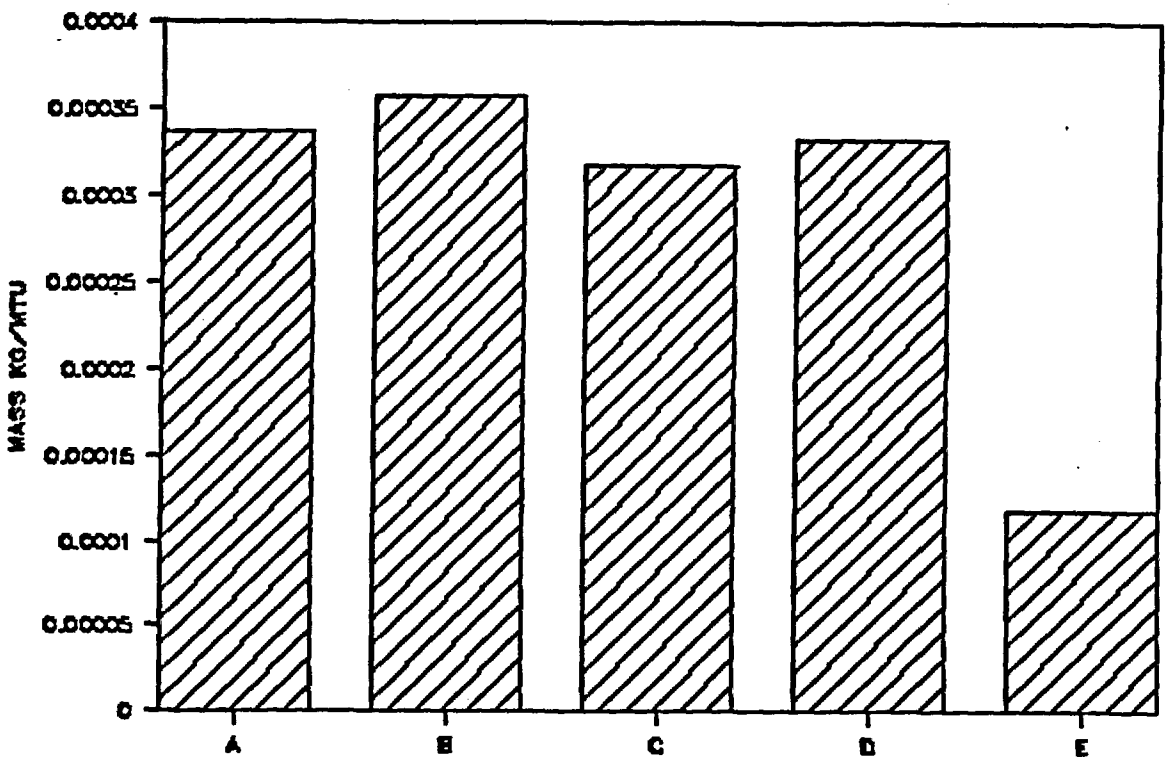

Note: A = ORIGEN-calculated results for H.B. Robinson 2, using existing cross-sections

B = ORIGEN-calculated results for H.B. Robinson 2, using newly generated cross-sections

C = ORIGEN-calculated results for Turkey Point 3, using existing cross-sections

D = ORIGEN-calculated results for Turkey Point 3, using newly generated cross-sections

E = Average of H.B. Robinson 2 and Turkey Point 3 measured data

Figure 3-32

^{247}Cm – ORIGEN Results vs. Measured Data for Problems 2.4 and 2.5

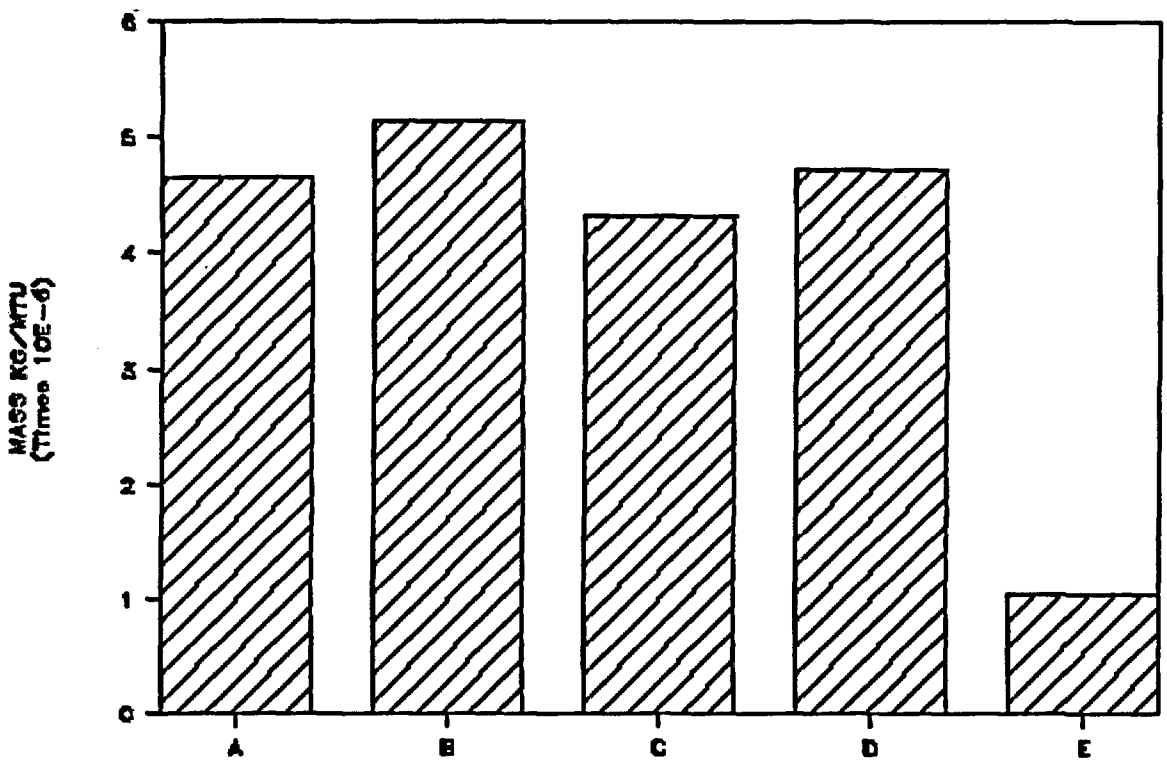

Note: A = ORIGEN-calculated results for H.B. Robinson 2, using existing cross-sections

B = ORIGEN-calculated results for H.B. Robinson 2, using newly generated cross-sections

C = ORIGEN-calculated results for Turkey Point 3, using existing cross-sections

D = ORIGEN-calculated results for Turkey Point 3, using newly generated cross-sections

E = Average of H.B. Robinson 2 and Turkey Point 3 measured data

Figure 3-33

^{248}Cm – ORIGEN Results vs. Measured Data for Problems 2.4 and 2.5

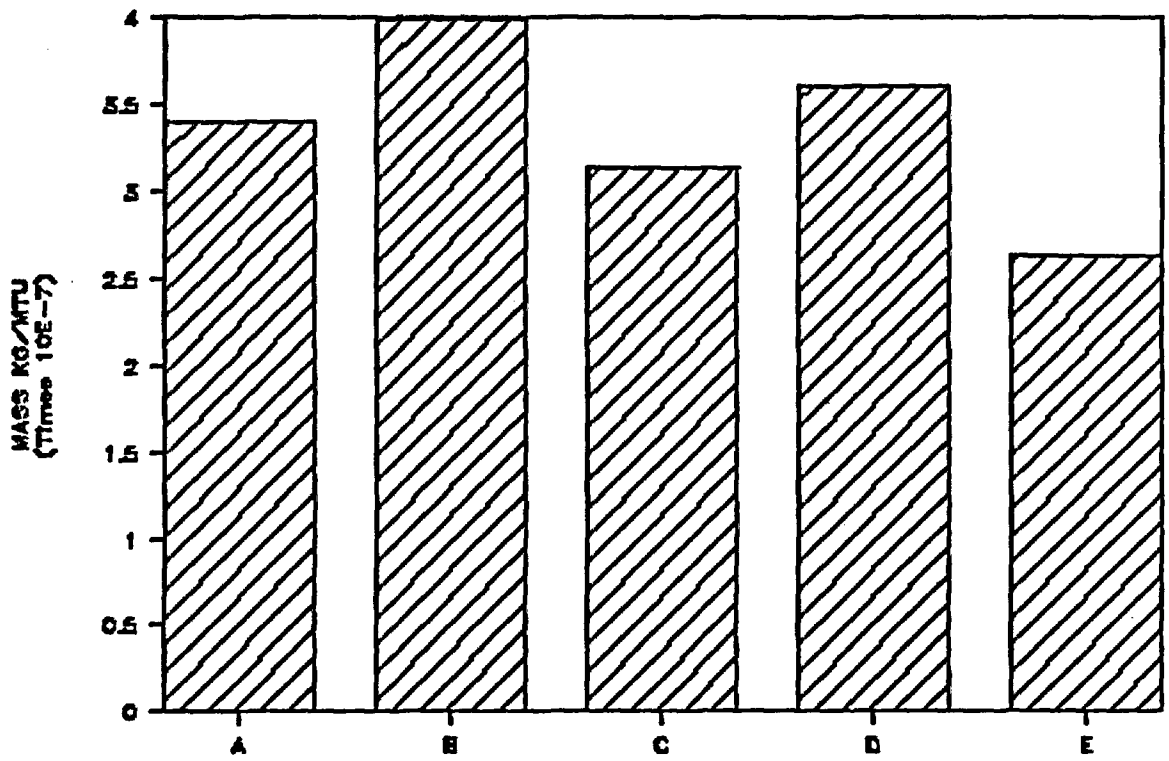

Note: A = ORIGEN-calculated results for H.B. Robinson 2, using existing cross-sections

B = ORIGEN-calculated results for H.B. Robinson 2, using newly generated cross-sections

C = ORIGEN-calculated results for Turkey Point 3, using existing cross-sections

D = ORIGEN-calculated results for Turkey Point 3, using newly generated cross-sections

E = Average of H.B. Robinson 2 and Turkey Point 3 measured data

Figure 3-34

^{106}Ru – ORIGEN Results vs. Measured Data for Problems 2.4 and 2.5

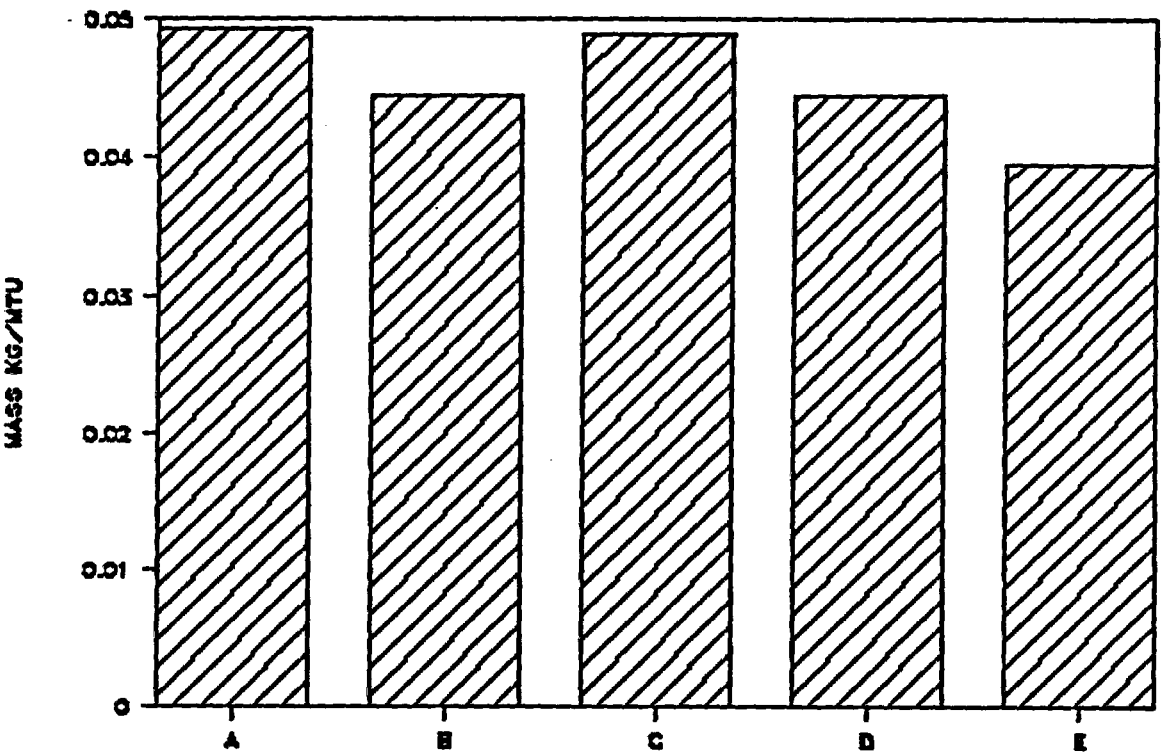

Note: A = ORIGEN-calculated results for H.B. Robinson 2, using existing cross-sections

B = ORIGEN-calculated results for H.B. Robinson 2, using newly generated cross-sections

C = ORIGEN-calculated results for Turkey Point 3, using existing cross-sections

D = ORIGEN-calculated results for Turkey Point 3, using newly generated cross-sections

E = Average of H.B. Robinson 2 and Turkey Point 3 measured data

Figure 3-35

^{134}Cs – ORIGEN Results vs. Measured Data for Problems 2.4 and 2.5

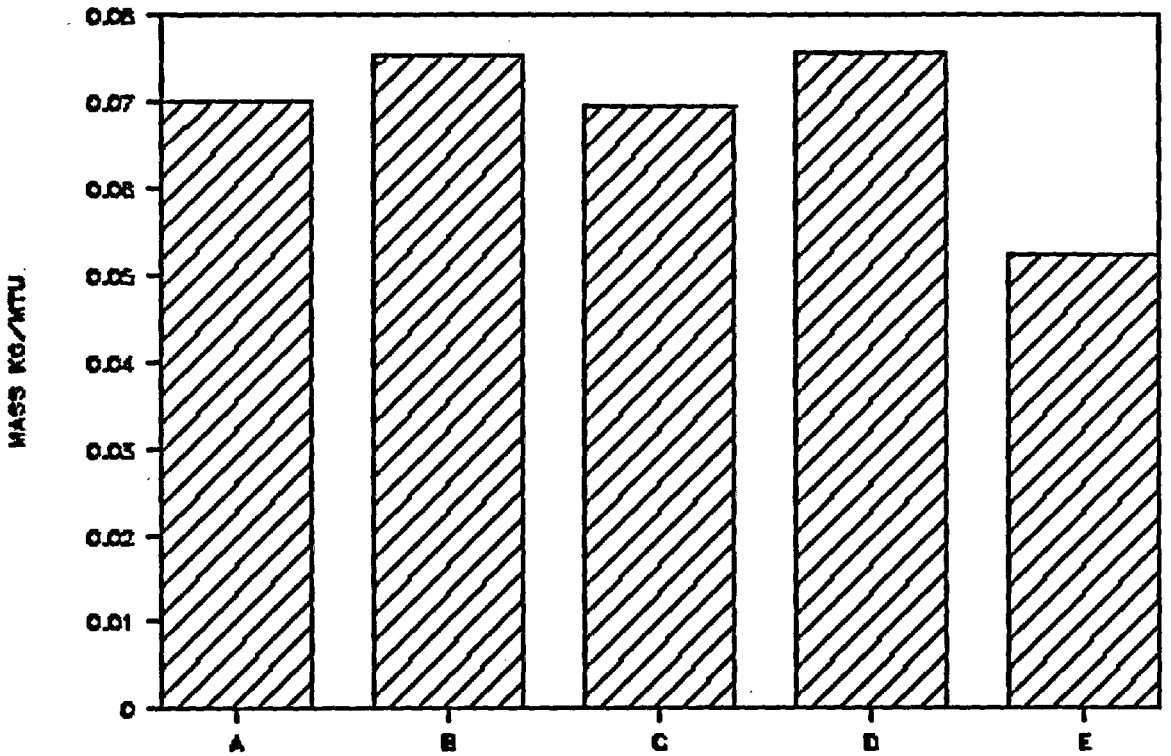

Note: A = ORIGEN-calculated results for H.B. Robinson 2, using existing cross-sections

B = ORIGEN-calculated results for H.B. Robinson 2, using newly generated cross-sections

C = ORIGEN-calculated results for Turkey Point 3, using existing cross-sections

D = ORIGEN-calculated results for Turkey Point 3, using newly generated cross-sections

E = Average of H.B. Robinson 2 and Turkey Point 3 measured data

Figure 3-36

^{137}Cs – ORIGEN Results vs. Measured Data for Problems 2.4 and 2.5

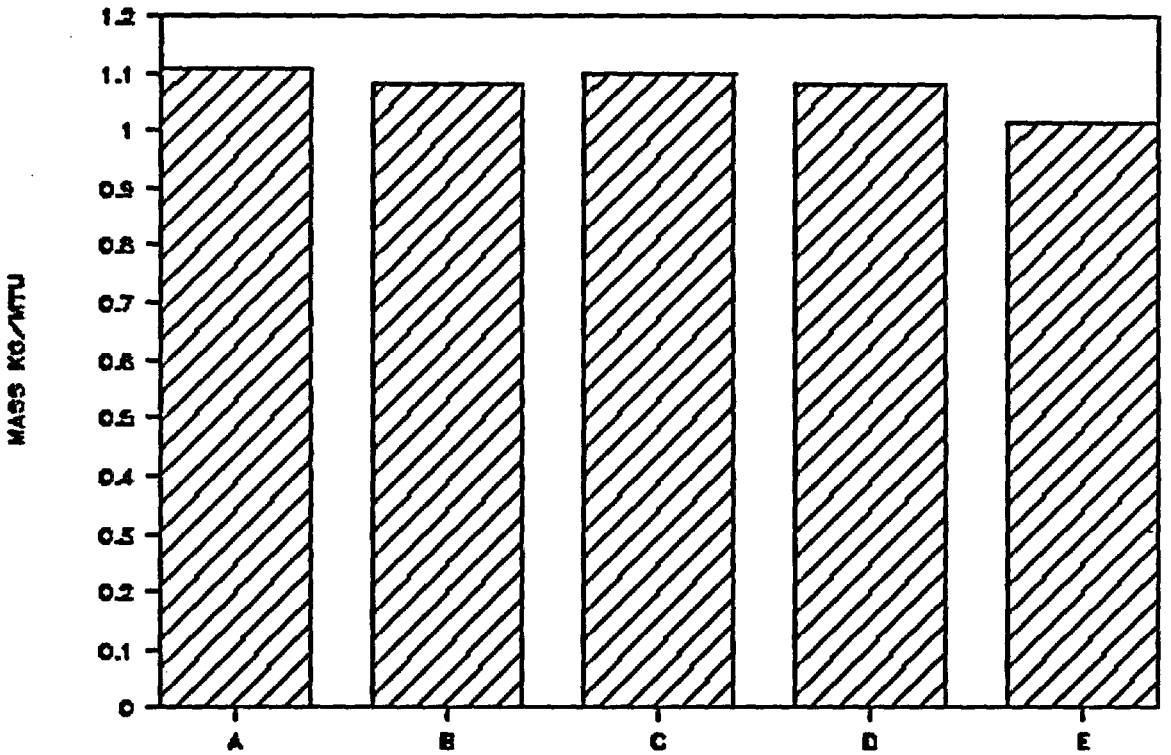

Note: A = ORIGEN-calculated results for H.B. Robinson 2, using existing cross-sections

B = ORIGEN-calculated results for H.B. Robinson 2, using newly generated cross-sections

C = ORIGEN-calculated results for Turkey Point 3, using existing cross-sections

D = ORIGEN-calculated results for Turkey Point 3, using newly generated cross-sections

E = Average of H.B. Robinson 2 and Turkey Point 3 measured data

Figure 3-37

^{144}Ce – ORIGEN Results vs. Measured Data for Problems 2.4 and 2.5

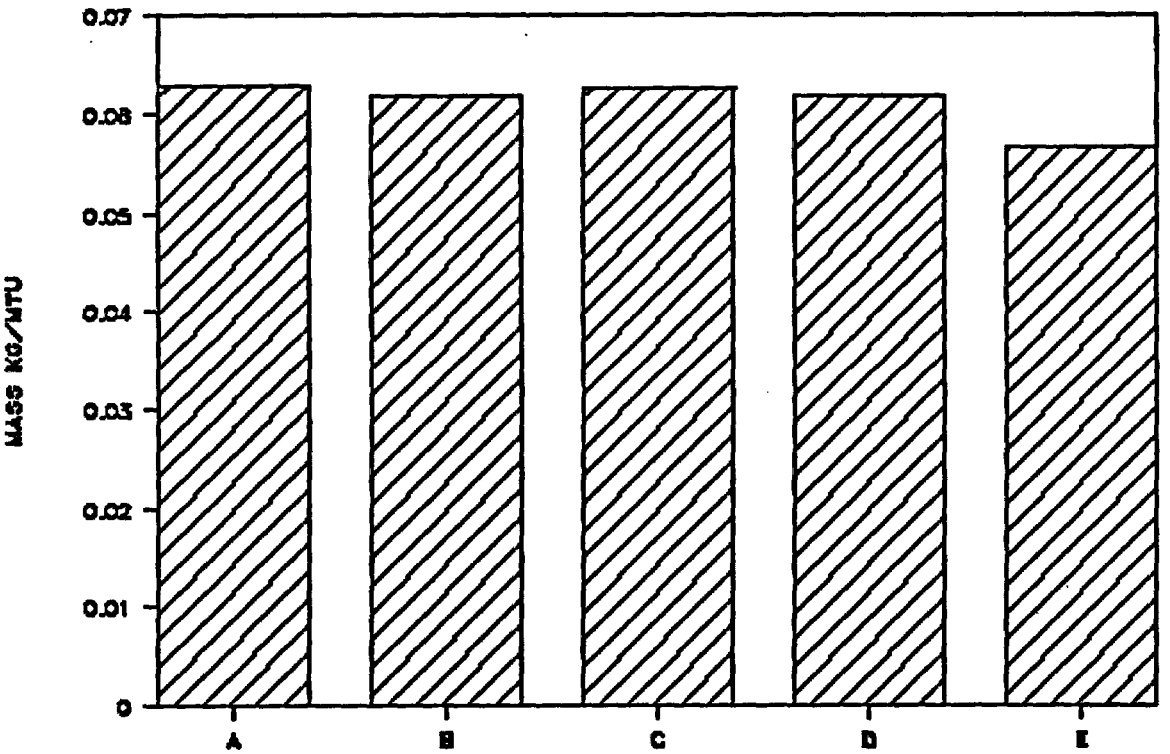

Note: A = ORIGEN-calculated results for H.B. Robinson 2, using existing cross-sections

B = ORIGEN-calculated results for H.B. Robinson 2, using newly generated cross-sections

C = ORIGEN-calculated results for Turkey Point 3, using existing cross-sections

D = ORIGEN-calculated results for Turkey Point 3, using newly generated cross-sections

E = Average of H.B. Robinson 2 and Turkey Point 3 measured data

Figure 3-38

^{3}H – ORIGEN Results vs. Measured Data for Problems 2.4 and 2.5

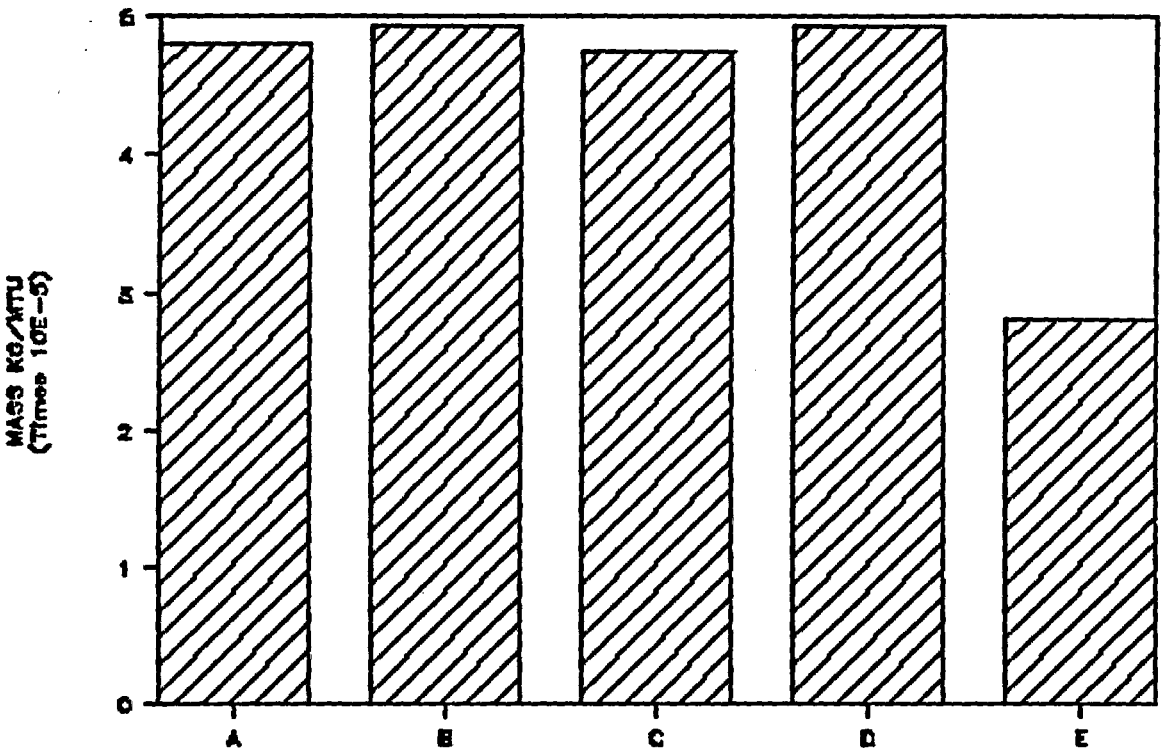

Note: A = ORIGEN-calculated results for H.B. Robinson 2, using existing cross-sections

B = ORIGEN-calculated results for H.B. Robinson 2, using newly generated cross-sections

C = ORIGEN-calculated results for Turkey Point 3, using existing cross-sections

D = ORIGEN-calculated results for Turkey Point 3, using newly generated cross-sections

E = Average of H.B. Robinson 2 and Turkey Point 3 measured data

Figure 3-39

^{129}I – ORIGEN Results vs. Measured Data for Problems 2.4 and 2.5

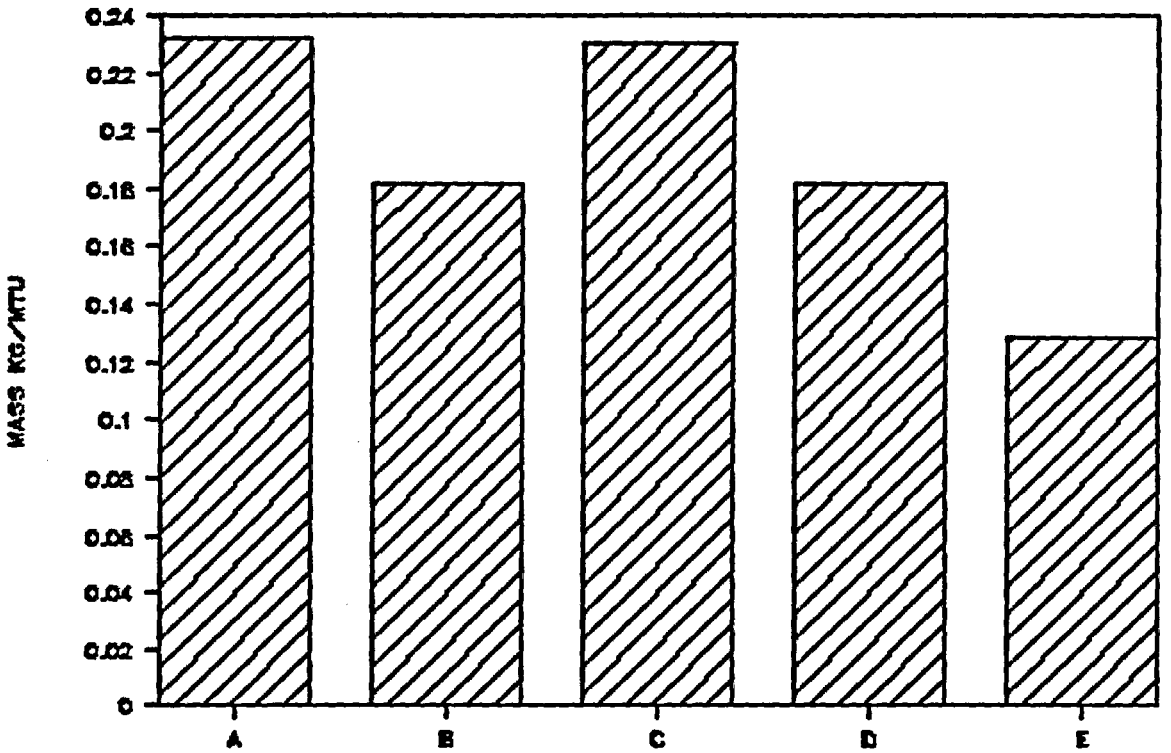

Note: A = ORIGEN-calculated results for H.B. Robinson 2, using existing cross-sections

B = ORIGEN-calculated results for H.B. Robinson 2, using newly generated cross-sections

C = ORIGEN-calculated results for Turkey Point 3, using existing cross-sections

D = ORIGEN-calculated results for Turkey Point 3, using newly generated cross-sections

E = Average of H.B. Robinson 2 and Turkey Point 3 measured data

ORIGEN/S estimates of the concentrations of transplutonic isotopes in spent fuel did not compare favorably with measured values. Differences of 20 to over 300 percent were observed. With the exception of ^{242m}Am, ^{242}Cm, and ^{243}Cm, ORIGEN/S overpredicted transplutonic isotope concentrations. For waste management purposes, then, ORIGEN/S predictions should probably be viewed as conservative.

Comparisons of measured fission product activities with ORIGEN/S predictions showed agreement to within 6 to 75 percent. This disagreement may be due in part to calibration errors of detector instruments when the original measurements were made. It may also be due to isotope removal by chemical interaction: if it is true, as believed, that cesium, iodine, and tritium react preferentially with the zircaloy cladding and may be removed from the fuel pellet during reactor operation, then the removal will be reflected in the measurements of these elements in spent fuel pellets. For the isotopes for which measurements were taken, ORIGEN/S consistently overpredicted the mass of the fission product present.

More accurate calculations of plutonium and transplutonics may require the use of computer programs with more neutron energy groups, with time-varying neutron spectra, and perhaps with a one-dimensional spatial treatment of the neutron flux.

3.2 ANSIDECH/BURNUP

3.2.1 Code Description

The computer programs ANSIDECH and BURNUP were developed to estimate the fission-product thermal energy release from light water reactor fuel. The program ANSIDECH implements American National Standard ANSI/ANS-5.1-1979. The program BURNUP can be used to estimate the fraction of fission events occurring in ^{235}U, ^{238}U, and ^{239}Pu, one of the required inputs to ANSIDECH.

ANSIDECH uses two ANS methods (Reference 6) for computing fission-product afterheat power. One is a simplified and conservative method in which all fissions are assumed to occur in ^{235}U. The other method, a detailed one, accounts for fission in ^{235}U, ^{238}U, and ^{239}Pu. A short review of these two methods follows.

We begin with the detailed method. When the operating history of a reactor can be represented by a histogram of N time intervals with constant power $P_{i\alpha}$ from fissionable nuclide i during irradiation period α, then the fission-product afterheat power (uncorrected for neutron capture) from fissionable nuclide i is given by the following equations:

$$P'_{di}(t,T) = \sum_{\alpha=1}^{N} \frac{P_{i\alpha} F_i(t_\alpha, T_\alpha)}{Q_i} \qquad (3.2.1)$$

$$t_1 = t,\ t_2 = t + T_1,\ \ldots,\ t_N = t + \sum_{\alpha=1}^{N-1} T_\alpha \qquad (3.2.2)$$

$$T = \sum_{\alpha=1}^{N} T_\alpha\ , \qquad (3.2.3)$$

where

T_α = the duration of irradiation period α (s)

t_α = the elapsed time after irradiation period α (s)

T_α = the time after cessation of fission(s)

Q_i = total recoverable energy per fission for nuclide i (MeV per fission)

The value of Q_i includes fission fragment and neutron kinetic energy, prompt gamma energy, the energy of gamma and beta radiation from complete decay of fission products, and the energy of gamma and beta radiation from capture reactions in all fuel, coolant, and structural materials. The units of $P_{i\alpha}$ and P'_{di} must be the same. In Equation 3.2.1, F_i, the decay heat power t_α seconds after an irradiation period of T_α seconds, is found from

$$F_i(t_\alpha, T_\alpha) = F_i(t_\alpha, \infty) - F_i(t_\alpha + T_\alpha, \infty) \qquad (3.2.4)$$

The values of F_i (t_α,) for ^{235}U, ^{238}U, and ^{239}Pu can be calculated from formulas given in Tables 3-20, 3-21, and 3-22.

The total fission-product afterheat power is given by

$$P_d(t,T) = P'_d(t,T) \cdot G(t) \qquad (3.2.5)$$

$$P'_d(t,T) = \sum_{i=1}^{3} P'_{di}(t,T), \qquad (3.2.6)$$

Table 3-20

Parameters for ^{235}U Thermal Fission Function F(t,T)*

α	λ
6.5057E-01**	2.2138E+01
5.1264E-01	5.1587E-01
2.4384E-01	1.9594E-01
1.3850E-01	1.0314E-01
5.5440E-02	3.3656E-02
2.2225E-02	1.1681E-02
3.3088E-03	3.5870E-03
9.3015E-04	1.3930E-03
8.0943E-04	6.2630E-04
1.9567E-04	1.8906E-04
3.2535E-05	5.4988E-05
7.5595E-06	2.0958E-05
2.5232E-06	1.0010E-05
4.9948E-07	2.5438E-06
1.8531E-07	6.6361E-07
2.6608E-08	1.2290E-07
2.2398E-09	2.7213E-08
8.1641E-12	4.3714E-09
8.7797E-11	7.5780E-10
2.5131E-14	2.4786E-10
3.2176E-16	2.2384E-13
4.5038E-17	2.4600E-14
7.4791E-17	1.5699E-14

Source: Reference 6. (Table extracted from American National Standard ANSI/ANS-5.1-1979 with permission of the publishers, the American Nuclear Society.)

* $F(t,T) = \sum_{i=1}^{23} \frac{\alpha_i}{\lambda_i} e^{-\lambda_i t} (1-e^{-\lambda_i T})$ MeV/Fission

$F(T,\infty) = F(t,10^{13})$

t and T in seconds

** Read as 6.5057×10^{-1}.

Table 3-21

Parameters for ^{238}U Fast Fission Function F(t,T)*

α	λ
1.2311E+0**	3.2881E+0
1.1486E+0	9.3805E-1
7.0701E-1	3.7073E-1
2.5209E-1	1.1118E-1
7.1870E-2	3.6143E-2
2.8291E-2	1.3272E-2
6.8382E-3	5.0133E-3
1.2322E-3	1.3655E-3
6.8409E-4	5.5158E-4
1.6975E-4	1.7873E-4
2.4182E-5	4.9032E-5
6.6356E-6	1.7058E-5
1.0075E-6	7.0465E-6
4.9894E-7	2.3190E-6
1.6352E-7	6.4480E-7
2.3355E-8	1.2649E-7
2.8094E-9	2.5548E-8
3.6236E-11	8.4782E-9
6.4577E-11	7.5130E-10
4.4963E-14	2.4188E-10
3.6654E-16	2.2739E-13
5.6293E-17	9.0536E-14
7.1602E-17	5.6098E-15

Source: Reference 6. (Table extracted from American National Standard ANSI/ANS-5.1-1979 with permission of the publishers, the American Nuclear Society.)

* $F(t,T) = \sum_{i=1}^{23} \frac{\alpha_i}{\lambda_i} e^{-\lambda_i t} (1-e^{-\lambda_i T})$ MeV/Fission

$F(T,\infty) = F(t,10^{13})$

t and T in seconds

** Read as 1.2311×10^{0}.

Table 3-22

Parameters for ^{239}Pu Thermal Fission Function F(t,T)*

α	λ
2.083E-01**	1.002E+01
3.853E-01	6.433E-01
2.213E-01	2.186E-01
9.460E-02	1.004E-01
3.531E-02	3.728E-02
2.292E-02	1.435E-02
3.946E-03	4.549E-03
1.317E-03	1.328E-03
7.052E-04	5.356E-04
1.432E-04	1.730E-04
1.765E-05	4.881E-05
7.347E-06	2.006E-05
1.747E-06	8.319E-06
5.481E-07	2.358E-06
1.671E-07	6.450E-07
2.112E-08	1.278E-07
2.996E-09	2.466E-08
5.107E-11	9.378E-09
5.730E-11	7.450E-10
4.138E-14	2.426E-10
1.088E-15	2.210E-13
2.454E-17	2.640E-14
7.557E-17	1.380E-14

Source: Reference 6. (Table extracted from American National Standard ANSI/ANS-5.1-1979 with permission of the publishers, the American Nuclear Society.)

* $F(t,T) = \sum_{i=1}^{23} \frac{\alpha_i}{\lambda_i} e^{-\lambda_i t} (1-e^{-\lambda_i T})$ MeV/Fission

$F(T,\infty) = F(t,10^{13})$

t and T in seconds

** Read as 2.083×10^{-1}.

with i = 1,2,3 representing ^{235}U (thermal fission), ^{239}U (fast fission), and ^{238}Pu (thermal fission). Here, ^{235}U includes all other fissionable nuclides not explicitly mentioned (i.e., all others are assumed to behave as does ^{235}U). G(t) is a correction factor used to account for neutron capture in fission products. For shutdown times of $t < 10^4$ s, operating times of $T < 1.2614 \times 10^8$ s (four years), and $\psi < 3.0$, G(t) is found from

$$G(t) = 1.0 + (3.24 \times 10^{-6} + 5.23 \times 10^{-10} t) T^{0.4} \psi, \qquad (3.2.7)$$

where ψ is the number of fissions per initial fissile atom. For shutdown times in the range of $10^4 < t < 10^9$ s, Table 3-23 provides a tabulation of the maximum correction factors, $G_{max}(t)$, to apply.

The decay heat power should also be obtained by using the following simplified method. It is assumed that the decay heat power from fissile isotopes other than ^{235}U is identical to that of ^{235}U and that the fission rate is constant over the operating history of the level corresponding to the maximum power P_{max}. Only the infinite operating period data for ^{235}U are used. This simplified method overestimates decay heat power, especially with respect to LWR cores containing an appreciable amount of plutonium.

For finite reactor operating time, T, the decay heat power without neutron absorption in fission products is

$$P'_d(t,T) = 1.02 \frac{P_{max}}{Q} \left[F(t,\infty) - F(t+T,\infty) \right], \qquad (3.2.8)$$

where F and Q are for ^{235}U.

Table 3-23

Ratio of Decay Heat with Absorption to Values without Absorption*

Time after Shutdown (sec)	$G_{max}(t)$	Time after Shutdown (sec)	$G_{max}(t)$
1.0	1.020	1.5E+5	1.130
1.5	1.020	2.0E+5	1.131
2.0	1.020	4.0E+5	1.126
4.0	1.021	6.0E+5	1.124
6.0	1.022	8.0E+5	1.123
8.0	1.022	1.0E+6	1.124
1.0E+1	1.022	1.5E+6	1.125
1.5E+1	1.022	2.0E+6	1.127
2.0E+1	1.022	4.0E+6	1.134
4.0E+1	1.022	6.0E+6	1.146
6.0E+1	1.022	8.0E+6	1.162
8.0E+1	1.022	1.0E+7	1.181
1.0E+2	1.023	1.5E+7	1.233
1.5E+2	1.024	2.0E+7	1.284
2.0E+2	1.025	4.0E+7	1.444
4.0E+2	1.028	6.0E+7	1.535
6.0E+2	1.030	8.0E+7	1.586
8.0E+2	1.032	1.0E+8	1.598
1.0E+3	1.033	1.5E+8	1.498
1.5E+3	1.037	2.0E+8	1.343
2.0E+3	1.039	4.0E+8	1.065
4.0E+3	1.048	6.0E+8	1.021
6.0E+3	1.054	8.0E+8	1.012
8.0E+3	1.060	1.0E+9	1.007
1.0E+4	1.064		
1.5E+4	1.074		
2.0E+4	1.081		
4.0E+4	1.098		
6.0E+4	1.111		
8.0E+4	1.119		
1.0E+5	1.124		

Source: Reference 6. (Table extracted from American National Standard ANSI/ANS-5.1-1979 with permission of the publishers, the American Nuclear Society.)

* Ratio based on following assumptions: ^{235}U thermal fission for four years; no depletion; typical LWR spectrum.

The computer program BURNUP implements the five-step method outlined below to estimate the relative power from ^{235}U, ^{238}U, and ^{239}Pu. This method is based on the observation that $P_{i\alpha}/Q_i = N'_{i\alpha}$, where $N'_{i\alpha}$ is the number of fissions of nuclide i in time period .

Step 1. Beginning with the first irradiation period, estimate the cumulative number of fissions, N_α, by all nuclides through the end of the irradiation period by the following expression:

$$N_\alpha = \frac{5.3930 \times 10^{23}}{\bar{Q}_\alpha} B_\alpha \qquad (3.2.9)$$

where N_α is the total number of fissions per kilogram of uranium, B_α is the fuel burnup in units of MWD/kgU, and $\bar{Q}_\alpha$ is the burnup averaged energy in MeV for all fissions of all isotopes through the end of irradiation period α. The constant in Equation 3.2.9 is obtained as follows:

$$5.3930 \times 10^{23} = \frac{1 \text{ MeV}}{1.60209 \times 10^{-13} \text{ watt-sec}} \cdot \frac{86400 \text{ sec}}{\text{day}} \cdot \frac{10^6 \text{ watts}}{1 \text{ MW}} \qquad (3.2.10)$$

Tables 3-24 and 3-25 provide correlations that can be used to estimate the value of $\bar{Q}_\alpha$ for pressurized water reactors and boiling water reactors, respectively.

Step 2. Estimate the cumulative number of fissions by ^{238}U and ^{239}Pu through the end of irradiation period α using the correlations given in Tables 3-24 and 3-25 for PWRs and BWRs, respectively.

Table 3-24

Correlations for Average MeV/Fission and Total ^{238}U and ^{239}Pu Atoms Fissioned for PWRs

---

Average MeV/fission:

$$\bar{Q}_\alpha = 200 + 5.2342\, E^{-1.0858}\, B_\alpha^{\,.11559 \ln B_\alpha}$$

Total atoms fissioned per kgU:

for ^{238}U

$$N_{i\alpha} = 1.7038 \times 10^{20}\, E^{-.17202}\, B_\alpha^{\,1.0574}$$

for ^{239}Pu

$$N_{i\alpha} = 2.7165 \times 10^{20}\, E^{-.90385}\, B_\alpha^{\,1.6125}$$

E = ^{235}U enrichment in weight percent

B_α = burnup in MWD/kgU at the end of time period α

Note: These correlations are based on results of CorSTAR analyses of 15x15 Westinghouse fuel assemblies using a version of the code LEOPARD. The correlations were developed for the following range of parameters:

$$1.5 \leq E \leq 3.5$$

$$1 \leq B_\alpha \leq 5 + 10 \cdot E$$

Table 3-25

Correlations for Average MeV/Fission and Total ^{238}U and ^{239}Pu Atoms Fissioned for BWRs

---

Average MeV/fission:

$$\bar{Q}_\alpha = 200 + 8.2112E^{(-.35234)}\, V_\alpha^{(.045316)}\, B_\alpha^{(.066524 + .027002\, \ln B_\alpha)}$$

Total atoms fissioned per kgU:*

for ^{238}U

$$N_{i\alpha} = 1.7923 \times 10^{20}\, E^{-.24103}\, B_\alpha^{1.0583} \qquad (V=20\%)$$

$$N_{i\alpha} = 1.5603 \times 10^{20}\, E^{-.26939}\, B_\alpha^{1.0587} \qquad (V=50\%)$$

for ^{239}Pu

$$N_{i\alpha} = 1.9941 \times 10^{20}\, E^{-1.0176}\, B_\alpha^{1.7198} \qquad (V=20\%)$$

$$N_{i\alpha} = 1.8505 \times 10^{20}\, E^{-1.1043}\, B_\alpha^{1.7499} \qquad (V=50\%)$$

E = ^{235}U enrichment in weight percent

B_α = burnup in MWD/kgU at time α

V_α = exposure average void percentage at time α

If V_α is not known, use V_α = 35% as the best estimate and V_α = 50% for a conservative estimate

---

Note: These correlations are based on results of CorSTAR analyses of 8x8 General Electric fuel assemblies using a version of the code LEOPARD. The correlations were developed for the following range of parameters:

$$1.1 \leq E \leq 3.5$$

$$1 \leq B_\alpha \leq 5 + 10 \cdot E$$

* To estimate the number of atoms fissioned for average void percentages between 20% and 50%, use linear interpolation.

Step 3. Calculate the cumulative number of ^{235}U fissions through the end of irradiation period α by subtracting the total number of ^{238}U and ^{239}Pu fissions calculated in Step 2 above from the total number of all fissions of all nuclides calculated in Step 1.

Step 4. For each of the nuclides, ^{235}U, ^{238}U, and ^{239}Pu, calculate the number of fissions that occur during irradiation period α by subtracting the total number of fissions that occurred through the end of time step α - 1 from the total number that occurred through the end of time step α.

$$N_{i\alpha}' = N_{i\alpha} - N_{i\alpha-1} \qquad (3.2.11)$$

Step 5. Repeat steps 1 through 4 for each irradiation period.

3.2.2 Description of Benchmark Problems

ANSIDECH/BURNUP was used to estimate the decay thermal power for benchmark problems 2.1, 2.2, and 2.3. See Section 3.1.2 for a description of these problems.

3.2.3 Benchmarking Results and Conclusions

3.2.3.1 Pressurized Water Reactor Afterheat Generation — ANS Standard (Benchmark Problem 2.1)

Results of ANSIDECH/BURNUP predictions of decay thermal power are summarized in Table 3-26. Compared with ORIGEN/S calculations, for time periods

Table 3-26

Decay Thermal Power Prediction, in Watts

Problem Number	Time (Years)	ORIGEN Prediction Using Generated Cross-Sections	ANSI-Short Method w/o G-Fctr	ANSI-Short Method w/ G-Fctr	ANSI-Long Method w/o G-Fctr	ANSI-Long Method w/ G-Fctr
2.1.1	1	6550	5546	7681	6169	8544
	3	1690	1284	2052	1453	2323
	10	405	453	506	382	426
	30	228	273	275	228	230
	100	43.7	51.1	51.1	43.1	43.1
	300	0.426	0.445	0.445	0.394	0.394
	1000	0.00812	0.00206	0.00206	0.00371	0.00371
	3000	0.008	0.00192	0.00192	0.00348	0.00348
	10000	0.00771	0.00192	0.00192	0.0034	0.0034
2.1.2	1	8600	8033	11127	8029	11121
	3	2560	2139	3419	2053	3282
	10	711	881	983	658	734
	30	396	532	536	395	398
	100	75.4	99.6	99.6	74.5	74.5
	300	0.733	0.867	0.867	0.677	0.677
	1000	0.0134	0.004	0.004	0.00599	0.00599
	3000	0.0132	0.00381	0.00381	0.00568	0.00568
	10000	0.0127	0.00366	0.00366	0.00545	0.00545
2.1.3	1	10500	9474	13122	7257	10051
	3	3350	2835	4533	2159	3452
	10	983	1328	1481	888	990
	30	533	803	810	535	540
	100	101	150	150	101	101
	300	0.978	1.31	1.31	0.914	0.914
	1000	0.0178	0.0061	0.0061	0.0077	0.0077
	3000	0.0175	0.00581	0.00581	0.00735	0.00735
	10000	0.0169	0.00561	0.00561	0.00701	0.00701
2.1.4	1	9260	6936	9607	7649	10595
	3	3070	2094	3347	2221	3551
	10	937	990	1104	854	953
	30	509	599	603	514	518
	100	96.7	112	112	97.1	97.1
	300	0.936	0.975	0.975	0.88	0.88
	1000	0.0174	0.00457	0.00457	0.00756	0.00756
	3000	0.0166	0.00436	0.00436	0.00725	0.00725
	10000	0.0163	0.00421	0.00421	0.00695	0.00695
2.1.5	1	9550	9100	12604	7611	10542
	3	3110	2747	4392	2181	3486
	10	931	1298	1448	855	953
	30	506	785	792	515	519
	100	96.1	147	147	97.2	97.2
	300	0.93	1.28	1.28	0.881	0.881
	1000	0.0172	0.006	0.006	0.00749	0.00749
	3000	0.017	0.00571	0.00571	0.00736	0.00736
	10000	0.0164	0.00552	0.00552	0.006967	0.006967

ranging from 1 to 30 years following shutdown, the ANS Standard with G-factor corrections provides a conservative estimate of decay heat. For time periods of 30 to 100 years following shutdown, the ANS Standard provides a realistic estimate of decay heat, typically within plus 5 percent to minus 2 percent of ORIGEN/S predictions. From 100 to 300 years following shutdown, the ANS Standard slightly underestimates decay heat generation, by as much as 5 percent to 8 percent. After 300 years, generally considered the end of significant heat generation, the ANS Standard predictions begin to deviate from ORIGEN/S predictions.

Figures 3-40 through 3-44 show the predicted decay heat values using the ANS Standard methods for the five subproblems of benchmark problem 2.1. Figures 3-45 through 3-48 show the relative differences between the predictions using the different ANS Standard methods and the predictions using the code ORIGEN/S.

Sensitivity analyses using the ANSIDECH program indicate that the decay heat generation rate after 10 years of cooling is relatively insensitive to reactor operating conditions. For the fuel assemblies and ranges of operating conditions examined, a variation of less than plus or minus 4 percent in decay heat generation was seen for typical variations in reactor power levels and irradiation histories. The principal variables governing decay heat generation rate after 10 years of cooling are fuel assembly burnup, initial enrichment, and time in the reactor. The time-dependent power history of the fuel assembly is of secondary importance.

3.2.3.2 Boiling Water Reactor Afterheat Generation — ANS Standard (Benchmark Problem 2.2)

Table 3-27 provides a summary of ANS decay heat predictions for benchmark problem 2.2. For time periods of 1 to 30 years following shutdown, the ANS Standard with G-factor corrections provides a conservative estimate of decay heat. For time periods of 30 to 100 years following shutdown, the ANS Standard provides a realistic estimate of decay heat, typically to within 0 percent to

Figure 3-40

ANSIDECH/BURNUP—Predicted Decay Heat Generation Rate vs. Time for Benchmark Problem 2.1.1

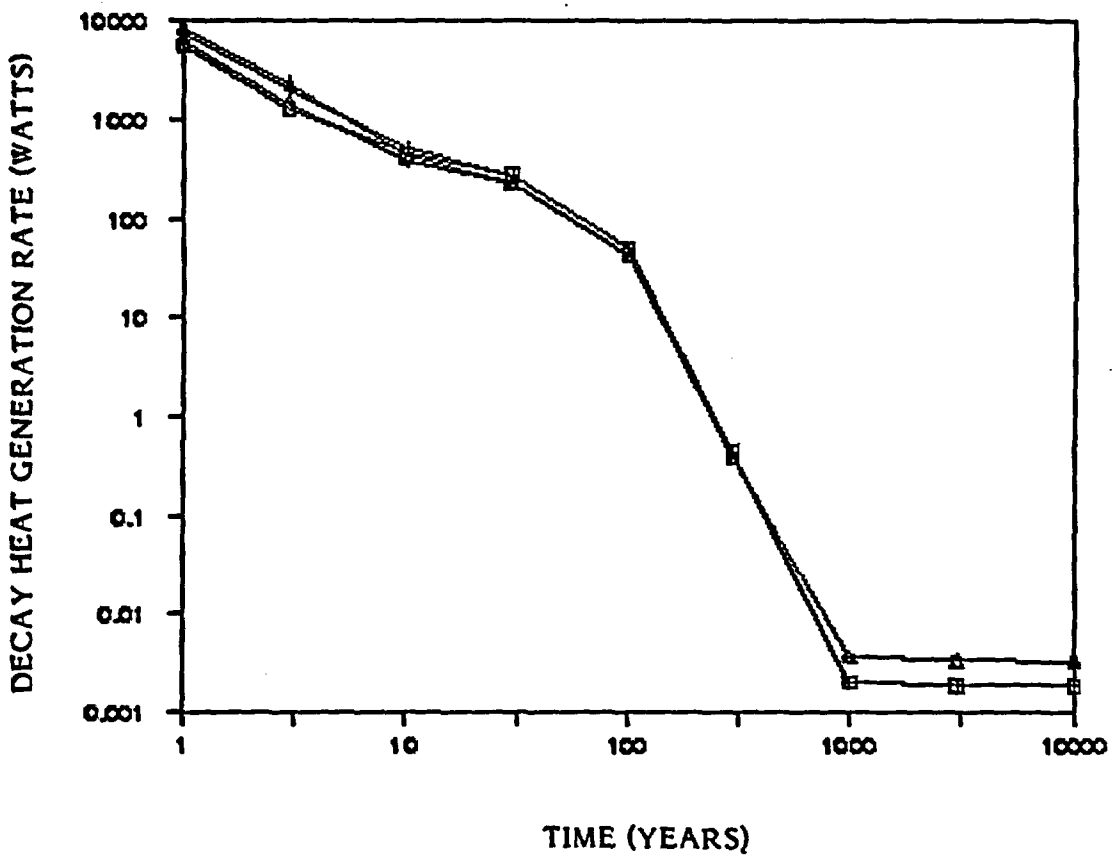

- □ ANSIDECH/BURNUP—predicted value using short method without G-factor
- \+ ANSIDECH/BURNUP—predicted value using short method with G-factor
- ◇ ANSIDECH/BURNUP—predicted value using long method without G-factor
- △ ANSIDECH/BURNUP—predicted value using long method with G-factor

Figure 3-41

ANSIDECH/BURNUP—Predicted Decay Heat Generation Rate vs. Time for Benchmark Problem 2.1.2

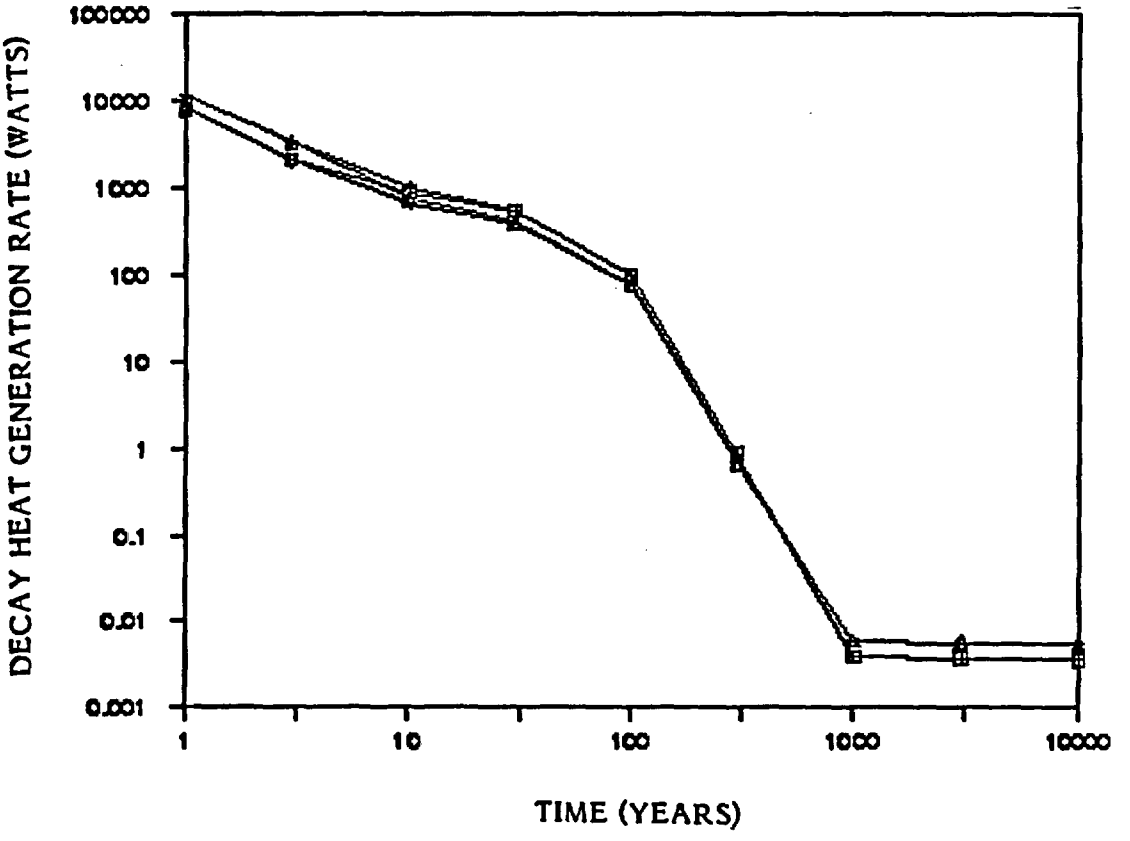

- ▫ ANSIDECH/BURNUP—predicted value using short method without G-factor
- \+ ANSIDECH/BURNUP—predicted value using short method with G-factor
- ◇ ANSIDECH/BURNUP—predicted value using long method without G-factor
- △ ANSIDECH/BURNUP—predicted value using long method with G-factor

Figure 3-42

ANSIDECH/BURNUP—Predicted Decay Heat Generation Rate vs. Time for Benchmark Problem 2.1.3

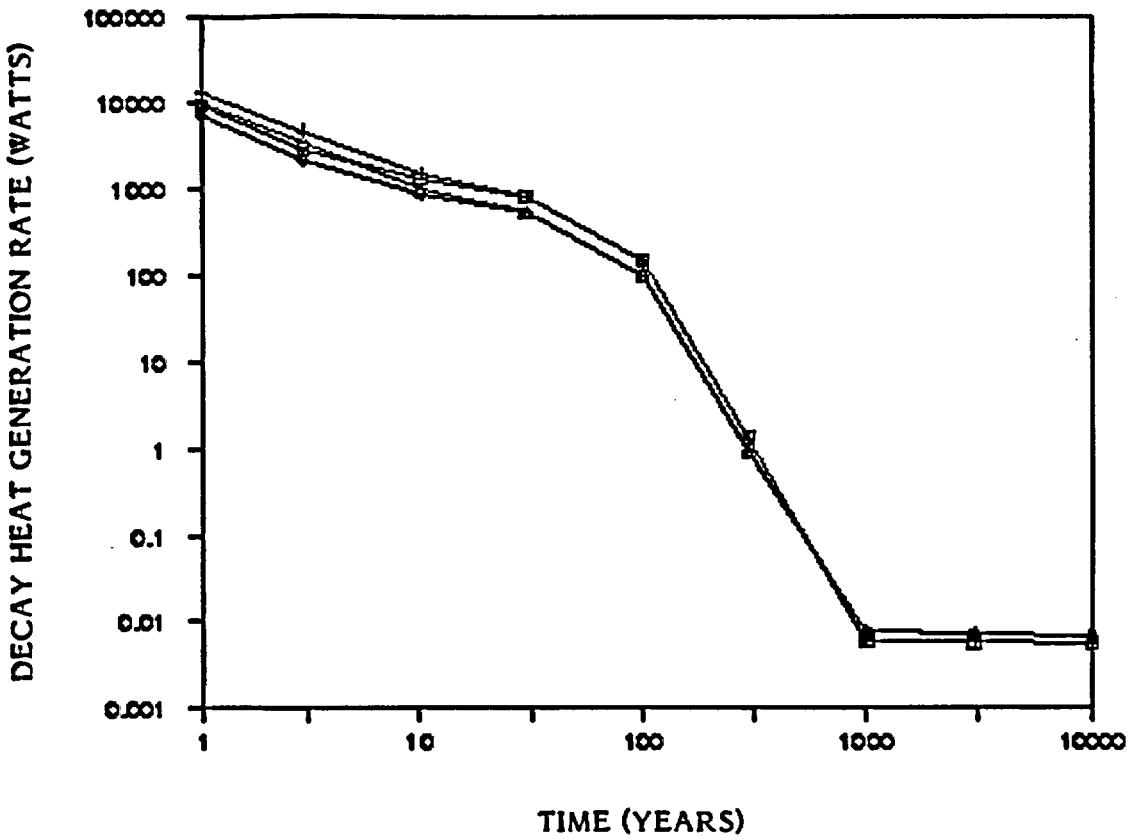

- ▫ ANSIDECH/BURNUP—predicted value using short method without G-factor
- \+ ANSIDECH/BURNUP—predicted value using short method with G-factor
- ◇ ANSIDECH/BURNUP—predicted value using long method without G-factor
- △ ANSIDECH/BURNUP—predicted value using long method with G-factor

Figure 3-43

ANSIDECH/BURNUP—Predicted Decay Heat Generation Rate vs. Time for Benchmark Problem 2.1.4

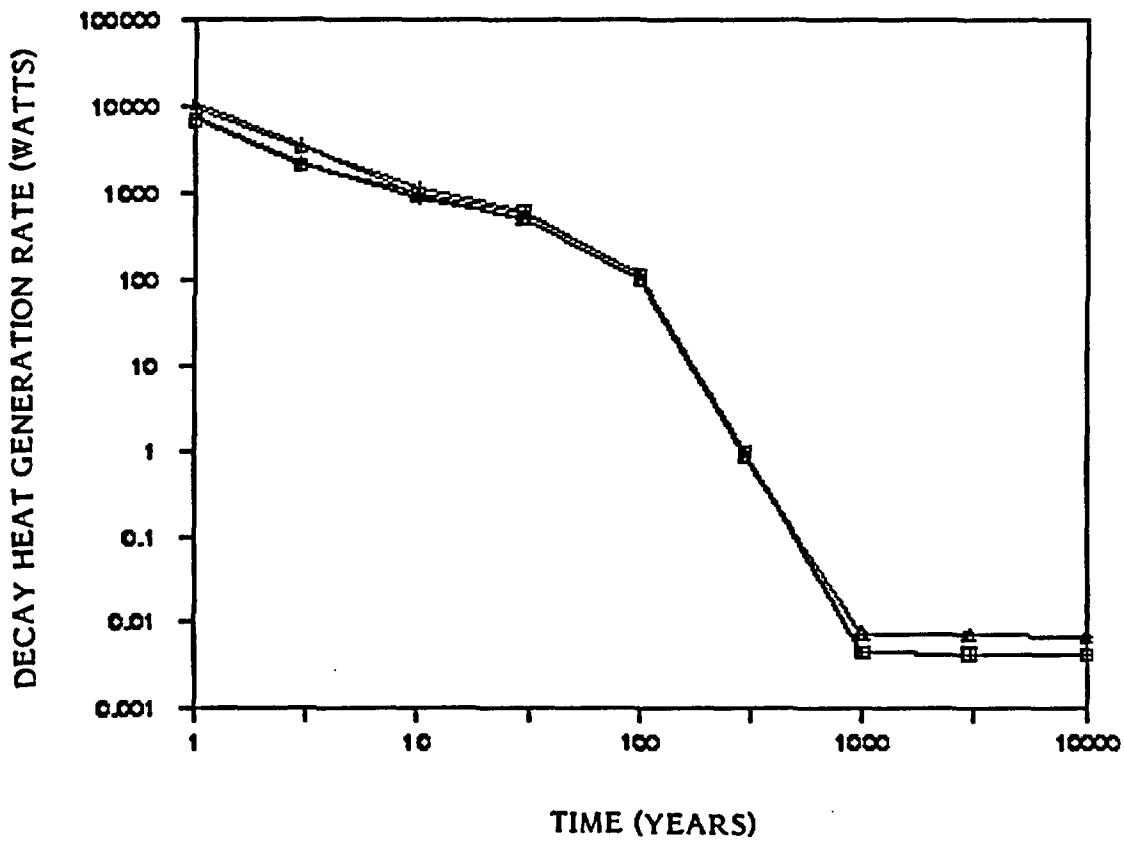

- ANSIDECH/BURNUP—predicted value using short method without G-factor
- \+ ANSIDECH/BURNUP—predicted value using short method with G-factor
- ◇ ANSIDECH/BURNUP—predicted value using long method without G-factor
- △ ANSIDECH/BURNUP—predicted value using long method with G-factor

Figure 3-44

ANSIDECH/BURNUP—Predicted Decay Heat Generation Rate vs. Time for Benchmark Problem 2.1.5

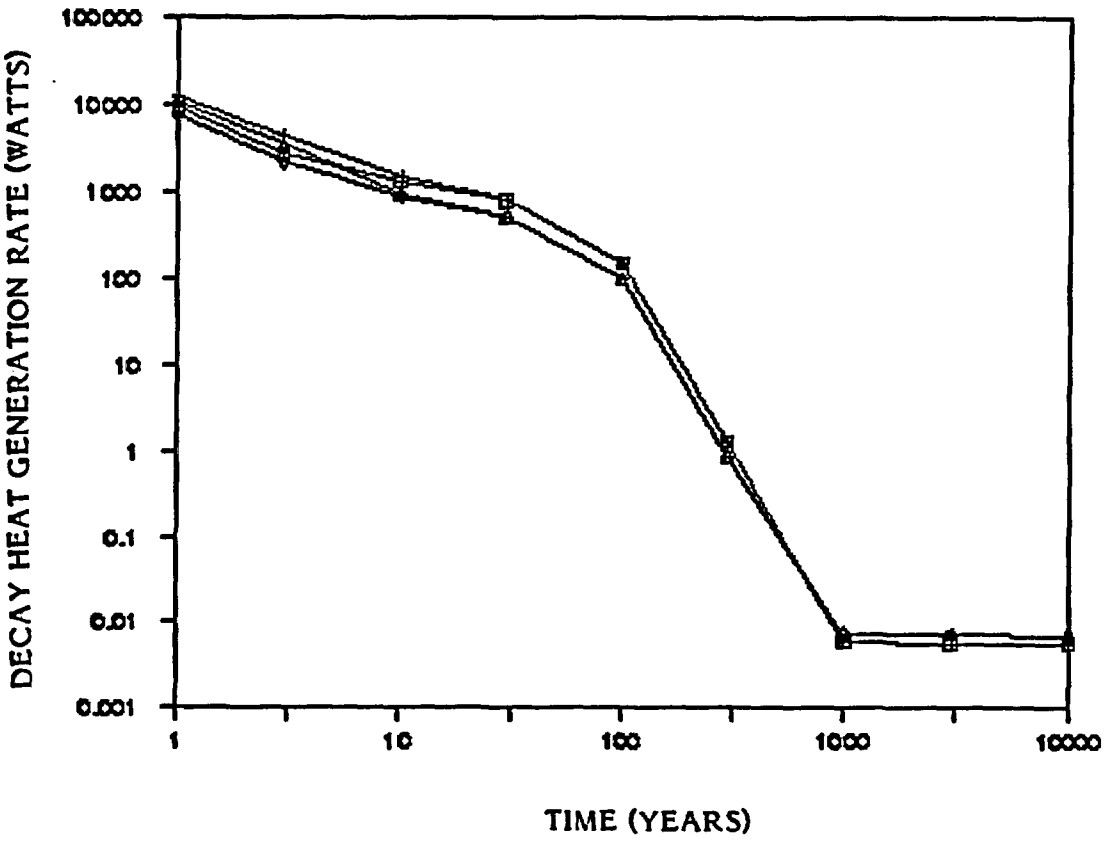

- ▫ ANSIDECH/BURNUP—predicted value using short method without G-factor
- \+ ANSIDECH/BURNUP—predicted value using short method with G-factor
- ◇ ANSIDECH/BURNUP—predicted value using long method without G-factor
- △ ANSIDECH/BURNUP—predicted value using long method with G-factor

Figure 3-45

Comparison of ANSIDECH/BURNUP–Predicted Decay Heat Generation Rates Based on Short Method without G-Factor for Problems 2.1.1 through 2.1.5

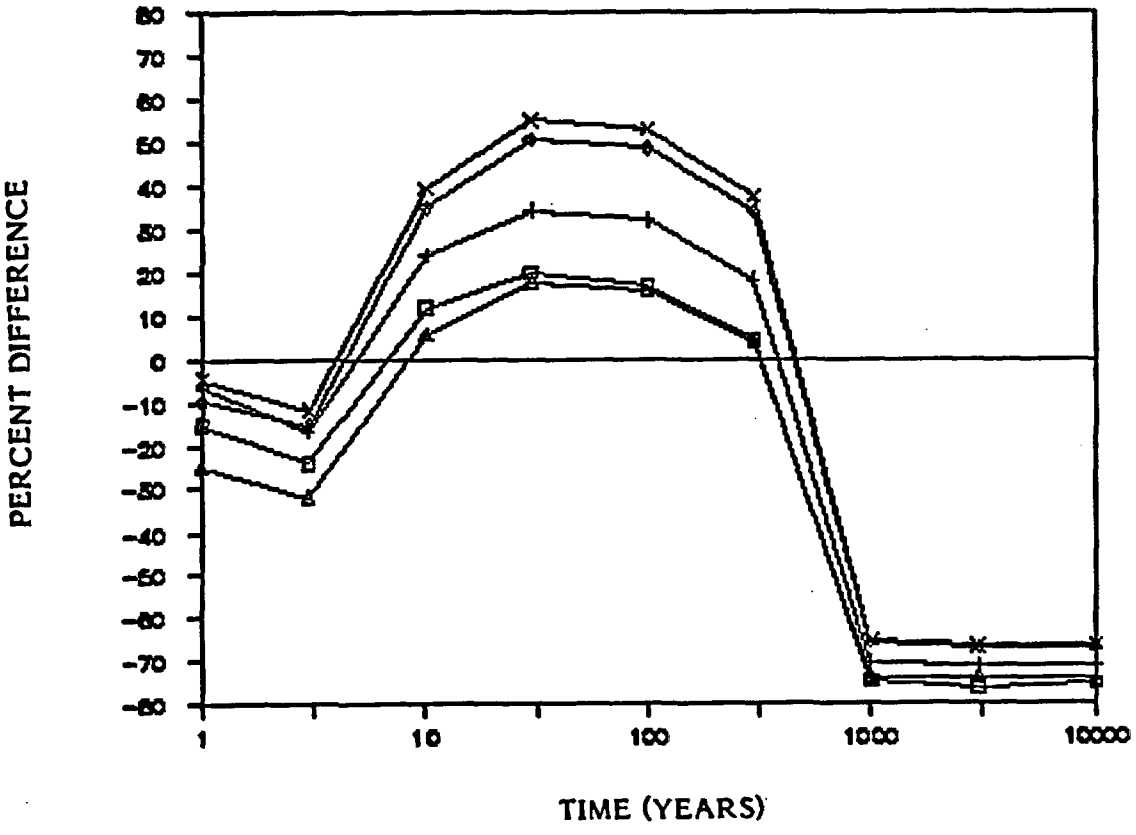

□ Problem 2.1.1
\+ Problem 2.1.2
◇ Problem 2.1.3
△ Problem 2.1.4
× Problem 2.1.5

Figure 3-46

Comparison of ANSIDECH/BURNUP–Predicted Decay Heat Generation Rates Based on Short Method Using G-Factor for Problems 2.1.1 through 2.1.5

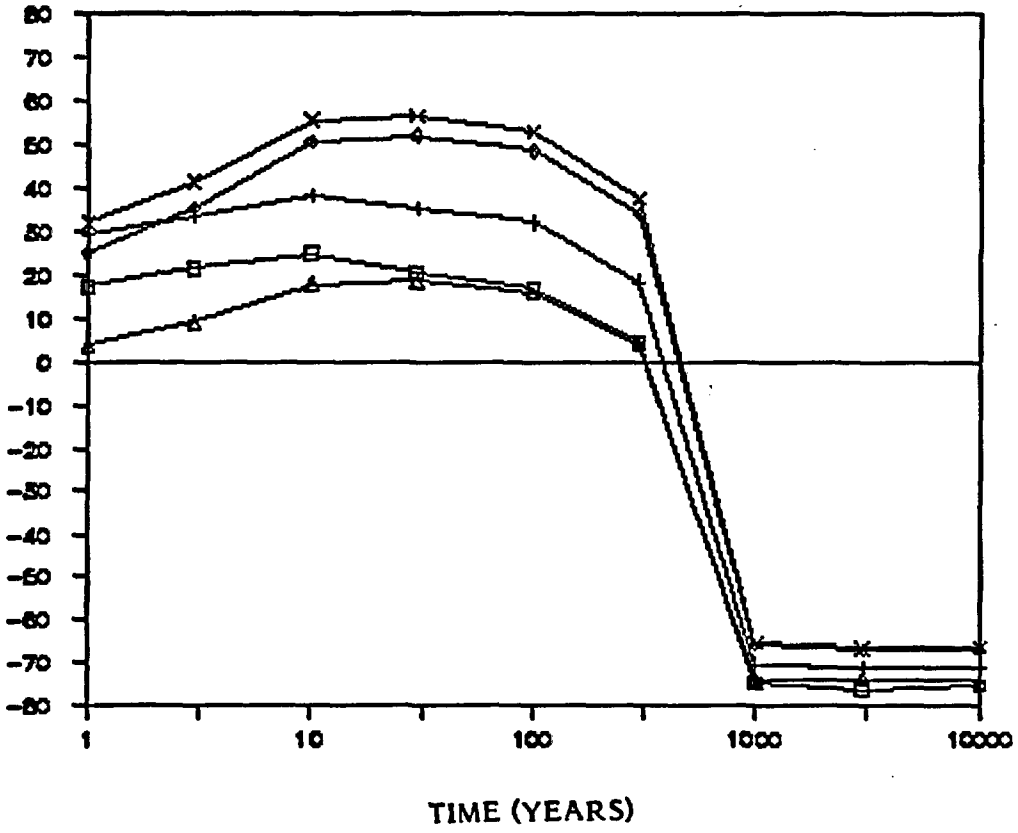

□ Problem 2.1.1
\+ Problem 2.1.2
◇ Problem 2.1.3
△ Problem 2.1.4
× Problem 2.1.5

Figure 3-47

Comparison of ANSIDECH/BURNUP—Predicted Decay Heat Generation Rates Based on Long Method without G-Factor for Problems 2.1.1 through 2.1.5

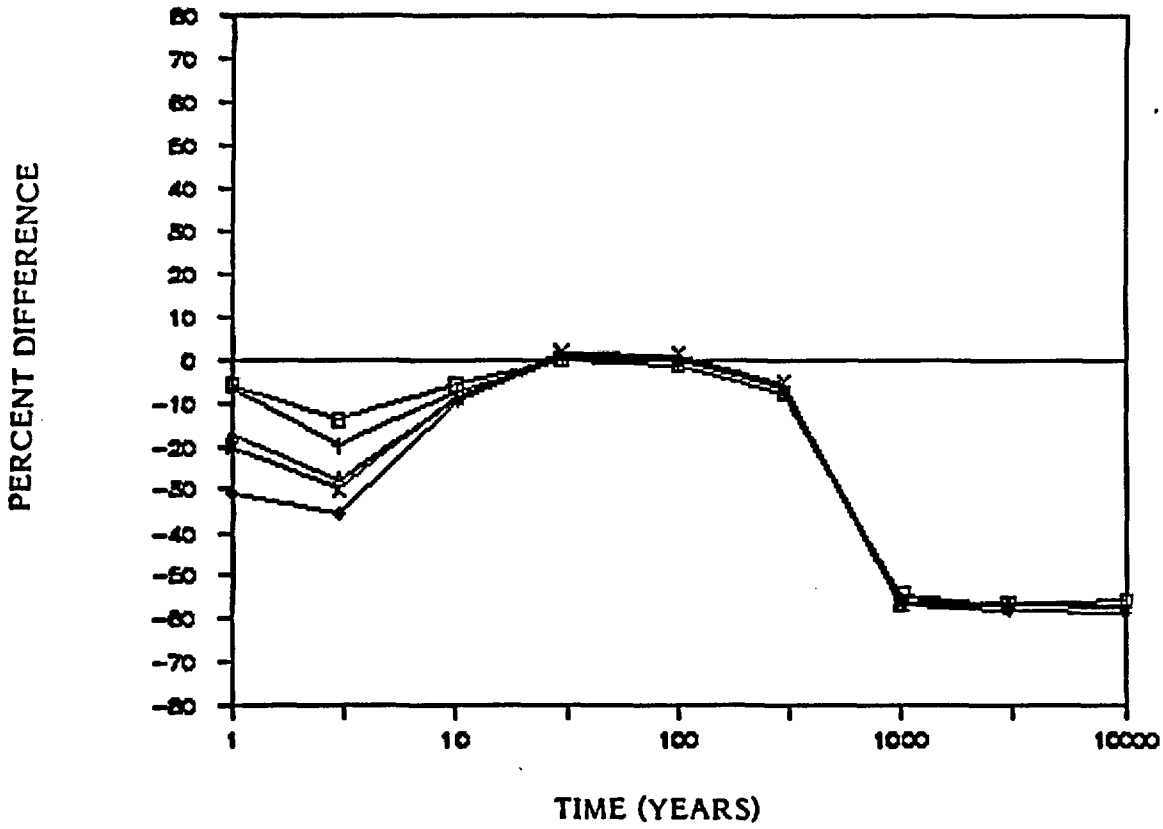

□ Problem 2.1.1
\+ Problem 2.1.2
◇ Problem 2.1.3
△ Problem 2.1.4
× Problem 2.1.5

Figure 3-48

Comparison of ANSIDECH/BURNUP—Predicted Decay Heat Generation Rates Based on Long Method Using G-Factor for Problems 2.1.1 through 2.1.5

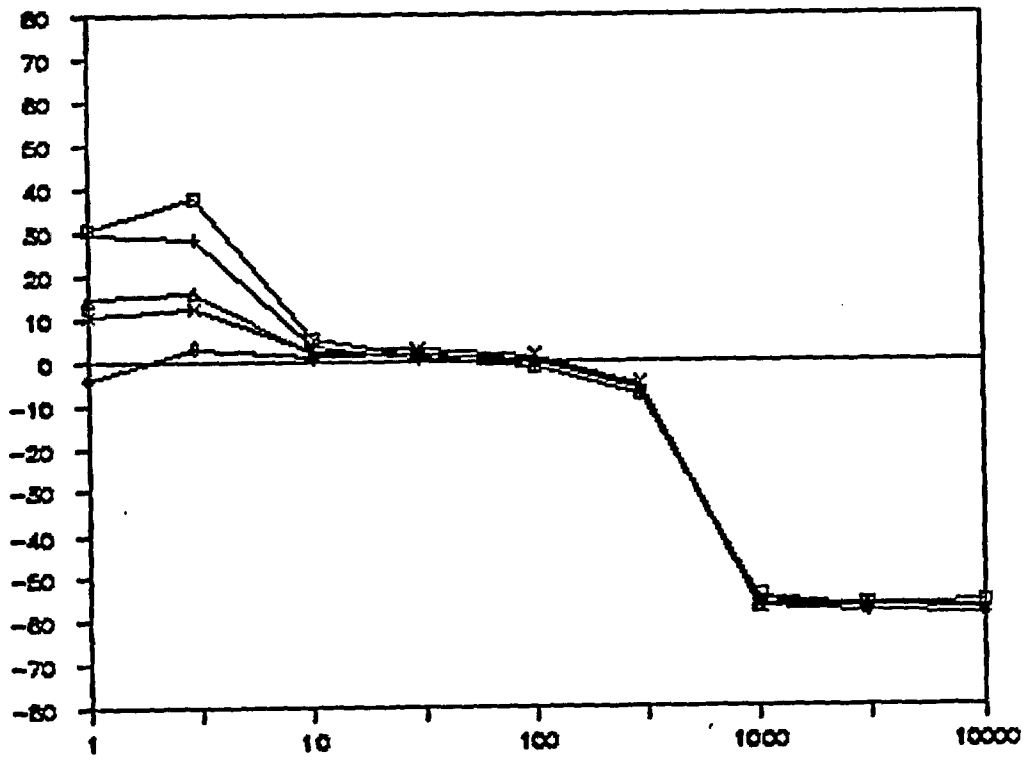

□ Problem 2.1.1
\+ Problem 2.1.2
◇ Problem 2.1.3
△ Problem 2.1.4
× Problem 2.1.5

Table 3-27

Decay Thermal Power Prediction, in Watts

Problem Number	Time (Years)	ANSI-Short Method w/o G-Factor	ANSI-Short Method w/G-Factor	ANSI-Long Method w/o G-Factor	ANSI-Long Method w/G-Factor	ORIGEN Prediction Using Generated Cross-Sections
2.2.1	1	3963	5489	4230	6136	4760
	3	917	1466	1044	1670	1210
	10	324	361	271	303	291
	30	195	197	162	163	165
	100	36.5	36.5	30.6	30.6	31.7
	300	0.318	0.318	0.28	0.28	0.31
	1000	0.00147	0.00147	0.0027	0.0027	0.00601
	3000	0.00137	0.00137	0.00254	0.00254	0.00592
	10000	0.00137	0.00137	0.00248	0.00248	0.00571
2.2.2	1	5477	7586	5338	7393	5760
	3	1458	2331	1370	2191	1670
	10	601	670	469	523	502
	30	363	366	281	284	284
	100	67.9	67.9	53	53	54.5
	300	0.591	0.591	0.475	0.475	0.526
	1000	0.00273	0.00273	0.00363	0.00363	0.00906
	3000	0.0026	0.0026	0.00343	0.00343	0.00893
	10000	0.00249	0.00249	0.0033	0.0033	0.00862
2.2.3	1	6496	8997	4895	6780	7120
	3	1961	3135	1455	2326	2220
	10	927	1034	600	669	664
	30	561	565	361	365	368
	100	105	105	68.3	68.3	70.2
	300	0.913	0.913	0.617	0.617	0.679
	1000	0.00428	0.00428	0.00521	0.00521	0.0125
	3000	0.00408	0.00408	0.00498	0.00498	0.0123
	10000	0.00394	0.00394	0.00476	0.00476	0.0119
2.2.4	1	5413	7498	5933	8218	7250
	3	1634	2613	1726	2760	2370
	10	772	862	672	750	742
	30	467	471	404	408	409
	100	87.4	87.4	76.3	76.3	77.9
	300	0.761	0.761	0.69	0.69	0.754
	1000	0.00357	0.00357	0.00577	0.00577	0.0139
	3000	0.0034	0.0034	0.00553	0.00553	0.0137
	10000	0.00329	0.00329	0.0053	0.0053	0.0132
2.2.5	1	7044	9756	5992	8300	7530
	3	2099	3355	1707	2729	2410
	10	979	1092	673	750	738
	30	592	596	405	408	407
	100	111	111	76.5	76.5	77.5
	300	0.964	0.964	0.691	0.691	0.75
	1000	0.00449	0.00449	0.00568	0.00568	0.0138
	3000	0.00426	0.00426	0.00557	0.00557	0.0136
	10000	0.00415	0.00415	0.00531	0.00531	0.0131
2.2.6	1	7044	9756	6150	8518	7350
	3	2099	3355	1727	2761	2380
	10	979	1092	673	751	737
	30	592	596	406	409	406
	100	111	111	76.5	76.5	77.4
	300	0.964	0.964	0.692	0.692	0.749
	1000	0.00449	0.00449	0.00569	0.00569	0.0138
	3000	0.00426	0.00426	0.00557	0.00557	0.0136
	10000	0.00415	0.00415	0.00531	0.00531	0.0131

minus 4 percent of ORIGEN/S predictions. In these instances, ANSIDECH may be slightly nonconservative. After 100 to 300 years, the ANS Standard slightly underestimates decay heat generation, by as much as 8 percent to 11 percent. After 300 years, generally considered the end of significant heat generation, the ANS Standard begins to deviate significantly from ORIGEN/S predictions.

Figures 3-49 through 3-54 provide graphs of the decay heat predictions as a function of time using the ANS Standard for the six subproblems in problem 2.2. Figures 3-55 through 3-58 show the relative differences between the ORIGEN/S predictions and the ANS Standard predictions of decay heat.

Sensitivity analyses indicated that, after 10 years of cooling time, the decay heat generation rate is relatively insensitive to operating conditions. For typical variations in reactor power level and irradiation history, a 1 percent variation in decay heat generation rate was observed. The principal variables affecting decay heat rate are fuel assembly burnup, initial enrichment, and time in the reactor. The time-dependent power history is not of primary importance at time periods beyond 10 years after reactor shutdown.

3.2.3.3 Turkey Point Unit 3 Afterheat Power Study (Benchmark Problem 2.3)

Table 3-28 summarizes the ANSIDECH/BURNUP estimates of decay heat generation rate for Turkey Point Unit 3 fuel assemblies. As this table shows, the ANS Standard for fission products overestimates fission-product decay heat rate by 25 to 30 percent for fuel that is two and one-half to three years out of the reactor. While the ANS Standard was meant to apply only to the fission-product decay heat rate, a comparison of the ANS Standard predictions of fission product heat to the total measured heat from these fuel assemblies indicates that the ANS Standard estimate of total decay heat is still generally conservative, ranging from 3 percent to 8 percent over measured values. Figure 3-59 provides a comparison of ANS Standard predictions with measured fission product and total decay heat generation rates for Problem 2.3.

Figure 3-49

ANSIDECH/BURNUP—Predicted Decay Heat Generation Rate vs. Time for Benchmark Problem 2.2.1

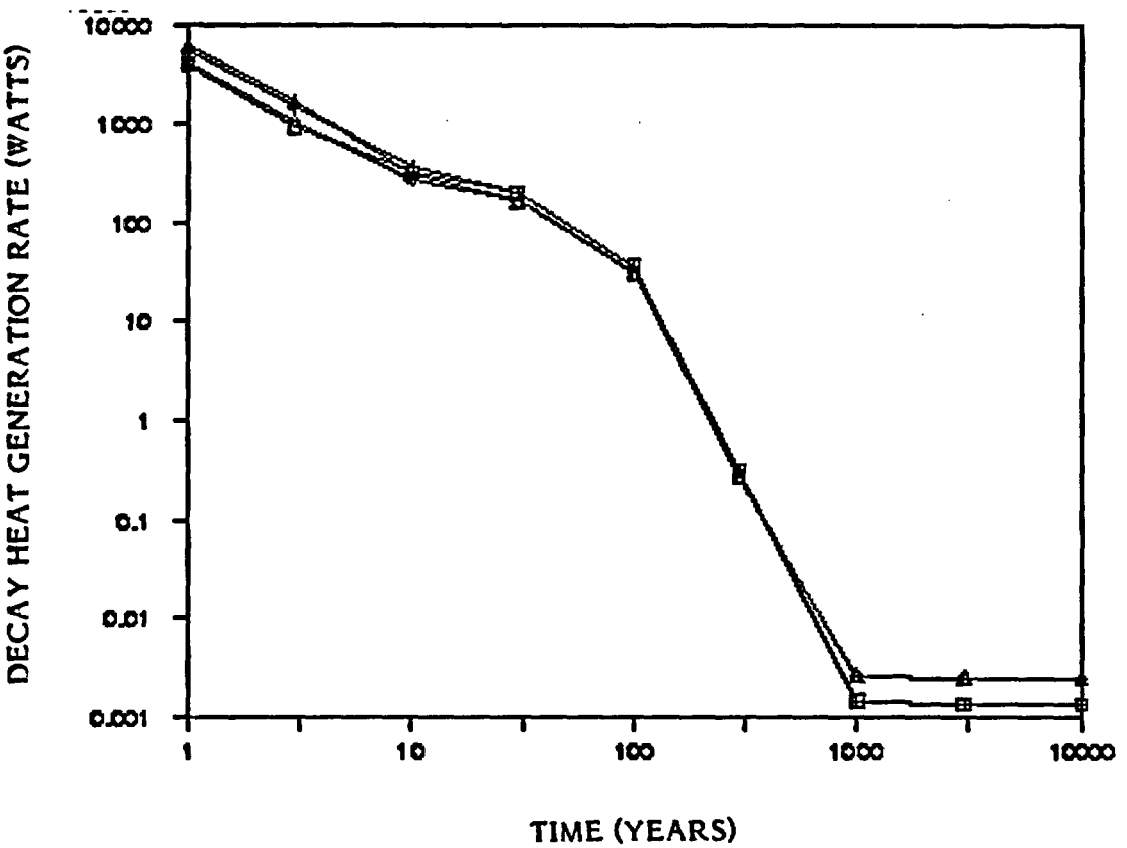

- ▫ ANSIDECH/BURNUP—predicted value using short method without G-factor
- \+ ANSIDECH/BURNUP—predicted value using short method with G-factor
- ◇ ANSIDECH/BURNUP—predicted value using long method without G-factor
- △ ANSIDECH/BURNUP—predicted value using long method with G-factor

Figure 3-50

ANSIDECH/BURNUP—Predicted Decay Heat Generation Rate vs. Time for Benchmark Problem 2.2.2

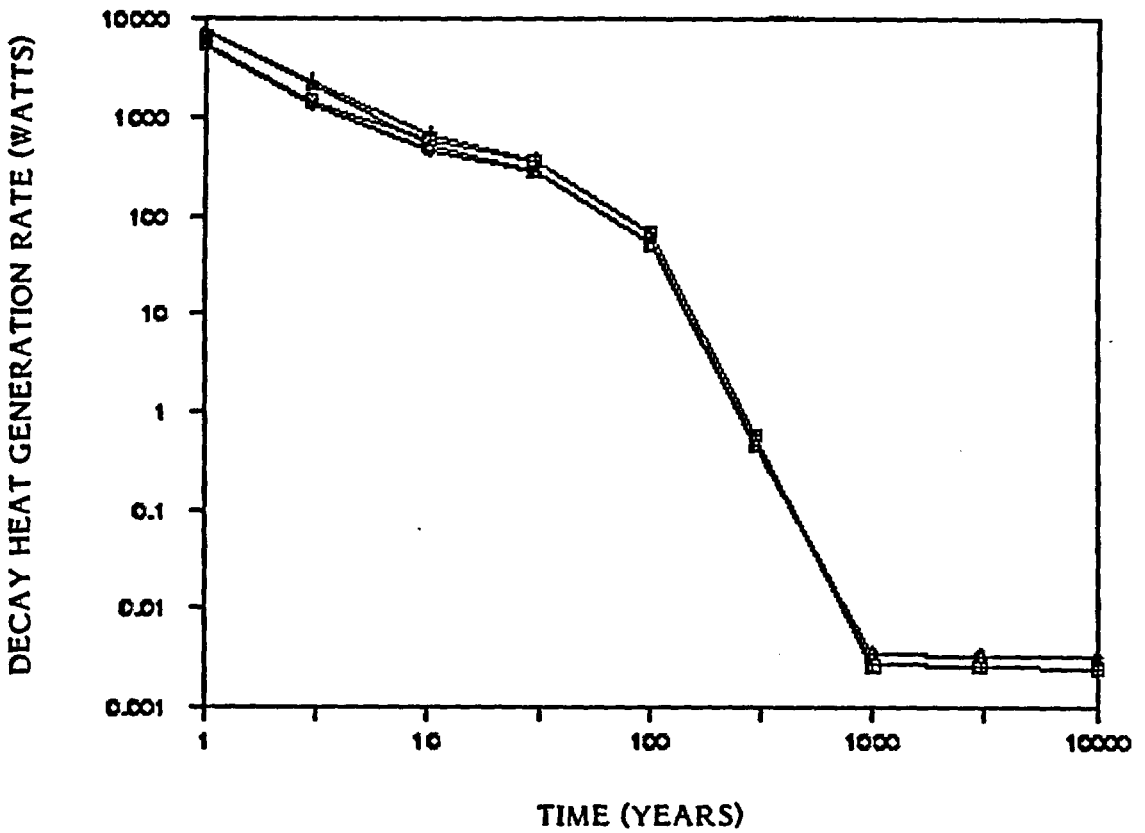

- ANSIDECH/BURNUP—predicted value using short method without G-factor
- \+ ANSIDECH/BURNUP—predicted value using short method with G-factor
- ◇ ANSIDECH/BURNUP—predicted value using long method without G-factor
- △ ANSIDECH/BURNUP—predicted value using long method with G-factor

Figure 3-51

ANSIDECH/BURNUP—Predicted Decay Heat Generation Rate vs. Time for Benchmark Problem 2.2.3

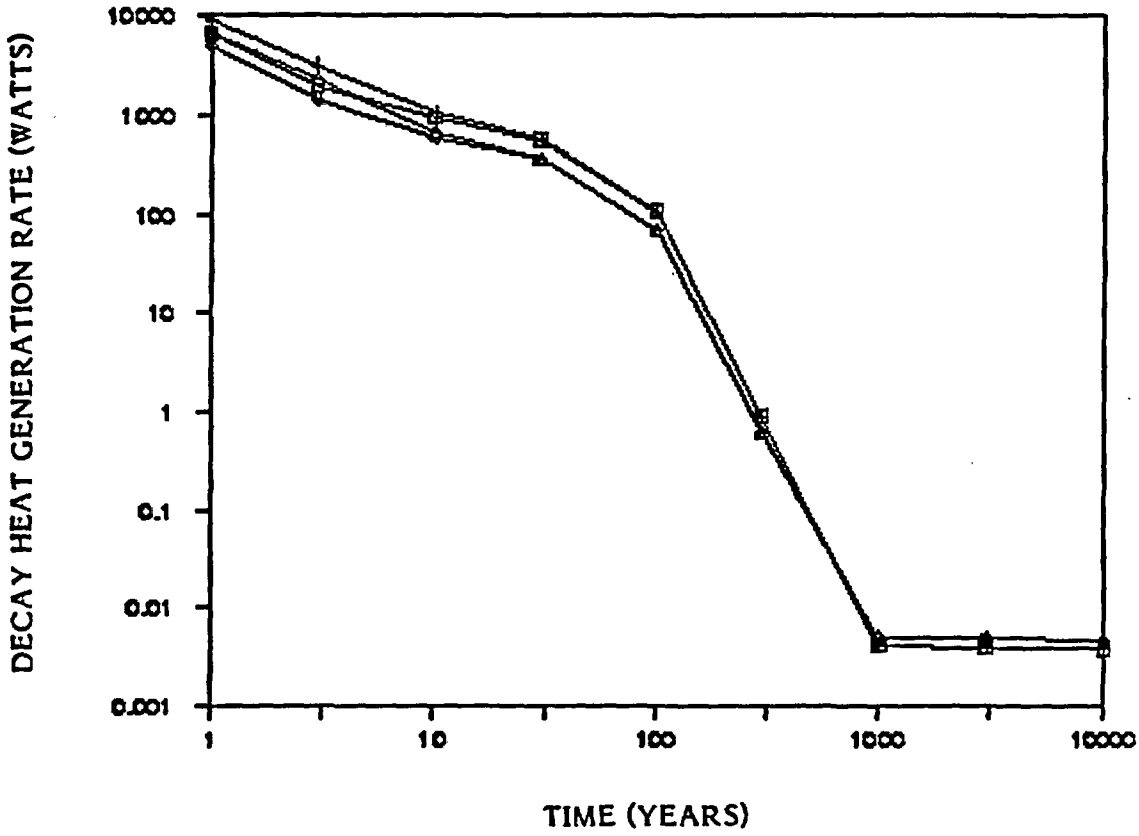

- □ ANSIDECH/BURNUP—predicted value using short method without G-factor
- \+ ANSIDECH/BURNUP—predicted value using short method with G-factor
- ◇ ANSIDECH/BURNUP—predicted value using long method without G-factor
- △ ANSIDECH/BURNUP—predicted value using long method with G-factor

Figure 3-52

ANSIDECH/BURNUP—Predicted Decay Heat Generation Rate vs. Time for Benchmark Problem 2.2.4

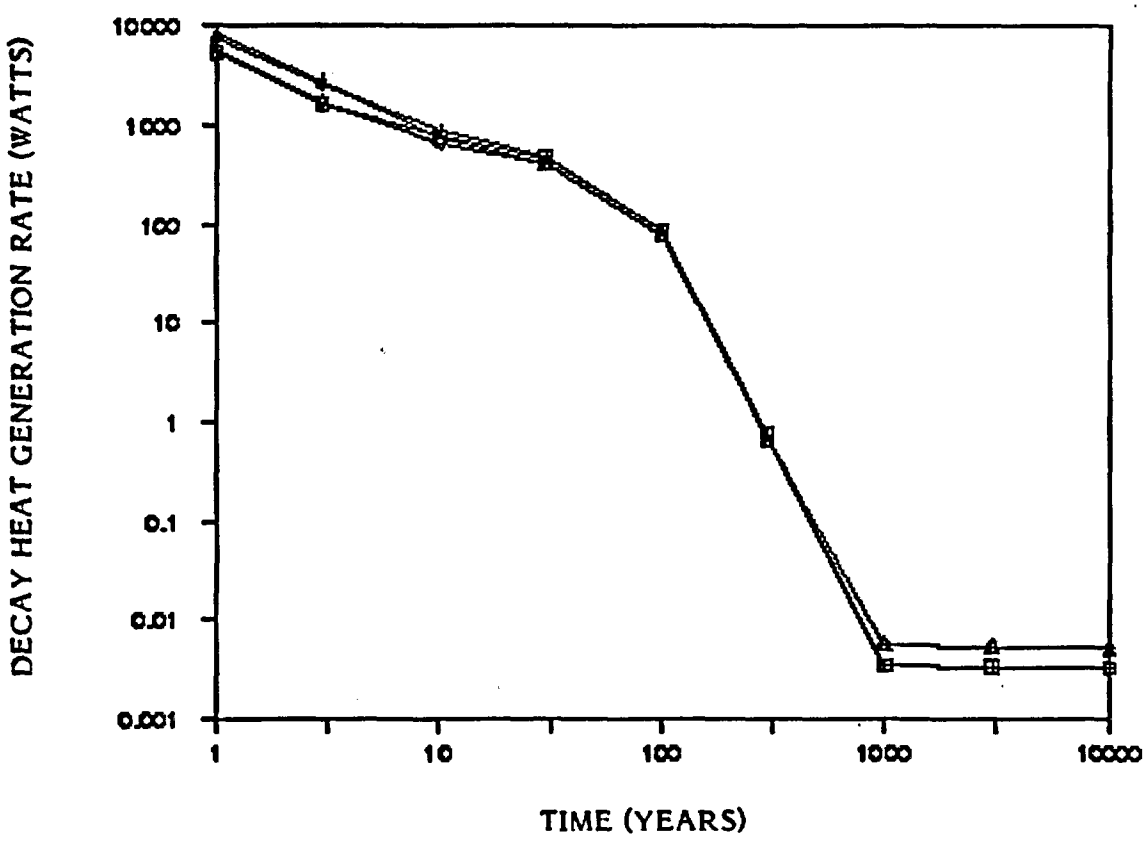

- ANSIDECH/BURNUP—predicted value using short method without G-factor
- \+ ANSIDECH/BURNUP—predicted value using short method with G-factor
- ◇ ANSIDECH/BURNUP—predicted value using long method without G-factor
- △ ANSIDECH/BURNUP—predicted value using long method with G-factor

Figure 3-53

ANSIDECH/BURNUP—Predicted Decay Heat Generation Rate vs. Time for Benchmark Problem 2.2.5

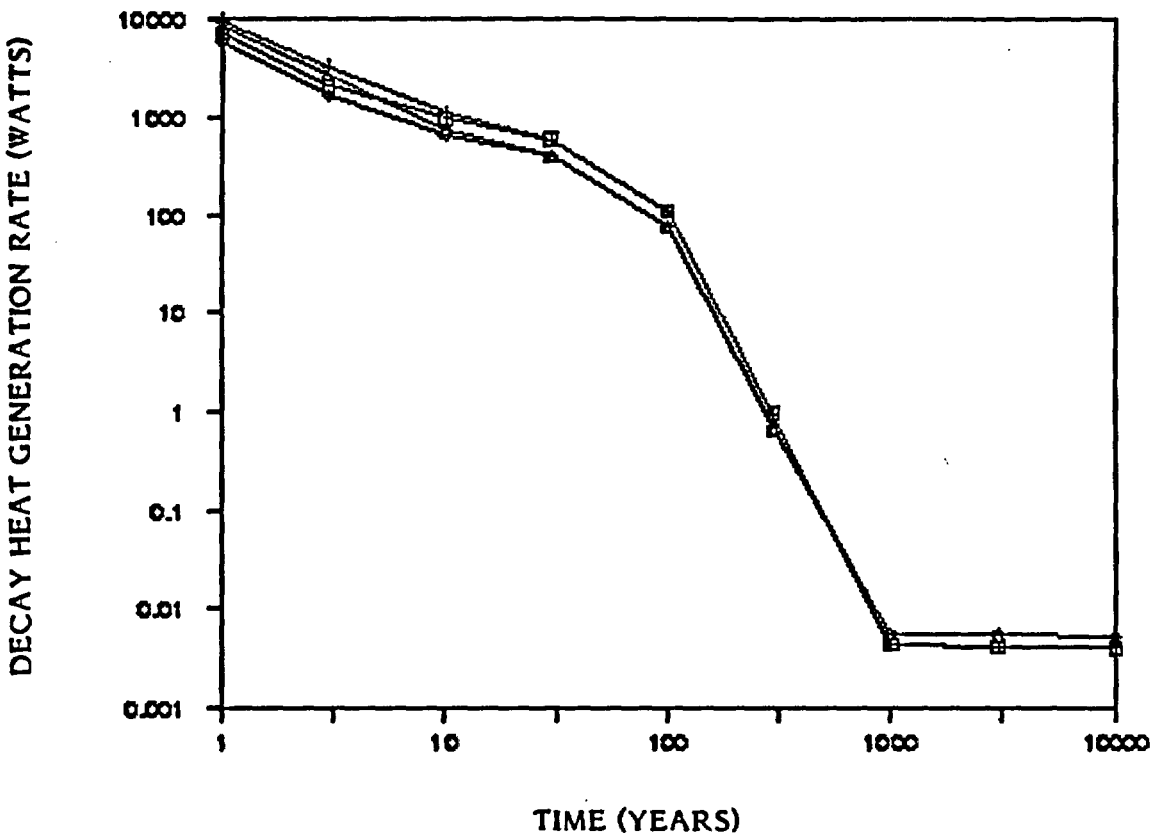

- □ ANSIDECH/BURNUP—predicted value using short method without G-factor
- \+ ANSIDECH/BURNUP—predicted value using short method with G-factor
- ◇ ANSIDECH/BURNUP—predicted value using long method without G-factor
- △ ANSIDECH/BURNUP—predicted value using long method with G-factor

Figure 3-54

ANSIDECH/BURNUP—Predicted Decay Heat Generation Rate vs. Time for Benchmark Problem 2.2.6

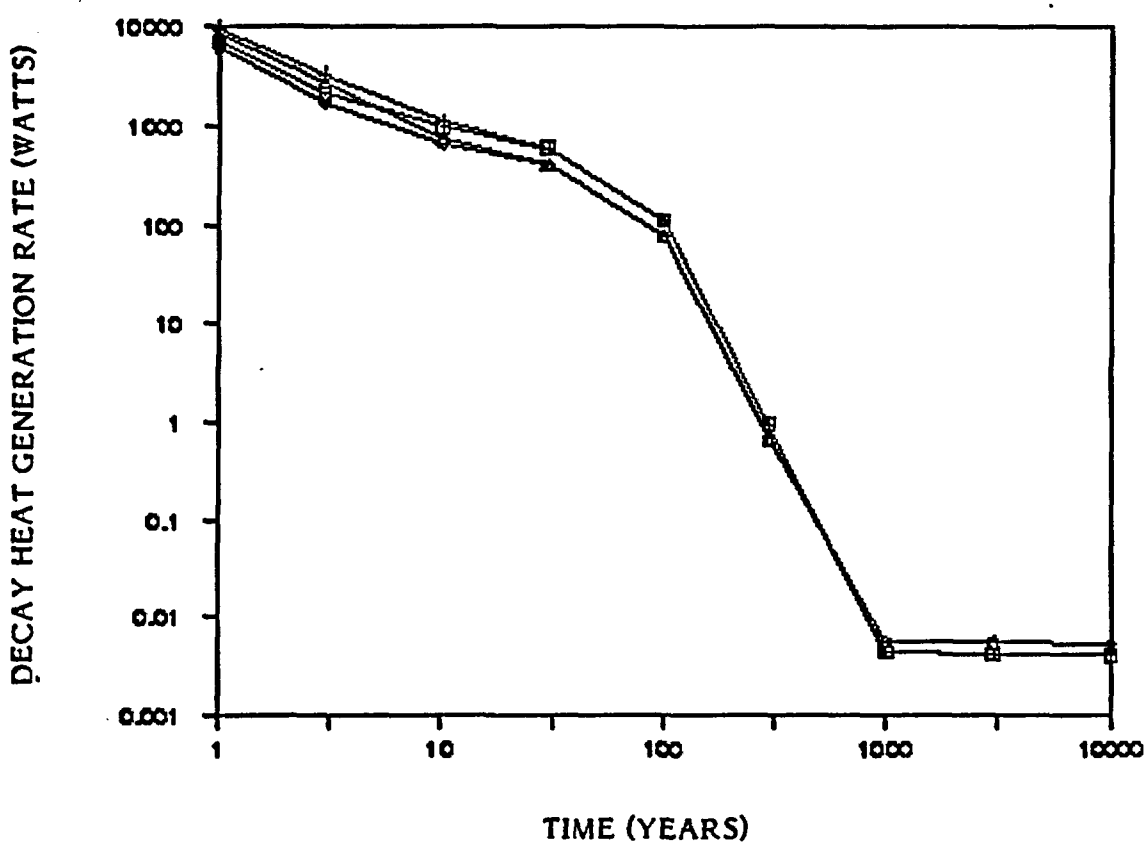

- □ ANSIDECH/BURNUP—predicted value using short method without G-factor
- \+ ANSIDECH/BURNUP—predicted value using short method with G-factor
- ◇ ANSIDECH/BURNUP—predicted value using long method without G-factor
- △ ANSIDECH/BURNUP—predicted value using long method with G-factor

Figure 3-55

Comparison of ANSIDECH/BURNUP–Predicted Decay Heat Generation Rates Based on Short Method without G-Factor for Problems 2.2.1 through 2.2.6

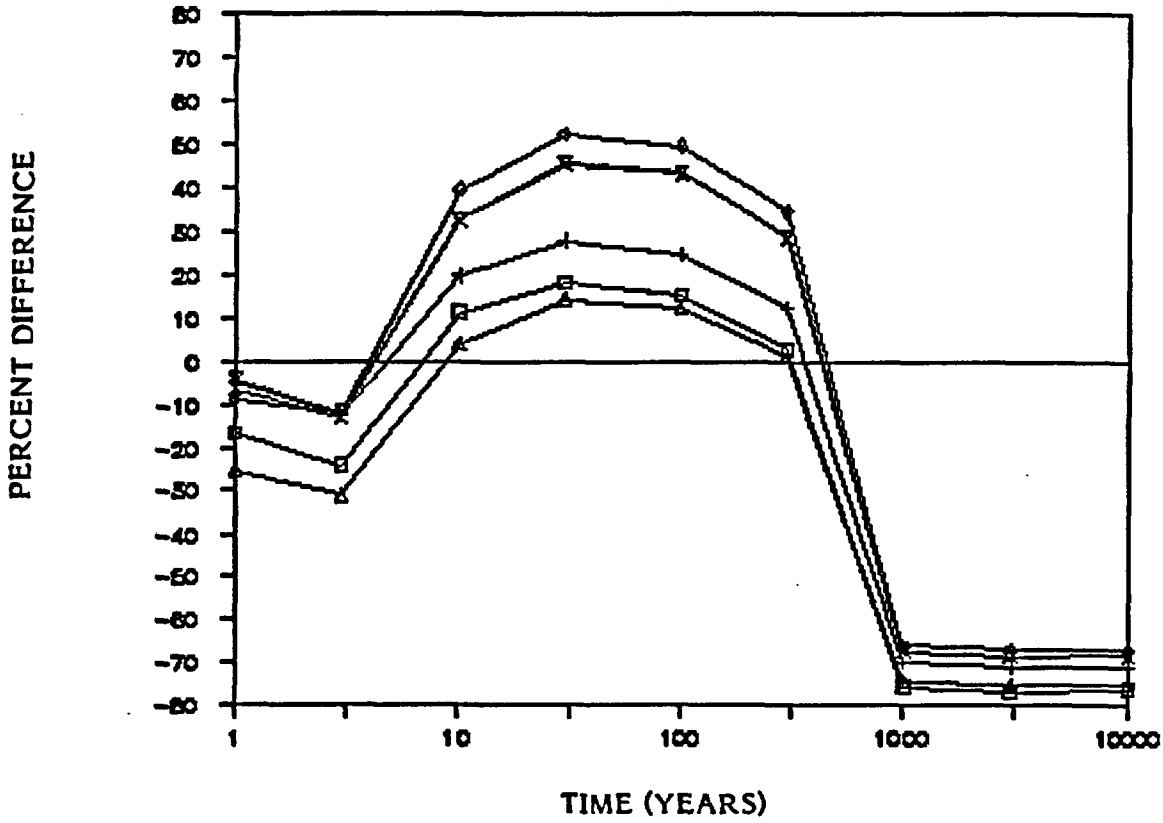

□ Problem 2.2.1
\+ Problem 2.2.2
◇ Problem 2.2.3
△ Problem 2.2.4
× Problem 2.2.5
▽ Problem 2.2.6

Figure 3-56

Comparison of ANSIDECH/BURNUP–Predicted Decay Heat Generation Rates Based on Short Method Using G-Factor for Problems 2.2.1 through 2.2.6

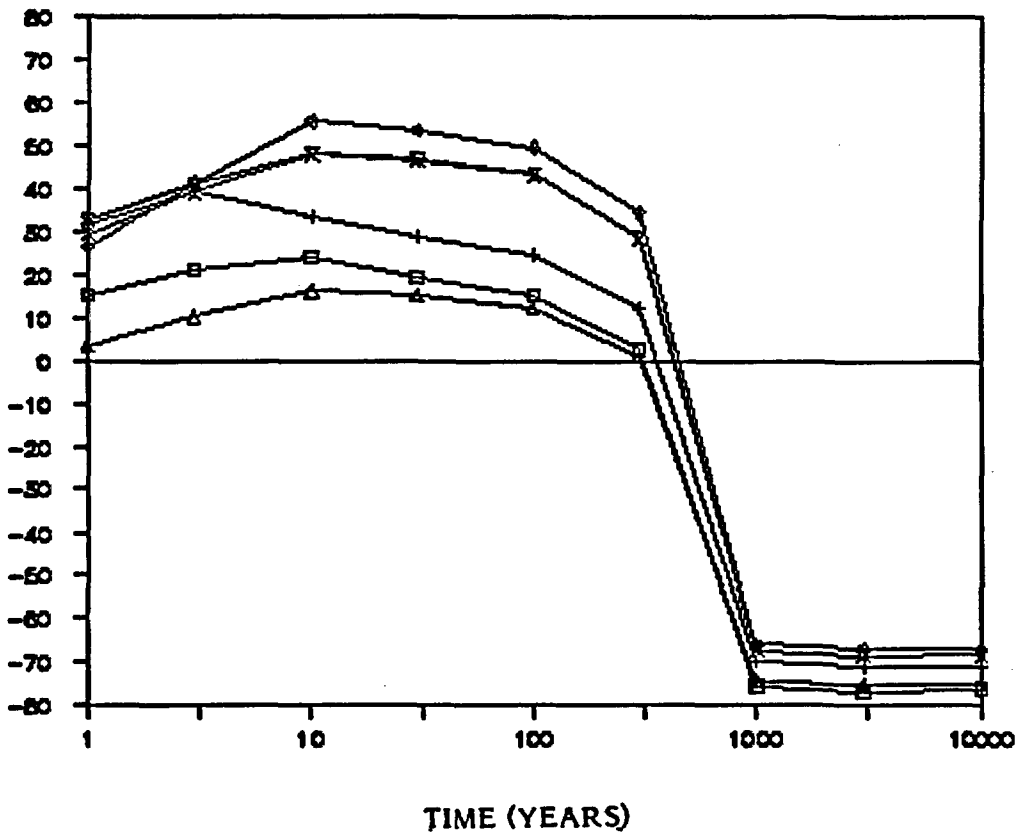

□ Problem 2.2.1
+ Problem 2.2.2
◇ Problem 2.2.3
△ Problem 2.2.4
× Problem 2.2.5
▽ Problem 2.2.6

Figure 3-57

Comparison of ANSIDECH/BURNUP–Predicted Decay Heat Generation Rates Based on Long Method without G-Factor for Problems 2.2.1 through 2.2.6

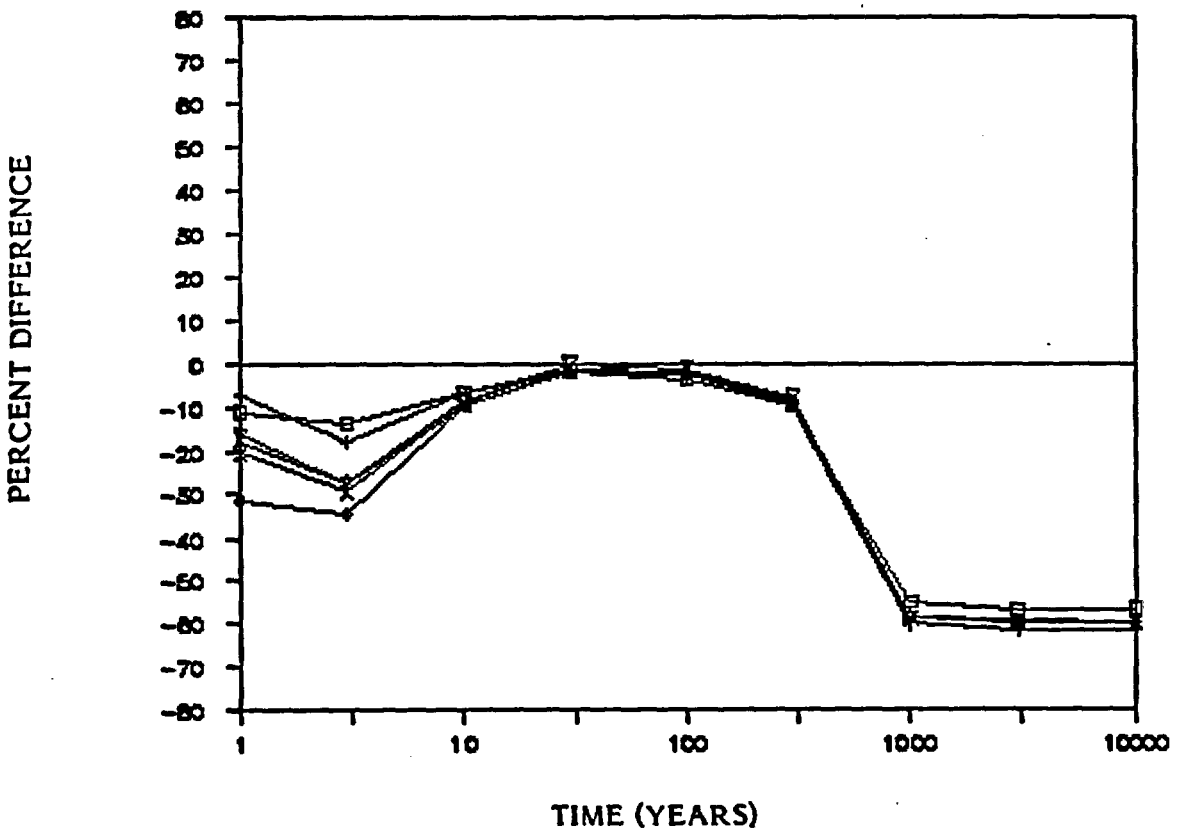

□ Problem 2.2.1
+ Problem 2.2.2
◇ Problem 2.2.3
△ Problem 2.2.4
× Problem 2.2.5
▽ Problem 2.2.6

Figure 3-58

Comparison of ANSIDECH/BURNUP—Predicted Decay Heat Generation Rates Based on Long Method Using G-Factor for Problems 2.2.1 through 2.2.6

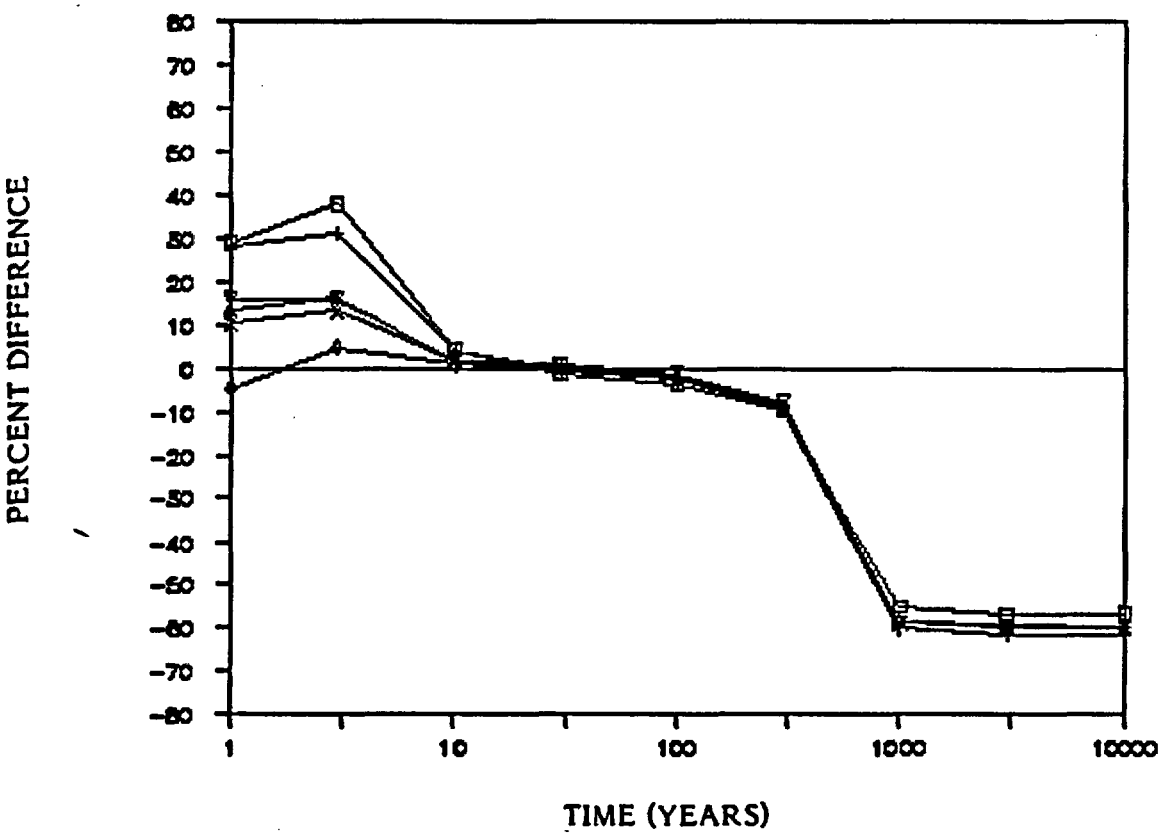

□ Problem 2.2.1
+ Problem 2.2.2
◇ Problem 2.2.3
△ Problem 2.2.4
× Problem 2.2.5
▽ Problem 2.2.6

Table 3-28

Decay Thermal Power Prediction, in Watts

Problem Number	Time (Years)	ANSI-Short Method w/o G-Fctr	ANSI-Short Method w/ G-Fctr	ANSI-Long Method w/o G-Fctr	ANSI-Long Method w/ G-Fctr	ORIGEN Predictions		Measured Value
						Existing Cross-Sections	Generated Cross-Sections	
2.3.1	864	2793	4403	2473	3898	3380	3320	3039
					Lights	118	127	
					Actinides	205	226	
					Total	3703	3673	3392
2.3.2	962	2509	3991	2195	3491	3040	3000	2767
					Lights	116	125	
					Actinides	206	222	
					Total	3362	3347	3114
	1143	2053	3281	1745	2789	2450	2410	2139
					Lights	107	116	
					Actinides	191	207	
					Total	2748	2733	2462
2.3.3	963	2339	3720	2039	3243	2780	2740	2508
					Lights	108	115	
					Actinides	171	187	
					Total	3059	3042	2810

Figure 3-59

ANSI Standard vs. Measured Data for
Benchmark Problems 2.3.1 through 2.3.3

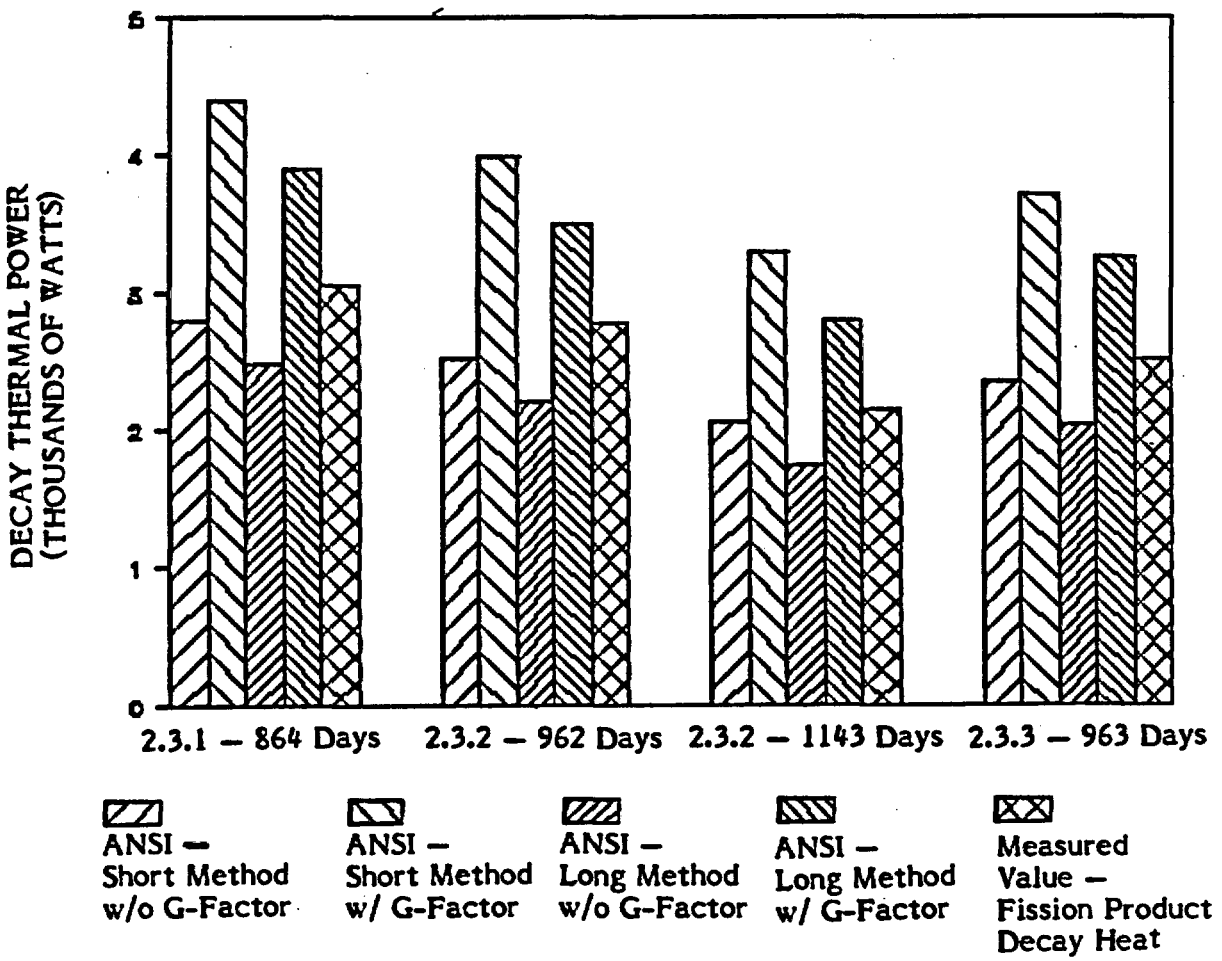

3.3 Code Comparison and Evaluation

In Sections 3.1 and 3.2, the capabilities of the codes ORIGEN/S and ANSIDECH/BURNUP were evaluated with respect to the calculation of decay heat generation rate and radionuclide inventories. Here we compare and evaluate the codes' decay heat predictions.

From a review of the data presented earlier in this chapter, together with an understanding of the operating characteristics of the codes, the following conclusions were reached:

- ORIGEN/S and ANSIDECH/BURNUP provide similar estimates of decay heat generation rate at times of importance to high level waste management (10 to 300 years following discharge from reactor).
- Only limited measurements of spent-fuel decay heat generation rates are available. However, compared with those that are available, the ORIGEN/S and ANSIDECH estimates of decay heat generation rate are conservative.
- Few measurements of spent fuel isotopic composition are available. ORIGEN estimates of spent fuel isotopic composition are good for uranium isotopes, fair to poor for plutonium isotopes, poor to unacceptable for transuranics other than plutonium and acceptable to marginally acceptable for fission products.
- If better estimates of spent fuel isotopic composition than those presented here are required, it is recommended that a computer code with several neutron energy groups, a time-varying neutron flux and time-varying cross section be used.

3.4 References for Chapter 3

1. Bell, M.J. ORIGEN: The ORNL Isotope Generation and Depletion Code. ORNL-4728. Oak Ridge National Laboratory. May 1973.
2. Oak Ridge National Laboratory. Documentation for CCC-217/ORIGEN Computer Code Package. June 1977.
3. Bennett, David E. SANDIA-ORIGEN User's Manual. NUREG/CR-0985. Sandia Laboratories. October 1979.

4. Herman, O.W., et al. ORIGEN-S Scale System Module to Calculate Fuel Depletion, Actinide Transmutation, Fission Product Buildup and Decay, and Associated Source Terms. NUREG/CR-0200, vol. 2, Section F1. October 1981.

5. Bateman, H. I. Proceedings of the Cambridge Philosophical Society 15 (1910): 423.

6. American Nuclear Society. American National Standard for Decay Heat Power in Light Water Reactors. ANSI/ANS-5.1-1979. Lagrange Park, Illinois, 1979.

7. Ryman, J.C.; Herman, O.W.; Webster, C.C.; and Parks, C.V. Fuel Inventory and Afterheat Power Studies of Uranium-Fueled Pressurized Water Reactor Fuel Assemblies Using the SAS2 and ORIGEN-S Modules of Scale with an ENDF/B-V Updated Cross Section Library. NUREG/CR-2397. September 1982.

8. Croff, A.G., et al. Revised Uranium-Plutonium Cycle PWR and BWR Models for the ORIGEN Computer Code. ORNL/TM-6051. Oak Ridge National Laboratory. September 1978.

9. General Electric. Standard Safety Analysis Report. BWR/6. Docket STN 50-447. 1973.

10. Schmittroth, F.; Neely, G.J.; and Krogness, J.C. Comparison of Measured and Calculated Decay Heat for Spent Fuel Near 2.5 Years of Cooling Time. TC 1759. August 1980.

11. U.S. Nuclear Regulatory Commission. Operating Status Report, Licensed Operating Reactors. NUREG 0020. Vols. 1-4.

12. Atkins, S.D. Destructive Examination of 3-Cycle LWR Fuel Rods from Turkey Point Unit 3 for the CLIMAX-Spent Fuel Test. HEDL-TME 80-89. Hanford Engineering and Development Laboratories. June 1981.

13. Campbell, D.O., and Buxton, S.R. "Dissolution Studies." In LWR Fuel Reprocessing and Recycle Program Quarterly Report for Period January 1 to March 31, 1976. ORNL/TM-5447. Oak Ridge National Laboratory. May 1976.

14. Campbell, D.O., and Buxton, S.R. "Hot-Cell Studies." In LWR Fuel Reprocessing and Recycle Program Quarterly Report for Period April 1 to June 30, 1976. ORNL/TM-5547. Oak Ridge National Laboratory. July 1976.

15. Campbell, D.O. "Hot Cell Studies." In LWR Fuel Reprocessing and Recycle Program Quarterly Report for Period July 1 to September 30, 1976. ORNL/TM-5660. Oak Ridge National Laboratory. November 1976.

16. Campbell, D.O.; Buxton, S.R.; Beatty, R.L.; and Pattison, W.L. "Hot-Cell Studies." In LWR Fuel Reprocessing and Recycle Program Quarterly Report for Period October 1 to December 31, 1976. ORNL/TM-5760. Oak Ridge National Laboratory. February 1977.

17. Campbell, D.O.; Buxton, S.R.; and Pattison, W.L. "Hot-Cell Studies." In LWR Fuel Reprocessing and Recycle Program Quarterly Report for Period April 1 to June 30, 1977. ORNL/TM-5987. Oak Ridge National Laboratory. August 1977.

18. Vaughen, V.C.A., et al. "Building 4507 Hot-Cell Operations." In LWR Fuel Reprocessing and Recycle Program Quarterly Report for Period April 1 to June 30, 1977. ORNL/TM-5987. Oak Ridge National Laboratory. August 1977.

4. BENCHMARKING OF ENVIRONMENTAL-PATHWAY AND DOSE-TO-MAN CODES

4.1 PATH1/DOSHEM

4.1.1 Code Description

The PATH1 code (Reference 1) uses a generalized approach to the simulation of radionuclide transport from the groundwater through the environment and food chain to man. The code is flexible in that it is not tied to any specific site characteristics. The Environmental Transport Submodel of PATH1 requires that the study area be divided into a number of compartments, with radionuclide movement between these compartments represented by a system of linear differential equations. The user must specify the transfer and decay coefficients for this system of compartments. In the Transport-to-Man Submodel, radionuclide ingestion is calculated on the basis of simple food chains and concentration ratios, while the amount of each radionuclide inhaled is determined from the amount of radionuclide-containing soil suspended in the air. These calculated ingestion and inhalation rates are input to the Sandia Dose and Health Effects Model, DOSHEM (Reference 2), which simply applies the appropriate dose factors in the calculation of committed dose.

PATH1 assumes that the environmental transport of radionuclides takes place between zones. Each zone is divided into four subzones: sediment, groundwater, surface water, and soil. Each of these subzones is uniform in its physical characteristics. All subzones have a liquid and solid component between which the radionuclides present in the subzone are partitioned. Radionuclide input is possible into one or more of these subzones. Flows between zones involve both water and solid material and are assumed to take place only from the surface-water subzone of one zone to the surface-water subzone of another zone. Water and solid material may also move from a subzone to a sink, so that the associated radionuclides are removed from the system. The decay of a radionuclide is also mathematically represented as a compartmental transfer, even though the daughter radionuclide will occupy the same physical subzone as the parent. The process may be described in terms of the following system of linear differential equations:

$$f_i'(t) = R_i(t) + \sum_{j=1}^{i-1} a_{ji} f_j(t) - \left[k_i + \sum_{\substack{j=1 \\ j \neq i}}^{M} a_{ij} \right] f_i(t) + \sum_{j=i+1}^{M} a_{ji} f_j(t) , \quad (4.1.1)$$

where

$f_i'(t)$ = rate of change of radionuclide in compartment i at time t (atoms/yr)

M = number of compartments (number of zones x number of subzones per zone x number of radionuclides)

$f_i(t)$ = amount of radionuclide present in compartment i at time t (atoms)

$R_i(t)$ = rate of radionuclide input to compartment i (atoms/yr)

a_{ij} = coefficient of radionuclide transfer from compartment i to compartment j (yr^{-1})

k_i = rate of radionuclide transfer from compartment i to a sink (yr^{-1})

This system of equations is solved in PATH1 through the use of a direct integration routine. In calling up this routine within the program, the user must specify a relative error bound, the basic solution method, and the iteration method.

PATH1 gives the user the option of making changes directly to the transfer coefficients (a_{ij}) to account for special effects such as the escape of radon gas from subzones.

Total radionuclide amount (A) in each phase are given by

$$AS = \left[\frac{(KD)(MS)}{(KD)(MS)+VM}\right] A \qquad (4.1.2a)$$

and

$$AW = \left[1 - \frac{(KD)(MS)}{(KD)(MS)+VM}\right] A \qquad (4.1.2b)$$

The partitioning of a radionuclide concentration in each subzone between the solid and liquid components is given by the distribution coefficient

$$k_d = \frac{\text{concentration of radionuclide sorbed on solids}}{\text{concentration of radionuclide dissolved in water}}$$

$$= \frac{AS/MS}{AW/VM}, \qquad (4.1.3)$$

where

AS = amount of radionuclide sorbed on solids (atoms)
AW = amount or radionuclide dissolved in water (atoms)
MS = mass of solid (kilograms)
VM = volume of water (liters)

Surface-water radionuclide concentrations are used to calculate the foliar deposition of radionuclides due to sprinkler irrigation of crops. A fraction of these deposited radionuclides are assumed to be incorporated within the body of the plant and subsequently consumed by man. PATH1 is also designed to consider a weathering half-life for radionuclides deposited on plant leaves. Direct human ingestion of surface-water radionuclides can take place through the drinking water pathway. In the case of drinking and sprinkler irrigation, the

PATH1 user can specify whether suspended particulates have been removed from the water. Two other surface-water exposure pathways considered in the code are fish consumption and external exposure from swimming.

Radionuclides in the soil subzone can be transferred to vegetation through root uptake. These radionuclides can be ingested by humans directly through the consumption of vegetation or indirectly through the milk or meat pathways. Inhalation of windblown contaminated soil is another soil exposure pathway considered by PATH1. External exposure to radiation emanating from the soil (both surface and airborne) is also considered.

Two versions of the PATH1 code were developed for the NRC by Sandia National Laboratories. The first version, which was benchmarked in this study, calculates time-dependent radionuclide concentrations in environmental subzones. It was this version of the code that was in place at the Brookhaven National Laboratory Computing Center at the outset of the study. The second version, which has been named the "methodology version" by Sandia, calculates steady-state radionuclide concentrations. Only this second version of PATH1 writes a file containing radionuclide ingestion, inhalation, and external exposure information for input to the dose and health effects code DOSHEM. For the time-dependent version of PATH1, these inputs to DOSHEM must be manually coded from the PATH1 output.

4.1.2 Description of Benchmark Problems

4.1.2.1 Hypothetical Repository — Radiological Assessment (Benchmark Problem 3.0)*

Problem Statement. This problem deals with the environmental transport of a chain of seven radionuclides, their entry into the food chain, and their eventual consumption and resultant dose to man. In addition to receiving doses through ingestion, man also receives doses via inhalation of resuspended soil, immersion

---

* Problem number refers to number used in preceding report (see Reference 3, Chapter 1).

in air containing resuspended soil, and exposure due to radiation from the ground surface and swimming in contaminated water. The problem has been adapted from a problem used in the sensitivity analysis of the PATH1 code (Reference 3). The purpose of the problem is to test the capabilities of radiological assessment codes to deal with those aspects of radionuclide transport and dose to man that are most important for a high-level waste repository. The problem assumes that the transfer rates or radionuclides between subzones of a watershed system (sediment, surface water, groundwater, and soil) are proportional to the radionuclide amounts in the compartments.

Physical Specifications and Assumptions. A stream flows along the major axis of a half-ellipse that forms the boundary of a watershed (see Figure 4-1). A high-level waste repository is located 43 km west of the stream at a point 175 km downstream. The watershed below the repository is rectangular, with the dimensions given in Figure 4-2. Areas for each of the watershed segments are given in Figure 4-3. Three zones are identified in Figure 4-1. Within each zone there are four physical subzones: surface water, groundwater, sediment, and soil. In the case of any particular zone, the radionuclides are distributed uniformly within each physical subzone. Transfer of water and solid between zones can take place only from the surface-water subzone of one zone to the surface-water subzone of another zone. The distance of the repository from the stream of Zone 1 is not used directly in the calculation. It is assumed that the repository is far enough away so that the input of radionuclides to the groundwater subzone is reasonably uniform across the extent of the compartment. The first zone is associated with a 40-km-long section of stream below the repository. The second zone is associated with a 201-km^2 elliptical lake. The volume of the lake is assumed to equal the volume of water that enters the lake from upstream during a three-month period. The third zone follows a 40-km section of stream below the lake. The water and solid input rates for the lake and each of the stream segments are given in Figure 4-4. Water input is assumed to originate entirely from groundwater at a rate of 2.7E7 L/yr/m from both sides of the stream or lake. Solid input to the surface water is assumed to follow from

Figure 4-1

Watershed Zones

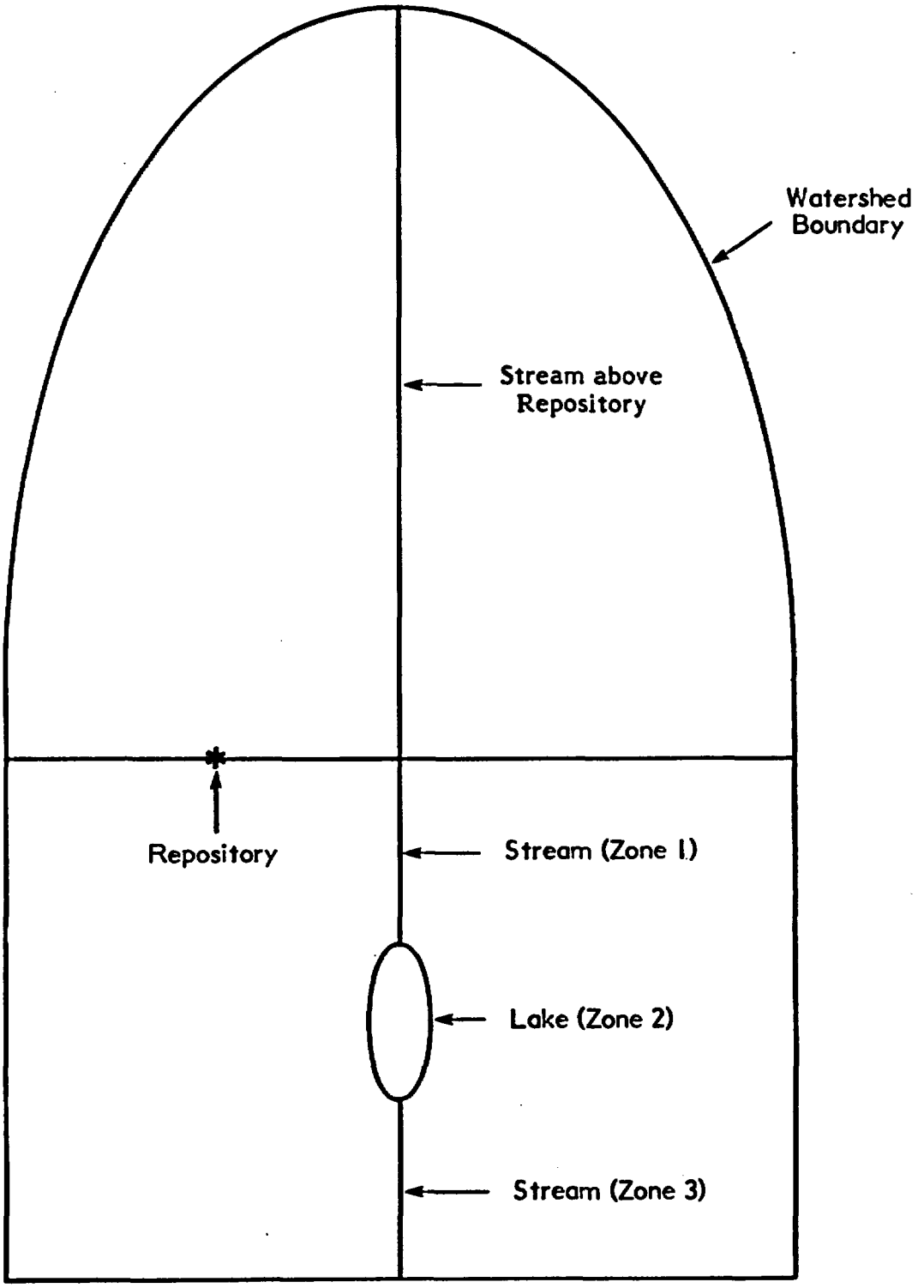

Figure 4-2

Watershed Dimensions

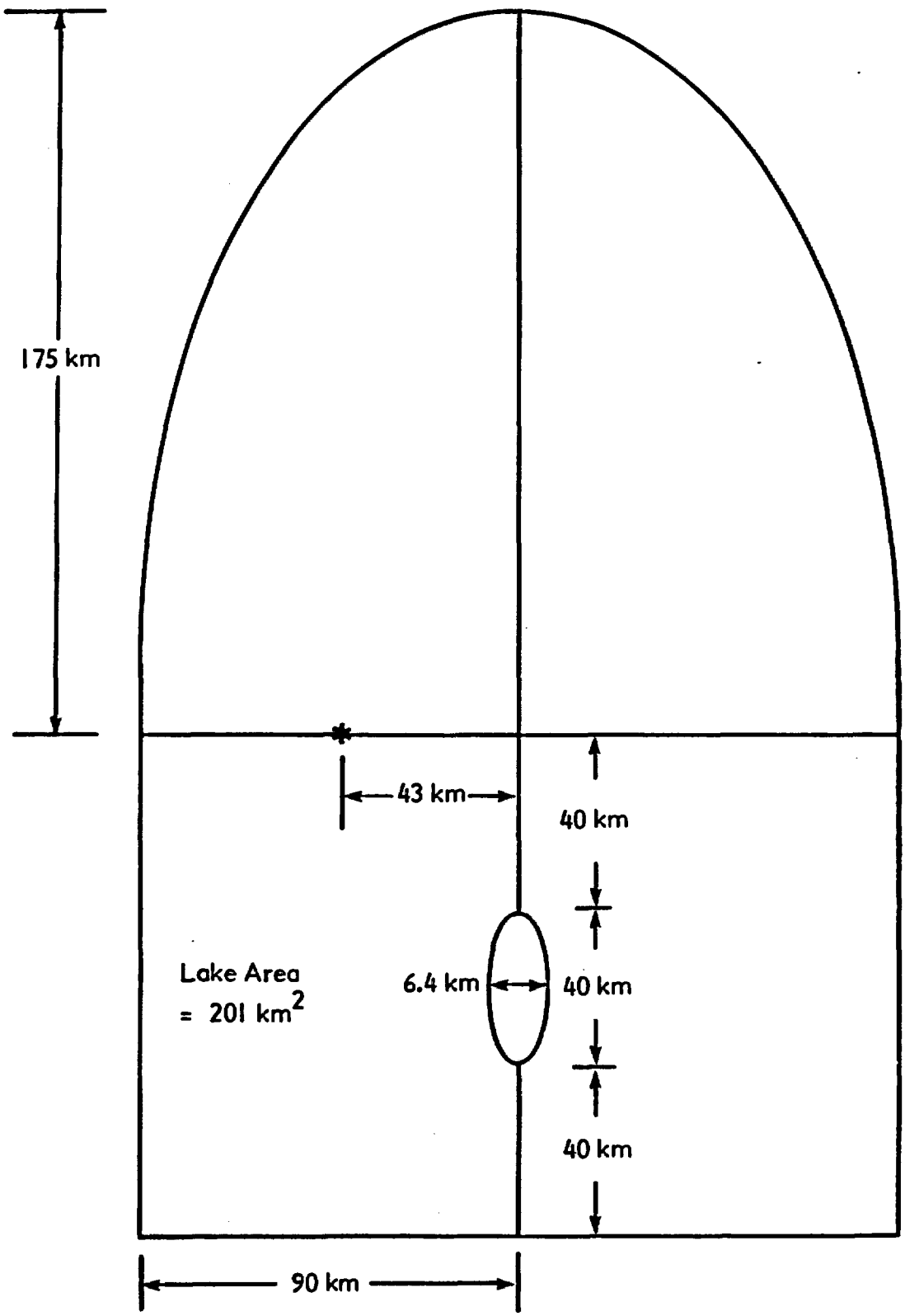

Figure 4-3

Watershed Areas

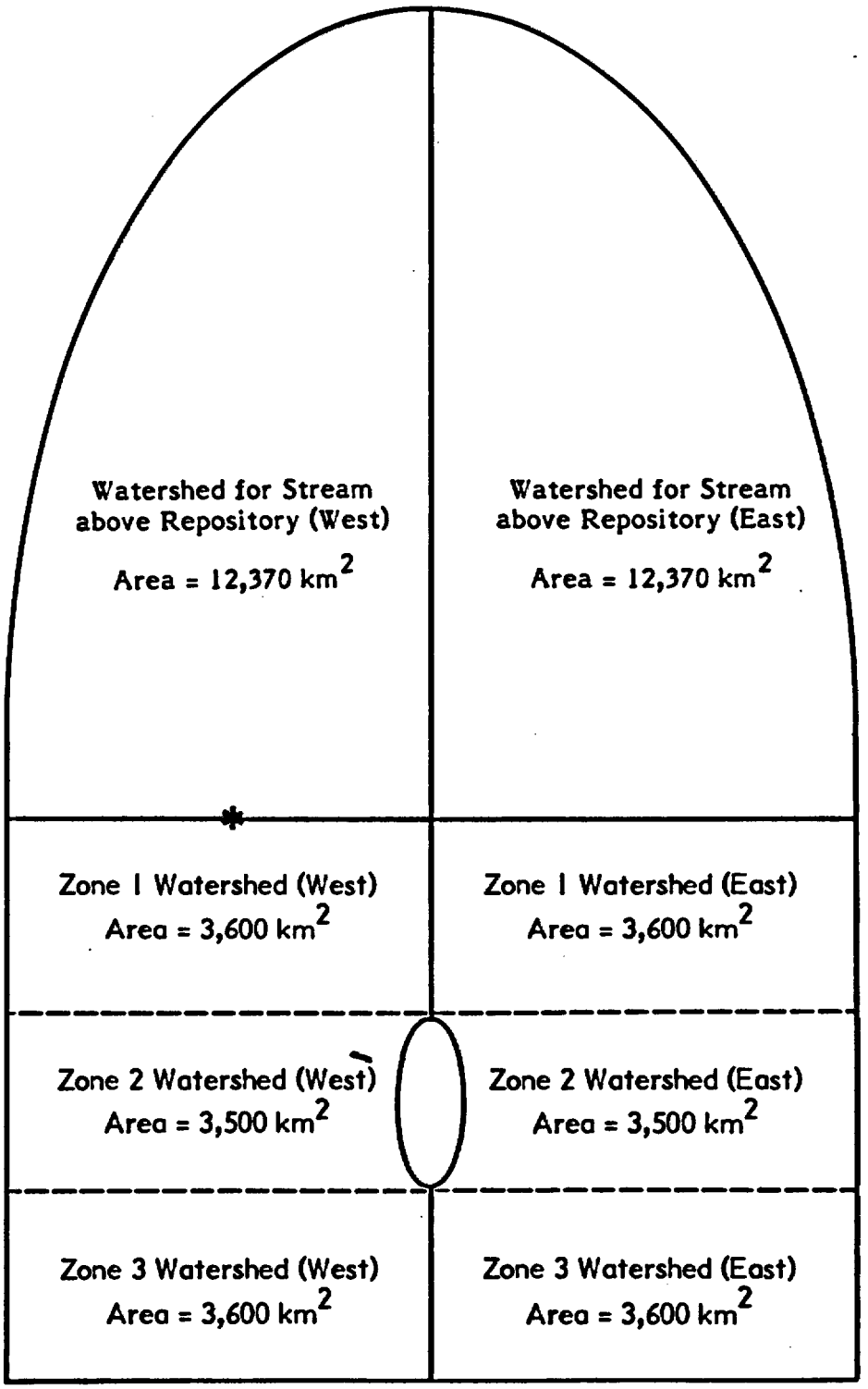

Figure 4-4

Water and Solid Input Rates for the Stream and Lake Segments. Water Input is Assumed to Originate Entirely from Groundwater at a Rate of 2.7E7 L/yr/m from Each Side of the Stream. Solid Input is Based upon a Watershed Erosion Rate of 5cm/1,000 yr and a Soil Density of 2.8E3 kg/m^3, with 67 Percent of the Eroded Material Suspended and 33 percent Carried in Solution.

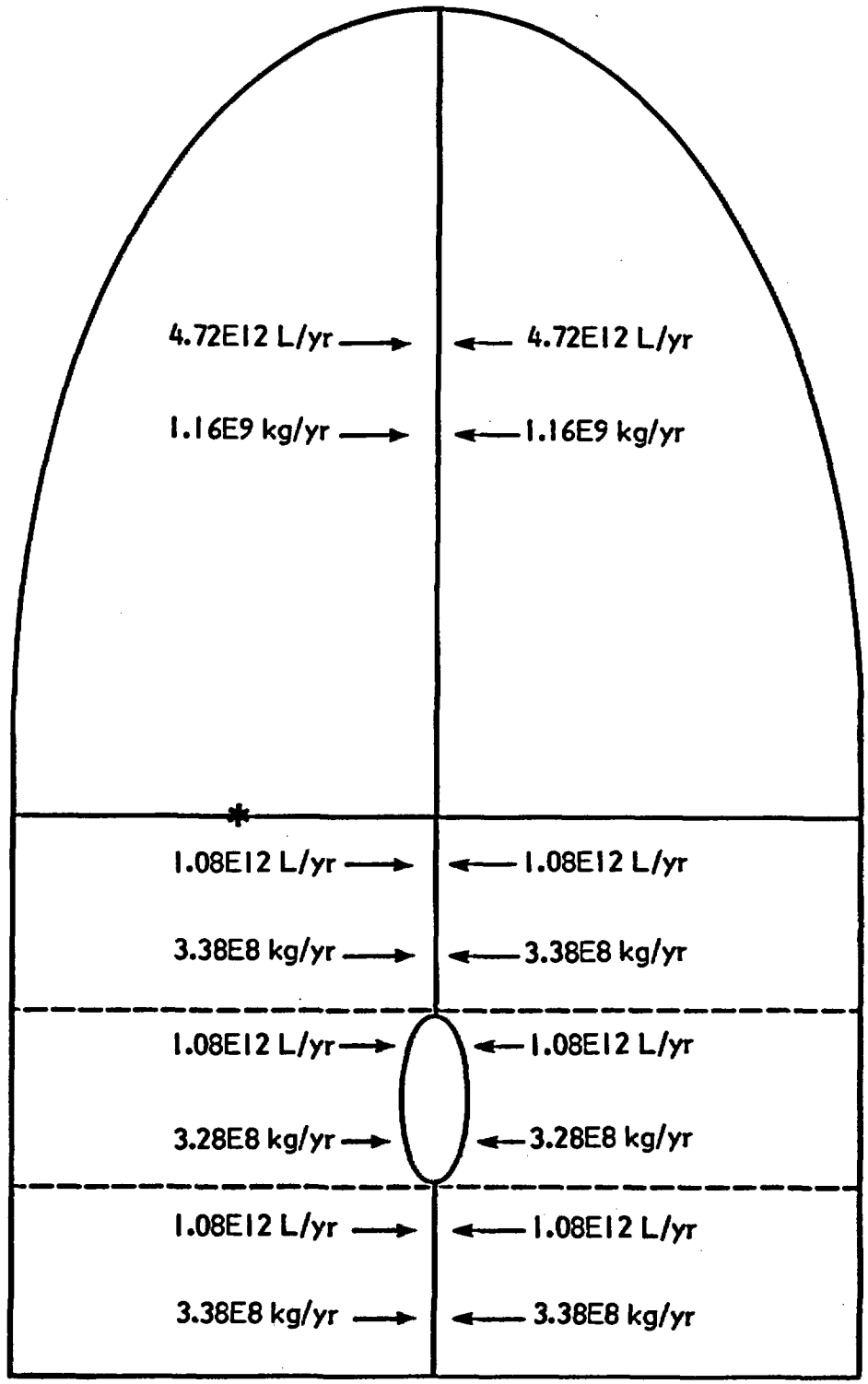

a watershed erosion rate of 5 cm/1,000 yr and a soil density of 2.8E3 kg/m^3, with 67 percent of the eroded material suspended and 33 percent carried in solution.

The cross-sections of Zones 1 and 3 along with subzone heights and widths are shown in Figure 4-5. The cross-section for Zone 2 is shown in Figure 4-6. The characteristics of the soil, surface water, sediment, and groundwater subzones for each zone are given in Figure 4-7. On the basis of the characteristics given in Figure 4-7 and the dimensions of each subzone, the quantities of water and solid are calculated for each subzone and presented in Figures 4-8 through 4-10 for Zones 1, 2, and 3, respectively. Although no doses are to be calculated for individuals in Zone 3, that dose calculation has been included in the problem statement for future problem iterations.

The transfers of water and solid between subzones and zones are shown schematically in Figure 4-11. For Zones 1 and 3, it is assumed that the surface-water and soil subzones exchange the equivalent of one soil pore volume of water per year due to overbank flooding, and that the transfer of solid between these two subzones involves an exchange of 0.1 percent of the soil mass per year. For all three zones, the transfer of water from the soil to the groundwater subzone is based on an assumed infiltration rate of 0.6 m/yr. In the case of each zone, 10 percent of the sediment solid and associated water is assumed to be exchanged between the sediment and surface-water subzones each year. For Zone 2, the exchange of water and solid between the lake and the soil is based on an assumed 0.3 m/yr sprinkler irrigation rate, with half the water and solid applied to the soil being returned to the lake. For the purposes of this problem, no water loss from the soil is assumed to occur due to plant uptake. In Zone 2, there is a transfer of solid and associated water from the sediment subzone to a sink. This transfer represents the 75 percent of incoming sediment that is trapped by the lake. The water and solid flow rates are specified for each zone in Figures 4-12 through 4-14.

Within each subzone, the radionuclide concentrations associated with the water (Ci/L) and solid (Ci/kg) components are determined by the distribution coefficient, k_d. The K_d values for each radionuclide under consideration are given in Table 4-1 for each of the four compartments. These values are to be used for all three zones of the system.

Figure 4-5

Cross-Section for Zones 1 and 3 (Drawing Not to Scale)

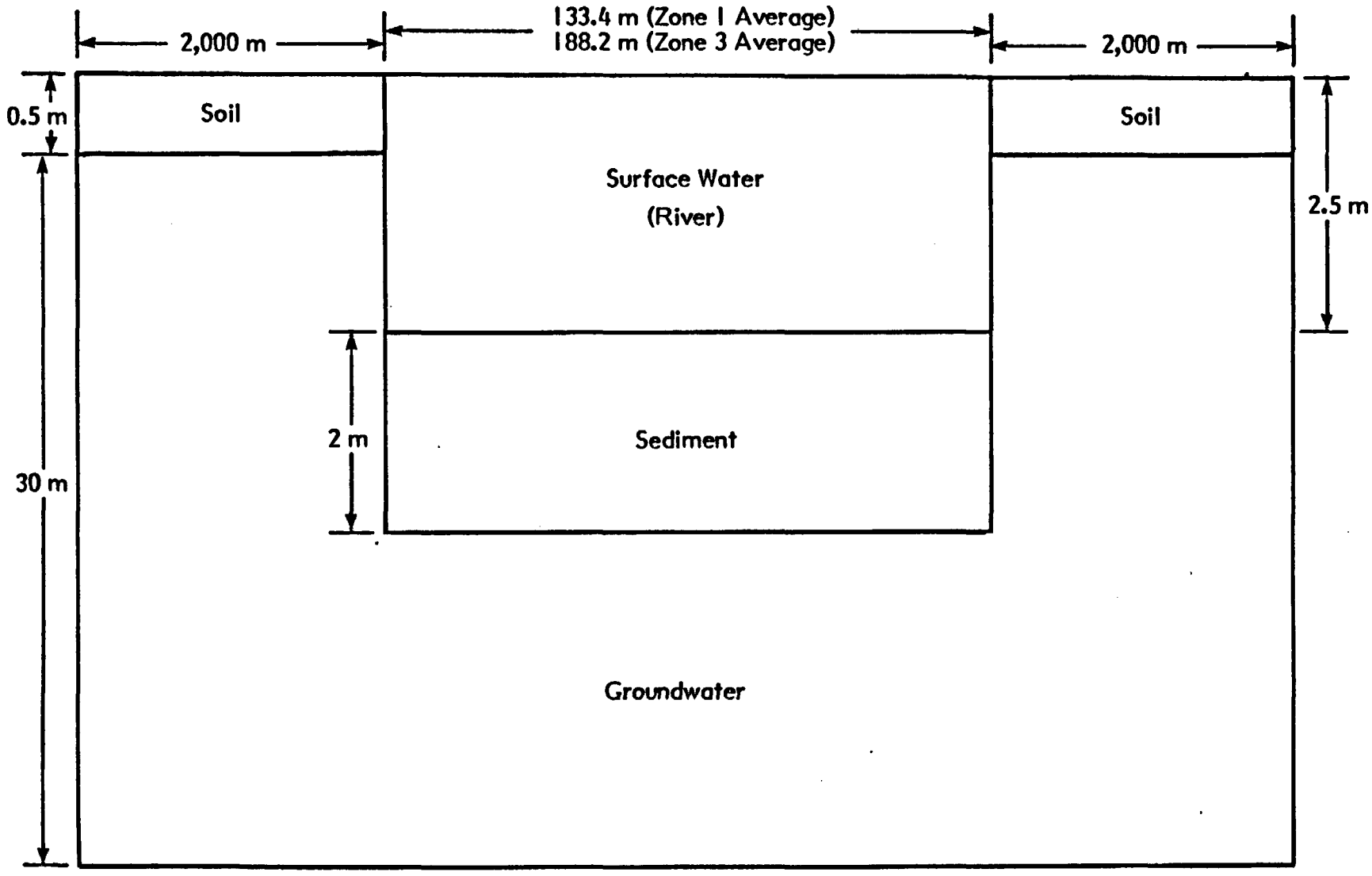

Figure 4-6

Cross-Section for Zone 2 (Drawing Not to Scale)

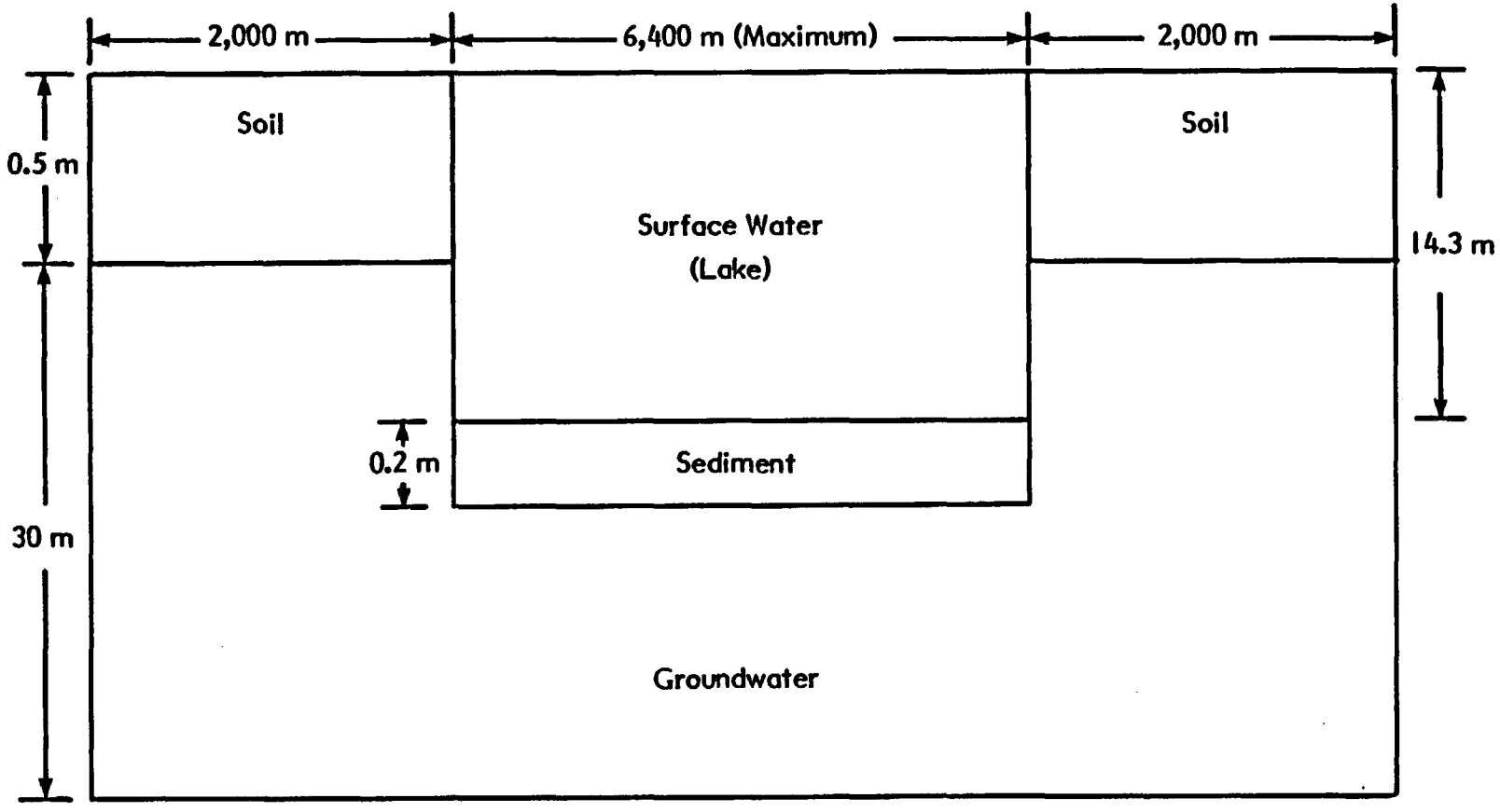

Figure 4-7

Characteristics of the Soil, Surface Water, Sediment, and Groundwater Subzones for Each of the Three Zones

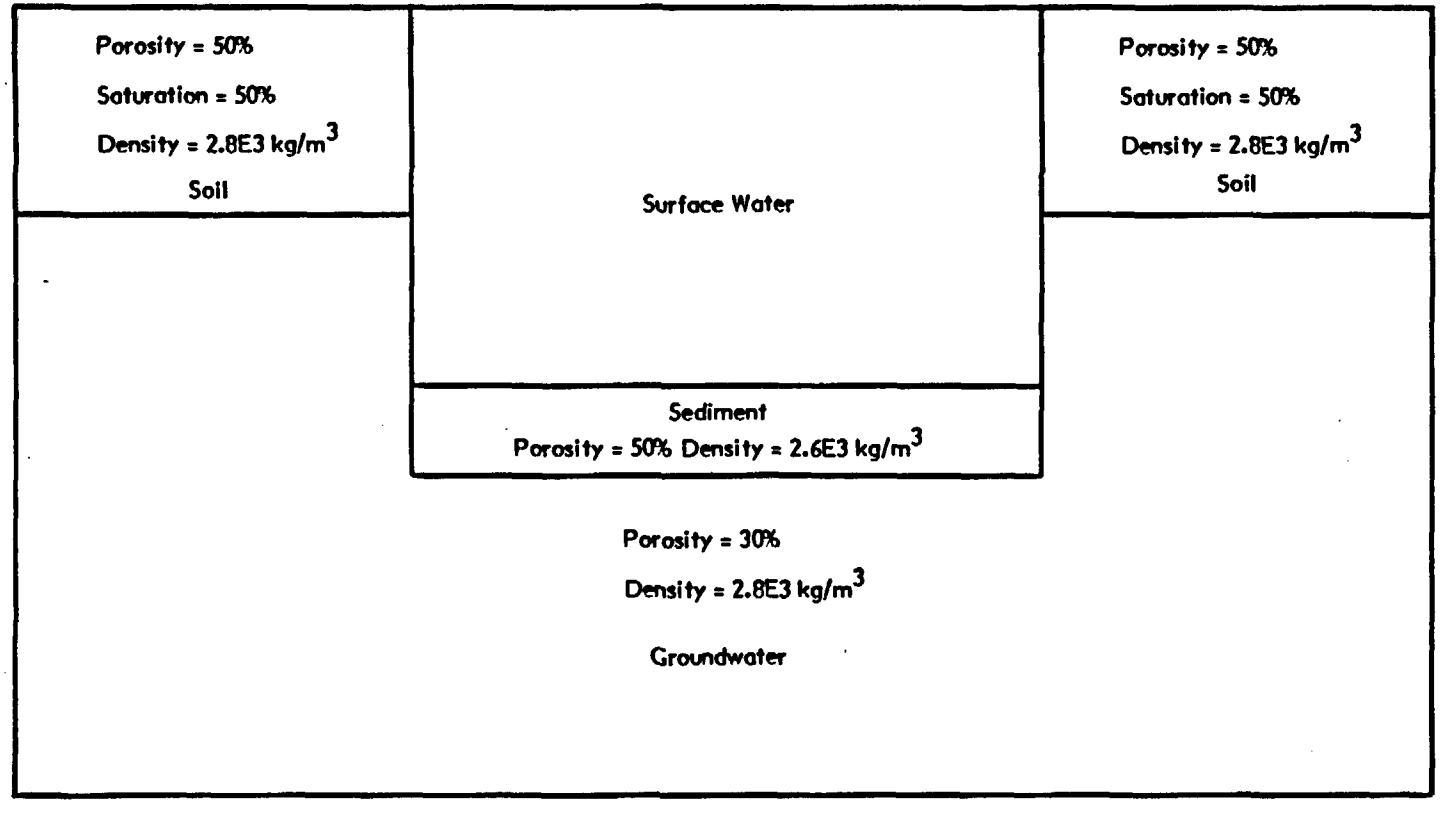

Figure 4-8

Zone 1: Water and Solid Amounts for Each Subzone

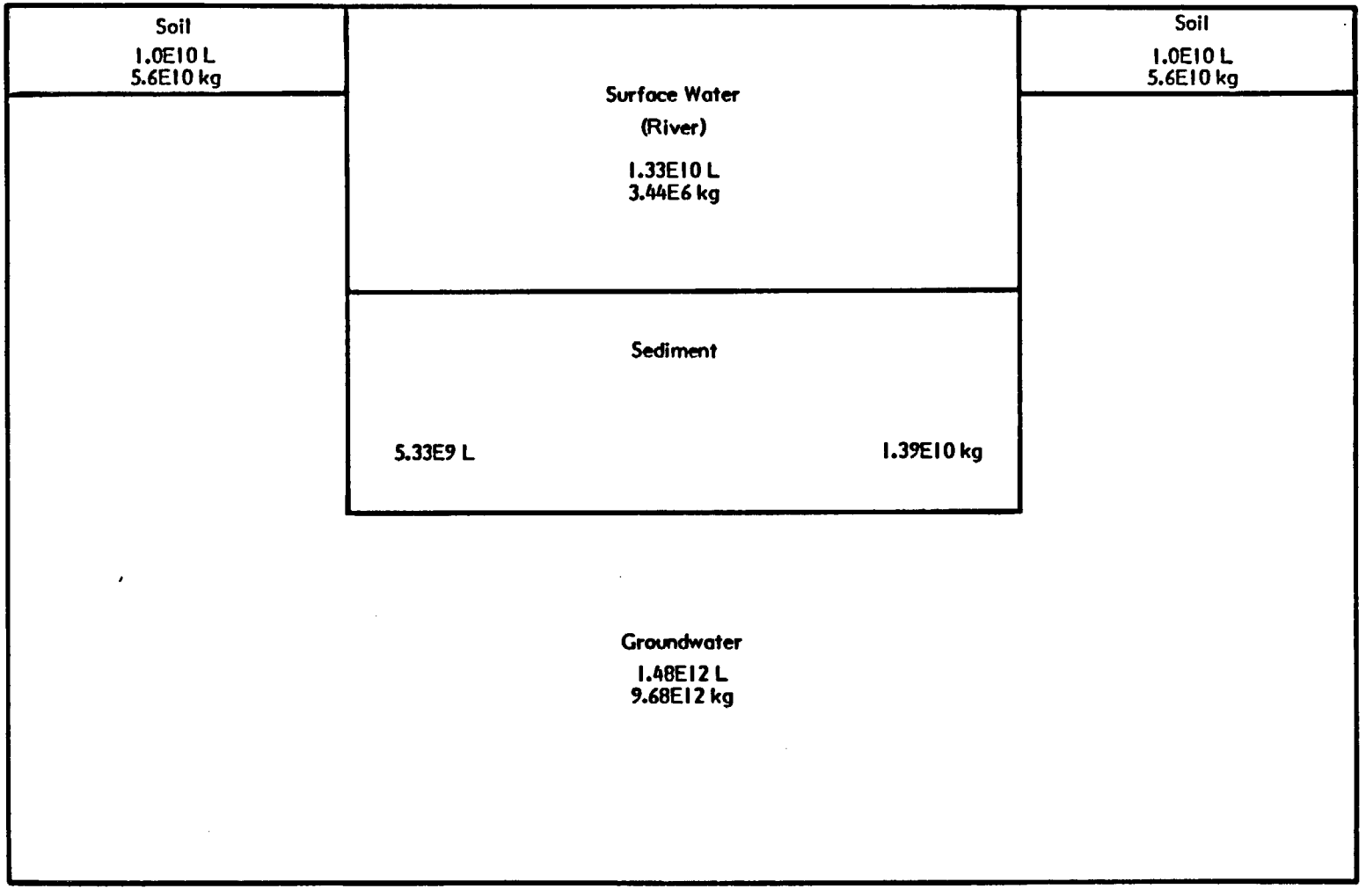

Figure 4-9

Zone 2: Water and Solid Amounts for Each Subzone

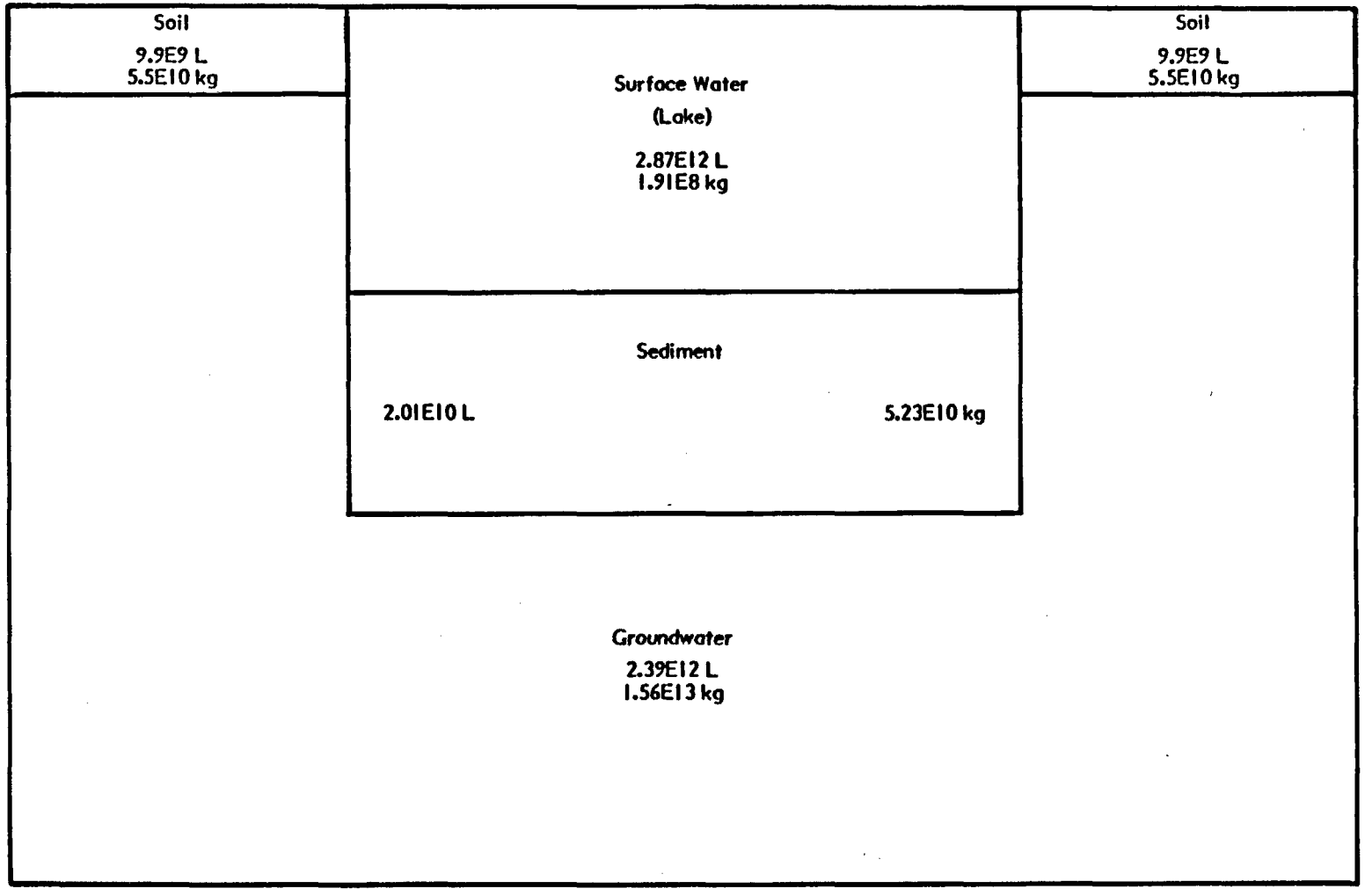

Figure 4-10

Zone 3: Water and Solid Amounts for Each Subzone

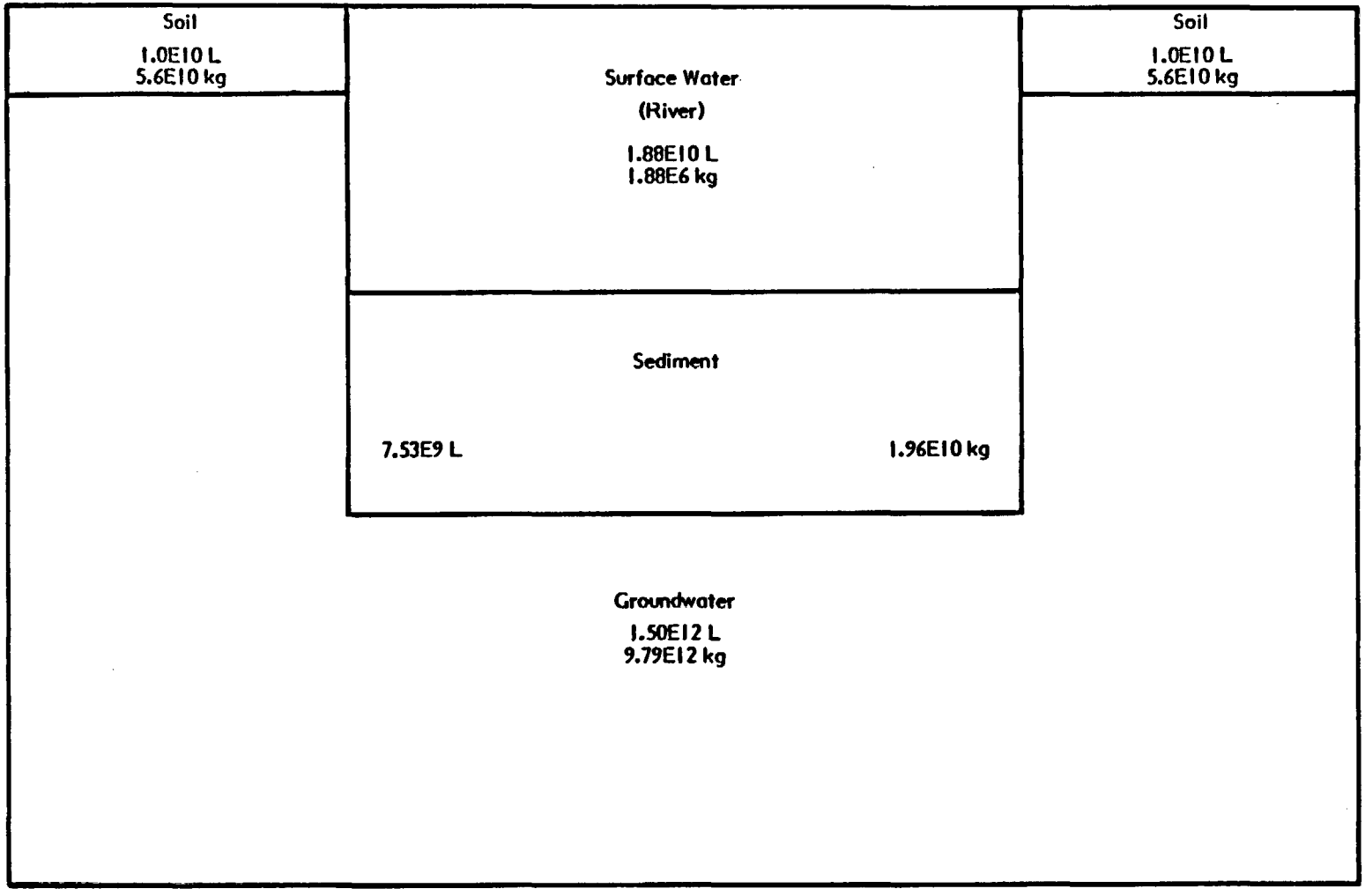

Figure 4-11

Water (L) and Solid (S) Transfers between
Subzones and Zones

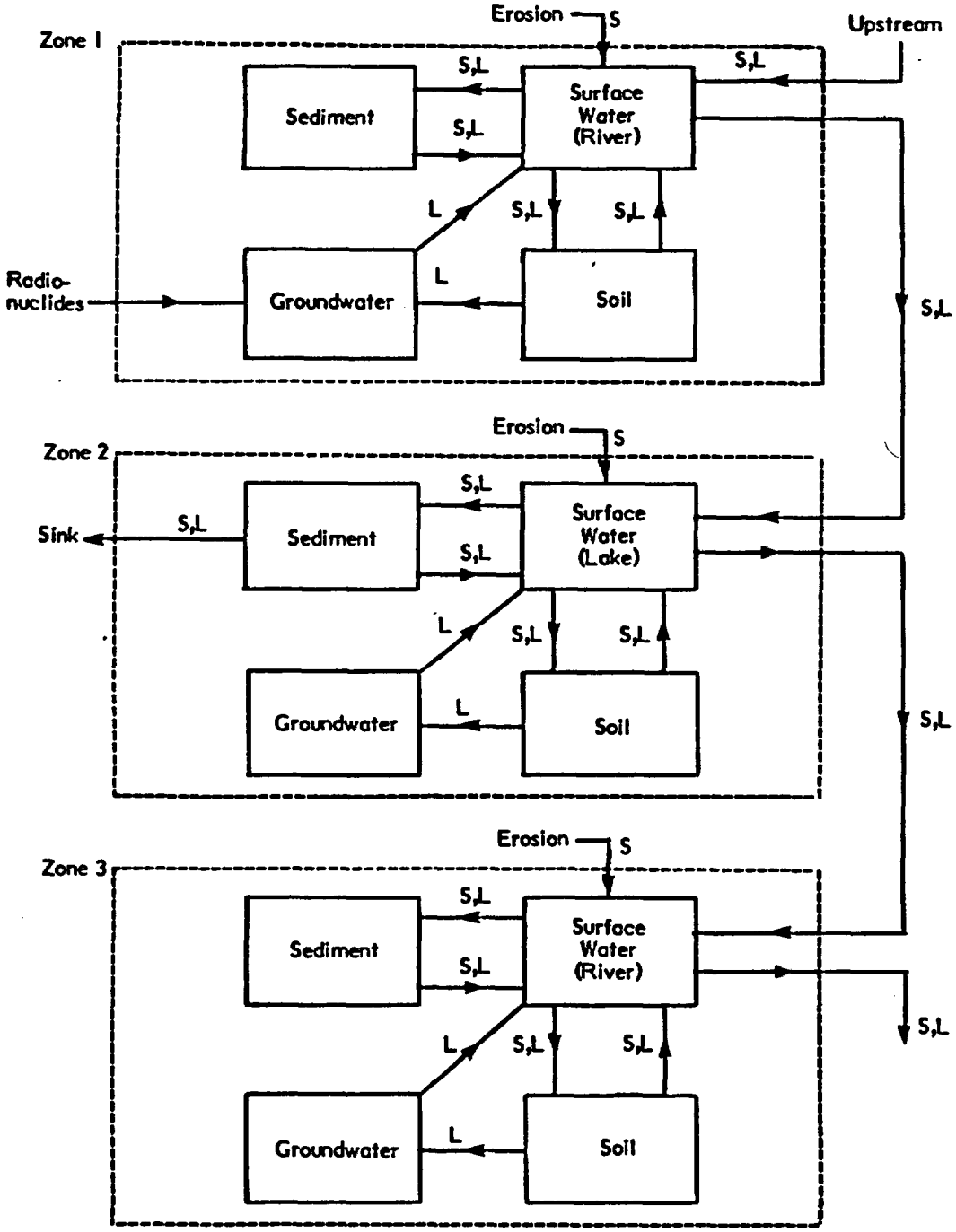

Figure 4-12

Water and Solid Flows between Subzones of Zone 1. Exchange of Water between Surface Water and Soil is Based upon Assumed Exchange of One Pore Volume of Water per Year Due to Overbank Flooding. Transfer of Solid between These Two Subzones is Based upon Exchange of 0.1 Percent Soil Mass per Year.

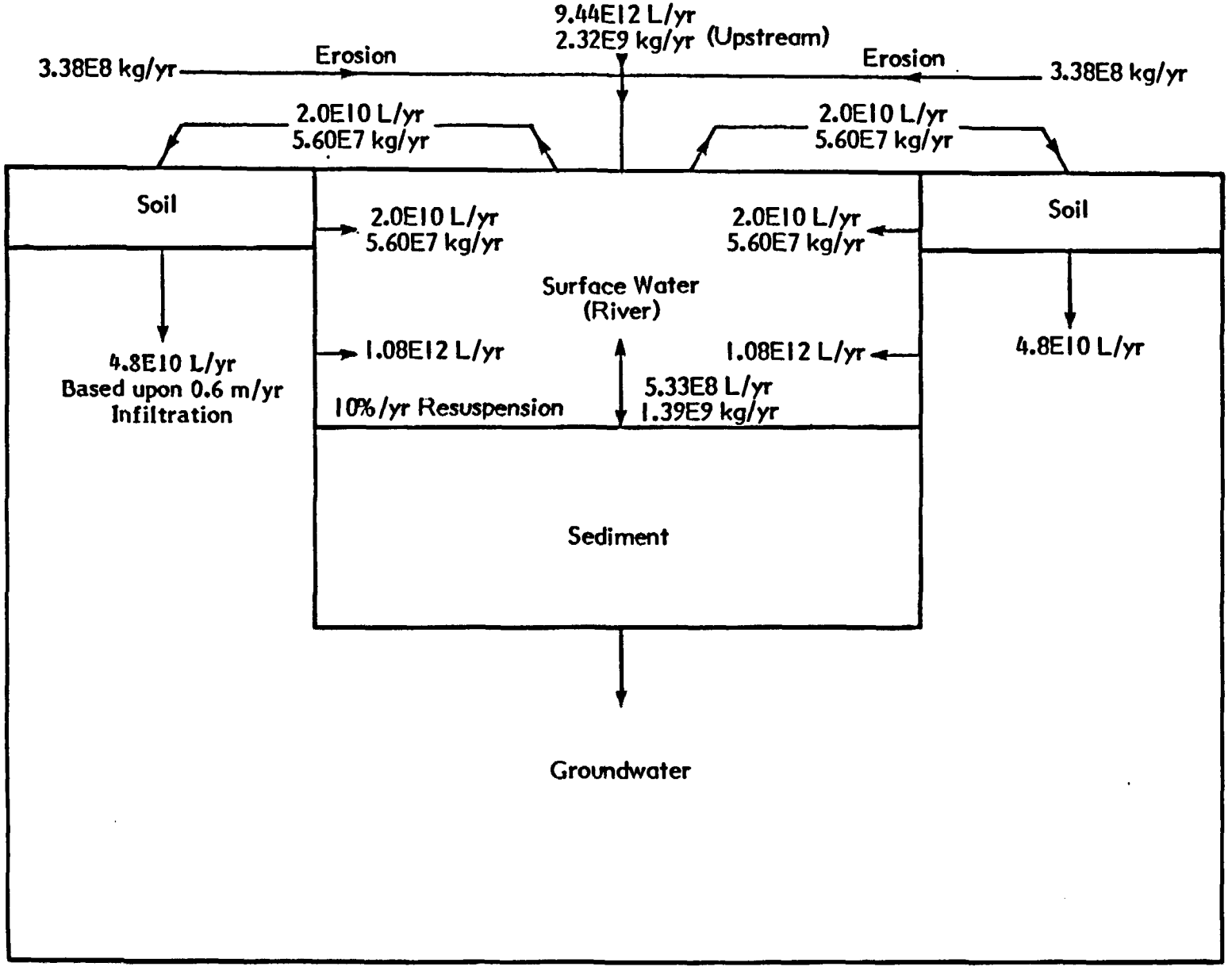

Figure 4-13

Water and Solid Flows between Subzones of Zone 2. Exchange of Water and Solid between Lake and Soil is Based upon Assumed 0.3 m/yr Irrigation Rate, with Half the Water and Solid Applied to the Soil Being Returned to the Lake.

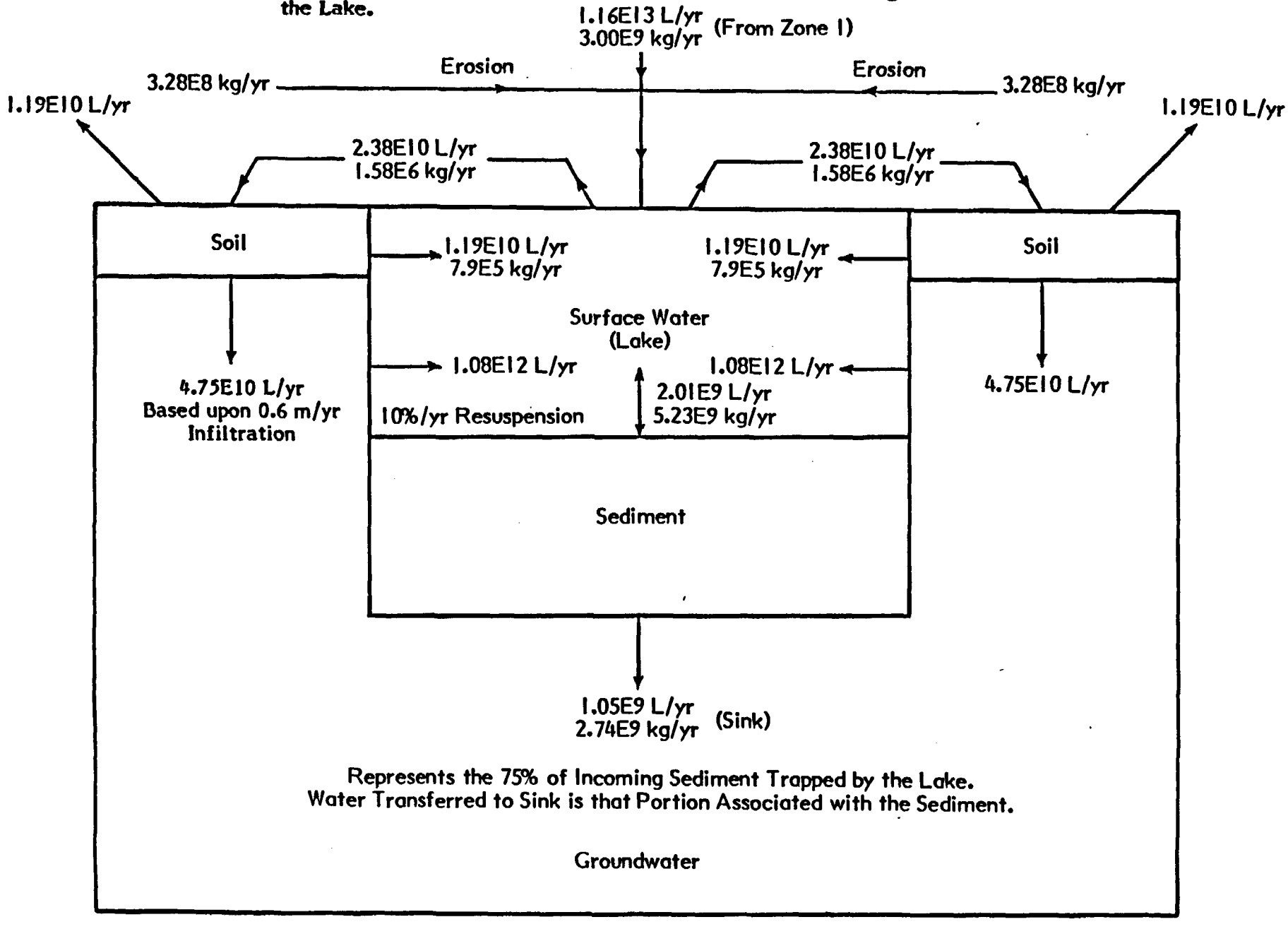

Figure 4-14

Water and Solid Flows between Subzones of Zone 3. Rationale for Exchange of Water and Solids between Surface Water and Soil is Same as for Zone 1.

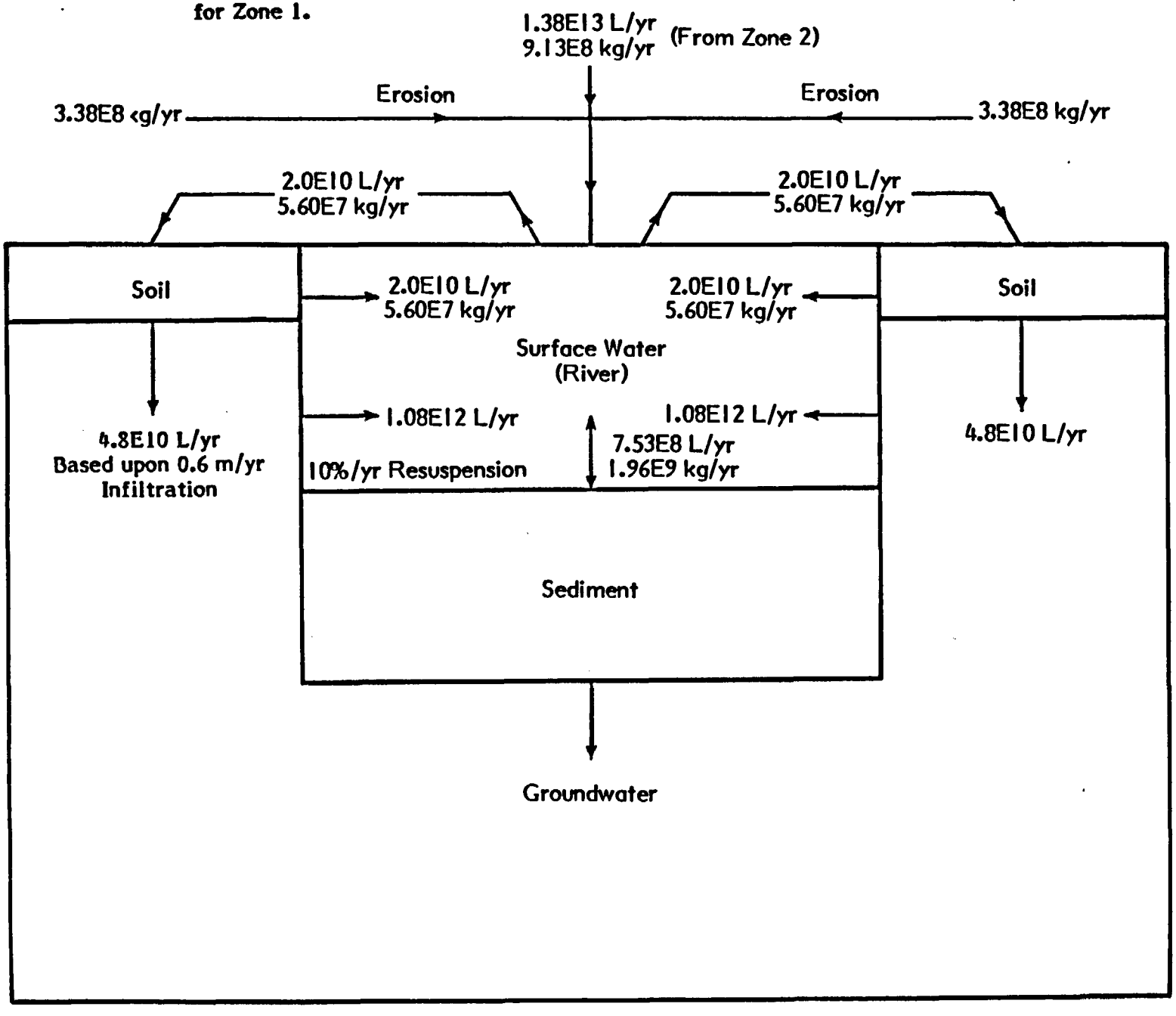

Table 4-1

Radionuclide Distribution Coefficients (L/kg) for Each Subzone

Radionuclide	Distribution Coefficient			
	Sediment	Surface Water	Groundwater	Soil
^{242}Pu	50,000	100,000	5,000	1,000
^{238}U, ^{234}U	5,000	10,000	500	10
^{230}Th	50,000	100,000	50,000	10,000
^{226}Ra	5,000	50,000	5,000	10
^{222}Rn	0	0	0	0
^{210}Pb	5,000	10,000	500	10

Note: Values apply to all three zones.

As water and solid components are transferred between subzones, the radionuclide associated with each component moves along. When the radionuclide reaches a new subzone, it is reassigned to water and solid components according to the subzone's relative amounts of water and solid and its distribution coefficient. The radionuclide input rates for the groundwater compartment of Zone 1 for an entire 10,000-year simulation period are given in Table 4-2. At the beginning of the simulation, the radionuclide concentration in all subzones is assumed to be zero.

Once the gas ^{222}Rn is formed, it is assumed to be removed to the atmosphere with the following rate constants in all three zones: sediment (6,070 yr^{-1}), surface water (364,000 yr^{-1}), groundwater (0.0 yr^{-1}), and soil (51.4 yr^{-1}). The removal of ^{222}Rn from surface water and sediment is, in effect, instantaneous. The rate for soil is based on a value of 3.6×10^{-5} Ci per m^2 (of land surface area) per year per pCi/g of ^{226}Ra in soil (Reference 4).

The radiation exposure to an individual is assumed to take place in Zone 2 and is a function of radionuclide concentrations in the soil and surface water. From the soil (see Figure 4-15, radionuclides are transferred to vegetation through root uptake. Radionuclides are also transferred to vegetation by means of sprinkler irrigation. For this problem, it is assumed that the suspended river sediments are included in this irrigation water. The vegetation is eaten by man and cattle. The milk or beef derived from the cattle is, in turn, consumed by man. Exposure also occurs due to radiation emanating directly from the ground. To calculate this exposure, it is necessary to know the surface radionuclide "concentration" in Ci/m^2. For the purpose of arriving at this surface concentration, one should assume an effective soil depth of 2.5 cm, a soil density of 2.8 $E3kg/m^3$, and a porosity of zero in this topmost layer. Contaminated soil particles are blown into the air and inhaled by man. Direct radiation from this cloud of particles can also contribute to human exposure. The exposure due to direct inhalation of ^{222}Rn has been neglected for the purposes of this benchmark problem. Uptake of ^{222}Rn by plants is assumed to be zero.

Man can receive a dose from radionuclides in the water both directly and indirectly (see Figure 4-16). A direct dose can be received by drinking the water

Table 4-2

Radionuclide Input Rates for the Groundwater Subzone of Zone 1

Radionuclide*	Half-Life (yr)	Input Rate		
		Ci/yr	g/yr	Atoms/yr
^{242}Pu	3.763E5	0.6	153	3.80E23
^{238}U	4.468E9	1.0	2.97E6	7.52E27
^{234}U	2.445E5	0.7	112	2.88E23
^{230}Th	7.7E4	0.8	39.6	1.04E23
^{226}Ra	1,600	0.8	0.808	2.16E21
^{222}Rn	0.01048	0.8	5.20E-6	1.41E16
^{210}Pb	22.3	0.8	0.0105	3.00E19

* Decay chain.

Figure 4-15

Exposure Pathways Based upon Radionuclide Concentrations in the Soil

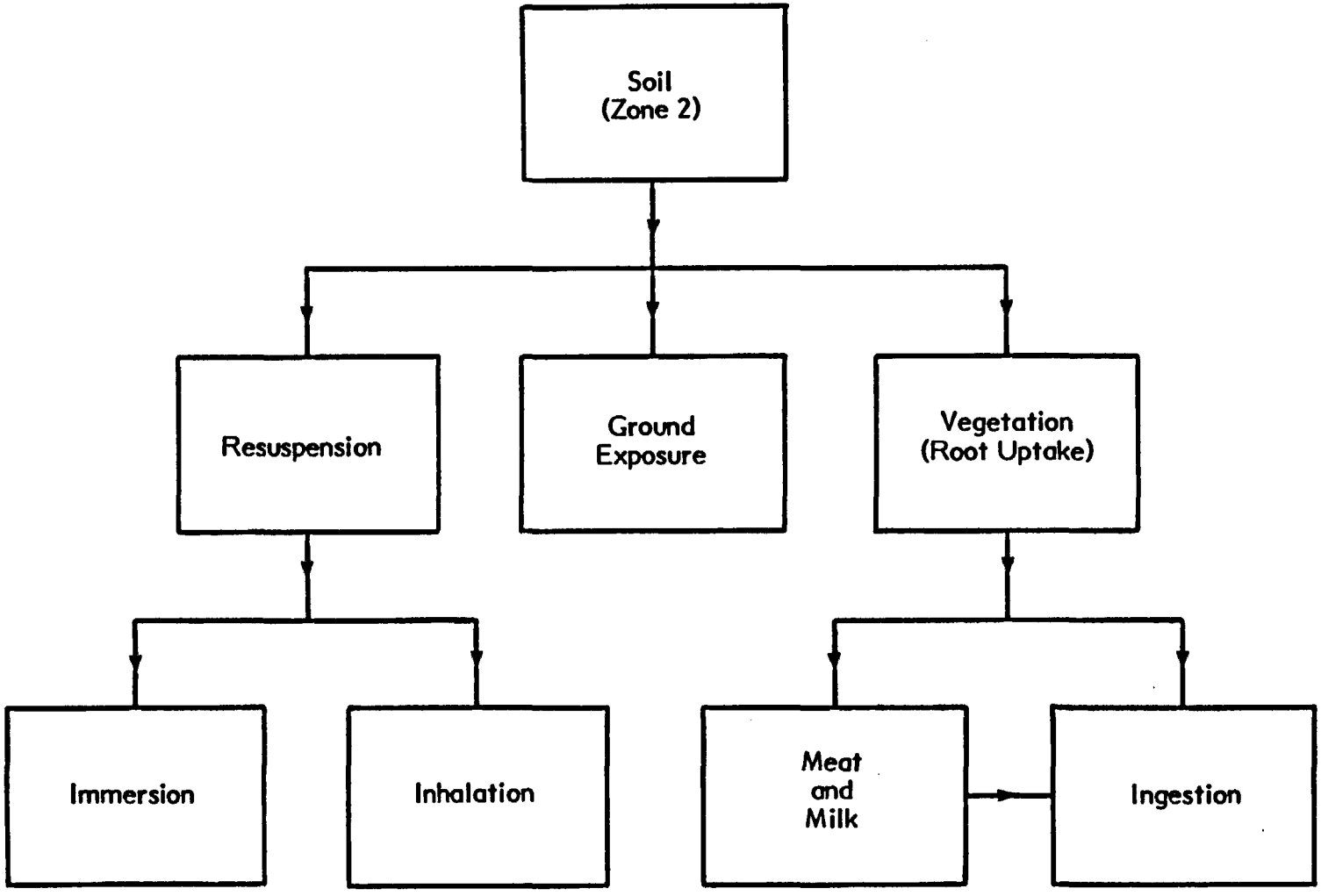

Figure 4-16

Exposure Pathways Based upon Radionuclide Concentrations in Surface Water

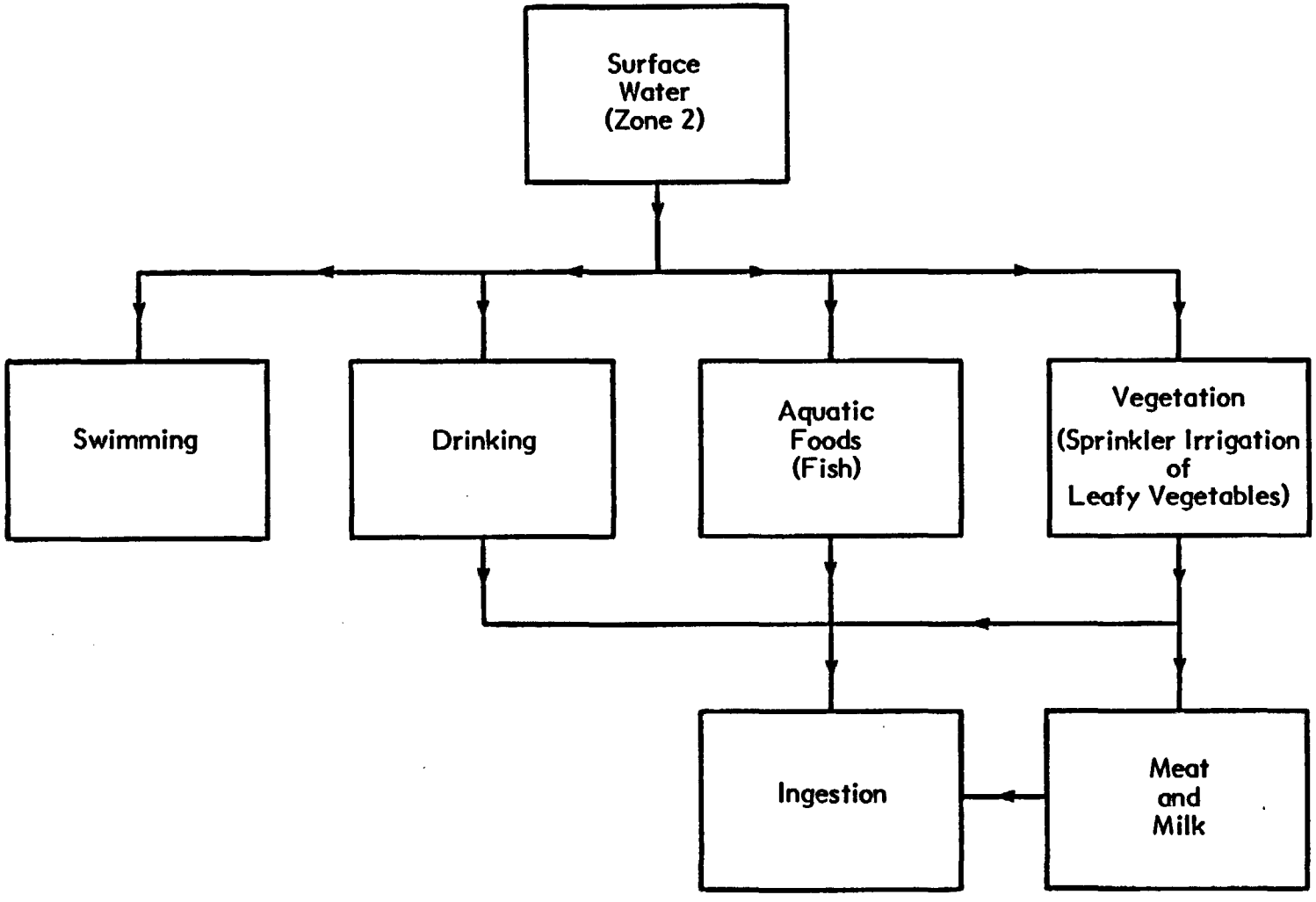

or swimming in it. An indirect dose can be received by ingesting fish from contaminated water, vegetation that has been subjected to sprinkler irrigation with contaminated water, and meat and milk from cattle that have been fed with contaminated water and vegetation. For purposes of this problem, it is assumed that all the water, vegetables, milk, and beef consumed by an individual in Zone 2 are contaminated. Furthermore, it is assumed that all food and water consumed by dairy and beef cattle are contaminated. Drinking water for man and cattle is assumed to contain suspended sediment. The parameters required for this calculation of ingestion, inhalation, and external exposure are given in Table 4-3.

From the soil and surface-water radionuclide concentrations in Zone 2, the dose to an individual is calculated by using the following concentration and dose factors, together with the usage and exposure parameters given in Table 4-3:

- Concentration factors for food for each element
  - Fish (Ci/kg per Ci/L)
  - Vegetables (Ci/kg plant per Ci/kg soil)
  - Milk (Ci/kg milk per Ci/day intake)
  - Meat (Ci/kg meat per Ci/day intake)
- Dose factors for ingestion, inhalation, ground exposure, air immersion, and water submersion for each radionuclide and organ

For this benchmark problem, the concentration and dose factors given in Tables 4-4 through 4-8 are to be used. The inhalation and ingestion dose factors given in Tables 4-7 and 4-8 represent a 70-year intake with a dose commitment time of 70 years following the onset of intake.

Output Specifications. The dose in rem by radionuclide and organ is to be calculated for the following numbers of years after the onset of radionuclide input to the groundwater compartment of Zone 1: 100, 200, 300, 400, 500, 600, 700, 800, 900, 1,000, 2,000, 3,000, 4,000, 5,000, 6,000, 7,000, 8,000, 9,000, and 10,000.

Table 4-3

Usage and Exposure Parameters Pertaining to Zone 2

Parameter	Value
Sprinkler irrigation	33.33 L/m^2/month
Vegetation density (for both human and animal consumption)	5.2 kg/m^2
Irrigation time	62 days
Weathering half-life for radionuclides deposited on plant leaves	14 days
Fraction of radionuclide deposited on leaves that is transferred to the plant	0.25
Vegetable consumption by humans	190 kg/yr
Water consumption by humans	370 L/yr
Consumption of plants by dairy cows	50 kg/day
Consumption of plants by beef cattle	50 kg/day
Dairy cow drinking rate	60 L/day
Beef cattle drinking rate	50 L/day
Meat consumption by humans	95 kg/yr
Milk consumption by humans	100 L/yr
Fish consumption by humans	6.9 kg/yr
Air submersion	8,760 hr/yr for 70 years
Soil exposure	2,920 hr/yr for 70 years
Swimming	15 hr/yr for 70 years

Table 4-3 (Continued)

Parameter	Value
Soil resuspension factor (radionuclide concentration in air ÷ radionuclide concentration in soil)	3.5E-9 kg/m^3
Breathing rate for humans	8,000 m^3/yr
Exposure time for humans	70 years
Dose commitment time	70 years after start of exposure
Simulation period	10,000 years
Soil depth for exposure	2.5 cm

Table 4-4

Concentration Ratios for Freshwater Fish

Radionuclide	Concentration Ratio (Ci/kg fish per Ci/L water)
^{242}Pu	3.5
^{238}U	2.0
^{234}U	2.0
^{230}Th	30
^{226}Ra	50
^{210}Pb	100

Source: Reference 5.

Table 4-5

Concentration Ratios for Vegetation, Milk, and Meat

Radionuclide	Vegetation* (Ci/kg) Vegetation per (Ci/kg) Soil	Milk (Ci/L) Milk per (Ci/day) Intake	Meat (Ci/kg) Meat per (Ci/day) Intake
^{242}Pu	2.5E-4	2.5E-8	5.0E-3
^{238}U	2.5E-3	6.0E-4	5.0E-3
^{234}U	2.5E-3	6.0E-4	5.0E-3
^{230}Th	4.2E-3	2.5E-6	5.0E-3
^{226}Ra	1.4E-3	2.0E-4	9.9E-4
^{210}Pb	6.8E-2	1.0E-5	9.9E-4

Source: Reference 5.

* Wet weight for vegetation and dry weight for soil.

Table 4-6

External Dose Factors

Radionuclide	Ground Exposure (rem/hr per μCi/m^2)		Water Immersion (rem/hr per μCi/m^3)		Air Submersion (rem/hr per μCi/m^3)	
	Skin	Body	Skin	Body	Skin	Body
^{242}Pu	1.60E-8	1.10E-9	3.60E-9	1.10E-10	1.60E-6	5.10E-8
^{238}U	6.32E-7	3.52E-7	9.32E-7	7.36E-8	8.11E-4	3.38E-5
^{234}U	5.08E-7	7.32E-9	1.24E-8	1.18E-9	5.28E-6	5.18E-7
^{230}Th	1.00E-7	7.82E-9	4.41E-9	1.22E-9	1.88E-6	5.45E-7
^{226}Ra	1.55E-5	1.28E-5	5.03E-6	3.26E-6	2.89E-3	1.51E-3
^{210}Pb	1.70E-8	1.30E-8	3.60E-7	3.00E-9	3.36E-4	2.69E-6

Source: Reference 6.

Table 4-7

Inhalation Dose Factors for 70-Year Exposure and 70-Year Commitment

Radionuclide	Dose Factor (rem/μCi/yr)						
	Total Body	Bone	Thyroid	Liver	Kidneys	Lungs	GI-LLI
^{242}Pu	7.63E+3	3.02E+5	0	4.33E+4	3.26E+4	1.18E+4	2.83E+0
^{238}U	7.90E+1	1.34E+3	0	0	3.11E+2	3.31E+3	2.39E+0
^{234}U	9.00E+1	1.46E+3	0	0	3.54E+2	3.78E+3	2.67E+0
^{230}Th	7.09E+3	2.63E+5	0	1.17E+4	5.70E+4	4.16E+4	2.61E+0
^{226}Ra	1.55E+4	1.54E+4	0	5.35E-1	1.52E+1	8.47E+3	2.06E+1
^{210}Pb	1.28E+2	3.71E+3	0	1.00E+3	3.34E+3	1.90E+3	2.55E+0

Source: Reference 6.

Table 4-8

Ingestion Dose Factors for 70-Year Exposure and 70-Year Commitment

Radionuclide	Dose Factor (rem/μCi/yr)						
	Total Body	Bone	Thyroid	Liver	Kidneys	Lungs	GI-LLI
^{242}Pu	9.16E-1	3.63E+1	0	5.13E+0	3.92E+0	0	4.57E+0
^{238}U	3.16E+0	5.27E+1	0	0	1.22E+1	0	3.85E+0
^{234}U	3.60E+0	5.75E+1	0	0	1.39E+1	0	4.30E+0
^{230}Th	2.84E+0	1.02E+2	0	5.84E+0	2.85E+1	0	4.21E+0
^{226}Ra	1.16E+4	1.54E+4	0	4.01E-1	1.14E+1	0	2.32E+1
^{210}Pb	3.54E+1	9.26E+2	0	2.79E+2	8.35E+2	0	3.79E+0

Source: Reference 6.

4.1.2.2 Hypothetical Repository — Radiological Assessment (Benchmark Problem 3.0A)

This problem is identical to the preceding one (problem 3.0), except that no ^{222}Rn physical removal is allowed.

4.1.2.3 Hypothetical Repository — Radiological Assessment (Benchmark Problem 3.0B)

This problem is identical to problem 3.0A, with the following exceptions:

- All seven radionuclides are input directly to the suface-water compartment of Zone 1
- The groundwater compartment of Zone 1 is assumed to contain an infinitesimal solid and water content
- All doses are calculated for Zone 1 rather than Zone 2. In these calculations, the water transfer between stream and soil is assumed to include sprinkler irrigation. The usage and exposure parameters given in Table 4-3 are used.

4.1.2.4 Hypothetical Repository — Radionuclide Daughter Ingrowth (Benchmark Problem 3.1)

This problem is identical to problem 3.0, except that only ^{242}Pu is input (at the rate of 0.6 Ci/yr) and the six daughter radionuclides are produced through chain decay.

4.1.2.5 Hypothetical Repository — Radionuclide Daughter Ingrowth (Benchmark Problem 3.1A)

This problem is identical to problem 3.0A, except that only ^{242}Pu is input (at the rate of 0.6 Ci/yr) and the six daughter radionuclides are produced through chain decay.

4.1.2.6 Hypothetical Repository – Radionuclide Daughter Ingrowth (Benchmark Problem 3.1B)

This problem is identical to problem 3.0B, except that only ^{242}Pu is input and the six daughter radionuclides are produced through chain decay.

4.1.2.7 Hypothetical Repository – ^{14}C and ^{129}I Exposure (Benchmark Problem 3.2)

In this benchmark problem, the physical dimensions, subzone solid and water contents, and intersubzone solid and water transfers are the same as in problem 3.0. The exposure of humans to ^{14}C and ^{129}I occurs in Zone 2 according to the usage and exposure parameters given in Table 4-3.

The rates at which ^{14}C and ^{129}I are input to the surface-water compartment are 1 Ci/yr and 0.1 Ci/yr, respectively. The environmental transport parameters and dose factors for ^{14}C and ^{129}I are given in Tables 4-9 and 4-10. No loss of ^{14}C to the atmosphere is assumed.

4.1.2.8 Hypothetical Repository – ^{14}C and ^{129}I Exposure (Benchmark Problem 3.2A)

This problem is identical to problem 3.2, except that the groundwater subzone is assigned an infinitesimal solid and water content and all doses are calculated in Zone 1.

4.1.3 Benchmarking Results and Conclusions

Since the benchmark problems were adapted from a problem originally used in the sensitivity analysis of the PATH1 code, little difficulty was encountered in preparing the input data sets; essentially the only problems were the practical ones associated with the cumbersome PATH1 input format. The selection of parameters for the differential equation solver turned out to involve a trial-and-error process. The PATH1 user must specify two parameters that control the

Table 4-9

Environmental Transport Parameters for ^{14}C and ^{129}I

	^{14}C	^{129}I
Input Rate	1.0 Ci/yr	0.1 Ci/yr
	0.224 g/yr	566 g/yr
	9.65E21 atoms/yr	2.64E24 atoms/yr
Half-life (yr)	5,730	1.57E7
Distribution Coefficient, K_d		
Sediment (L/kg)	0	100
Surface water (L/kg)	0	1,000
Groundwater (L/kg)	0	10
Soil (L/kg)	0	1
Concentration Ratios*		
Freshwater fish (L/kg)	4.6E3	15
Vegetation (kg/kg)**	5.5	2.0E-2
Milk (day/L)	1.2E-2	6.0E-3
Meat (day/kg)	3.1E-2	2.9E-3

* Reference 7.

** Dry weight for soil; wet weight for vegetation.

Table 4-10

Dose Factors for ^{14}C and ^{129}I

	^{14}C	^{129}I
External Dose Factors*		
Ground exposure(rem/hr per μ Ci/m^2)		
Skin	0.0	7.5E-7
Body	0.0	4.5E-7
Water immersion (rem/hr per μ Ci/m^3)		
Skin	3.8E-9	3.3E-8
Body	0.0	1.7E-8
Air submersion (rem/hr per μ Ci/m^3)		
Skin	3.5E-6	3.9E-5
Body	1.4E-8	1.8E-5
Inhalation Dose Factors (rem/(μCi/yr))**		
Total body	2.98E-2	4.8E-1
Bone	1.59E-1	1.73E-1
Thyroid	2.98E-2	3.86E2
Liver	2.98E-2	1.47E-1
Kidneys	2.98E-2	3.17E-1
Lungs	4.97E-3	0
GI-LLI	2.98E-2	1.55E-2
Ingestion Dose Factors (rem/(μCi/yr))**		
Total body	3.97E-2	6.41E-1
Bone	1.98E-1	2.29E-1
Thyroid	3.97E-2	5.03E2
Liver	3.97E-2	1.96E-1
Kidneys	3.97E-2	4.23E-1
Lungs	3.97E-2	0
GI-LLI	3.97E-2	3.11E-2

* Reference 5.

** Reference 6; 70-year exposure, 70-year commitment.

operation of the differential equation solver GEARB. The first parameter, EPS, is the relative error bound, which acts as a limit for the root mean square normalized error estimate calculated by GEARB. If the error is calculated to exceed EPS, then the initial step size is divided by 10 and the process is repeated. This reduction of step size is allowed a maximum number of ten times before the calculation is aborted. The second parameter, MF, is the "method flag," which is a combinaton of the basic method (METH) and the iteration method (MITER) indicators as follows:

$$MF = 10 \times METH + MITER, \tag{4.1.4}$$

where

METH	= 1	means the Adams methods
METH	= 2	means the backward differentiation formulas, or stiff methods of Gear
MITER	= 0	means functional iteration (no partial derivatives needed)
MITER	= 1	means the chord method with analytic Jacobian
MITER	= 2	means the chord method with Jacobian calculated internally by finite differences
MITER	= 3	means the chord method with the Jacobian replaced by a diagonal approximation based on a directional derivative

The PATH1 examples given in Reference 4-8 (a self-teaching guide) use an EPS of 1.0E-10 and a method flag of 21. Although this choice will yield accurate results for radionuclide input to a surface-water compartment, there will probably be convergence problems in the case of direct radionuclide input to the groundwater compartment. To obtain reasonable running times, achieve accept-

able accuracy, and avoid nonconvergence for this latter case, values of 1.0E-3 and 23 were selected for the parameters EPS and MF, respectively.

A complete list of PATH1-calculated doses by radionuclide, organ, and time can be found in the microfiche output accompanying this report. Presented here graphically are some of the more interesting results for dose to the bone, which represents the largest of the organ doses for the radionuclides considered. One should bear in mind that the doses calculated here do not represent values that would be obtained using inputs from an actual analysis. The radionuclide input rates given in Table 4-2 were chosen simply for the convenience of normalization.

Benchmark problems 3.0 and 3.0A both involve the input of seven radionuclides to the groundwater compartment of Zone 1, with the dose being delivered to the maximally exposed individual in Zone 2. In benchmark problem 3.0, the ^{222}Rn is assumed to be physically removed from the subzones of Zones 1 and 2 according to the rates given in Section 4.1.2.1. No ^{222}Rn removal is assumed for benchmark problem 3.0A. The time-dependent bone dose for both of these benchmark problems is shown in Figure 4-17. The magnitude of the bone dose is significantly higher for problem 3.0A than for problem 3.0, since ^{222}Rn decays into ^{210}Pb, which is an important contributor to the bone dose. In both cases, the dose is still increasing after 10,000 years. On the other hand, the dose rapidly reaches steady state when the radionuclides are directly input to the surface-water compartment of Zone 1 (see Figure 4-18).

Benchmark problems 3.1, 3.1A, and 3.1B are the same as problems 3.0, 3.0A, and 3.0B, except that only ^{242}Pu is input. For groundwater input of ^{242}Pu (problem 3.1), as was the case when all seven radionuclides were input, the calculated bone dose does not even approach steady state after 10,000 years (see Figure 4-19). At this time (see Figure 4-20), the inhalation contribution to this does amounts to only about 12 percent. For ^{242}Pu input to the surface-water subzone of Zone 1 (problem 3.1B), the bone dose reaches steady state after about 2,500 years (see Figure 4-21). This is a much longer time than was required for the steady-state condition to be reached when all seven radionuclides were input to the stream (compare with Figure 4-18). The reason for this lag in the

Figure 4-17

Time-Dependent Bone Dose Calculated for Benchmark Problem 3.0 (Groundwater Radionuclide Input with ^{222}Rn Physical Removal) and Benchmark Problem 3.0A (Groundwater Radionuclide Input without ^{222}Rn Physical Removal)

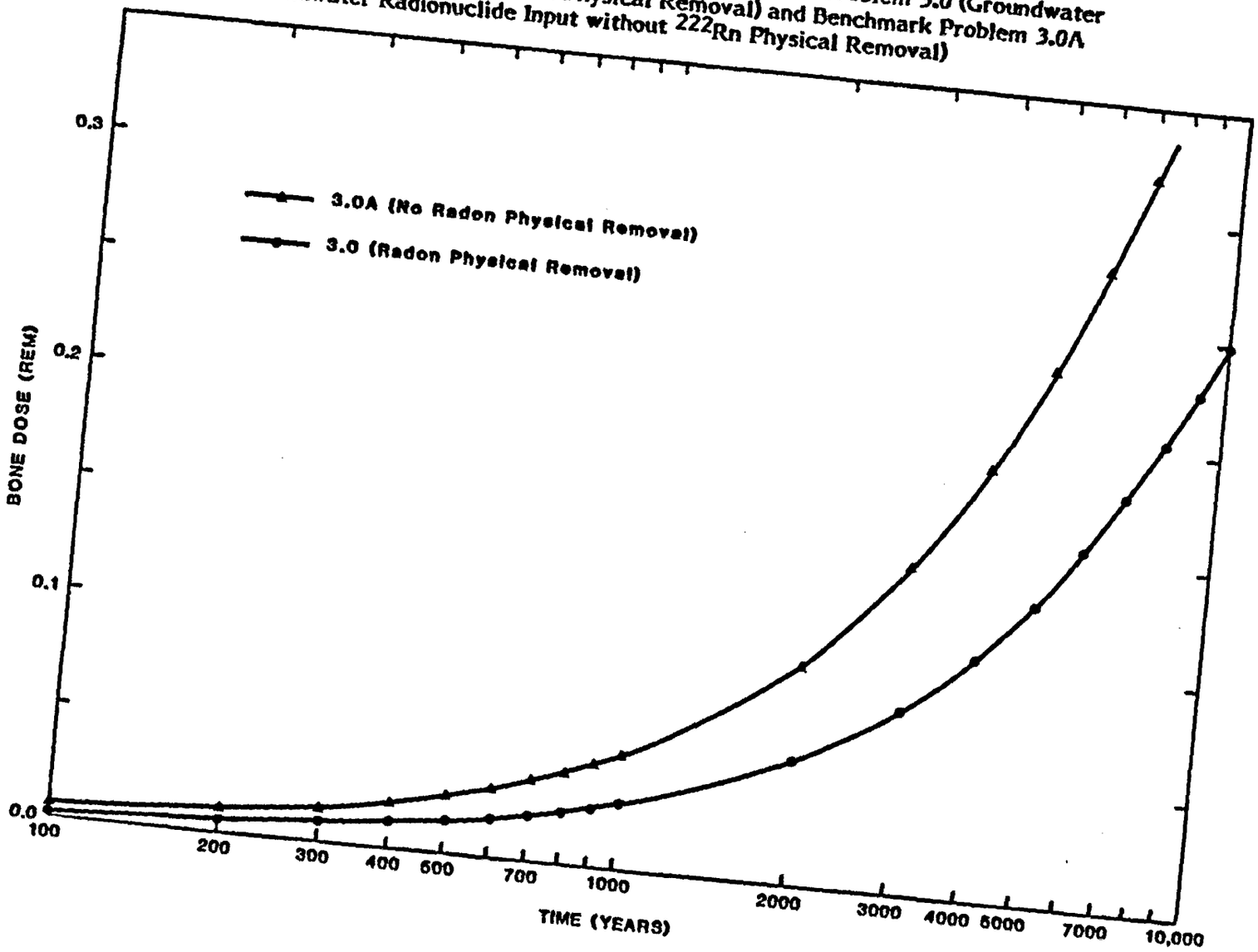

Figure 4-18

Time-Dependent Bone Dose Calculated for Benchmark Problem 3.0B (Surface-Water Radionuclide Input with ^{222}Rn Physical Removal)

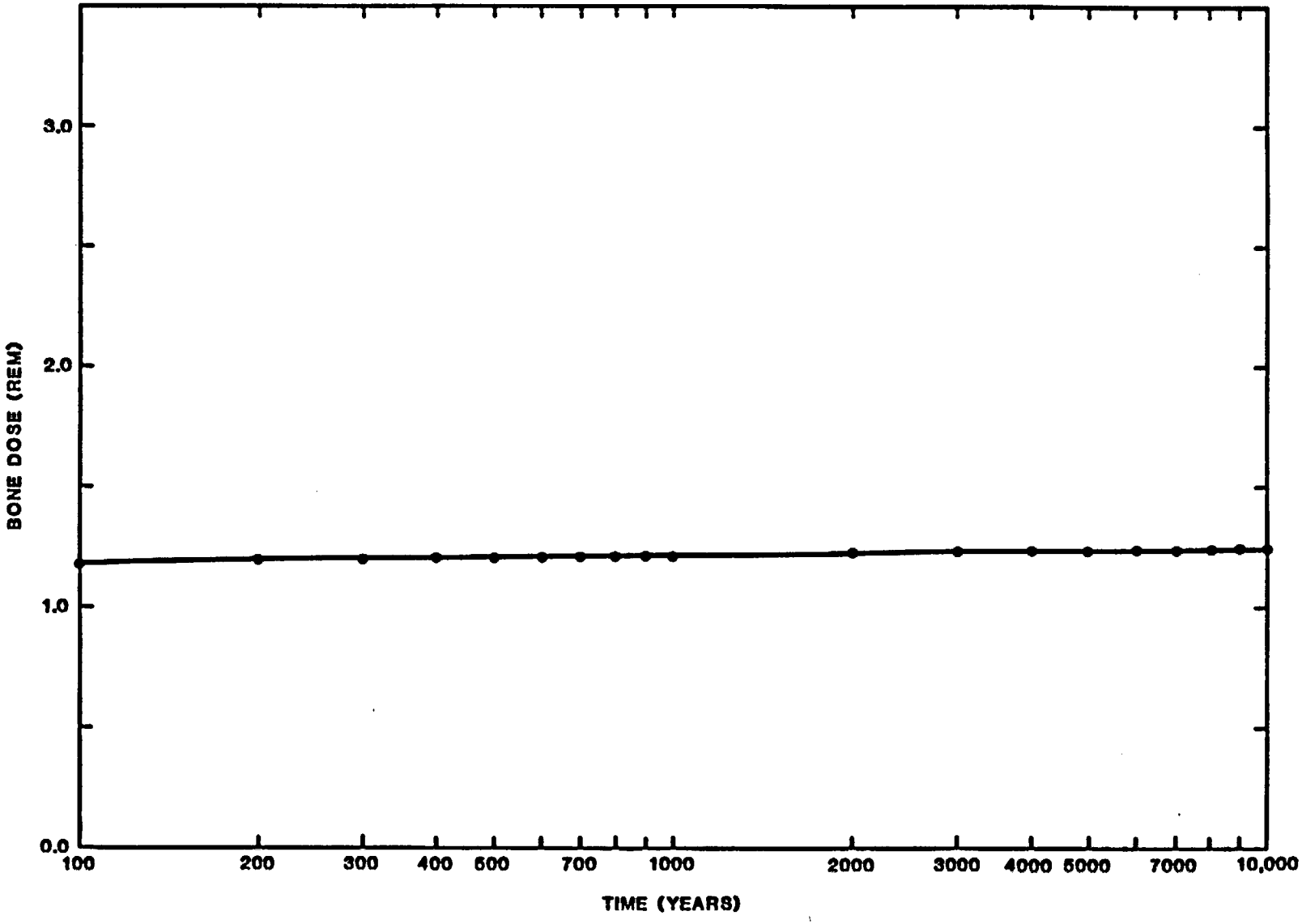

Figure 4-19

Time-Dependent Bone Dose Calculated for Benchmark Problem 3.1 (Only ^{242}Pu Input to the Groundwater). Values the Same for Benchmark Problem 3.1A. Dose Contribution from Daughter Radionuclides Relatively Small.

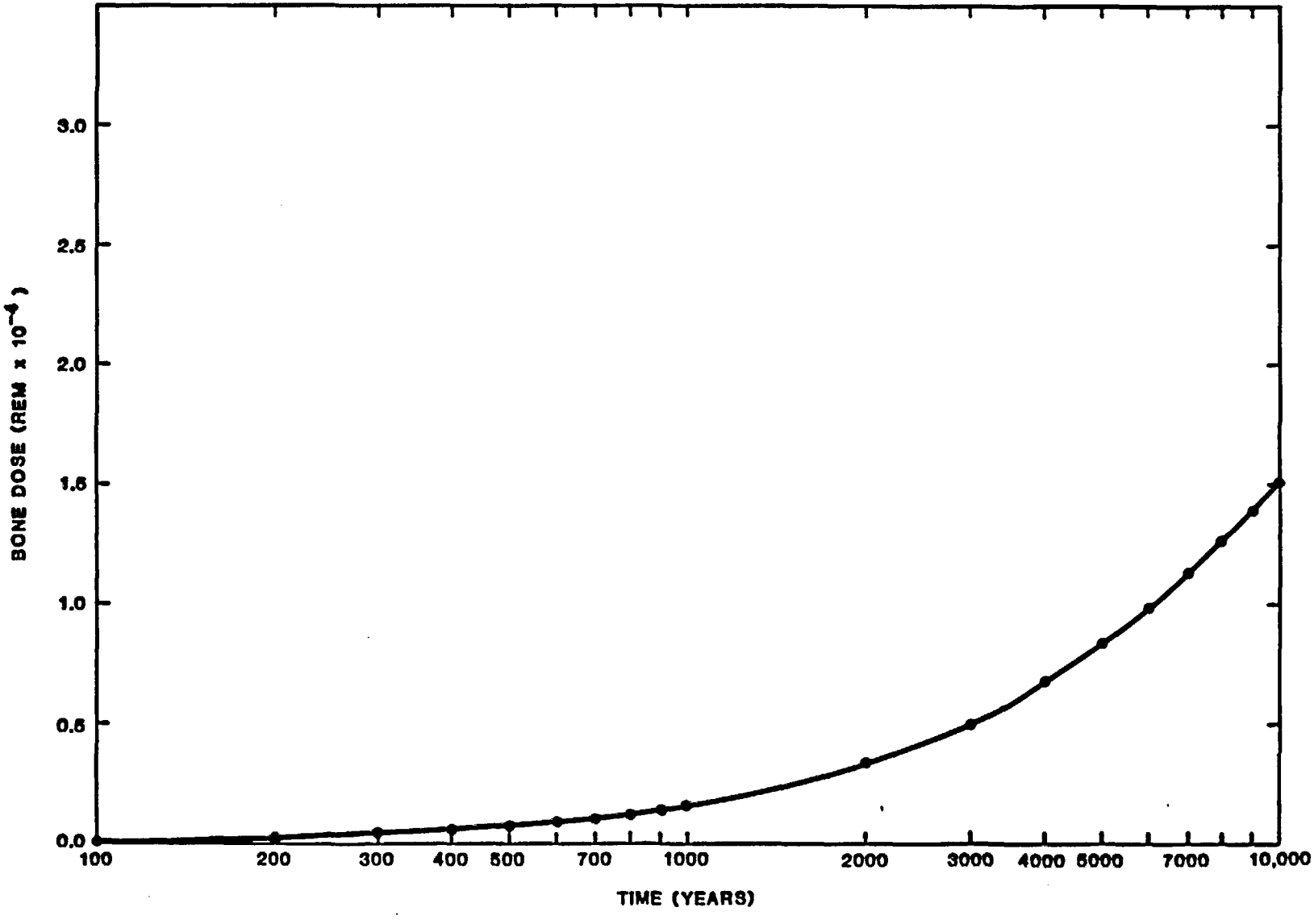

Figure 4-20

Ratio of Inhalation to Ingestion Bone Dose for Benchmark Problem 3.1. Same for Problem 3.1A.

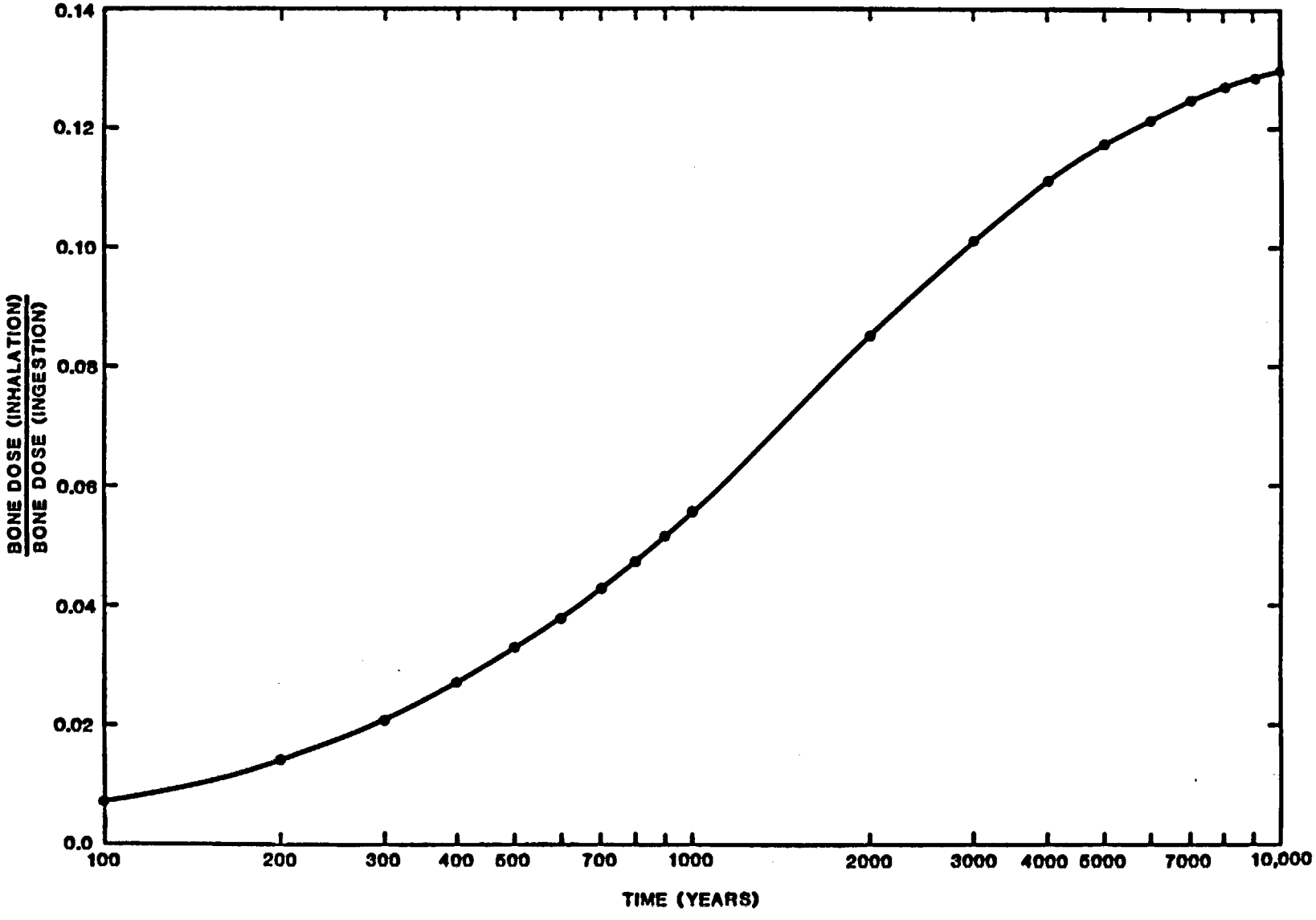

Figure 4-21

Time-Dependent Bone Dose Calculated for Benchmark Problem 3.1 (Only ^{242}Pu Input to the Surface Water). Dose Contribution from Daughter Radionuclides Relatively Small.

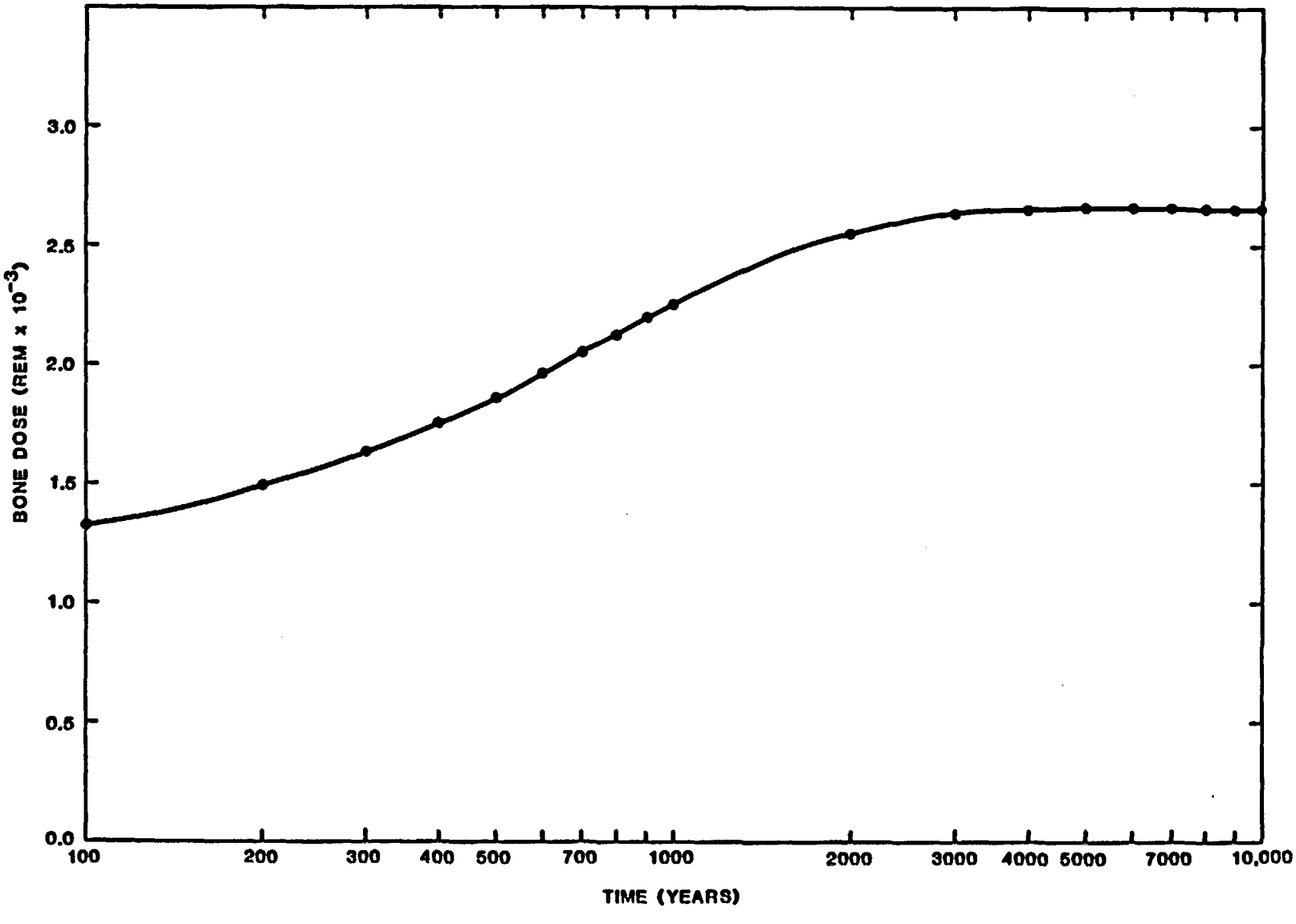

case of ^{242}Pu is the importance of the inhalation dose, which contributes 45 percent of the dose during steady-state conditions (see Figure 4-22). The fact that the inhalation dose requires a buildup of radionuclides in the soil, whereas the ingestion dose does not, explains the longer time for the bone dose to reach steady state in the case of ^{242}Pu input alone.

4.2 CELLTRANS

4.2.1 Code Description

The code CELLTRANS was developed at the outset of this benchmarking effort to check the calculations of PATH1/DOSHEM. The codes differ from one another in the way the linear differential equations of compartment transfer are solved. In CELLTRANS, no compartment transfer is specified for radioactive decay. Instead, decay of a parent is treated as a source term for the daughter. This assumption reduces the order of the transfer matrix by a factor of seven. Furthermore, the radionuclide concentration in a surface-water subzone, when multiplied by the flow out of that subzone, is treated as a source term for the surface-water subzone of the next zone downstream. This means that the transfer matrix can be broken down into a number of 4x4 submatrices, which can be solved rapidly by use of the eigenvalue method. The use of this method means that the calculation can be performed on a microcomputer. In fact, CELLTRANS was developed and tested on a microcomputer before being transferred to the National Institutes of Health (NIH) computing facility used by NRC. The direct integration procedure for solving the compartmental transfer equations, as used in PATH1, is generally too time consuming for a microcomputer.

For a particular zone, the transfer of a radionuclide, A, between subzones can be expressed mathematically as follows:

$$\frac{dA_i}{dt} = \sum_{j=1}^{N} B_{ij}A_j + Q_{Ai} , \qquad (4.2.1)$$

Figure 4-22

Ratio of Inhalation to Ingestion Bone Dose for Benchmark Problem 3.1B

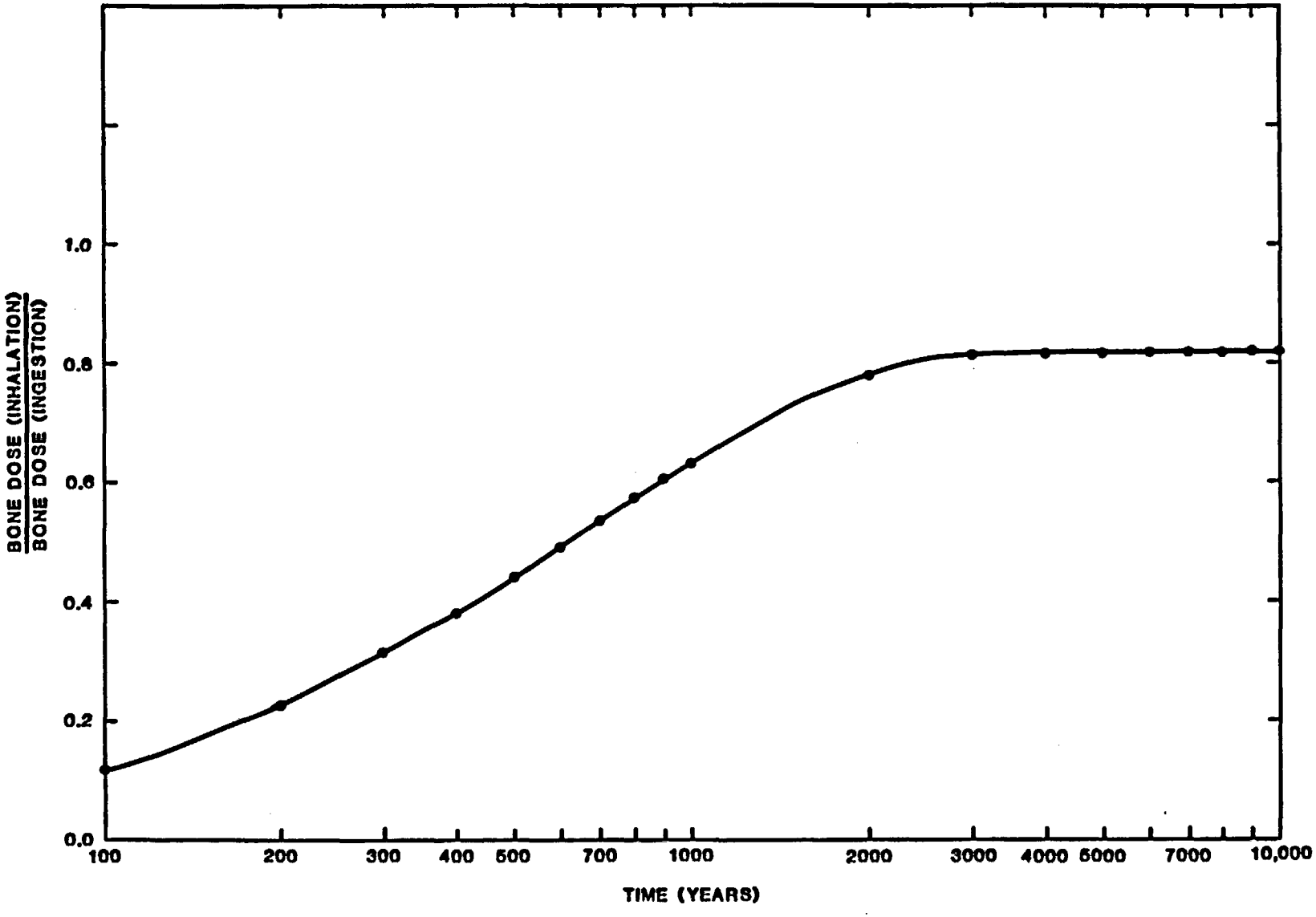

where

A = number of atoms of radionuclide A in subzone i

$$B_{ii} = -\sum_{\substack{j=1 \\ j\neq i}}^{N} B_{ji} - \lambda_i - \sum_{k=1}^{N_s} S_{ki} \qquad (4.2.2)$$

$$B_{ij} = \frac{1}{M_{sj} + \frac{V_{Lj}}{K_{dj}}} \left(\frac{dM_s}{dt}\right)_{ij} + \frac{1}{M_{sj}K_{dj}+V_{Lj}} \left(\frac{dV_L}{dt}\right)_{ij} \qquad (4.2.3)$$

$B_{\substack{ij \\ i\neq j}}$ = transfer coefficient (positive or zero) for transfers from subzone j to subzone i (yr^{-1})

Q_{Ai} = input rate of radionuclide A to subzone i (atoms/yr)

N = number of subzones = 4 (groundwater, surface water, sediment, and soil)

In addition to accounting for direct input of radionuclide A to subzone i, the term Q_{Ai} will also reflect the input of radionuclide A due to the radioactive decay of the parent of A occurring in subzone i. If subzone i is the surface-water subzone, the term Q_{Ai} will also include the input of radionuclide A from the surface-water subzone upstream. The transfer coefficient for radionuclide transfer out of subzone i is given by:

$$B_{ii} = -\sum_{\substack{j=1 \\ j\neq i}}^{N} B_{ji} - \lambda_i - \sum_{k=1}^{N_s} S_{ki} \,, \qquad (4.2.2)$$

where

B_{ii} = negative sum of all transfer coefficients (B_{ij} for $i \neq j$) transfers out of subzone i (yr^{-1}))

λ_i = decay rate for radionuclide A for subzone i (yr^{-1}) (includes both radioactive decay and physical decay from subzone i)

S_{ki} = transfer coefficient for physical transfer of radionuclide A from subzone i to sink k (yr^{-1})

N_s = number of sinks for subzone i

The radionuclide transfer coefficients associated with the physical movement of water and soil between subzones or between a subzone and a sink are calculated as follows:

$$B_{ij} = \frac{1}{M_{sj} + \frac{V_{Lj}}{K_{dj}}} \left(\frac{dM_s}{dt}\right)_{ij} + \frac{1}{M_{sj}K_{dj} + V_{Lj}} \left(\frac{dV_L}{dt}\right)_{ij} , \qquad (4.2.3)$$

where

M_{sj} = mass solid in subzone j (kg)

V_{Lj} = volume of water in subzone j (L)

$\left(\frac{dM_s}{dt}\right)_{ij}$ = transfer rate for mass from subzone j to subzone i (kg/yr)

$\left(\frac{dV_L}{dt}\right)_{ij}$ = transfer rate for water from subzone j to subzone i (L/yr)

K_{dj} = distribution coefficient for subzone j (L/kg)

The solution method for Equation 4.2.1 in CELLTRANS requires determination of the eigenvalues and eigenvectors of the transfer matrix $||B||$ with elements B_{ij}. The matrix $||P||$, with the $||B||$ matrix eigenvectors as columns, can be used to generate a transformed subzone inventory vector $|y|$ as follows:

$$|A| = ||P||\ |y| \tag{4.2.4}$$

With this substitution, Equation 4.2.1 becomes

$$||P||\ \frac{d|y|}{dt} = ||B||\ ||P||\ |y| + |Q| \tag{4.2.5}$$

Multiplying both sides of Equation 4.2.5 from the left by the inverse of $||P||$ gives

$$\frac{d|y|}{dt} = ||P||^{-1}\ ||B||\ ||P||\ |y| + ||P||^{-1}\ |Q| \tag{4.2.6}$$

$$\frac{d|y|}{dt} = ||D||\ |y| + ||P||^{-1}|Q|, \tag{4.2.7}$$

where $||D||$ is the diagonal matrix of eigenvalues ($\lambda 1, \lambda 2 \ldots \lambda N$) of the matrix $||B||$. Equation 4.2.7 can be solved to yield the transformed inventory vector components:

$$y_i(t_m) = \left(\frac{\hat{Q}_{mi}}{\lambda_i} - \frac{K}{\lambda_i^2}\right)\left(1-e^{-\lambda_i(t_m-t_{m-1})}\right) + \frac{K}{\lambda_i}(t_m-t_{m-1}) + y(t_{m-1})\ e^{-\lambda_i(t_m-t_{m-1})}, \tag{4.2.8}$$

where

K = $\dfrac{\hat{Q}_{mi} - \hat{Q}_{m1-i}}{t_m - t_{m-1}}$

$\hat{Q}_{mi}$ = $(||P||^{-1}\ |Q_m|)_i$

t_m = time at the end of the mth time interval (yr)

$|Q_m|$ = vector of subzone radionuclide input rates at time t_m (atoms/yr)

The actual subzone concentrations can then be determined by use of Equation 4.2.4.

The solution given by Equation 4.2.8 is based upon an assumed linear variation of $|Q|$ within the time interval (t_{m-1},t_m). Depending upon the length of the time interval, this is a reasonable approximation even for source terms associated with the decay of a parent radionuclide. When running CELLTRANS, the user should begin with logarithmically spaced time steps that subsequently can be refined until no significant change is observed in the calculated radionuclide concentrations within each subzone. This was the procedure used in the PATH1-CELLTRANS comparison.

4.2.2 Description of Benchmark Problems

The specification of benchmark problems is identical to that given in Section 4.1.2 for the PATH1/DOSHEM code.

4.2.3 Benchmarking Results and Conclusions

A dose-by-dose comparison of PATH1/DOSHEM and CELLTRANS showed differences only in the third significant digit.

4.3 BIODOSE

4.3.1 Code Description

The remaining codes benchmarked in this project do not account separately for the liquid and solid components of the groundwater, surface water, sediment, and soil subzones. Only the code BIODOSE accounts for the long-term transfer of radionuclides between subzones, and even it cannot account for the groundwater subzone or for the presence of multiple zones.

In the BIODOSE code* the amount of radionuclide in river water, Aw (atoms), is given by

$$\frac{dA_w}{dt} = -\left[F + I\,\frac{D\,AR(sed)}{d} + K_{rs}\,AR(sed)\,v_w\right]\frac{A_w}{V_w} + \left(\frac{I + R - E}{B_{rt}\,\theta\,V_s}\right)A_s + \left(\frac{D\,AR(sed)}{K_{rs}\,d}\right)\frac{A_{sed}}{V_{sed}} + Q \qquad (4.3.1)$$

The amounts of radionuclide in the sediment, Ased, and soil, As, are given by the following two equations:

$$\frac{dA_{sed}}{dt} = -\left[\frac{D\,AR(sed)}{d\,K_{rs}} + AR(sed)\,v_w + I\,R_s\right]\frac{A_{sed}}{V_{sed}} + \frac{S_t AR(soil)}{V_s}\,A_s + \left[\frac{D\,AR(sed)}{d} + K_{rs}\,AR(sed)\,v_w\right]\frac{A_w}{V_w} \qquad (4.3.2)$$

$$\frac{dA_s}{dt} = -\left[\frac{I + R - E}{B_{rt}\,\theta} + M_r + S_t\,AR(soil)\right]\frac{A_s}{V_s} + \frac{I}{V_w}\,A_w + I\,R_s\,\frac{A_{sed}}{V_{sed}} \qquad (4.3.3)$$

The variables appearing in Equation 4.3.1 through 4.3.3 are described below:

---

* For a more detailed description, see Reference 1 in Chapter 1 and References 9 and 10 in Chapter 4.

A_w = amount of radionuclide in river water (atoms)

A_{sed} = amount of radionuclide in sediment (atoms)

A_s = amount of radionuclide in topsoil (atoms)

R = average yearly rainfall on the topsoil (m^3/yr)

E = average yearly evapotranspiration from the topsoil (m^3/yr)

F = net outflow rate of the river ($m^{3/yr}$)

θ = volumetric water content of the topsoil

d = average diffusion depth (m)

V_w = river water volume (m^3)

V_{sed} = sediment volume (m^3)

V_s = soil volume (m^3)

AR(sed) = sediment surface area (m^2)

AR(soil) = soil surface area (m^2)

I = irrigation rate (m^3/yr)

D = diffusion coefficient into sediment (m^2/yr)

K_{rs} = distribution coefficient for sediment

B_{rt} = retardation factor for topsoil

v_w = sedimentation rate from the river (m/yr)

S_t = erosion rate of topsoil (m/yr)

Q = radionuclide input rate (atoms/yr)

R_s = ratio of suspended sediment to river water

BIODOSE can calculate radionuclide amounts and concentrations not only for the river water, river sediment, and topsoil compartments but also for estuary water, estuary sediment, plume water, and ocean water. These last four compartments were not, however, included in the benchmark problem simulation. Equations 4.3.1 through 4.3.3 apply to a given radionuclide. One of the most

important assumptions in BIODOSE is that radionuclide decay can be neglected. This is a valid assumption only if the decay rate is low when compared with the compartmental transfer rates. This means that BIODOSE cannot adequately handle benchmark problem 3.1B, which involves radionuclide daughter ingrowth from ^{242}Pu atoms input directly to the stream compartment. Furthermore, BIODOSE cannot handle ^{222}Rn input, transport, and decay.

4.3.2 Adaptation of Benchmark Problems to BIODOSE Input Requirements

The greatest problem encountered in running benchmark problems 3.0B, 3.1B, and 3.2A with BIODOSE was the lack of any straightforward relationship between problem specification and the code's required environmental input parameters. To allow a fair comparison to be made between BIODOSE and the codes PATH1/DOSHEM and CELLTRANS, it was essential that the parameters selected for Equations 4.3.1 through 4.3.3 be such that the transfer matrix for each radionuclide would correspond to the matrix given in the CELLTRANS intermediate output (see Figures 4-23 through 4-29). The BIODOSE input parameter selections required to generate these matrices are given in Tables 4-11 and 4-12. To set the water removal rate by plants equal to zero, it was necessary to set the population dose input parameters, (RATE(b), b=1,5) and FVEG(1), equal to zero. The RATE array give the production rate per animal of the five different types of animal products considered in BIODOSE. FVEG(1) is the fraction of the irrigation rate used for irrigation of vegetation for human consumption. Although this assumption would give incorrect population doses, it does not affect the calculated dose to the maximally exposed individual, which is the quantity of interest in the benchmark problems. Since only one irrigation rate (I) can be used in a BIODOSE run, an average value of 3.686E8 m^3/yr was used for benchmark problem 3.0B. The choice of an irrigation rate will affect only the time-dependent radionuclide concentrations, not the steady-state values. For benchmark problem 3.1B, the irrigation rate chosen was the rate of 4.184E8 m^3/yr associated with ^{242}Pu. Since the irrigation rates derived for ^{14}C and ^{129}I were much different, separate BIODOSE runs were made for these two radionuclides.

Figure 4-23

Transfer Matrix for ^{242}Pu, Based upon CELLTRANS Output (Problems 3.0B and 3.1B)

A

$\frac{dA}{dt}$

	Sediment	Water	Soil
Sediment	-0.1	0.389E3	0
Water	0.1	-0.129E4	0.136E-2
Soil	0	0.315E2	-0.136E-2

Figure 4-24

Transfer Matrix for ^{238}U and ^{234}U, Based upon CELLTRANS Output (Problem 3.0B)

A

$\frac{dA}{dt}$

	Sediment	Water	Soil
Sediment	-0.1	0.291E3	0
Water	0.1	-0.119E4	0.361E-1
Soil	0	0.243E2	-0.361E-1

Figure 4-25

Transfer Matrix for ^{230}Th, Based upon CELLTRANS Output (Problem 3.0B)

A

$\frac{dA}{dt}$	Sediment	Water	Soil
Sediment	-0.1	0.389E3	0
Water	0.1	-0.129E4	0.104E-2
Soil	0	0.315E2	-0.104E-2

Figure 4-26

Transfer Matrix for ^{226}Ra, Based upon CELLTRANS Output (Problem 3.0B)

A

$\frac{dA}{dt}$	Sediment	Water	Soil
Sediment	-0.1004	0.375E3	0
Water	0.1	-0.128E4	0.361E-1
Soil	0	0.304E2	-0.365E-1

Figure 4-27

Transfer Matrix for ^{210}Pb, Based upon CELLTRANS Output (Problem 3.0B)

A

	Sediment	Water	Soil
Sediment	-0.131	0.291E3	0
Water	0.1	-0.119E4	0.361E-1
Soil	0	0.243E2	-0.672E-1

$\frac{dA}{dt}$

Figure 4-28

Transfer Matrix for ^{14}C, Based upon CELLTRANS Output (Problem 3.2A)

A

	Sediment	Water	Soil
Sediment	-0.1	0.401E-2	0
Water	0.1	-0.875E3	2.0
Soil	0	3.01	-2.0

$\frac{dA}{dt}$

Figure 4-29

Transfer Matrix for ^{129}I, Based upon CELLTRANS Output (Problem 3.2A)

$\frac{dA}{dt}$

A

	Sediment	Water	Soil
Sediment	-0.1	83.1	0
Water	0.1	-0.964E3	0.304
Soil	0	9.08	-0.304

Table 4-11

BIODOSE Transfer Parameters for Benchmark Problems 3.0B and 3.1B

Transfer Parameter	Radionuclide-Dependent Transfer Parameters						
	^{242}Pu	^{238}U	^{234}U	^{230}Th	^{226}Ra	^{222}Rn	^{210}Pb*
Irrigation rate (m^3/yr) (I)	4.184E8	3.234E8	3.234E8	4.184E8	4.048E8	–	3.234E8
Diffusion coefficient into sediment (m^2/yr) (D)	1939	1453	1453	1939	1869	–	1453
Distribution coefficient for sediment (K_{rs})	4848	3633	3633	4848	4674	–	3633
Inverse retardation factor for topsoil ($1/B_{rt}$)	1.30E-4	4.46E-3	4.46E-3	9.99E-5	3.61E-3	–	8.31E-3

Radionuclide-Independent Transfer Parameters

(R)	Average yearly rainfall on topsoil (m^3/yr) = 0	(d)	Average diffusion depth (m) = 2
(E)	Average yearly evapotranspiration from topsoil (m^3/yr) = 0	(S_t)	Erosion rate of topsoil (m/yr) = 0
(F)	Net outflow rate of river (m^3/yr) = 1.16E10	(M_r)	Water removal rate by plants (m^3/yr) = 0
(v_w)	Sedimentation rate from river (m/yr) = 0	(V_w)	Water volume (m^3) = 1.33E7
(Θ)	Volumetric water content of topsoil = 0.5**	(V_{sed})	Sediment volume = 1.067E7
(R_s)	Ratio of suspended sediment to river water = 0	AR(sed)	Sediment surface area (m^2) = 5.336E6
		AR(soil)	Topsoil surface area (m^2) = 1.60E8

* Exact matchup not possible for ^{210}Pb, since BIODOSE does not allow for radioactive decay.

** Strictly speaking, this value should be 0.25; but, since only the product of Θ and B_{rt} is used in calculating the soil concentrations, the choice of Θ alone is not important.

Table 4-12

BIODOSE Transfer Parameters for Benchmark Problem 3.2A

Transfer Parameter	Radionuclide	
	^{14}C	^{129}I
Irrigation rate (m^3/yr) (I)	4.0E7	1.21E8
Diffusion coefficient into sediment (m^2/yr) (D)	0.225	414
Distribution coefficient for sediment (K_{rs})	0.562	1035
Inverse retardation factor for topsoil ($1/B_{rt}$)	2.0	0.101

The soil density is used by BIODOSE to convert radionuclide concentrations by volume to concentrations by dry weight of soil. These concentrations by weight are in turn used in the calculation of root uptake of radionuclides, external exposure to ground radiation, and atmospheric concentration of radionuclides due to soil resuspension. Since BIODOSE requires the use of a bulk soil density, a value of 1.4E03 kg/m^3 (based upon a 50 percent porosity), rather than the 2.8E03 kg/m^3 used in PATH1/DOSHEM and CELLTRANS, was input to the program. As stated earlier, BIODOSE does not keep track of the liquid and solid radionuclide concentrations in each compartment. In the case of the topsoil, BIODOSE assumes that all the radionuclide is associated with the solid component. In PATH1/DOSHEM and CELLTRANS, this division between the liquid and solid components is calculated by use of the distribution coefficient, K_d. In practice, however, these two approaches give essentially the same calculated radionuclide concentrations by weight of soil if the K_d value is 10 or greater or if the soil-related pathways are not important.

The calculation of an external dose from ground exposure requires the use of an effective soil depth, which is assumed to be 2.5 cm for all the benchmark problems. The BIODOSE code, however, does not let the user input an effective-depth value directly; instead, it calculates the value as the ratio of the soil volume to the soil area, or 50 cm. This BIODOSE-calculated effective depth of 50 cm would lead to an external dose that is a factor of 20 too high. The user can, however, input a shielding factor of 0.05 to rectify this problem. In practice, a value of 0.10 was used for the shielding factor, since the benchmark problem description requires that actual soil density rather than bulk density be used in the calculation of "surface concentration."

Before the benchmark problems could be run, all of the dose factors in BIODOSE had to be adjusted for the radionuclides of interest. This would not have been difficult except for the fact that the standard ingestion and inhalation dose factors in BIODOSE are based upon a 50-year uptake and commitment time. If the user specifies a greater uptake and commitment time, such as 70 years, BIODOSE will convert the 50-year factor to a 70-year factor by use of the radionuclide half-life in the organ of interest. Consequently, the ingestion and inhalation dose factors in Tables 4-7, 4-8, and 4-10 had to be converted to a 50-year basis before input to BIODOSE. After this conversion had been carried out, it was discovered that BIODOSE does not internally convert the inhalation dose

factor to the time basis supplied by the user. The 70-year inhalation dose factors were therefore input directly. The soil and water exposure dose factors in Tables 4-6 and 4-10 had to be multiplied by 50 to be made consistent with the hr/yr usage basis of BIODOSE. These external dose factors were then converted within BIODOSE to the 70-year exposure period. BIODOSE does not calculate the external dose due to exposure to radioactive dust. In addition to the modifications just described, the following unit changes were made for the dose factors:

Ingestion:	(rem/ (μCi/yr)) to (mrem/ (pCi/yr))
Inhalation:	(rem/ (μCi/yr)) to (mrem/pCi/yr))
Surface Exposure:	(rem/hr per μ Ci/m^2) to (mrem/hr per pCi/m^2)
Water Exposure:	(rem/hr per μ Ci/m^3) to (mrem/hr per pCi/L)

Unlike the other computer codes considered in this study, BIODOSE does not allow the user to input directly a radionuclide source term for the river-water subzone. Instead, the user is required to supply, as a function of radionuclide and time, the number of curies of high-level waste stored per MWe-yr of power production. In calculating the dose in rem, BIODOSE assumes that the activity associated with one MWe-yr of power production is delivered annually to the river-water subzone. The rationale for these units is given in the user's manual for the NUTRAN system (Reference 10), of which the code BIODOSE is a member.

4.3.3 Benchmarking Results and Conclusions

The following three methods can be used in BIODOSE for the calculation of radionuclide concentrations: steady state, quasi—steady state, and time varying. With the steady-state option, BIODOSE calculates steady-state concentrations in all subzones, even if the time to reach steady state is longer than the period between inventory changes (and therefore emission rate changes). With the quasi—steady state option, concentrations in all subzones except the topsoil are assumed to be in a state of equilibrium with the instantaneous topsoil concentration. The topsoil concentration is treated as time varying. The quasi—steady

state method can accommodate only a constant input rate for each radionuclide during what is called the maximum limit of irrigation time. This value, together with an "interval factor" between irrigations, must be specified by the user. For the benchmark problems, the maximum limit of irrigation and the interval factor were chosen as 10,000 years and 1, respectively. With the time-varying option, the radionuclide concentrations in all compartments are allowed to vary with time, as is the rate of radionuclide input to the river-water compartment.

All three of the options just described were used in the running of the benchmark problems with BIODOSE. The doses calculated with the steady-state option agreed with those obtained with the quasi—steady state option at sufficiently long times. The doses calculated with the time-varying option made no sense at all. There appears to be a problem with the use of this option, although the exact nature of the problem has yet to be ascertained. The code developers have been notified of this.

BIODOSE-calculated doses using the quasi—steady state option show good agreement with those calculated by PATH1/DOSHEM and CELLTRANS, except in the case of ^{210}Pb, a radionuclide for which chain decay plays an important role in determining subzone concentrations. Figures 4-30 and 4-31 show only a small difference between the time-dependent bone doses calculated by CELLTRANS and BIODOSE for ^{242}Pu and ^{230}Th, respectively. This difference can be attributed to the fact that a composite irrigation rate was used in the simulation of benchmark problem 3.0B. A more significant discrepancy between the CELLTRANS and BIODOSE bone dose calculations occurs for ^{210}Pb (see Figure 4-32). The reason for this discrepancy is the inability of BIODOSE to account for radionuclide buildup and decay. A detailed comparison of BIODOSE-calculated doses with doses obtained from the other codes is given in Section 4.6.

4.4 PABLM

4.4.1 Code Description

The PABLM code is designed to calculate the dose to an individual or population due to atmospheric deposition of radionuclides or the release of radionuclides to

Figure 4-30

Time-Dependent ^{242}Pu Bone Dose Calculated by CELLTRANS and BIODOSE for Benchmark Problem 3.0B

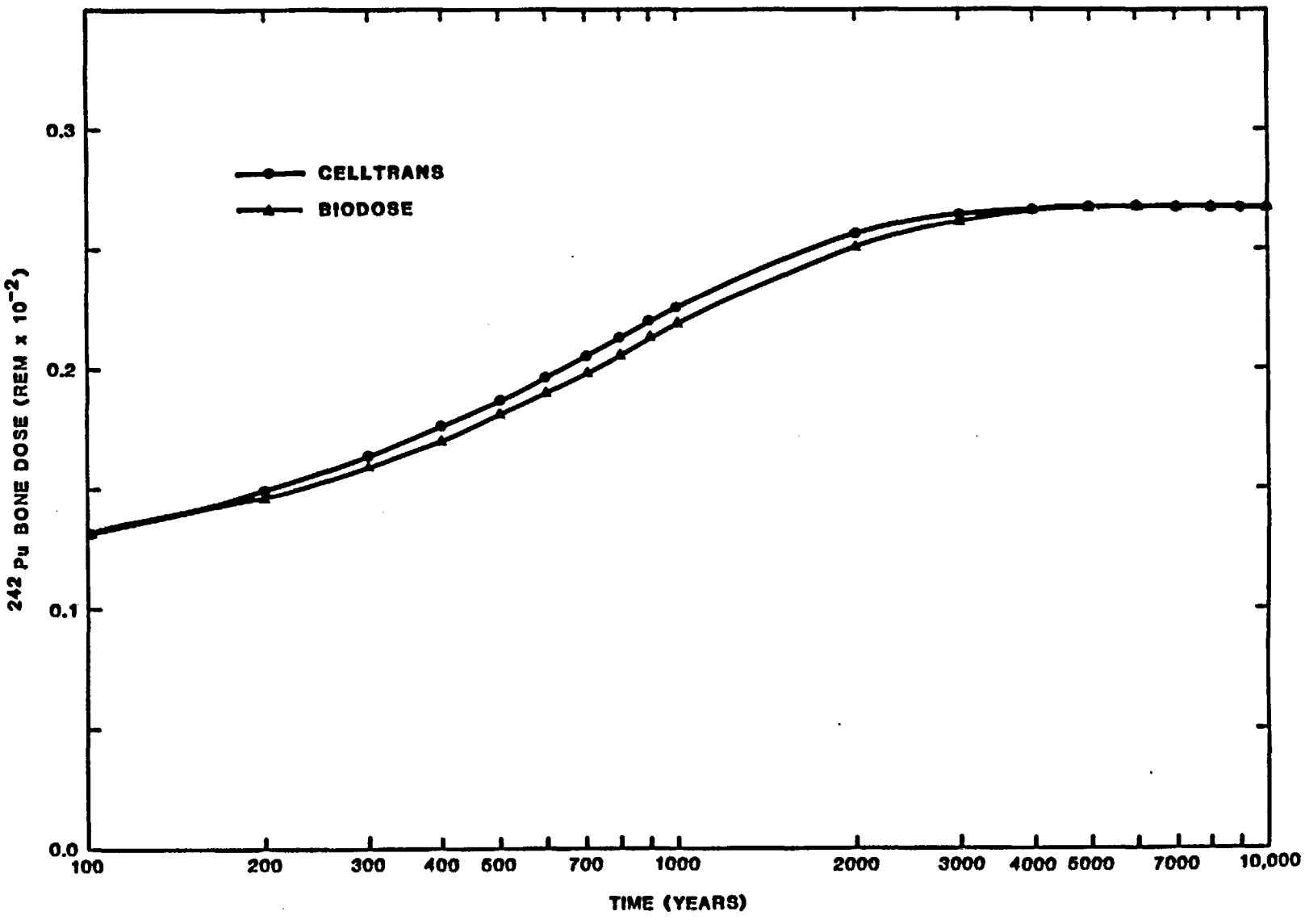

Figure 4-31

Time-Dependent ^{230}Th Bone Dose Calculated by CELLTRANS and BIODOSE for Benchmark Problem 3.0B

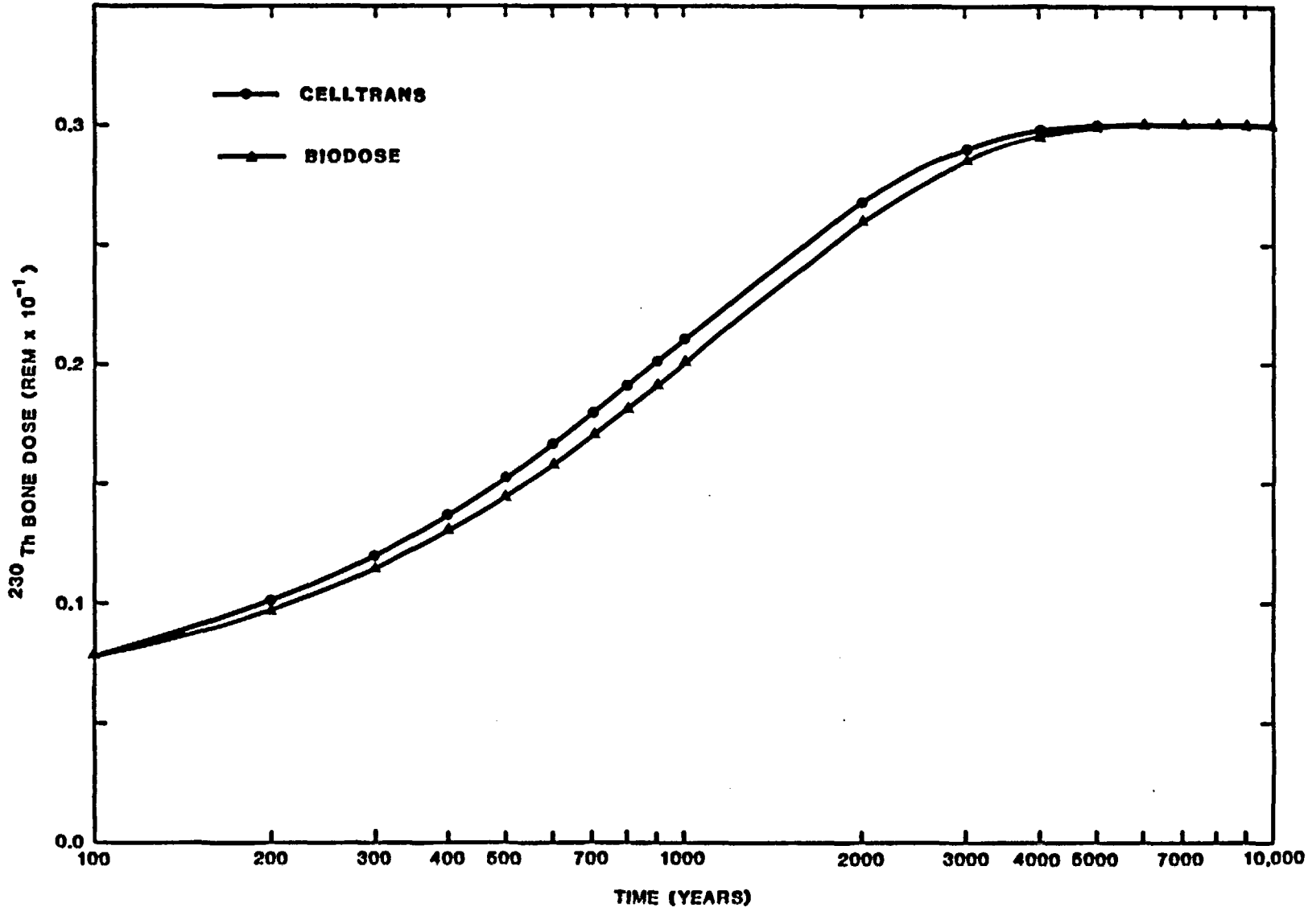

Figure 4-32

Time-Dependent ^{210}Pb Bone Dose Calculated by CELLTRANS and BIODOSE for Benchmark Problem 3.0B

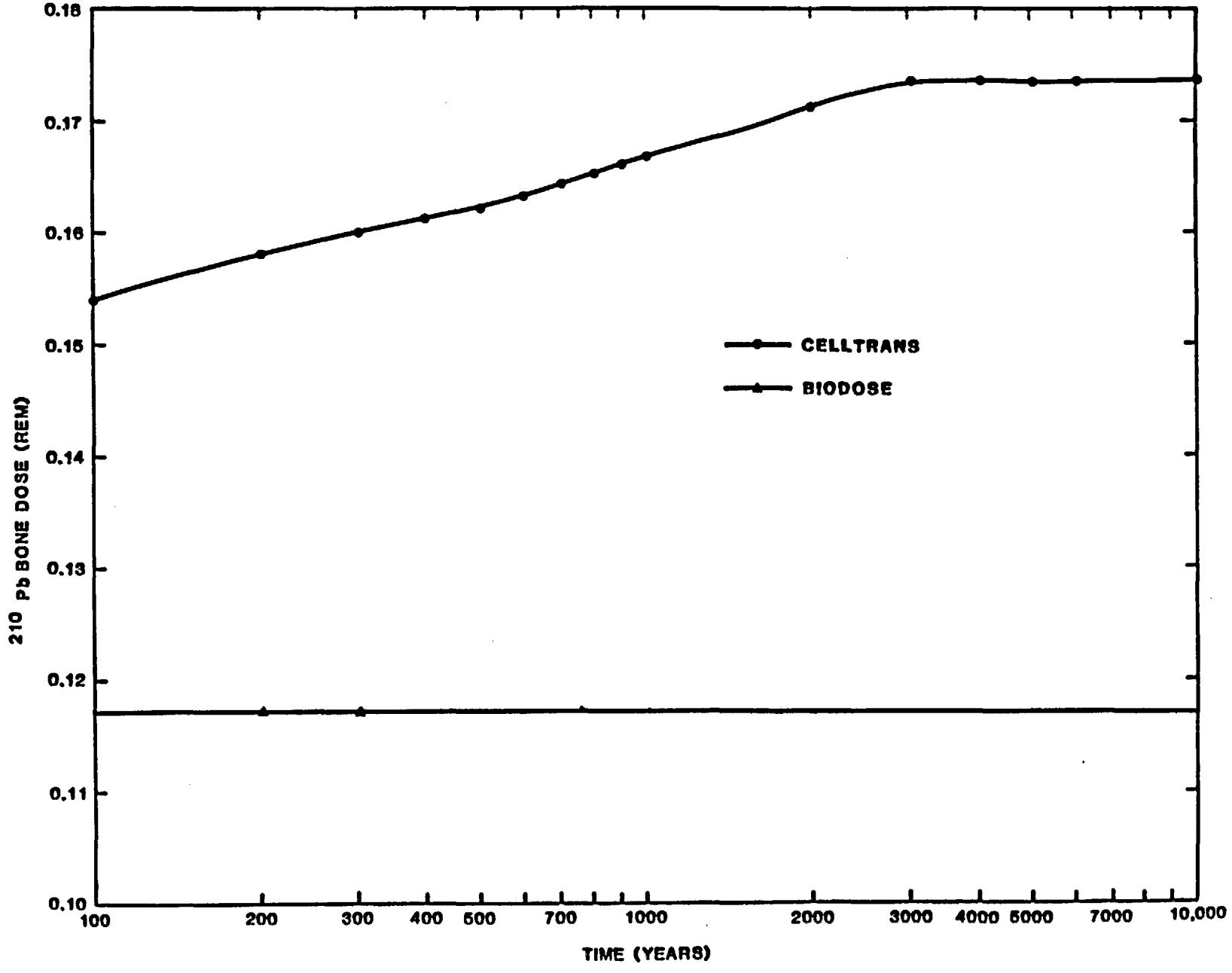

a water body (Reference 5).* The dose calculations in PABLM consider exposure to radionuclides deposited on the ground or on crops due to contaminated irrigation water, radionuclides in drinking water, radionuclides in aquatic foods raised in contaminated water, and radionuclides in bodies of water where people might swim. For vegetation, PABLM considers both direct deposition on leaves and uptake through roots. No dose is calculated for inhalation of contaminated soil particles.

The code has a number of limitations with respect to its general-purpose application to high level waste repository analysis. We list here the major limitations:

- Since PABLM was originally designed for the analysis of nuclear reactors, its simulation period is limited to the generally accepted dose commitment time of 70 years.
- The only means considered for water input to the soil is sprinkler irrigation.
- The only method considered for radionuclide removal from sediment and topsoil is radioactive decay. For long-lived radionuclides, concentrations in water, soil, and sediment do not have a chance to reach steady state in PABLM.
- The feed and water consumption rates for beef and dairy cattle are fixed within the program, as is the fraction of direct deposition retained on plant leaves.
- The user has no control over the river-to-sediment radionuclide transfer parameter of 25,300 L $m^{-2} yr^{-1}$.
- For the calculation of external irradiation dose from contaminated soil, radionuclide deposition is assumed to take place on a uniform thin sheet.
- In the calculation of plant uptake of radionuclides from the soil, a soil "surface density" of 224 kg/m^2 is assumed and cannot be changed by the code user.

---

* See also Reference 1 in Chapter 1.

- The organ-specific dose factors for ingestion are calculated within PABLM from an input library containing effective energy deposition values, fractional transfer coefficients, and biological half-lives by organ. There is no provision for the user to input dose factors directly.

PABLM differs from the other codes covered in this study in the way it calculates ^{14}C concentrations in vegetation and animal product. The concentration of ^{14}C in vegetation, C_{14Cv}, is calculated as

$$C_{14Cv} = C_{14Cw}F_{cv}, \tag{4.4.1}$$

where

C_{14Cw} = pCi ^{14}C/L ÷ carbon concentration in irrigated water (kg/L)

F_{cv} = the fraction of carbon in total vegetation (0.09)

The concentration of ^{14}C in the animal product, C_{14Ca}, is given by

$$C_{14Ca} = \left[\frac{C_{14CF}Q_F + C_{14Caw}Q_{aw}}{F_{cF}Q_F + F_{cw}Q_{aw}}\right]F_{ca}, \tag{4.4.2}$$

where

C_{14CF} = the concentration of ^{14}C in feed or forage as calculated by Equation 4.4.1, so that $C_{14C} = (C_{14Cv})$ (pCi/kg)

F_{cF} = the fraction of carbon in animal feed (0.09)

F_{cw} = the fraction of carbon in animal drinking water (2.0×10^{-5} kg/L)

C_{14Caw} = the concentration of ^{14}C in animal drinking water (pCi/kg)

F_{ca} = the fraction of carbon in animal product (milk = 0.07, meat = 0.24)

Q_F = animal feed consumption (kg/day)

Q_{aw} = animal water consumption (kg/day)

4.4.2 Adaptation of Benchmark Problems to PABLM Input Requirements

Since PABLM allows no direct radionuclide input to the environment other than the input to stream water, the following benchmark problems could not be run: 3.0, 3.0A, 3.1, and 3.1A. The lack of a groundwater subzone prevented PABLM from being used to solve problem 3.2. Finally, the 70-year maximum simulation time allowed by PABLM is not sufficient to permit ^{242}Pu ingrowth, so that the solution of problem 3.1B was not meaningful. The problem was, however, run for the sake of completeness. This left problems 3.0B and 3.2A for the PABLM benchmarking. For both of these problems, the following parameters were found to be set within the code itself and consequently were not changed to reflect the benchmark problem inputs:

- Dairy cow feed consumption rate = 55 kg/day (versus 50 kg/day for problems 3.0B and 3.2A)
- Beef cow feed consumption rate = 68 kg/day (versus 50 kg/day for problems 3.0B and 3.2A)
- Soil depth for root uptake by vegetation = 16 cm (versus 50 cm for problems 3.0B and 3.2A)
- Soil depth for surface exposure calculation = 0 cm (versus 2.5 cm for problems 3.0B and 3.2A)
- Organ weight for liver = 1,800 g (versus 1,700 g implicit in the calculation of dose factors presented in Table 4-8)
- Organ weight for kidney = 310 g (versus 360 g implicit in the calculation of dose factors presented in Table 4-8)

Other parameters that are set within the code are the fraction of direct deposition retained on the plant (0.25) and the half-life for weathering removal (14 days). These values, however, are identical to those specified for the benchmark problems.

The bioaccumulation factors given in the PABLM default input libraries were compared with those given in Tables 4-4, 4-5, and 4-9. On the basis of this comparison, the following changes for Iodine were made in the Food Transfer Coefficient Library:

- For milk, 1.0E-2 day/L was changed to 6.0E-3 day/L
- For beef, 2.0E-2 day/kg was changed to 2.9E-3 day/kg

For all the radionuclides considered in this study, the factor giving the fraction of activity passing through in the water treatment facility was set equal to one. As mentioned earlier, PABLM does not use bioaccumulation factors for carbon but instead uses Equations 4.4.1 and 4.4.2 to calculate ^{14}C concentrations in vegetation and animal product.

The external dose factors given in Tables 4-6 and 4-10 matched those given in the PABLM default library GRDFLIB. The reconciliation of ingestion dose factors, however, presented a problem. A special computer program was written to calculate does rate factors using data from the PABLM default library ORGLIB. These factors were then compared with those given in Table 4-8. On the basis of this comparison and information presented in Reference 11, the following changes were made to ORGLIB:

- For ^{242}Pu, the fraction of the radionuclide transferred to the bone was changed from 0.45 to 0.80. The fraction transferred to the liver was changed from 0.45 to 0.15.
- For ^{242}Pu, the physical half-life of the radionuclide in the bone was changed from 36,500 days to 73,000 days. The half-life for ^{242}Pu in the liver was changed from 14,600 days to 30,000 days.
- For ^{226}Ra, the following dose information was added for the liver and kidneys:

	Biological Half-life (Days)	Fraction Reaching Organ	MeV/ Disintegration
Liver	10	1.2E-4	110
Kidney	10	6.0E-4	110

4.4.3 Benchmarking Results and Conclusions

With the exception of ^{14}C, the primary reason for the differences between the doses calculated by PABLM and those calculated by PATH1/DOSHEM and CELLTRANS is the difference in the way soil radionuclide concentrations are calculated. In PATH1/DOSHEM and CELLTRANS, the soil is treated as a uniform subzone with specific dimensions. The input of river water to this subzone in liters per year is specified separately from the sprinkler irrigation rate, which is given in liters/m^2/year. The total amount of river water deposited in the soil during the year is assumed to include the amount due to sprinkler irrigation. PABLM, on the other hand, does not have a soil subzone but instead uses the sprinkler irrigation rate and the soil "surface density" to establish the Ci/kg soil concentrations required for the calculation of plant uptake of radionuclides by roots. For benchmark problems 3.0B and 3.2A, this results in PABLM's calculating a radionuclide input rate per kilogram of soil that is a factor of five greater than the rate calculated by PATH1/DOSHEM and CELLTRANS. The soil concentrations calculated by PABLM also tend to be higher, since, other than radioactive decay, no mechanism is provided for the removal of radionuclides from the soil.

A less important reason for the differences between the PABLM versus other dose calculations is the PABLM assumption, in calculating root uptake, that all radionuclides in the topsoil are associated with the dry soil. Although PATH1/DOSHEM and CELLTRANS assume that only the radionuclides associated with the solid component of the soil are available for root uptake, the high soil K_d values mean that virtually all of the radionuclides in the soil compartment will be associated with the solid component. For ^{129}I, this assumption, taken by itself, will cause the ^{129}I soil concentration to be overestimated by only 15 percent. Compensating for these factors, however, is the fact that, according to the specifications of benchmark problems 3.0B and 3.2A, the proportion of

suspended sediments in the water added to the soil is greater than the proportion in the river water itself. (Water used for sprinkler irrigation, however, does have the same proportion.) For radionuclides with high river-water K_d values, this has an important effect. For example, in the case of ^{129}I(K_d = 1,000 L/kg), the factor of five mentioned earlier is reduced to 1.7. For ^{230}Th (K_d = 100,000 L/kg), the factor becomes 0.48, meaning that the PATH1/DOSHEM and CELLTRANS radionuclide addition rates per unit weight of soil are a factor of two greater than those calculated by PABLM. Another compensating factor is that PABLM has a maximum simulation time equal to the dose commitment time (70 years). Soil concentrations of radionuclides sometimes take over 1,000 years to reach steady state in the soil (see Figures 4-31 and 4-32). The factors discussed above account for the BIODOSE overprediction of the ^{129}I dose and underprediction of the ^{242}Pu, ^{210}Pb, and ^{230}Th doses. Another reason for the underprediction of the ^{242}Pu dose is that PABLM does not account for the inhalation pathway.

During the course of the PABLM benchmarking, it was discovered that the code's calculations of skin doses for ^{238}U were several orders of magnitude too small. It was suspected that the long ^{238}U half-life was causing a computational error in the calculation of the soil concentrations. When a separate run was made with the half-life of ^{234}U substituted for that of ^{238}U, the problem was corrected. The calculated ^{238}U doses to the other organs were also found to be more reasonable after the substitution was made.

The most striking result of the PABLM benchmarking, however, was the conservative estimate of the ^{14}C dose based upon the uptake model presented in Section 4.4.1. For all organs except the skin, these ^{14}C doses calculated by PABLM were a factor of 75 greater than those calculated by PATH1/DOSHEM, CELLTRANS, and BIODOSE. A comparison of all PABLM-calculated doses with doses calculated by the other codes covered in this study is given in Section 4.6.

4.5 LADTAP

4.5.1 Code Description

The LADTAP code (Reference 12)* is a computerized version of NRC Regulatory Guide 1.109 (Reference 7). As such, the user has only limited control over the parameters used in the dose calculation. The pathways for ingestion and external exposure are the same ones used in the PABLM code. No inhalation dose is calculated by LADTAP. With respect to the benchmark problems included in this study, the following parameters can be specified in the LADTAP input data:

- Fish consumption (kg/yr)
- Water consumption (L/yr)
- Swimming (hr/yr)
- Irrigation rate (L/m^2/month)
- Yield (kg/m^2)
- Growing period (days)
- Individual consumption of vegetables, milk, and beef (kg/yr)

The doses calculated by LADTAP are for one year of facility operation and a 50-year commitment period. These calculated doses must be multiplied by 70 for comparison with doses calculated by the other codes. This will overestimate the dose, however, since a 70-year-old individual will not be able to receive a full committed dose. The amount of overestimation will depend upon the physical half-life of the radionuclide in the particular organ of interest.

---

* See also Reference 1 in Chapter 1.

4.5.2 Adaptation of Benchmark Problems to LADTAP Input Requirements

As in the case of the BIODOSE and PABLM codes, benchmark problems 3.0B, 3.1B, and 3.2A were simulated. The 3.1B simulation is not that meaningful in the case of LADTAP, since the code does not explicitly account for chain decay or time-dependent processes. No attempt was made to change the default bioaccumulation and dose factors in the LADTAP input files. Even if one wanted to change these factors, the format of the input files would make this quite difficult.

4.5.3 Benchmarking Results and Conclusions

In practice, one would probably not run LADTAP for a high level waste repository assessment. The code was included in this benchmarking study as a "zero order" model against which the performance of the other codes could be judged. The comparison presented in Section 4.6 shows that the LADTAP-calculated doses were generally within a factor of two to three of those calculated by PATH1/DOSHEM and CELLTRANS. From the point of view of code evaluation, one problem with the LADTAP output format is that the breakdown of dose to an organ by radionuclide is given only to the nearest percent.

4.6 Code Comparison and Evaluation

In Sections 4.1 through 4.3, the capabilities of the codes PATH1/DOSHEM, CELLTRANS, and BIODOSE were evaluated with respect to the calculation of time-dependent doses to maximally exposed individuals. To provide some common ground for comparison between all the codes, the 10,000-year dose by organ and radionuclide has been selected as the output parameter for evaluation. This method of comparison will, however, introduce some bias against the codes PABLM and LADTAP, which have short simulation times. In spite of this drawback, the 10,000-year doses represent the values that would be of interest in an actual radiological assessment.

From a review of Tables 4-13 through 4-20, together with an understanding of the operating characteristics of the codes, the following conclusions were reached:

- The 10,000-year doses calculated by PATH1/DOSHEM and CELLTRANS are virtually identical. The results from the two codes for other time periods also show this close agreement. This finding constitutes a verification of the two codes' methods for solving compartmental equations.

- Contrary to the documentation, the PATH1/DOSHEM code does not calculate an external dose to the skin. Only the external total body dose is calculated. Also, contrary to the documentation, the DOSHEM binary format dose factor library contains an external dose factor for ^{222}Rn.

- There is good agreement between BIODOSE and PATH1/DOSHEM-CELLTRANS, with the following exceptions:

  - The ^{210}Pb doses are underpredicted by BIODOSE, because the code does not account for the ingrowth of ^{210}Pb due to chain decay from ^{226}Ra. The ^{226}Ra skin dose for benchmark problem 3.0B is underpredicted, since BIODOSE does not account for ^{226}Ra ingrowth due to ^{230}Th decay.

  - Since BIODOSE does not explicitly account for chain decay, only ^{242}Pu doses are calculated for benchmark problem 3.1B.

  - The ^{129}I skin dose calculated by BIODOSE is 15 percent greater than that calculated by CELLTRANS, because BIODOSE is not able to account for the low ^{129}I Kd value for the soil.

- Dose calculations from PABLM show good agreement with those from PATH1/DOSHEM and CELLTRANS only when the soil concentration is not an important factor in the calculation.

- Even if PABLM could simulate the transport of radionuclides beyond the dose commitment time, there would still be a problem, since the radionuclide library in PABLM does not account for the full decay chain.

- The ^{14}C uptake model used in PABLM gives ^{14}C doses that are a factor of 75 higher than the ^{14}C doses calculated by PATH1/DOSHEM, CELLTRANS, and BIODOSE, all of which use the concentration-factor method for calculating ^{14}C uptake.

Table 4-13

Comparison of Calculated Doses by Organ and Radionuclide for Benchmark Problem 3.0 at 10,000 Years after Radionuclide Input Begins

Organ	Radionuclide	Total Dose (Rem)				
		PATH1/ DOSHEM	CELLTRANS	BIODOSE	PABLM	LADTAP
Skin	^{242}Pu		0.472E-6			
	^{238}U		0.150E-5			
	^{234}U		0.822E-6			
	^{230}Th		0.193E-5			
	^{226}Ra		0.923E-5			
	^{222}Rn		0.0			
	^{210}Pb		0.114E-6			
	All		0.141E-4			
Total Body	^{242}Pu	0.388E-5	0.386E-5			
	^{238}U	0.810E-4	0.810E-4			
	^{234}U	0.642E-4	0.641E-4			
	^{230}Th	0.593E-5	0.596E-5			
	^{226}Ra	0.966E-1	0.963E-1			
	^{222}Rn	0.878E-11	0.0			
	^{210}Pb	0.461E-2	0.462E-2			
	All	0.101E+0	0.101E+0			
Bone	^{242}Pu	0.152E-3	0.152E-3			
	^{238}U	0.134E-2	0.134E-2			
	^{234}U	0.102E-2	0.102E-2			
	^{230}Th	0.209E-3	0.209E-3			
	^{226}Ra	0.128E+0	0.128E+0			
	^{222}Rn	0.0	0.0			
	^{210}Pb	0.121E+0	0.121E+0			
	All	0.251E+0	0.251E+0			
Thyroid	^{242}Pu					
	^{238}U					
	^{234}U					
	^{230}Th					
	^{226}Ra					
	^{222}Rn					
	^{210}Pb					
	All					

Table 4-13 (Continued)

Organ	Radionuclide	Total Dose (Rem) PATH1/ DOSHEM	CELLTRANS	BIODOSE	PABLM	LADTAP
Liver	^{242}Pu	0.216E-4	0.215E-4			
	^{238}U	0.0	0.0			
	^{234}U	0.0	0.0			
	^{230}Th	0.118E-4	0.118E-4			
	^{226}Ra	0.333E-5	0.333E-5			
	^{222}Rn	0.0	0.0			
	^{210}Pb	0.363E-1	0.364E-1			
	All	0.363E-1	0.364E-1			
Kidneys	^{242}Pu	0.165E-4	0.164E-4			
	^{238}U	0.310E-3	0.310E-3			
	^{234}U	0.248E-4	0.247E-3			
	^{230}Th	0.575E-4	0.578E-4			
	^{226}Ra	0.943E-4	0.947E-4			
	^{222}Rn	0.0	0.0			
	^{210}Pb	0.109E+0	0.109E+0			
	All	0.110E+0	0.110E+0			
Lungs	^{242}Pu	0.681E-6	0.681E-6			
	^{238}U	0.149E-7	0.149E-7			
	^{234}U	0.119E-7	0.120E-7			
	^{230}Th	0.156E-5	0.157E-5			
	^{226}Ra	0.975E-8	0.982E-8			
	^{222}Rn	0.0	0.0			
	^{210}Pb	0.167E-7	0.167E-7			
	All	0.229E-5	0.231E-5			
GI-LLI	^{242}Pu	0.170E-4	0.169E-4			
	^{238}U	0.978E-4	0.977E-4			
	^{234}U	0.766E-4	0.765E-4			
	^{230}Th	0.818E-5	0.822E-5			
	^{226}Ra	0.193E-3	0.193E-3			
	^{222}Rn	0.0	0.0			
	^{210}Pb	0.495E-3	0.494E-3			
	All	0.888E-3	0.886E-3			

Table 4-14

Comparison of Calculated Doses by Organ and Radionuclide for Benchmark Problem 3.0A at 10,000 Years after Radionuclide Input Begins

Organ	Radionuclide	Total Dose (Rem) PATH1/ DOSHEM	CELLTRANS	BIODOSE	PABLM	LADTAP
Skin	^{242}Pu		0.472E-6			
	^{238}U		0.150E-5			
	^{234}U		0.822E-6			
	^{230}Th		0.193E-5			
	^{226}Ra		0.923E-5			
	^{222}Rn		0.0			
	^{210}Pb		0.314E-6			
	All		0.143E-4			
Total Body	^{242}Pu	0.386E-5	0.386E-5			
	^{238}U	0.810E-4	0.810E-4			
	^{234}U	0.642E-4	0.641E-4			
	^{230}Th	0.593E-5	0.596E-5			
	^{226}Ra	0.969E-1	0.963E-1			
	^{222}Rn	0.159E-3	0.0			
	^{210}Pb	0.121E-1	0.122E-1			
	All	0.109E+0	0.109E+0			
Bone	^{242}Pu	0.152E-3	0.152E-3			
	^{238}U	0.134E-2	0.134E-2			
	^{234}U	0.103E-2	0.102E-2			
	^{230}Th	0.209E-3	0.209E-3			
	^{226}Ra	0.128E+0	0.128E+0			
	^{222}Rn	0.0	0.0			
	^{210}Pb	0.318E+0	0.318E+0			
	All	0.449E+0	0.449E+0			
Thyroid	^{242}Pu					
	^{238}U					
	^{234}U					
	^{230}Th					
	^{226}Ra					
	^{222}Rn					
	^{210}Pb					
	All					

Table 4-14 (Continued)

Organ	Radionuclide	Total Dose (Rem) PATH1/ DOSHEM	CELLTRANS	BIODOSE	PABLM	LADTAP
Liver	^{242}Pu	0.215E-4	0.215E-4			
	^{238}U	0.0	0.0			
	^{234}U	0.0	0.0			
	^{230}Th	0.118E-4	0.118E-4			
	^{226}Ra	0.334E-5	0.333E-5			
	^{222}Rn	0.0	0.0			
	^{210}Pb	0.955E-1	0.959E-1			
	All	0.955E-1	0.959E-1			
Kidneys	^{242}Pu	0.164E-4	0.164E-4			
	^{238}U	0.310E-3	0.310E-3			
	^{234}U	0.248E-3	0.247E-3			
	^{230}Th	0.575E-4	0.578E-4			
	^{226}Ra	0.946E-4	0.947E-4			
	^{222}Rn	0.0	0.0			
	^{210}Pb	0.286E+0	0.287E+0			
	All	0.287E+0	0.288E+0			
Lungs	^{242}Pu	0.681E-6	0.681E-6			
	^{238}U	0.149E-7	0.149E-7			
	^{234}U	0.119E-7	0.120E-7			
	^{230}Th	0.156E-5	0.157E-5			
	^{226}Ra	0.983E-8	0.982E-8			
	^{222}Rn	0.0	0.0			
	^{210}Pb	0.469E-7	0.469E-7			
	All	0.232E-5	0.234E-5			
GI-LLI	^{242}Pu	0.169E-4	0.169E-4			
	^{238}U	0.978E-4	0.977E-4			
	^{234}U	0.766E-4	0.765E-4			
	^{230}Th	0.819E-5	0.822E-5			
	^{226}Ra	0.193E-3	0.193E-3			
	^{222}Rn	0.0	0.0			
	^{210}Pb	0.130E-2	0.130E-2			
	All	0.169E-2	0.169E-2			

Table 4-15

Comparison of Calculated Doses by Organ and Radionuclide for Benchmark Problem 3.0B at 10,000 Years after Radionuclide Input Begins

Organ	Radionuclide	Total Dose (Rem) PATH1/ DOSHEM	CELLTRANS	BIODOSE	PABLM	LADTAP*
Skin	^{242}Pu		0.325E-4	0.326E-4	0.24E-5	
	^{238}U		0.613E-4	0.626E-4	0.84E-7	
	^{234}U		0.345E-4	0.351E-4	0.90E-4	
	^{230}Th		0.353E-3	0.353E-3	0.20E-4	
	^{226}Ra		0.215E-2	0.152E-2	0.30E-2	
	^{222}Rn		0.0	0.0	0.29E-2	
	^{210}Pb		0.182E-5	0.747E-6	0.34E-5	
	All		0.263E-2	0.200E-2	0.60E-2	
Total Body	^{242}Pu	0.696E-4	0.696E-4	0.696E-4	0.31E-4	0.256E-4
	^{238}U	0.217E-3	0.217E-3	0.218E-3	0.17E-3	
	^{234}U	0.147E-3	0.146E-3	0.147E-3	0.15E-3	
	^{230}Th	0.865E-3	0.867E-3	0.866E-3	0.17E-3	
	^{226}Ra	0.782E+0	0.779E+0	0.758E+0	0.75E+0	0.98E+0
	^{222}Rn	0.912E-6	0.0	0.0	0.0	
	^{210}Pb	0.662E-2	0.663E-2	0.447E-2	0.50E-2	0.66E-3
	All	0.790E+0	0.787E+0	0.764E+0	0.76E+0	0.994E+0
Bone	^{242}Pu	0.266E-2	0.267E-2	0.270E-2	0.12E-2	0.103E-2
	^{238}U	0.306E-2	0.305E-2	0.307E-2	0.29E-2	
	^{234}U	0.234E-2	0.233E-2	0.234E-2	0.23E-2	
	^{230}Th	0.302E-1	0.302E-1	0.303E-1	0.57E-2	
	^{226}Ra	0.103E+1	0.103E+1	0.100E+1	0.99E+0	0.135E+1
	^{222}Rn	0.0	0.0	0.0	0.0	
	^{210}Pb	0.173E+0	0.173E+0	0.117E+0	0.13E+0	0.92E-1
	All	0.124E+1	0.124E+1	0.115E+1	0.11E+1	0.147E+1
Thyroid	^{242}Pu					
	^{238}U					
	^{234}U					
	^{230}Th					
	^{226}Ra					
	^{222}Rn					
	^{210}Pb					
	All					0.263E-6

* Due to the LADTAP percentage roundoff limitation, the LADTAP-calculated ^{242}Pu doses are taken from the benchmark problem 3.1B results.

Table 4-15 (Continued)

Organ	Radionuclide	Total Dose (Rem) PATH1/ DOSHEM	CELLTRANS	BIODOSE	PABLM	LADTAP*
Liver	^{242}Pu	0.379E-3	0.379E-3	0.379E-3	0.16E-3	0.142E-3
	^{238}U	0.0	0.0	0.0	0.0	
	^{234}U	0.0	0.0	0.0	0.0	
	^{230}Th	0.170E-2	0.171E-2	0.170E-2	0.33E-3	0.16E-3
	^{226}Ra	0.269E-4	0.269E-4	0.263E-4	0.25E-4	0.44E-5
	^{222}Rn	0.0	0.0	0.0	0.0	
	^{210}Pb	0.522E-1	0.522E-1	0.352E-1	0.37E-1	0.279E-1
	All	0.543E-1	0.543E-1	0.373E-1	0.38E-1	0.285E-1
Kidneys	^{242}Pu	0.288E-3	0.288E-3	0.288E-3	0.13E-3	0.11E-3
	^{238}U	0.709E-3	0.707E-3	0.712E-3	0.65E-3	0.24E-3
	^{234}U	0.565E-3	0.563E-3	0.566E-3	0.55E-3	0.24E-3
	^{230}Th	0.831E-2	0.832E-2	0.831E-2	0.17E-2	0.14E-2
	^{226}Ra	0.762E-3	0.764E-3	0.744E-3	0.71E-3	0.40E-3
	^{222}Rn	0.0	0.0	0.0	0.0	0.0
	^{210}Pb	0.156E+0	0.156E+0	0.106E+0	0.12E+0	0.78E-1
	All	0.167E+0	0.167E+0	0.117E+0	0.12E+0	0.819E-1
Lungs	^{242}Pu	0.469E-4	0.469E-4	0.470E-4		
	^{238}U	0.626E-6	0.627E-6	0.640E-6		
	^{234}U	0.502E-6	0.502E-6	0.511E-6		
	^{230}Th	0.287E-3	0.288E-3	0.287E-3		
	^{226}Ra	0.230E-5	0.230E-5	0.162E-5		
	^{222}Rn	0.0	0.0	0.0		
	^{210}Pb	0.391E-6	0.392E-6	0.158E-6		
	All	0.337E-3	0.338E-3	0.337E-3		0.263E-6
GI-LLI	^{242}Pu	0.184E-3	0.185E-3	0.185E-3	0.17E-3	0.93E-4
	^{238}U	0.223E-3	0.223E-3	0.224E-3	0.24E-3	0.38E-3
	^{234}U	0.174E-3	0.174E-3	0.175E-3	0.19E-3	0.97E-4
	^{230}Th	0.117E-2	0.117E-2	0.117E-2	0.0	0.16E-3
	^{226}Ra	0.156E-2	0.155E-2	0.152E-2	0.0	0.15E-2
	^{222}Rn	0.0	0.0	0.0	0.0	0.0
	^{210}Pb	0.710E-3	0.710E-3	0.479E-3	0.0	0.34E-3
	All	0.402E-2	0.402E-2	0.375E-2	0.60E-3	0.259E-2

* Due to the LADTAP percentage roundoff limitation, the LADTAP-calculated ^{242}Pu doses are taken from the benchmark problem 3.1B results.

Table 4-16

Comparison of Calculated Doses by Organ and Radionuclide for Benchmark Problem 3.1 at 10,000 Years after Radionuclide Input Begins

Organ	Radionuclide	Total Dose (Rem)				
		PATH1/ DOSHEM	CELLTRANS	BIODOSE	PABLM	LADTAP
Skin	^{242}Pu		0.472E-6			
	^{238}U		0.928E-12			
	^{234}U		0.345E-14			
	^{230}Th		0.582E-16			
	^{226}Ra		0.162E-15			
	^{222}Rn		0.0			
	^{210}Pb		0.178E-17			
	All		0.472E-6			
Total Body	^{242}Pu	0.386E-5	0.386E-5			
	^{238}U	0.492E-10	0.493E-10			
	^{234}U	0.269E-12	0.267E-12			
	^{230}Th	0.181E-15	0.189E-15			
	^{226}Ra	0.151E-11	0.152E-11			
	^{222}Rn	0.213E-20	0.0			
	^{210}Pb	0.714E-13	0.270E-13			
	All	0.386E-5	0.386E-5			
Bone	^{242}Pu	0.152E-3	0.152E-3			
	^{238}U	0.812E-9	0.814E-9			
	^{234}U	0.430E-12	0.426E-11			
	^{230}Th	0.658E-14	0.663E-14			
	^{226}Ra	0.200E-11	0.201E-11			
	^{222}Rn	0.0	0.0			
	^{210}Pb	0.187E-11	0.188E-11			
	All	0.152E-3	0.152E-3			
Thyroid	^{242}Pu					
	^{238}U					
	^{234}U					
	^{230}Th					
	^{226}Ra					
	^{222}Rn					
	^{210}Pb					
	All					

Table 4-16 (Continued)

Organ	Radionuclide	Total Dose (Rem) PATH1/ DOSHEM	CELLTRANS	BIODOSE	PABLM	LADTAP
Liver	^{242}Pu	0.214E-4	0.215E-4			
	^{238}U	0.0	0.0			
	^{234}U	0.0	0.0			
	^{230}Th	0.372E-15	0.376E-15			
	^{226}Ra	0.522E-16	0.524E-16			
	^{222}Rn	0.0	0.0			
	^{210}Pb	0.562E-12	0.567E-12			
	All	0.214E-4	0.215E-4			
Kidneys	^{242}Pu	0.164E-4	0.164E-4			
	^{238}U	0.188E-9	0.188E-9			
	^{234}U	0.104E-11	0.103E-11			
	^{230}Th	0.181E-14	0.183E-14			
	^{226}Ra	0.148E-14	0.149E-14			
	^{222}Rn	0.0	0.0			
	^{210}Pb	0.168E-11	0.170E-11			
	All	0.164E-4	0.164E-4			
Lungs	^{242}Pu	0.679E-6	0.681E-6			
	^{238}U	0.931E-14	0.927E-14			
	^{234}U	0.502E-16	0.502E-16			
	^{230}Th	0.466E-16	0.474E-16			
	^{226}Ra	0.170E-18	0.173E-18			
	^{222}Rn	0.0	0.0			
	^{210}Pb	0.258E-18	0.261E-18			
	All	0.679E-6	0.681E-6			
GI-LLI	^{242}Pu	0.169E-4	0.169E-4			
	^{238}U	0.593E-10	0.595E-10			
	^{234}U	0.322E-12	0.319E-12			
	^{230}Th	0.259E-15	0.261E-15			
	^{226}Ra	0.302E-14	0.303E-14			
	^{222}Rn	0.0	0.0			
	^{210}Pb	0.766E-14	0.771E-14			
	All	0.169E-4	0.169E-4			

Table 4-17

Comparison of Calculated Doses by Organ and Radionuclide for Benchmark Problem 3.1A at 10,000 Years after Radionuclide Input Begins

Organ	Radionuclide	Total Dose (Rem) PATH1/ DOSHEM	CELLTRANS	BIODOSE	PABLM	LADTAP
Skin	^{242}Pu		0.472E-6			
	^{238}U		0.928E-12			
	^{234}U		0.345E-14			
	^{230}Th		0.582E-16			
	^{226}Ra		0.162E-15			
	^{222}Rn		0.0			
	^{210}Pb		0.494E-17			
	All		0.472E-6			
Total Body	^{242}Pu	0.383E-5	0.386E-5			
	^{238}U	0.492E-10	0.493E-10			
	^{234}U	0.269E-12	0.267E-12			
	^{230}Th	0.187E-15	0.189E-15			
	^{226}Ra	0.151E-11	0.152E-11			
	^{222}Rn	0.249E-14	0.0			
	^{210}Pb	0.189E-12	0.191E-12			
	All	0.383E-5	0.386E-5			
Bone	^{242}Pu	0.150E-3	0.152E-3			
	^{238}U	0.812E-9	0.814E-9			
	^{234}U	0.430E-11	0.426E-11			
	^{230}Th	0.658E-14	0.663E-14			
	^{226}Ra	0.200E-11	0.201E-11			
	^{222}Rn	0.0	0.0			
	^{210}Pb	0.494E-11	0.499E-11			
	All	0.150E-3	0.152E-3			
Thyroid	^{242}Pu					
	^{238}U					
	^{234}U					
	^{230}Th					
	^{226}Ra					
	^{222}Rn					
	^{210}Pb					
	All					

Table 4-17 (Continued)

Organ	Radionuclide	Total Dose (Rem) PATH1/ DOSHEM	CELLTRANS	BIODOSE	PABLM	LADTAP
Liver	^{242}Pu	0.213E-4	0.215E-4			
	^{238}U	0.0	0.0			
	^{234}U	0.0	0.0			
	^{230}Th	0.372E-15	0.376E-15			
	^{226}Ra	0.522E-16	0.524E-16			
	^{222}Rn	0.0	0.0			
	^{210}Pb	0.149E-11	0.150E-11			
	All	0.213E-4	0.215E-4			
Kidneys	^{242}Pu	0.162E-4	0.164E-4			
	^{238}U	0.188E-9	0.188E-9			
	^{234}U	0.104E-11	0.103E-11			
	^{230}Th	0.181E-14	0.183E-14			
	^{226}Ra	0.148E-14	0.149E-14			
	^{222}Rn	0.0	0.0			
	^{210}Pb	0.445E-11	0.450E-11			
	All	0.162E-4	0.164E-4			
Lungs	^{242}Pu	0.679E-6	0.681E-6			
	^{238}U	0.931E-14	0.927E-14			
	^{234}U	0.502E-16	0.502E-16			
	^{230}Th	0.466E-16	0.474E-16			
	^{226}Ra	0.170E-18	0.173E-18			
	^{222}Rn	0.0	0.0			
	^{210}Pb	0.729E-18	0.739E-18			
	All	0.679E-6	0.681E-6			
GI-LLI	^{242}Pu	0.168E-4	0.169E-4			
	^{238}U	0.593E-10	0.595E-10			
	^{234}U	0.322E-12	0.319E-12			
	^{230}Th	0.259E-15	0.261E-15			
	^{226}Ra	0.302E-14	0.303E-14			
	^{222}Rn	0.0	0.0			
	^{210}Pb	0.202E-13	0.204E-13			
	All	0.168E-4	0.169E-4			

Table 4-18

Comparison of Calculated Doses by Organ and Radionuclide for Benchmark Problem 3.1B at 10,000 Years after Radionuclide Input Begins

Organ	Radionuclide	Total Dose (Rem)				
		PATH1/ DOSHEM	CELLTRANS	BIODOSE	PABLM	LADTAP
Skin	^{242}Pu		0.325E-4	0.032E-4	0.24E-5	0.0
	^{238}U		0.561E-11			
	^{234}U		0.365E-15			
	^{230}Th		0.658E-18			
	^{226}Ra		0.123E-17			
	^{222}Rn		0.0			
	^{210}Pb		0.621E-21			
	All		0.325E-4	0.326E-4	0.24E-5	0.0
Total Body	^{242}Pu	0.695E-4	0.696E-4	0.696E-4	0.31E-4	0.256E-4
	^{238}U	0.468E-11	0.468E-11			
	^{234}U	0.150E-15	0.150E-15			
	^{230}Th	0.133E-17	0.133E-17			
	^{226}Ra	0.392E-16	0.391E-16			
	^{222}Rn	0.337E-21	0.0			
	^{210}Pb	0.123E-17	0.124E-17			
	All	0.695E-4	0.696E-4	0.696E-4	0.31E-4	0.256E-4
Bone	^{242}Pu	0.266E-2	0.267E-2	0.270E-2	0.12E-2	0.103E-2
	^{238}U	0.260E-10	0.260E-10			
	^{234}U	0.236E-14	0.231E-14			
	^{230}Th	0.461E-16	0.460E-16			
	^{226}Ra	0.505E-16	0.505E-16			
	^{222}Rn	0.0	0.0			
	^{210}Pb	0.323E-16	0.324E-16			
	All	0.266E-2	0.267E-2	0.270E-2	0.12E-2	0.103E-2
Thyroid	^{242}Pu					0.597E-11
	^{238}U					
	^{234}U					
	^{230}Th					
	^{226}Ra					
	^{222}Rn					
	^{210}Pb					
	All					0.597E-11

Table 4-18 (Continued)

Organ	Radionuclide	Total Dose (Rem) PATH1/ DOSHEM	CELLTRANS	BIODOSE	PABLM	LADTAP
Liver	^{242}Pu	0.379E-3	0.379E-3	0.379E-3	0.16E-3	0.142E-3
	^{238}U	0.0	0.0			
	^{234}U	0.0	0.0			
	^{230}Th	0.259E-17	0.259E-17			
	^{226}Ra	0.132E-20	0.132E-20			
	^{222}Rn	0.0	0.0			
	^{210}Pb	0.971E-17	0.977E-17			
	All	0.379E-3	0.379E-3	0.379E-3	0.16E-3	0.142E-3
Kidneys	^{242}Pu	0.288E-3	0.288E-3	0.288E-3	0.13E-3	0.109E-3
	^{238}U	0.602E-11	0.602E-11			
	^{234}U	0.560E-15	0.559E-15			
	^{230}Th	0.126E-16	0.126E-16			
	^{226}Ra	0.373E-19	0.374E-19			
	^{222}Rn	0.0	0.0			
	^{210}Pb	0.291E-16	0.292E-16			
	All	0.288E-3	0.288E-3	0.288E-3	0.13E-3	0.109E-3
Lungs	^{242}Pu	0.469E-4	0.469E-4	0.470E-4		0.597E-11
	^{238}U	0.573E-13	0.575E-13			
	^{234}U	0.532E-17	0.531E-17			
	^{230}Th	0.536E-18	0.536E-18			
	^{226}Ra	0.131E-20	0.132E-20			
	^{222}Rn	0.0	0.0			
	^{210}Pb	0.135E-21	0.136E-21			
	All	0.469E-4	0.469E-4	0.470E-4		0.597E-11
GI-LLI	^{242}Pu	0.184E-3	0.185E-3	0.185E-3	0.17E-3	0.934E-4
	^{238}U	0.190E-11	0.190E-11			
	^{234}U	0.173E-15	0.173E-15			
	^{230}Th	0.176E-17	0.176E-17			
	^{226}Ra	0.762E-19	0.761E-19			
	^{222}Rn	0.0	0.0			
	^{210}Pb	0.132E-18	0.133E-18			
	All	0.184E-3	0.185E-3	0.185E-3	0.17E-3	0.934E-4

Table 4-19

Comparison of Calculated Doses by Organ and Radionuclide for Benchmark Problem 3.2 at 10,000 Years after Radionuclide Input Begins

Organ	Radionuclide	Total Dose (Rem) PATH1/ DOSHEM	CELLTRANS	BIODOSE	PABLM	LADTAP
Skin	^{14}C		0.290E-9			
	^{129}I		0.279E-7			
	All		0.282E-7			
Total Body	^{14}C	0.940E-4	0.943E-4			
	^{129}I	0.316E-5	0.316E-5			
	All	0.971E-4	0.975E-4			
Bone	^{14}C	0.469E-3	0.471E-3			
	^{129}I	0.112E-5	0.112E-5			
	All	0.470E-3	0.472E-3			
Thyroid	^{14}C	0.940E-4	0.943E-4			
	^{129}I	0.247E-2	0.247E-2			
	All	0.256E-2	0.256E-2			
Liver	^{14}C	0.940E-4	0.943E-4			
	^{129}I	0.964E-6	0.962E-6			
	All	0.950E-4	0.953E-4			
Kidneys	^{14}C	0.940E-4	0.943E-4			
	^{129}I	0.208E-5	0.208E-5			
	All	0.961E-4	0.964E-4			
Lungs	^{14}C	0.940E-4	0.943E-4			
	^{129}I	0.0	0.0			
	All	0.940E-4	0.943E-4			
GL-LLI	^{14}C	0.940E-4	0.943E-4			
	^{129}I	0.153E-6	0.153E-6			
	All	0.942E-4	0.945E-4			

Table 4-20

Comparison of Calculated Doses by Organ and Radionuclide for Benchmark Problem 3.2A at 10,000 Years after Radionuclide Input Begins

Organ	Radionuclide	Total Dose (Rem) PATH1/ DOSHEM	CELLTRANS	BIODOSE	PABLM	LADTAP
Skin	^{14}C		0.345E-9	0.344E-9	0.34E-9	
	^{129}I		0.278E-6	0.329E-6	0.25E-4	
	All		0.279E-6	0.329E-6	0.25E-4	
Total Body	^{14}C	0.112E-3	0.112E-3	0.114E-3	0.84E-2	
	^{129}I	0.443E-5	0.444E-5	0.449E-5	0.22E-4	
	All	0.116E-3	0.117E-3	0.118E-3	0.84E-2	0.299E-3
Bone	^{14}C	0.558E-3	0.561E-3	0.564E-3	0.42E-1	0.147E-2
	^{129}I	0.152E-5	0.153E-5	0.154E-5	0.23E-5	0.707E-6
	All	0.560E-3	0.562E-3	0.566E-3	0.42E-1	0.147E-2
Thyroid	^{14}C	0.112E-3	0.112E-3	0.114E-3	0.84E-2	0.320E-3
	^{129}I	0.335E-2	0.335E-2	0.336E-2	0.51E-2	0.276E-2
	All	0.346E-2	0.346E-2	0.347E-2	0.14E-1	0.308E-2
Liver	^{14}C	0.112E-3	0.112E-3	0.114E-3	0.84E-2	0.297E-3
	^{129}I	0.131E-5	0.131E-5	0.131E-5	0.19E-5	0.626E-6
	All	0.113E-3	0.114E-3	0.115E-3	0.84E-2	0.297E-3
Kidneys	^{14}C	0.112E-3	0.112E-3	0.114E-3	0.84E-2	0.297E-3
	^{129}I	0.282E-5	0.282E-5	0.283E-5	0.42E-5	0.134E-5
	All	0.115E03	0.115E-3	0.117E-3	0.84E-2	0.298E-3
Lungs	^{14}C	0.112E-3	0.112E-3	0.114E-3	0.84E-2	0.295E-3
	^{129}I	0.0	0.0	0.0	0.0	0.0
	All	0.112E-3	0.112E-3	0.114E-3	0.84E-2	0.295E-3
GL-LLI	^{14}C	0.112E-3	0.112E-3	0.114E-3	0.84E-2	0.295E-3
	^{129}I	0.207E-6	0.207E-6	0.208E-6	0.35E-6	0.959E-7
	All	0.112E-3	0.113E-3	0.114E-3	0.84E-2	0.295E-3

- The LADTAP code gave doses that were generally within a factor of two to three of those calculated with PATH1/ DOSHEM and CELLTRANS.

4.7 References for Chapter 4

1. Helton, J.C., and Kaestner, P.C. Risk Methodology for Geologic Disposal of Radioactive Waste: Model Description and User's Manual for the Pathways Model. NUREG/CR-1636, vol. 1. SAND78-1711AN.

2. Runkle, G.E., and Cranwell, R.M. "User's Manual for the Dosimetry and Health Effects Model." (Rough draft.) Sandia National Laboratories. July 1981.

3. Helton, J.C., and Iman, R.L. Risk Methodology for Geologic Disposal of Radioactive Waste: Sensitivity Analysis of the Environmental Transport Model. NUREG/CR-1636, vol. 2. December 1980.

4. Blanchard, R.L.; Fowler, T.W.; Horton, T.R.; and Smith, J.W. "Potential Health Effects of Radioactive Emissions from Active Surface and Underground Uranium Mines." Nuclear Safety 23-4 (July-August 1982).

5. Napier, B.A.; Kennedy, W.E., Jr.; and Soldat, J.K. PABLM—A Computer Program to Calculate Accumulated Radiation Doses from Radionuclides in the Environment. PNL-3209. UC-70. March 1980.

6. Runkle, G.E.; Cranwell, R.M.; and Johnson, J.D. Risk Methodology for Geologic Disposal of Radioactive Waste: Dosimetry and Health Effects. NUREG/CR-2166. July 1981.

7. U.S. Nuclear Regulatory Commission, Office of Standards Development. Calculation of Annual Doses to Man from Routine Releases of Reactor Effluents for the Purpose of Evaluating Compliance with 10 CFR Part 50, Appendix I. NRC Regulatory Guide 1.109.

8. Runkle, G.E., and Finley, N.C. Dosimetry and Health Effects Self-Teaching Curriculum. NUREG/CR-2422. SAND 81-2488. March 1983.

9. Duffy, J.J., and Bogar, G.P. User's Manual for the Biosphere and Dose Simulation Program BIODOSE. TR-1797-3. UCRL-15188. January 1980.

10. Koplik, C.M.; Nalbandian, J.Y.; and Scott, J.I. User's Guide to NUTRAN: A Computer Program for Long-Term Repository Safety Analysis. TR-3854-5. Reading, Mass.: Analytic Sciences Corporation, June 1983.

11. Hoenes, G.R., and Soldat, J.K., Age Specific Radiation Dose Commitment Factors for a One Year Chronic Intake. NUREG-0172. November 1977.

12. Simpson, D.B., and McGill, B.L. User's Manual for LADTAP II — Computer Program for Calculating Radiation Exposure to Man from Routine Release of Nuclear Reactor Liquid Effluents. NUREG/CR-1276. ORNL/NUREG/TDMC-1. May 1980.

APPENDIX A

Method for Estimating U-234 Control of Enriched Uranium

ORIGEN results for benchmark problems 2.4 and 2.5 were in poor agreement with measured U-234 data. Since U-234 is a precursor of Ra-226, a potentially important radionuclide in estimating dose-to-man, better agreement was desired. In reviewing the benchmark problem inputs, the most likely source of error was the fuel initial U-234 content. To improve our estimate of U-234 content the following method was used.

Step 1: Estimate the number of enriching stages required to produce U-235 of the desired product enrichment. From Reference Benedict and Pigford (1957),

$$n_p = \frac{Ln\left(\frac{x_p^{235}(1 - x_f^{235})}{(1-x_p^{235})\, x_f^{235}}\right)}{Ln\ \beta^{235}}$$

where:

n_p = number of states in the enriching section of an ideal cascade

x_f^{235} = enrichment plant U-235 feed assay

x_p^{235} = enrichment plant U-235 product assay

$\beta^{235} = \sqrt{\alpha^{235}}$

α^{235} = separation factor for U-235

$$= \sqrt{\frac{\text{mass of } U^{235}}{\text{mass of } U^{238}} \frac{F_6}{F_6}}$$

Knowing the number of product stages, the U-234 content can be estimated by:

$$x_p^{234} = \frac{1}{1 - (\beta^{234})^{-n_p}(1 - 1/x_f^{234})}$$

where:

x_p^{234} = enrichment plant U-235 product

x_f^{234} = enrichment plant U-234 product assay

$\beta^{234} = \sqrt{\alpha^{234}}$

$\alpha^{234} = \sqrt{\frac{\text{mass of } U^{235}F_6}{\text{mass of } U^{238}F_6}}$

The U-234 product assay from a diffusion enrichment plant for typical U-235 enrichments are given in the attached worksheet.

Reference

Benedict, M. and T. H. Pigford, Nuclear Chemical Engineering, McGraw Hill, New York, 1957, p. 388.

Table 1

U-234 in Enriched Uranium

U-235 Enrichment	No. of Enriching Stages	U-234 Enrichment
1.0	161	0.008524
1.1	206	0.009694
1.2	247	0.010903
1.3	285	0.012149
1.4	320	0.013431
1.5	353	0.014746
1.6	383	0.016095
1.7	412	0.017476
1.8	439	0.018887
1.9	465	0.020328
2.0	489	0.021799
2.1	513	0.023298
2.2	535	0.024824
2.3	556	0.026378
2.4	577	0.027958
2.5	596	0.029564
2.6	615	0.031196
2.7	633	0.032852
2.8	651	0.034534
2.9	667	0.036240
3.0	684	0.037969
3.1	700	0.039723
3.2	715	0.041499
3.3	730	0.043299
3.4	744	0.045121
3.5	758	0.046966
3.6	772	0.048833
3.7	785	0.050722
3.8	798	0.052632
3.9	811	0.054564
4.0	823	0.056518
4.1	835	0.058493
4.2	847	0.060488
4.3	858	0.062505
4.4	869	0.064542
4.5	880	0.066600
4.6	891	0.068678
4.7	902	0.070776
4.8	912	0.072894
4.9	922	0.075033
5.0	932	0.077191